UNIVERSITY OF SOUTHAMPTON

MODULATION OF CCTα BY MEMBRANE BIOPHYSICS

BY

PAOLO FAGONE

DOCTOR OF PHILOSOPHY

DEPARTMENT OF CHEMISTRY

FACULTY OF SCIENCE

FEBRUARY 2003

UNIVERSITY OF SOUTHAMPTON

ABSTRACT

FACULTY OF SCIENCE

CHEMISTRY

Doctor of Philosophy

MODULATION OF CCTα BY MEMBRANE BIOPHYSICS

by Paolo Fagone

CCTα (CTP: phosphocholine cytidylyltransferase) catalyses the rate limiting step in the synthesis of phosphatidylcholine through the Kennedy pathway. CCTα, essentially inactive in solution, becomes active in the presence of lipid membranes, into which it partitions. Surface negative charge and torque tension were found to be membrane properties that modulate the enzyme activity.

Lipid monolayers and large unilamellar vesicles (LUVs) were examined as possible candidates to be used as model system of biological membranes. Using LUVs as model systems, the effect of surface charge, of torque tension and of lipid concentration on the CCTα activity were investigated.

A set of equations was derived attempting to distinguish between the partitioning of the enzyme onto vesicles and its activation. The preliminary results indicate that the torque tension affects mostly the enzyme partitioning whilst the surface charge affects mostly the enzyme activity.

"Fatti non foste a viver come bruti,
ma per seguir virtute e canoscenza"

("Man was not made to live as a beast,
but to pursue virtue and knowledge")

(*Inferno, Divina Commedia*, Dante Alighieri)

TABLE OF CONTENTS

TABLE OF CONTENTS I
LIST OF FIGURES VII
LIST OF TABLES XXII
ACKNOWLEDGMENTS XXIX
ABBREVIATIONS XXX

1 INTRODUCTION TO CCT 1-1

1.1 THE KEY ROLE OF CCT 1-2
1.2 BIBLIOGRAPHY 1-5

2 CELLULAR MEMBRANES 2-1

2.1 THE STRUCTURE OF BIOLOGICAL MEMBRANES 2-1
2.2 CELL ORGANELLES 2-3
2.3 LIPIDS 2-5
2.4 PHOSPHATIDYLCHOLINE BIOSYNTHETIC PATHWAYS 2-10
2.5 SACCHAROMYCES CEREVISIAE 2-10
2.6 CCT IN MAMMALS 2-12
2.6.1 CDP-choline pathway and phosphatidylethanolamine methylation pathway 2-12
2.6.2 CDP-choline pathway and the secretion of lipoproteins 2-14
2.6.3 CCT localization inside the cell 2-14
2.7 REFERENCES 2-15

3 CCTα 3-1

3.1 CCTα: GENE STRUCTURE 3-1
3.2 CCTα: PROTEIN STRUCTURE 3-3
3.3 CCT ISOFORMS: α, β1 AND β2 3-6
3.4 CCTα: ACTIVITY MODULATION 3-7

3.4.1 Phosphorylation/dephosphorylation *3-8*

3.4.2 Lipid modulation of CCTα activity *3-9*

3.5 CCTα AND CELL SIGNALLING 3-10

3.6 CCTα AND CELL CYCLE 3-11

3.7 REFERENCES 3-13

4 PHYSICAL CHEMISTRY OF MEMBRANES 4-1

4.1 THE HYDROPHOBIC EFFECT 4-1

4.2 SURFACES: FORCES, ENERGY AND TOPOLOGY 4-3

4.2.1 Geometric and thermodynamic variables *4-3*

4.2.2 Forces between lipids in monolayers *4-4*

4.3 ENERGIES IN MONOLAYERS AND BILAYERS: LATERAL EXPANSION AND BENDING 4-6

4.3.1 The surface chemical potential *4-6*

4.3.2 Surface elastic energy: extension and bending *4-8*

4.4 REFERENCES 4-11

5 PROTEIN FOLDING AND ENERGY 5-1

5.1 FOLDING AND STRUCTURES OF PROTEINS 5-1

5.1.1 α-helix and β-sheets *5-4*

5.1.2 Protein folding *5-4*

5.2 CYTOSOLIC AND MEMBRANE PROTEINS 5-5

5.2.1 Average hydropathy and hydrophobic moment *5-7*

5.3 ENERGY OF PARTITION 5-10

5.4 REFERENCES 5-11

6 VESICLES AND MONOLAYERS 6-1

6.1 LIPID MONOLAYERS 6-1

6.2 THE BILAYER/MONOLAYER CORRESPONDENCE 6-3

6.2.1 Intrinsic pressure and surface tention *6-4*

6.2.2 Free energy and chemical potential *6-8*

6.3 REFERENCES 6-10

7 LIPID MONOLAYER AND PRESSURE/AREA ISOTHERMS 7-1

7.1 PHOSPHOLIPIDS AND MONOLAYER ISOTHERMS 7-1
7.2 MATERIALS AND METHODS 7-3
7.2.1 Materials *7-3*
7.2.2 Pressure/area isotherms *7-4*
7.2.3 Head-group area measurement of mixed phospholipid monolayers *7-4*
7.2.4 Monolayer stability *7-4*
7.3 RESULTS 7-5
7.3.1 Pressure/area isotherms *7-5*
7.3.2 Head-group area in mixed DMPC/DOPC and DOPC/DOPE monolayers *7-7*
7.3.3 Monolayer stability *7-17*
7.4 DISCUSSION 7-20
7.4.1 Pressure/area isotherms *7-20*
7.4.2 Head-group area of DMPC/DOPC and DOPC/DOPE mixtures *7-22*
7.4.3 Monolayer stability *7-22*
7.5 CONCLUSIONS 7-23
7.6 REFERENCES 7-24

8 PEPTIDE ADSORPTION ONTO MONOLAYERS 8-1

8.1 ADSORPTION OF PROTEINS AT INTERFACE 8-1
8.2 PPF2 8-3
8.3 MATERIAL AND METHODS 8-5
8.3.1 Materials *8-5*
8.3.2 PPF2 synthesis, purification and characterisation *8-6*
8.3.3 PPF2 adsorption at the air/water interface *8-9*
8.3.4 PPF2 adsorption into DMPC and DOPC monolayers *8-10*
8.4 RESULTS 8-10
8.4.1 PPF2 adsorption at the air/water interface *8-10*
8.4.2 PPF2 adsorption into DMPC and DOPC monolayers *8-10*
8.5 CONCLUSIONS 8-15
8.5.1 PPF2 adsorption at the air/water interface *8-15*
8.5.2 PPF2 adsorption into DMPC or DOPC monolayer *8-16*
8.6 REFERENCES 8-17

9 UNILAMELLAR VESICLES 9-1

9.1 LARGE UNILAMELLAR VESICLES (LUVS) 9-1

9.2 LIGHT SCATTERING AND PARTICLE SIZING 9-3

9.2.1 Light scattering 9-3

9.2.2 Particle sizing 9-5

9.2.2.1 Unimodal analysis 9-5

9.2.2.2 Size Distribution Process (SDP) analysis 9-6

9.3 COAGULATION OF LUVS 9-8

9.4 MATERIALS AND METHODS 9-8

9.4.1 Materials 9-8

9.4.2 Sizing of standard latex particles 9-9

9.4.3 Preparation of LUV: F-T method 9-9

9.4.4 Freeze-Thaw effect on LUVs size 9-10

9.4.5 Vesicle stability 9-11

9.4.6 Anionic phospholipids and coagulation 9-11

9.5 RESULTS 9-12

9.5.1 Sizing of standard latex particles 9-12

9.5.2 Freeze-thaw effect on LUV size 9-12

9.5.3 Vesicle stability 9-19

9.5.4 Anionic phospholipids and coagulation 9-30

9.6 CONCLUSION 9-32

9.7 REFERENCES 9-33

10 CCTα ACTIVITY MODULATION 10-1

10.1 TORQUE TENSION, SURFACE CHARGE AND CCTα ACTIVITY 10-1

10.2 DOPC MIXTURES 10-6

10.3 ENZYMATIC ASSAY CONDITIONS 10-7

10.4 MATERIALS AND METHODS 10-9

10.4.1 Materials 10-9

10.4.2 Calcium removal from phosphocholine 10-10

10.4.3 Vesicle preparation 10-11

10.4.4 Enzymatic assay 10-11

10.4.5 TLC method *10-13*
10.5 RESULTS 10-14
10.5.1 DOPC/DOPE LUVs *10-14*
10.5.1.1 First set of experiments 10-14
10.5.1.2 Second set of experiments 10-17
10.5.1.3 Third set of experiments 10-17
10.5.1.4 Fourth set of experiments 10-17
10.5.1.5 Comparison of CCTα activity in DOPC/DOPE LUVs 10-21
10.5.2 DOPC/DOPA LUVs *10-26*
10.5.2.1 First set of experiments 10-27
10.5.2.2 Second set of experiments 10-27
10.5.2.3 DOPC/DOPA LUVs and CCTα activity 10-31
10.5.3 DOPC/DPPA system *10-33*
10.5.4 DOPC/OPA LUVs *10-35*
10.5.4.1 First set of experiments 10-35
10.5.4.2 Second set of experiments 10-37
10.5.4.3 CCTα activity in DOPC/OPA LUVs 10-37
10.5.5 DOPC/DOPS LUVs *10-40*
10.5.5.1 First set of experiments 10-41
10.5.5.2 Second set of experiments 10-41
10.5.5.3 DOPC/DOPS LUVs and CCTα activity 10-43
10.5.6 DOPC/DPPS LUVs *10-45*
10.5.7 DOPC/OPS LUVs *10-49*
10.5.7.1 First set of experiments 10-49
10.5.7.2 Second set of experiments 10-51
10.5.7.3 CCTα activity in DOPC/OPS LUVs 10-51
10.5.8 DOPC/OA LUVs *10-54*
10.6 CONCLUSIONS 10-56
10.6.1 Enzyme activity and substrate concentrations *10-56*
10.6.2 CCTα basal and maximal activity *10-58*
10.6.3 Enzyme activity variability and LUVs *10-63*

10.6.4 The basal activity and the reference lipid 10-65

10.6.5 Torque tension and surface charge 10-67

10.7 REFERENCES 10-68

11 CCTα PARTITIONING AND ACTIVATION 11-1

11.1 CCTα PARTITION 11-1

11.2 PARTITION CONSTANT AND ENZYME ACTIVITY 11-2

11.3 MATERIALS AND METHODS 11-6

11.3.1 Materials (see 11.2.1) 11-6

11.3.2 CCTα assay and vesicle preparation 11-7

11.3.3 Equilibrium and partition constants, specific enzymatic activity and standard deviation 11-7

11.4 RESULTS 11-8

11.4.1 CCTα partitioning 11-8

11.5 CONCLUSIONS 11-17

11.5.1 CCTα partition/activation 11-17

11.5.2 CCTα partitioning 11-18

11.5.3 Hypothesis of enzyme activity modulation 11-21

11.6 REFERENCES 11-23

12 CONCLUSIONS 12-25

12.1 REFERENCES 12-2

13 APPENDICES 13-1

14 GLOSSARY 14-1

LIST OF FIGURES

Figure 1.1 CDP-choline pathway, also known as Kennedy pathway. The synthesis of PtdCho from choline consists of three reactions catalysed by three enzymes: choline kinase (1) transfers a phosphate group from one molecule of ATP to choline to give phosphocholine and ADP; CCT (2) transfers the CMP-group from one molecule of CTP to phosphocholine giving CDP-choline and one molecule of pyrophosphate (PPi); finally, diacylglycerol: choline phosphotransferase (3) transfers the phosphocholine group from CDP-choline to one molecule of diacylglycerol giving PtdCho and CMP. 1-1

Figure 1.2 Different enzymes can convert phosphatidylcholine into other lipids. Phospholipase D (1) activity results in choline and phosphatidic acid that is converted into diacylglycerol and phosphate by the phosphatidate phosphohydrolase (2). Alternatively, phosphatidylcholine can be converted in diacylglycerol and phosphocholine by phospholipase C (3). Phospholipase A_2 convert the phosphatidylcholine in a molecule of fatty acid and one of lyso-phosphatidylcholine. 1-2

Figure 1.3 PtdCho hydrolysis products are involved in the regulation of several cell events. The PAF is synthesised through two different routes: the de novo pathway and the remodelling pathway, which starts from the 1-O-alkyl-*sn*-glycero-3-phosphocholine (lyso-phosphatidyl-choline). TNFs are molecules having systemic effects, which can cause systemic or endotoxic shock in high doses [5-7]. 1-3

Figure 1.4 Rod photoreceptor structure. The disks of photoreactive membranes are contained in the rod outer segmenr (ROS)..... 1-4

Figure 2.1 Eukaryote cells use membranes for the separation of the cellular space from the surrounding environment and for the maintenance of the internal compartmentalisation, through organelles which internal space is delimited by one or two membranes..... 2-2

Figure 2.2 Section of a phospholipid bilayer. The hydrophobic core in the bilayer separates the two aqueous regions at the two sides of the membrane. Spheres having different color represent different atoms: carbon in gray, hydrogen in white, oxygen in red and phosphorous in orange. the molecules of water are represented in a simple way by the two blue surfaces at the top and at the bottom of the lipid bilayer. 2-2

Figure 2.3 Simplified representation of the fluid mosaic model, which is currently the accepted structure that best describes most biological membranes... 2-3

Figure 2.4 The nuclear envelope is constituted by a double membrane. The genetic material is contained in the nuclear lumen; the molecule trafficking between the nuclear lumen and the cytoplasm is mediated by carrier protein and channels.2-4

Figure 2.5 Three fatty acids that may be found in biological membranes are stearic, palmitic and oleic acid. The oleic acid is an unsaturated fatty acid with one *cis* double bond. Other fatty acids may have longer chains and more than one *cis* double bond (all double bond found in fatty acids are *cis*-double bond). Mono-, di- and tri-glycerides are obtained by linking one, two or three fatty acids to the glycerol moiety through an ester bond. 2-7

Figure 2.6 Glycerol-ether-phospholipids are very similar to phosphoglycerides, although synthesised through a different biosynthetic pathway. The platelet activating factor (1.1) plays a fundamental role in preventing the platelet aggregation. The glycerol-ether-phospholipid is converted by a desaturase in plasmalogen, a glycerol-ether-phospholipid having an α-β unsaturation at the C-1 of glycerol. 2-7

Figure 2.7 Sphingomyelin and sphingolipids are two classes of lipids showing the sphingosine moiety. Sphingolipids, or glycolipids, are lipids in which one molecule of sugar or branched sugar is bound to the sphingosine. Galactocerebroside is largely contained in the myelin sheath. 2-9

Figure 2.8 Cholesterol is present only in eukaryotes and has no charge. The only polar group in the molecule is the hydroxyl function at the C-3. 2-9

Figure 2.9 Eukaryote accessible routes for the synthesis of phosphatidylcholine [2, 3]. 2-11

Figure 3.1 Structure of the Murine *ctpct* encoding for CCT. The entire CCT gene is ~ 26 kb long, while the CT cDNA is only ~ 1.5 kb [1]. Exons from II to IX (the first exon is not translated) are translated into the 367 amino acid sequence long CCTα. Domain N (residues 1-72) contains the nuclear localisation sequence; domain C (residues 73-236) contains the residues involved in the catalysis; domain M (residues 237-299) contains the lipid-binding domain; domain P (residues 300-367) contains the residues involved in phosphorylation/dephosphorylation. 3-3

Figure 3.2 CCTα is essentially inactive when in solution and becomes active when bound to the membrane. The membrane-binding domain M seems to be involved in the interaction with the lipid membrane. 3-9

Figure 3.3 Metabolic cycle of regeneration of PtdIns(4,5)P_2. I) DAG kinase; II) CDP-DAG synthase; III) PtdIns synthase; IV) PtdIns kinase; V) PtdInsP kinase; VI) PLC; VII) PtdInsP_2 kinase [51]. 3-11

Figure 3.4 PtdCho cycle. I) choline phosphotransferase; II) PLD; III) phosphatidate sphosphohydrolase; IV) PLC.....3-12

Figure 3.5 The four phases of a typical eukaryotic cell. G_1, S and G_2 phases form the interphase, during which the cell continues to grow. New DNA is synthesised during S phase and cell division occurs in M phase [51].....3-12

Figure 4.1 Amphipathic molecules cluster into three different structures to minimise their contact with the water: monolayers, vesicles and micelles. In all the three structures, the polar head-groups, represented by spheres, interact with the water while the acyl chains, represented by the tails, turn to the air or get in contact with other acyl chains.....4-1

Figure 4.2 Probable structure for methane hydrate. Clathrate cage model of water molecules surrounding a molecule of methane. The ordered structure of the water reduces the entropy of the system and drives the phenomenon of immiscibility of nonpolar molecules with water [1].....4-2

Figure 4.3 The two radii of curvature, r_1 and r_2, correspond to the radius of the two arcs of circumference defined by the two orthogonal planes xz and yz, being z perpendicular to the surface.....4-3

Figure 4.4 The force t(z) acting between lipids grouped together in an aqueous environment is function of the position z across the lipid molecule. F_h is the force acting between the lipid head-groups and derives from both electrostatic and hydrational effect; F_γ is the force acting at the water/acyl-chains interface and depends on the water interfacial tension tending to minimise the interfacial area; finally, F_c is the force acting between the acyl-chains.....4-5

Figure 4.5 The imbalance between the forces across a lipid monolayer determine the spontaneous mean curvature.....4-5

Figure 4.6 Hexagonal (H_I) and inverse hexagonal (H_{II}) phase are two simple examples of normal and inverse topology phases, respectively.....4-6

Figure 4.7 Surfaces can undergo two different types of deformation: extension of the surface area, under the lateral tension σ, and bending of the surface under the torque tension τ.....4-8

Figure 4.8 A monolayer constituted by type II lipids and in contact with the water through the polar head-groups can be free to bend (monolayer on the top) or can be constrained to remain flat (monolayer on the bottom). The flat monolayer is more stressed than the curved one and the increased exposure of the hydrophobic core to the water is one of the origins of the stress.....4-10

Figure 5.1 Polyglycine in α-helix structure. The representation on the left shows only those hydrogens (white balls), bound to the amide nitrogen (blue balls), involved in H-bond (dashed black lines) with the carbolic oxygen (red balls). The structure on the right shows only nitrogen and carbon (grey balls) atoms to highlight the backbone of the α-helix structure 5-1

Figure 5.2 Polyglycines arranged in parallel (up chains) and anti-parallel (down chains) β-sheets. The two structures show only those hydrogens (white balls) bound to the amide nitrogens (blue balls). The two β-sheets differ for the orientation of the chains and for the number of H-bonds (dashed black lines) between the shown hydrogen and the carbolic oxygen (red balls). Grey balls represent carbon atoms. The projections on the left show that β-sheets are flat structures. 5-2

Figure 5.3 Schematic representation of a haemoglobin molecule. The haemoglobin tertiary structure corresponds to the spatial diposition of all the amino acids that are not part of the same segment. Alternatively, the tertiary structure corresponds to the spatial diposition of the different secondary structures..... 5-2

Figure 5.4 Schematic representation of a porin molecule. The tertiary structure corresponds to the spatial diposition of all the amino acids that are not part of the same segment. Alternatively, the tertiary structure corresponds to the spatial position of the different secondary structures. 5-3

Figure 5.5 Quaternary structure of the haemoglobin complex. The four identical units, singularly shown in Figure 5.3, are represented with different colours..... 5-3

Figure 5.6 Four residues in a α-helix structure. Three consecutive amino acids are separated by 100°, whilst the n^{th} residue by **n**x100° from the first one. H_0, H_1, H_2 and H_n are the hydrophobicities of the four residues AA_0, AA_1, AA_2 and AA_n respectively. The hydrophobicity of each residue is resoluted by the sin and cos functions in two orthogonal components and perpendicular to the helix axis. 5-8

Figure 5.7 The above α-helices have the same hydrophilic (in grey) and hydrophobic (in black) residues and, consequently, the same hydrophobicity. The residues in the upper helix are ordered to form a hydrophobic strip, resulting in a high hydrophobic moment; the random disposition of the residues, in the lower helix, results in a low hydrophobic moment. 5-8

Figure 5.8 Protein classification as a function of their hydrophobic moment and hydrophobicity. Figure re-drawn from reference [11]. 5-9

Figure 5.9 α-helices with low hydrophobicity and high hydrophobic moments (a single α-helix is shown in the middle with the hydrophobic residues represented by the thick arc) can bundle in two different ways: through the polar

(on the left) or through the apolar (on the right) residues. The structure on the left exposes to the environment only the polar residues (decreasing the affinity for the membrane hydrophobic core), while the structure on the right exposes only the apolar residues (increasing the affinity for the membrane hydrophobic core). 5-9

Figure 6.1 Surface pressure versus area per molecule isotherm for a long-chain organic compound. The surface pressure and the area per molecule are given in arbitrary units, a.u. G= gaseous phase, E= expanded liquid phase, C= condensed liquid phase [1]. 6-1

Figure 6.2 Two possible ways in which monolayers collapse when the pressure between the lipids overcomes the collapsing pressure π_c. Alternatively, the monolayer structure can evolve into micelles or vesicles. 6-2

Figure 6.3 Lipids in vesicles and in monolayers may differ in their density. The hydrophobic effect is principally responsible for the close lipid packing in vesicles; on the contrary, lipid density in monolayer is not affected by the hydrophobic effect and can be changed reducing the total area available for the monolayer. 6-3

Figure 7.1 Pressure/area isotherms for saturated phosphatidylcholines on 0.1 M NaCl at 22°C. □, dibenheoylphosphocholine (C_{22}); O, distearoylphosphocholine (C_{18}); ×, dipalmitoyl-phosphocholine (C_{16}); Δ, dimyristoylphosphocholine (C_{14}); ∇, dicaprylphosphocholine (C_{10}). Figure from reference [2] 7-1

Figure 7.2 Pressure-area isotherms for L-α-dipalmitoylphosphatidyl-choline on 0.1 M NaCl at various temperatures. •, 34.6 °C; Δ, 29.5 °C; ■, 26.0 °C; ×, 21.1 °C; ○, 16.8 °C; ▲, 12.4 °C ; □, 6.2 °C. Figure from reference [2]. 7-2

Figure 7.3 Schematic representation of various lamellar phases found in PtdCho/water systems: (A) subgel, L_c; (B) gel (untilted chains) , L_β; (C) gel (tilted chains), $L_{\beta'}$; (D) rippled gel, $P_{\beta'}$; (E) liquid crystalline, L_α; (F) fully interdigitated gel, L_β^{int}; (G) partially interdigitated gel; (H) mixed. Cross-sectional view of the hydrocarbon chain arrangement in various chain packing modes (view is down the long axis of the chains): (I) orthorhombic; (J) quasi-hexagonal; (K) hexagonal. Figure and legend from reference [8] 7-3

Figure 7.4 DMPC isotherms recorded in two different conditions: 20 °C on 0.1 M NaCl (-magnesium) and 37 °C on 0.1 M NaCl, 0.1 M Tris-HCl, pH 7.2, 10 mM $MgCl_2$ (+ magnesium). 7-5

Figure 7.5 DOPC isotherms were recorded in two different conditions. One isotherm was recorded at 20 °C on 0.1 M NaCl (- magnesium). The second isotherm was recorded at 37 °C on 0.1 M NaCl, 0.1 M Tris-HCl at pH 7.2, and 10 mM $MgCl_2$ (+ magnesium). 7-6

Figure 7.6 DOPE isotherms were recorded in two different conditions. One isotherm was recorded at 20 °C on 0.1 M NaCl (- magnesium). The second isotherm was recorded at 37 °C on 0.1 M NaCl, 0.1 M Tris-HCl at pH 7.2 and 10 mM $MgCl_2$ (+ magnesium). 7-6

Figure 7.7 Head-group areas measured for mixtures with different DMPC/DOPC ratio. The head-group areas shown in this graph were measured after the third isocycle at 25 mM/m. Experimental conditions are reported in 7.2.2. The indicated values are reported in Table 7.1 7-7

Figure 7.8 Head-group areas measured for different DOPC/DOPE mixtures. The head-group areas shown were measured at 25 mN/m after the third isocycle. Experimental conditions are reported in 7.2.2. The indicated values are reported in Table 7.2 7-9

Figure 7.9 DMPC/DOPC head-group areas measured during the 1st cycle at 15 and 25 mN/m. The error bars correspond to ± the standard deviations calculated on two measurements. 7-10

Figure 7.10 DMPC/DOPC head-group areas measured at 15 and 25 mN/m after seven isocycles. The values plotted are the average of two separate measurements. 7-12

Figure 7.11 DOPC/DOPE head-group areas measured at 15 and 25 mN/m after one isocycle. The areas plotted correspond to the average of two separate measurements. 7-14

Figure 7.12 DOPC/DOPE head-group areas measured at 15 and 25 mN/m after seven isocycles. The plotted areas are the average of two separate measurements. 7-14

Figure 7.13 DMPC, DOPC and DOPE monolayer stability. 7-17

Figure 7.14 DOPE monolayer pressure/time isotherm was recorded on 0.1 M NaCl at 37 °C. The lipid chloroform solution was spread on the aqueous phase and the pressure monitored for more than two hours without any compression. 7-19

Figure 7.15 DOPE pressure/area isotherm of the monolayer whose pressure was monitored for two hours as shown in Figure 7.14 7-19

Figure 7.16 DOPC monolayer stability on a fixed area trough. 7-20

Figure 7.17 DMPC, DOPC and DOPE pressure/area isotherms recorded on 0.1 M NaCl at 20 °C (7.3.1). 7-21

Figure 7.18 DMPC, DOPC and DOPE pressure/area isotherms recorded on 0.1 M NaCl, 0.1 M Tris-HCl at pH 7.2, and 10 mM $MgCl_2$ (7.3.1). 7-21

Figure 7.19 The monolayer structure A could be reorganised to the final structure D through the intermediate B and C. The monolayer A, constituted by type II lipids, is under stress when constrained in a flat position. The first step in the reorganisation, B, could involve the formation of expanded domains "d" causing the initial increase of the monolayer area or alternatively, if the area is fixed, the increase of the lateral pressure. The following structure, C, corresponds to a structure halfway between the monolayer and the inversed phase showed in the structure D. 7-23

Figure 8.1 Hydrophobic moment profile of CCTα was calculated using the WIF scale (Table 5.1) and the Eisenberg algorithm (Eq. 5.2). The local hydrophobic moment (representing the average of a 31 residues window) has been normalized to the maximum value in the graph. 8-4

Figure 8.2 α-helical representation of the CCTα M-domain (segment 251-268) and PPF2. Charged residues are light blue, polar residues are sea-green and apolar residues are green. The hydrophobic strip formed by the apolar residues of the CCTα helix are involved in the binding to the membrane interface. PPF2 was used as model system of CCTα in the study of the torque tension effect on the partitioning of the enzyme on the lipid membrane. 8-5

Figure 8.3 MS-MS ES spectrum of PPF2. The spectrum represent the secondary fragmentation of the peak at m/z 1051.1 ($[M+2H]^{2+}$). 8-7

Figure 8.4 Fragmentation of an idealised peptide (protonated) in the ionizing chamber of a mass spectrometer. R1, R2, R3 and R4 refer to the lateral chain of the residues. 8-9

Figure 8.5 PPF2 adsorption at the air/water interface. 250 μl of 2.37 mM PPF2 where injected in 60 ml of buffer A. A magnetic stirrer was switched on for 20s after the injection of the PPF2 solution. 8-11

Figure 8.6 PPF2 adsorption at the air/water interface. 125 μl of 2.37 mM PPF2 where injected in 60 ml of buffer A. A magnetic stirrer was switched on for 20s after the injection of the PPF2 solution. 8-11

Figure 8.7 PPF2 adsorption at the air/water interface. 25 μl of 2.37 mM PPF2 where injected in 60 ml of buffer A. A magnetic stirrer was switched on for 20s after the injection of the PPF2 solution. 8-12

Figure 8.8 PPF2 adsorption at the air/water interface. 200 μl of 2.37 mM PPF2 where injected in 60 ml of buffer B 8-12

Figure 8.9 PPF2 adsorption at the air/water interface. 100 μl of 2.37 mM PPF2 where injected in 60 ml of buffer B. Magnetic stirrer was used for the black curves. 8-13

Figure 8.10 PPF2 adsorption into DMPC monolayer. 200 μl of 2.37 mM PPF2 where injected in 50 ml of buffer A (pH 7.2). The pressures in the figure legend correspond to the monolayer pressure measured before the addition of PPF2.....8-13

Figure 8.11. PPF2 adsorption into DMPC monolayers. 100 μl of 2.37 mM PPF2 where injected in 50 ml of buffer A (pH 7.2). The pressures in the legend correspond to the monolayer pressure measured before the addition of PPF2....8-14

Figure 8.12 PPF2 adsorption into DMPC monolayers. 80-200 μl of 2.37 mM PPF2 were injected in 50 ml of buffer B (pH 7.4). The pressures in the legend correspond to the monolayer pressure measured before the addition of PPF2 (the values in brackets).....8-14

Figure 8.13 PPF2 adsorption into DOPC monolayers. 200 or 160 μl of 2.37 mM PPF2 where injected in 50 ml of buffer A (pH 7.2). The pressures in the legend correspond to the monolayer pressure measured before the addition of PPF2, whilst the number in brackets refer to the volume of PPF solution injected beneath the monolayer.....8-15

Figure 8.14 Pressure increases as a function of the PPF2 concentration in solution. Each point is the average of the highest pressures reached during the adsorption experiments at the air/water interface shown from Figure 8.5 to Figure 8.9.....8-16

Figure 9.1 Bending energy in unit of $2kA/r_0^2$ as a function of the $|r/r_0|$ ratio, where k is the bending moduli, A is the head-group area, r_0 is the spontaneous radius of curvature and r is the vesicle radius of curvature. The bending energy has been calculated using the simplified version of Eq. 4.14: $g_{curv}=(1/2)k_M(c_1+c_2-2c_0)^2$, where $c_1=c_2=1/r$ and $c_0=1/r_0$.....9-2

Figure 9.2 A multilamellar vesicle, resembling the onion layer structure, is represented on the left, while a unilamellar vesicles is represented on the right. Clearly, the lipid area exposed to the external solution is larger for a unilamellar than for a moltilamellar vesicle.....9-2

Figure 9.3 Samples from 1 to 4 (9.4.2) were sized separately and analysed by unimodal analysis.....9-14

Figure 9.4 Unimodal analysis of sample 5 (black line) and sample 6 (red line)(9.4.2).....9-15

Figure 9.5 Sample 5 (red line) and 6 (black line)(9.4.2), previously sized by unimodal analysis (Figure 9.4), were sized by the SPD analysis and the result shown as intensity result.....9-16

Figure 9.6 Unimodal analysis of vesicles sampled during the step reported in Table 9.2: after the 6th step (black line), after the 7th step (red line) and after the first F-T cycle (green line).....9-17

Figure 9.7 Unimodal analysis of vesicles sampled during the steps reported in Table 9.2 and Table 9.3: after the 2nd F-T (black line), the 11th step (red line), the 4th F-T (green line) and the 5th F-T cycle (blue line).....9-18

Figure 9.8 Vesicle size after five consecutive F-T cycles following the four showed in Figure 9.7: after the 6th F-T (black line), the 7th F-T (red line), the 9th F-T and 30 second sonication (green line) and the 10th F-T (blue line).....9-19

Figure 9.9 DOPC LUVs were sized twice at t = 0 and t = 1.5 h. The size obtained at t = 0 h by unimodal analysis was 1303 ± 598 nm (black line), while at t = 1.5 h it was 1931 ± 895 nm (red line).....9-21

Figure 9.10. Intensity result of SDP analysis of DOPC LUVs sizing. The time gap between the first (black line) and the second measurement (red line) was 1.5 hours.....9-22

Figure 9.11. Mean peaks for DOPC LUVs size obtained from the intensity results of the SDP analysis, Figure 9.10.....9-23

Figure 9.12 DOPC/DOPE (1:1) LUVs were sized at t = 0 and t = 1.5 h. The size at t = 0 h, obtained by unimodal analysis, resulted 849 ± 395 nm (black line), while the size at t = 1.5 h resulted 984 ± 460 nm (red line).....9-24

Figure 9.13 DOPC/DOPE (1:1) LUVs were sized at t = 0 and t = 1.5 h. The SDP intensity results are shown as black and red line for t = 0 and t = 1.5 h respectively. All the sizes and standard deviations are reported in Table 9.6.....9-25

Figure 9.14 Mean size from the SDP analysis of the DOPC/DOPE(1:1) LUVs. The diameters and their standard deviation are reported in Table 9.6.....9-26

Figure 9.15 Unimodal results from DOPA LUVs sizing. Values for the twelve curves are given in Table 9.7.....9-28

Figure 9.16 SPD intensity analysis of the 12 DOPA LUVs sizing (Table 9.8). 9-30

Figure 10.1 Type II lipid monolayer adopting its spontaneous curvature (A) is torque tension free. When the monolayer (A) is constrained in a flat position (B), corresponding to a zero curvature, the torque tension and the bending energy (grey ellipses marked with E) of the monolayer increase. The release of part of the bending energy and reduction of the torque tension are the driving force of CCTα partition onto the monolayer(C)[1].....10-2

Figure 10.2 CCTα relative activity, S, is plotted as a function of the mole fraction of DOPC, x, in DMPC/DOPC mixtures (solid circles) and in DOPC/DOPE mixtures (open circles). The dotted line represents the theoretical enzyme relative activity as function of DOPE mole fraction [1]. 10-3

Figure 10.3 CCTα relative activity plotted as a function of the DOPC mole fraction, x, in DOPC/DOPE mixture. Data from Davies et al. [2]. 10-3

Figure 10.4 a) DMPC and DOPC have the same head-group, choline, but differ in the acyl chains, dimyristoyl and dioleoyl, respectively. DOPC and DOPE have the same hydrocarbon chains but differ in head-groups, choline and ethanolamine respectively. b) Flat monolayers of DMPC, DOPC and DOPE experience different torque tensions due to the different force distribution across the lipid layer. When the force at the hydrocarbon region, F_c, is similar to the force at the head-group region, F_h, the flat monolayer experiences a low tendency to bend (flat line in the middle of two DMPC molecules); the presence of the double bond in the oleoyl chains of DOPC causes an increase of F_c and the flat monolayer experiences a high tendency to bend (curved line in the middle of two DOPC molecules); the substitution of the choline group with the ethanolamine one in DOPE causes a decrease of F_h resulting in a further increase of the tendency to bend (curved line in the middle of two DOPE molecules). 10-4

Figure 10.5 Monomyristoylphosphocholine (lyso-MPC) and 1-*O*-octadecyl-2-*O*-methyl-*rac*-glycerophosphocholine (ET-O18) are type I amphipiles, which aggregates experience a reduced force acting across the hydrocarbon region (F_c in Figure 10.4) and in a positive spontaneous curvature (in opposition to the negative one characterising type II lipid such as DOPC). 10-5

Figure 10.6 CCTα activity is plotted as a function of the mole fraction of DOPE in the DOPC/DOPE mixture. The error bars correspond to ± the standard deviation of three different samples. All data are reported in Table 10.3. 10-15

Figure 10.7 CCTα relative activity (S) for the DOPC/DOPE mixtures. Relative activity was calculated using Eq. 10.1. Relative activity data are reported in Table 10.3. 10-16

Figure 10.8 CCTα activity is plotted as a function of the mole fraction of DOPE in the DOPC/DOPE mixture. The error bars correspond to ± the standard deviation of three different samples. All data are reported in Table 10.4. 10-18

Figure 10.9 CCTα relative activity S for the DOPC/DOPE mixtures. Relative activity was calculated using Eq. 10.1. Relative activity data are reported in Table 10.4. 10-18

Figure 10.10 CCTα activity is plotted as a function of the mole fraction of DOPE in the DOPC/DOPE mixture. The error bars correspond to ± the standard deviation of three different samples. All data are reported in Table 10.5.....10-19

Figure 10.11 CCTα relative activity S for the DOPC/DOPE. Relative activity was calculated using Eq. 10.1. Relative activity data are reported in Table 10.5. 10-20

Figure 10.12 CCTα activity is plotted as a function of the mole fraction of DOPE in the DOPC/DOPE mixture. The error bars correspond to ± the standard deviation of three different samples. All data are reported in Table 10.6.....10-22

Figure 10.13 CCTα relative activity S for the DOPC/DOPE. Relative activity was calculated using Eq. 10.1. Relative activity data are reported in Table 10.6. 10-22

Figure 10.14 Comparison of the four curves obtained for the CCTα activity as a function of the mole fraction of DOPE in the DOPC/DOPE lipid mixtures. The four curves are plotted singularly in Figure 10.6, Figure 10.8, Figure 10.10 and Figure 10.12. 10-23

Figure 10.15 The four curves in the above plot correspond to the CCTα relative activity reported previously and shown in Figure 10.7, Figure 10.9, Figure 10.11 and Figure 10.13.....10-24

Figure 10.16 Comparison of the CCTα activity measured in Basal CCTα activity was measured in absence of vesicles. The same enzyme was used for the second and the third set of experiments. The error bars correspond to ± the standard deviation of three different samples. 10-25

Figure 10.17 CCTα activity measured in presence of DOPC or DOPC/DOPE (4:6) LUVs. The enzyme used for the four sets of experiments came from three different aliquots of the first batch.....10-26

Figure 10.18 CCTα activity is plotted as a function of the mole fraction of DOPA in the DOPC/DOPA mixture. The error bars correspond to ± the standard deviation of three different samples. All data are reported in Table 10.10.....10-29

Figure 10.19 CCTα relative activity S for the DOPC/DOPA. Relative activity was calculated using Eq. 10.1. Relative activity data are reported in Table 10.10. 10-29

Figure 10.20 CCTα activity is plotted as a function of the mole fraction of DOPA in the DOPC/DOPA mixture. The error bars correspond to ± the standard deviation of three different samples. All data are reported in Table 10.11.....10-30

Figure 10.21 CCTα relative activity S for the DOPC/DOPA. Relative activity was calculated using Eq. 10.1 (10.4.4). Relative activity data are reported in Table 10.11. 10-30

Figure 10.22 The basal activity and the activity in presence of DOPC/DOPA LUVs show differences that could be due essentially to the different batch of enzyme used for the experiments. The enzyme from the first batch was used for the first set of experiments, whilst the enzyme from the second batch was used for the second set of experiments. 10-32

Figure 10.23 All the enzymatic relative activity curves obtained in the previous sets of experiments are plotted in the above graph. 10-32

Figure 10.24 Comparison of the two curves for the CCTα relative activity in the presence of DOPC/DOPA LUVs, shown separately in Figure 10.18 and Figure 10.20. 10-33

Figure 10.25 CCTα activity is plotted as a function of the mole fraction of DPPA in the DOPC/DPPA mixtures. The error bars correspond to ± the standard deviation of three different samples. All data are reported in Table 10.12. 10-34

Figure 10.26 CCTα relative activity S for the DOPC/DPPA. Relative activity was calculated using Eq. 10.1. Relative activity data are reported in Table 10.12. 10-35

Figure 10.27 CCTα activity plotted as a function of the mole fraction of OPA in the DOPC/OPA mixture. All data are reported in Table 10.13. 10-36

Figure 10.28 CCTα relative activity S for the DOPC/OPA. Relative activity was calculated using Eq. 10.1. Relative activity data are reported in Table 10.13. .. 10-37

Figure 10.29 CCTα activity plotted as a function of the mole fraction of DOPS in the DOPC/OPA mixture. The error bars correspond to ± the standard deviation of three different samples. All data are reported in Table 10.14. 10-38

Figure 10.30 CCTα relative activity S for the DOPC/OPA. Relative activity was calculated using Eq. 10.1. Relative activity data are reported in Table 10.14. .. 10-39

Figure 10.31 The two curves show a similar trend, even if the activity was found to be lower in the first set of experiments at low OPA mole fraction. The two curves are plotted singularly in Figure 10.27 and Figure 10.29. 10-39

Figure 10.32 The relative activity of CCTα shows an initial increase that is similar in both the curves at low OPA mole percentage. The two curves are plotted singularly in Figure 10.28 and Figure 10.30. 10-40

Figure 10.33 CCTα activity is plotted as a function of the mole fraction of DOPS in the DOPC/DOPS mixture. The error bars correspond to ± the standard deviation of three different samples. All data are reported in Table 10.16. 10-42

Figure 10.34 CCTα relative activity S for the DOPC/DOPS. Relative activity was calculated using Eq. 10.1. Relative activity data are reported in Table 10.16. 10-42

Figure 10.35 CCTα activity is plotted as a function of the mole fraction of DOPS in the DOPC/DOPS mixture. The error bars correspond to ± the standard deviation of three different samples. All data are reported in Table 10.17. 10-44

Figure 10.36 CCTα relative activity S for the DOPC/DOPA. Relative activity was calculated using Eq. 10.1. Relative activity data are reported in Table 10.17. 10-44

Figure 10.37 The three phospholipids differ in the charge and in the size of the polar head-group, being the acyl chain R1 (oleyl) the same. DOPC has a neutral zwitterion head-group (net charge 0), DOPS has a negatively charged zwitterion head-group (nominal charge –1) and DOPA has a negatively charge head-group (nominal charge –2). 10-45

Figure 10.38 CCTα activity showed no plateau or maximal activation even at high mole fraction of DOPS in mixture with DOPC. Curves from the first and the second set. 10-46

Figure 10.39 CCTα relative activity curves obtained from the first and the second set of experiments in the presence of DOPC/DOPS LUVs, and shown separately in Figure 10.34 and Figure 10.36. 10-46

Figure 10.40 The basal activity and the activity in presence of DOPC/DOPA LUVs show differences that could be due essentially to the different batch of enzyme used for the experiments. The enzyme from the first batch was used for the first set of experiments, whilst the enzyme from the second batch was used for the second set of experiments. Differently from the previous cases, the basal activity measured during the second set of experiments is higher than the activity measured in presence of DOPC vesicles. 10-47

Figure 10.41 CCTα activity is plotted as a function of the mole fraction of DPPS in the DOPC/DPPS mixture. The error bars correspond to ± the standard deviation of three different samples. All data are reported in Table 10.18. 10-48

Figure 10.42 CCTα relative activity S for the DOPC/DPPS. Relative activity was calculated using Eq. 10.1. Relative activity data are reported in Table 10.18. .. 10-48

Figure 10.43 CCTα activity plotted as a function of the mole fraction of OPS in the DOPC/OPS mixture. All data are reported in Table 10.19. 10-50

Figure 10.44 CCTα relative activity S for the DOPC/OPS. Relative activity was calculated using Eq. 10.1. Relative activity data are reported in Table 10.19. .. 10-51

Figure 10.45 CCTα activity plotted as a function of the mole fraction of DOPS in the DOPC/OPS mixture. The error bars correspond to ± the standard deviation of three different samples. All data are reported in Table 10.20. 10-52

Figure 10.46 CCTα relative activity S for the DOPC/OPS. Relative activity was calculated using Eq. 10.1. Relative activity data are reported in Table 10.20. .. 10-53

Figure 10.47 CCTα activity increases in a similar way in both the experiments with DOPC/OPS LUVs. The two curves are shown singularly in Figure 10.43 and Figure 10.45. 10-53

Figure 10.48 CCTα relative activity in the first set of experiments increases and shows a much higher activity than that obtained from the second set. The two curves are shown singularly in Figure 10.44 and Figure 10.46. 10-54

Figure 10.49 CCTα activity plotted as a function of the mole fraction of PA in the DOPC/OA mixture. The error bars correspond to ± the standard deviation of three different samples. All data are reported in Table 10.21. 10-55

Figure 10.50 CCTα relative activity S for the DOPC/OA lipid mixtures. Relative activity was calculated using Eq. 10.1. Relative activity data are reported in Table 10.21. 10-56

Figure 11.1 Double-reciprocal plot of Eq. 11.17. 11-5

Figure 11.2 CCTα, activity measured for different concentrations of DOPC/DOG (84:16). [CCTα] = 10 μg/ml= ~$2.4 \cdot 10^{-7}$ M. The error bars represent ± the standard deviation. 11-9

Figure 11.3 Double-reciprocal plots of CCTα partitioning into DOPC/DOG (84:16) LUVs and of the curve for the calculation of the standard deviation. [CCTα] = 10 μg/ml= ~$2.4 \cdot 10^{-7}$ M. Data are reported in Table 11.1 and Table 11.2. 11-10

Figure 11.4 CCTα activity measured for different concentrations of DOPC/DOPA (7:3). [CCTα] = 10 μg/ml= ~$2.4 \cdot 10^{-7}$ M. The error bars represent ± the standard deviation.....11-11

Figure 11.5 Double-reciprocal plot of the CCTα partitioning into DOPC/DOPA (7:3) LUVs and of the curve for the calculation of the standard deviation. [CCTα] = 10 μg/ml= ~$2.4 \cdot 10^{-7}$ M. Data are reported in Table 11.3 and Table 11.4.....11-12

Figure 11.6 CCTα activity measured for different concentrations of DOPC/DOPS (7:3). [CCTα] = 10 μg/ml= ~$2.4 \cdot 10^{-7}$ M. The error bars represent ± the standard deviation.....11-13

Figure 11.7 Double-reciprocal plots of CCTα partitioning into DOPC/DOPS (7:3) LUVs and of the curve for the calculation of the standard deviation. [CCTα] = 10 μg/ml= ~$2.4 \cdot 10^{-7}$ M. Data are reported in Table 11.5 and Table 11.6.....11-14

Figure 11.8 CCTα activity measured for different concentrations of DOPC/OA (1:1). [CCTα] = 10 μg/ml= ~$2.4 \cdot 10^{-7}$ M. The error bars represent ± the standard deviation.....11-15

Figure 11.9 Double-reciprocal plots of CCTα partitioning into DOPC/OA (1:1) LUVs and of the curve for the calculation of the standard deviation. [CCTα] = 10 μg/ml= ~$2.4 \cdot 10^{-7}$ M. Data are reported in Table 11.7 and Table 11.8.....11-16

Figure 11.10 Plot of the specific enzymatic activities and the partition constants reported in Table 11.9. The error bars correspond to ± the standard deviations reported in Table 11.10.....11-21

Figure 11.11 The hydrophobic interaction (light grey arrow), sensitive to the torque tension and the stored elastic energy, could the enzyme partition onto the vesicle surface. When the enzyme reaches the membrane surface, the membrane binding through the hydrophobic strip could aloud electrostatic interaction between the negatively charged lipids and the enzyme positively charged segment (5 lysine residues in the short segment 248-254, 3.1) to trigger the folding of CCTα into the active form.....11-23

LIST OF TABLES

Table 2.1 Approximate lipid compositions of different cell membranes [1]. 2-6

Table 2.2 Different phospholipids present in membranes. R_1 and R_2 are two acyl chains; only chain R_2 normally contains one or more double bonds..... 2-8

Table 3.1 Gene/domain structure of CCT obtained from the comparing of the Murine *ctpct* sequence with the protein amino acid sequence [1]..... 3-2

Table 3.2 CCTα amino acid sequence obtained from CCTα cDNA. 3-5

Table 4.1 Thermodynamic quantities for the transfer of non polar solutes from cyclo-hexane to water at 25 °C. n-hexane was transferred from n-hexane. Table from reference [1]..... 4-2

Table 5.1..... 5-6

Table 7.1 Head-group areas for the DMPC/DOPC mixtures. $A_{15}(1)$ and $A_{25}(1)$ are the head-group areas measured at 15 and 25 mN/m, respectively, during the first compression; $A_{15}(3)$ and $A_{25}(3)$ correspond to the head-group areas at 15 and 25 mN/m, respectively, after three cycles of compression and decompression. 7-8

Table 7.2 Head-group area for the DOPC/DOPE mixtures. $A_{15}(1)$ and $A_{25}(1)$ are the head-group areas measured at 15 and 25 mN/m, respectively, after one monolayer compression; $A_{15}(3)$ and $A_{25}(3)$ correspond to the head-group areas at 15 and 25 mN/m, respectively, after three cycles of compression and decompression..... 7-9

Table 7.3 DMPC/DOPC head-group areas measured at 15 mN/m during the first isocycle..... 7-11

Table 7.4 DMPC/DOPC head-group areas measured at 25 mN/m during the first isocycle..... 7-11

Table 7.5 DMPC/DOPC head-group areas measured at 15 mN/m after seven isocycles..... 7-13

Table 7.6 DMPC/DOPC head-group areas measured at 25 mN/m after seven isocycles..... 7-13

Table 7.7 DOPC/DOPE head-group areas measured at 15 mN/m after one isocycle..... 7-15

Table 7.8 DOPC/DOPE head-group areas measurement at 25 mN/m after one isocycle 7-15

Table 7.9 DOPC/DOPE head-group areas measured after seven isocycles at 15 mN/m. 7-16

Table 7.10 DOPC/DOPE head-group area measured at 25 mN/m after seven isocycles. 7-16

Table 8.1 Hydrophobic moment and hydrophobicity were calculated for CCTα(251-268) and for PPF2 using the WIF scale (Table 5.1) and the Eisenberg algorithm (Eq. 5.2). The hydrophobic moment per residue is indicated in brackets. 8-4

Table 8.2 Method used for the purification of PPF2. Aqueous solvent: H_2O with 0.1% TFA; organic solvent: CH_3CN with 0.1% TFA. 8-6

Table 8.3 Fragments and peaks for the MS-MS analysis of PPF2 (Figure 8.3). The two calculated values correspond to the M and to the isotopic M+1 peaks. .. 8-8

Table 9.1 Sample composition gives the diameter, in nm, of standard latex particles present in each sample. 9-9

Table 9.2 Steps for vesicle preparation by the Freeze-Thaw (F-T) method.. 9-10

Table 9.3 Extension of the F-T protocol reported in Table 9.2 9-11

Table 9.4 Vesicle size during the several steps constituting the Freeze- Thaw method. 9-13

Table 9.5 Size values for the curves reported in Figure 9.10 and Figure 9.119-20

Table 9.6 DOPC/DOPE (1:1) LUVs sizing. Intensity results and mean size obtained form SDP analysis. 9-20

Table 9.7 Unimodal results from DOPA LUVs sizing 9-27

Table 9.8 Intensity analysis of the SDP treatment of the data from the 12 sizings of DOPA LUVs 9-29

Table 9.9 Critical coagulation concentrations for DOPA LUVs 9-31

Table 9.10 DOPS titration using NaCl and $MgCl_2$. The value for $Mg^{2+}(a)$ was obtained using 150 mM BT buffer. 9-31

Table 9.11 Calculated and experimental *ccc* ratio obtained substituting data from Table 9.9 into Eq. 9.22 9-32

Table 9.12 Calculated and experimental *ccc* ratio obtained substituting data from Table 9.9 into Eq. 9.22 9-32

Table 10.1 Steps for the preparation of LUVs by the F-T method 10-12

Table 10.2 Difference between the four sets of experiment employing the DOPC/DOPE lipid mixtures. 10-14

Table 10.3 This tabulation reports CCTα activity and relative activity, S, measured in the presence of DOPC/DOPE LUVs. Relative activity was calculated using Eq. 10.1. All the data reported in the table are plotted in Figure 10.6 and Figure 10.7. 10-15

Table 10.4 This tabulation reports CCTα activity and relative activity, S, measured in the presence of DOPC/DOPE LUVs. Relative activity was calculated using Eq. 10.1. All the data reported in the table are plotted in Figure 10.8 and Figure 10.9. 10-16

Table 10.5 This tabulation reports CCTα activity and relative activity, S, measured in the presence of DOPC/DOPE LUVs. Relative activity was calculated using Eq. 10.1. All the data reported in the table are plotted in Figure 10.10 and Figure 10.11. 10-19

Table 10.6 This tabulation reports CCTα activity and relative activity, S, measured in the presence of DOPC/DOPE LUVs. Relative activity was calculated using Eq. 10.1. All the data reported in the table are plotted in Figure 10.12 and Figure 10.13. 10-20

Table 10.7 The table summarises all the CCTα activities reported in the previous tables. All the curves are plotted in Figure 10.14 10-23

Table 10.8 The table reports all the CCTα activities reported in the previous tables and plotted together in Figure 10.15 10-24

Table 10.9 Difference between the two sets of experiment employing the DOPC/DOPA lipid mixtures 10-27

Table 10.10 This tabulation reports CCTα activity and relative activity, S, measured in the presence of DOPC/DOPA LUVs. Relative activity was calculated using Eq. 10.1. All the data reported in the table are plotted in Figure 10.18 and Figure 10.19. 10-28

Table 10.11 This tabulation reports CCTα activity and relative activity, S, measured in the presence of DOPC/DOPA LUVs. Relative activity was calculated using Eq. 10.1. All the data reported in the table are plotted in Figure 10.20 and Figure 10.21. 10-28

Table 10.12 This tabulation reports CCTα activity and relative activity, S, measured in the presence of DOPC/DPPA LUVs. Relative activity was calculated using Eq. 10.1. All the data reported in the table are plotted in Figure 10.25 and Figure 10.26. 10-34

Table 10.13 This tabulation reports the CCTα activity and CCTα relative activity, S, measured in the presence of DOPC/OPA LUVs. Relative activity was calculated using Eq. 10.1. All the data reported in the table are plotted in Figure 10.27 and Figure 10.28. 10-36

Table 10.14 This tabulation reports CCTα activity and relative activity, S, measured in the presence of DOPC/OPA LUVs. Relative activity was calculated using Eq. 10.1. All the data reported in the table are plotted in Figure 10.29 and Figure 10.30. 10-38

Table 10.15 Difference between the two sets of experiment employing the DOPC/DOPS lipid mixtures 10-40

Table 10.16 This tabulation reports CCTα activity and relative activity, S, measured in the presence of DOPC/DOPS LUVs. Relative activity was calculated using Eq. 10.1. All the data reported in the table are plotted in Figure 10.33 and Figure 10.34. 10-41

Table 10.17 This tabulation reports CCTα activity and relative activity, S, measured in the presence of DOPC/DOPS LUVs. Relative activity was calculated using Eq. 10.1 (10.4.4). All the data reported in the table are plotted in Figure 10.35 and Figure 10.36 10-43

Table 10.18 This table reports CCTα activity and relative activity, S, measured in the presence of DOPC/DPPS LUVs. Relative activity was calculated using Eq. 10.1. All the data reported in the table are plotted in Figure 10.41 and Figure 10.42. 10-47

Table 10.19 This tabulation reports CCTα activity and relative activity, S, measured in the presence of DOPC/OPS LUVs. Relative activity was calculated using Eq. 10.1. All the data reported in the table are plotted in Figure 10.43 and Figure 10.44. 10-50

Table 10.20 This tabulation reports CCTα activity and relative activity, S, measured in the presence of DOPC/OPS LUVs. Relative activity was calculated

using Eq. 10.1. All the data reported in the table are plotted in Figure 10.45 and Figure 10.46. 10-52

Table 10.21 This tabulation reports CCTα activity and relative activity, S, measured in the presence of DOPC/OA LUVs. Relative activity was calculated using Eq. 10.1. All the data reported in the table are plotted in Figure 10.49 and Figure 10.50. 10-55

Table 11.1 CCTα partitioning into DOPC/DOG (84:16) LUVs. The least squares method was used for the linear regression. 11-9

Table 11.2 Data for the evaluation of the standard deviation for the results of CCTα partitioning into DOPC/DOG (84:16) LUVs. Lipid concentration ([L]) is expressed in mM. The least squares method was used for the linear regression. 11-10

Table 11.3 CCTα partitioning into DOPC/DOPA (7:3) LUVs. The least squares method was used for the linear regression. 11-11

Table 11.4 Data for the evaluation of the standard deviation for the results of CCTα partitioning into DOPC/DOPA (7:3) LUVs. Lipid concentration ([L]) is expressed in mM. The least squares method was used for the linear regression. 11-12

Table 11.5 CCTα partitioning into DOPC/DOPS (7:3) LUVs. The least squares method was used for the linear regression. 11-13

Table 11.6 Data for the evaluation of the standard deviation for the results of CCTα partitioning into DOPC/DOPS (7:3) LUVs. Lipid concentration ([L]) is expressed in mM. The least squares method was used for the linear regression. 11-14

Table 11.7 CCTα partitioning into DOPC/OA (7:3) LUVs. Lipid concentration ([L]) is expressed in mM; activity and standard deviation are expressed in $nmol \cdot min^{-1} mg^{-1}$. The least squares method was used for the linear regression 11-15

Table 11.8 Data for the evaluation of the standard deviation for the results of CCTα partitioning into DOPC/OA (1:1) LUVs. Lipid concentration ([L]) is expressed in mM. The least squares method was used for the linear regression. 11-16

Table 11.9 All the constants were calculated using the equations reported in 11.1 and 11.3.3. The specific enzymatic activation and the partition constant for the four lipid mixtures are plotted in Figure 11.10 11-17

Table 11.10 Standard deviation for the constants reported in Table 11.9. 11-17

Table 11.11 Partition constant for CCTα calculated using the method described herein (K_P) and calculated by Arnold *et al.* ($1/2 \cdot K_X$) [2]. The partition

constant determined by Arnold has been divided by two because they the used [L]/2 instead of [L] for the determination of K_X and K_P respectively (Eq. 11.1 and Eq. 11.7).....11-19

Table A-1 (DOPC/DOPE LUVs: first set of experiments).....13-1

Table A-2 (DOPC/DOPE LUVs: second set of experiments).....13-1

Table A-3 (DOPC/DOPE LUVs: third set of experiments).....13-2

Table A-4 (DOPC/DOPE LUVs: fourth set of experiments).....13-2

Table A-5 (DOPC/DOPA LUVs: first set of experiments).....13-3

Table A-6 (DOPC/DOPA LUVs: second set of experiments).....13-3

Table A-7 (DOPC/DOPS LUVs: first set of experiments).....13-4

Table A-8 (DOPC/DOPS LUVs: second set of experiments).....13-4

Table A-9 (DOPC/DPPA LUVs).....13-5

Table A-10 (DOPC/DPPS LUVs).....13-5

Table A-11 (DOPC/OPA and DOPC/OPS LUVs: first set of experiments).....13-6

Table A-12 (DOPC/OPA LUVs: second set of experiments).....13-6

Table A-13 (DOPC/OPS LUVs: second set of experiments).....13-7

Table A-14 (DOPC/OA LUVs: second set of experiments).....13-7

Table A-15 (CCTα partitioning into DOPC/DOG (84:16) LUVs).....13-8

Table A-16 (CCTα partitioning into DOPC/DOPA (7:3) LUVs).....13-8

Table A-17 (CCTα partitioning into DOPC/DOPS (7:3) LUVs).....13-8

Table A-18 (CCTα partitioning into DOPC/OAS (1:1) LUVs).....13-9

Table A- 19 Vesicles were diluted in buffer and sized measuring the light scattered at 90°. Vesicle diameter was estimated by SDP intensity analysis. Analysis conditions were: 300 seconds accumulation and automatic sampling time, 3-200 nm diameter range and 24 bins.....13-9

Table A- 20 Vesicles were diluted in buffer and sized measuring the light scattered at 90°. Vesicle diameter was estimated by SDP intensity analysis. Analysis conditions were: 300 seconds accumulation and automatic sampling time, 3-200 nm diameter range and 24 bins. 13-10

Table A- 21 Vesicles were diluted in buffer and sized measuring the light scattered at 90°. Vesicle diameter was estimated by SDP intensity analysis. Analysis conditions were: 300 seconds accumulation and automatic sampling time, 3-200 nm diameter range and 24 bins. 13-10

Table A- 22 Vesicles were diluted in buffer and sized measuring the light scattered at 90°. Vesicle diameter was estimated by SDP intensity analysis. Analysis conditions were: 300 seconds accumulation and automatic sampling time, 3-200 nm diameter range and 24 bins. 13-11

Table A- 23 Vesicles were diluted in buffer and sized measuring the light scattered at 90°. Vesicle diameter was estimated by SDP intensity analysis. Analysis conditions were: 300 seconds accumulation and automatic sampling time, 3-200 nm diameter range and 24 bins. 13-12

Table A- 24 Vesicles were diluted in buffer and sized measuring the light scattered at 90°. Vesicle diameter was estimated by SDP intensity analysis. Analysis conditions were: 300 seconds accumulation and automatic sampling time, 3-200 nm diameter range and 24 bins. 13-12

Table A- 25 Vesicles were diluted in buffer and sized measuring the light scattered at 90°. Vesicle diameter was estimated by SDP intensity analysis. Analysis conditions were: 300 seconds accumulation and automatic sampling time, 3-200 nm diameter range and 24 bins. 13-13

Table A- 26 Vesicles were diluted in buffer and sized measuring the light scattered at 90°. Vesicle diameter was estimated by SDP intensity analysis. Analysis conditions were: 300 seconds accumulation and automatic sampling time, 3-200 nm diameter range and 24 bins. 13-13

ACKNOWLEDGMENTS

The author wishes to thank:

The University of Southampton for funding.

Dr J. Frey for the use of his Langmuir trough; Dr G.J. Langley and J.M. Herniman for the ES-MS of the peptide PPF2; Dr M. Kriek, Dr W.S. Smith, R.J. Wood and Dr M. Dymond for their useful comments and suggestions on this thesis.

Prof. S. Jackowski for providing the CCTα and for useful comments.

Dr P.L. Roach, for the permission to use all the facilities available in his lab.

Prof. G.S. Attard for the time he spent in scientific discussions and comments and for his encouragement during the author's PhD.

Roberta Leonardi for comments, advice and assistance during the writing of this thesis.

The author also thanks his parents and his wife, Roberta Leonardi, for all the support and encouragement, the help and the love that they gave and will always give to him.

And finally, thanks to God.

ABBREVIATIONS

[^{125}I]TID	3-(trifluoromethyl)-3-(m[^{125}I]iodophenyl)diazirine
ACF	Autocorrelation function
ADP	Adenosine diphosphate
ATP	Adenosine triphosphate
BT	bis-Tris (2,2-Bis(hydroxymethyl)-2,2',2''-nitrilotriethanol)
CCT	CTP:phosphocholine cytidylyltransferase[a]
CDP	Cytidine diphosphate
CDP-Cho	CDP-choline
CET	CTP: phosphoethanolamine cytidylyltransferase
CMP	Cytidine monophosphate
CTP	Cytidine triphosphate
DAG	Diacylglycerol
DNA	Deoxyribonucleic acid
DOG	1,2-dioleoyl-*sn*-glycerol
DOPA	1,2-dioleoyl-*sn*-glycero-3-phosphatidic acid
DOPC	1,2-dioleoyl-*sn*-glycero-3-phosphocholine
DOPE	1,2-dioleoyl-*sn*-glycero-3-phosphoethanolamine
DOPS	1,2-dioleoyl-*sn*-glycero-3-phosphoserine
DPPA	1,2-dipalmitoyl-*sn*-glycero-3-phosphatidic acid
DPPS	1,2-dipalmitoyl-*sn*-glycero-3-phosphoserine
DZA	3-deaza-adenosine
ET-18-OCH$_3$	1-*O*-octadecyl-2-*O*-methyl-*rac*-glycero-3-phosphocholine
kcpm	10^3 count per minute
OA	Oleic acid

[a] Until 1998 no CCT isoform was known; therefore the generic denomination CCT is mantained when referring to findings reported in papers published before that year. The specific isoforms of the enzyme (CCTα, CCTβ, CCTβ1 and CCTβ2) are instead indicated when referring to papers published after 1998.

OPA	1-oleoyl-2-hydroxy-*sn*-glycero-3-phosphatidic acid
OPS	1-oleoyl-2-hydroxy-*sn*-glycero-3-phosphoserine
PAF	Platelet activating factor
PhoCho	Phosphocholine
PKC	Protein kinase C
PLA_2	Phospholipase A_2
PMET	Phosphatidylethanolamine methyltransferase
POPC	1-palmitoyl-2-oleoyl-*sn*-glycero-3-phosphocholine
PPi	Pyrophosphate
PtdCho	Phosphatidylcholine
PtdEtn	Phosphatidylethanolamine
PtdIns	Phosphatidylinositol
PtdSer	Phosphatidylserine
RNA	Ribonucleic acid
ROS	Rod outer segment
rt	room temperature
SDP	Size distribution processor
SDS	Sodium dodecylsulfate
SDS-PAGE	Sodium dodecylsulfate polyacrylamide gel electrophoresis
TFA	Trifluoroacetic acid
TNS	Tumour necrosis factor

1 Introduction to CCT

In 1957, Kennedy published the first data on the role played by CTP: phosphocholine cytidylyltransferase (CCT)[a] in phosphatidylcholine (PtdCho) synthesis and proposed the CDP-choline pathway (Figure 1.1), now known as Kennedy pathway, as one of the possible biochemical routes used by cells for PtdCho synthesis [1]. Since its discovery, hundreds of papers have been published on CCT, elucidating its regulation and role in cells. With the advent and the development of new scientific tools (in particular molecular biology) different CCT isoforms were discovered, increasing the understanding of its role and regulation in different organisms and mammal tissues [2, 3].

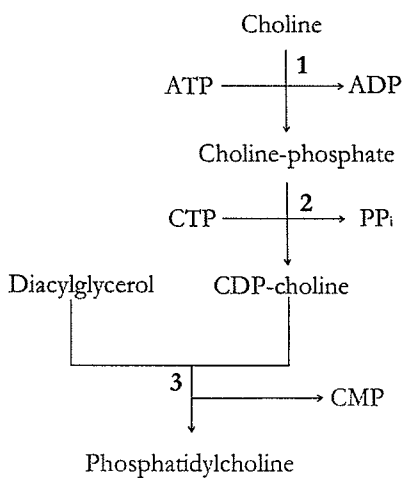

Figure 1.1 CDP-choline pathway, also known as Kennedy pathway. The synthesis of PtdCho from choline consists of three reactions catalysed by three enzymes: choline kinase (1) transfers a phosphate group from one molecule of ATP to choline to give phosphocholine and ADP; CCT (2) transfers the CMP-group from one molecule of CTP to phosphocholine giving CDP-choline and one molecule of pyrophosphate (PPi); finally, diacylglycerol: choline phosphotransferase (3) transfers the phosphocholine group from CDP-choline to one molecule of diacylglycerol giving PtdCho and CMP.

---

[a] Alternative synonyms are: CDP-choline pyrophosphorylase, CDP-choline synthetase, phosphorylcholine cytidylyltranspherase, and others. The name given by the Enzyme Commission (EC) is EC.2.7.7.15, which means the enzyme is a transferase (2.) that catalyses the transfer of the cytidylyl-phosphate group (7.7.) to the choline-phosphate (15). The Enzyme Commission (EC) was formed by the International Union of Pure and Applied Chemistry (IUPAC) for the development of a systematic numerical nomenclature of enzymes.

Different pathways of PtdCho synthesis have been found eukaryotes. However, the principal route in the synthesis of PtdCho, for most mammalian cells, is the Kennedy pathway, in which the conversion of phosphocholine to CDP-choline is the rate-limiting step [4]. Consequently, the role of CCT in the synthesis of PtdCho is critical in those organisms in which the Kennedy pathway is the preferential biosynthetic route.

1.1 The key role of CCT

Proteins and lipids constitute a major part of biological membranes and a wide range of membrane functions (such as compartmentalisation or storage) depends on membrane composition.

The homeostatic control of the lipid content in biological membranes is tightly regulated. PtdCho is the most abundant class of phospholipids present in membranes and it is both a membrane component and a synthetic precursor to other lipids, as shown in Figure 1.2 .

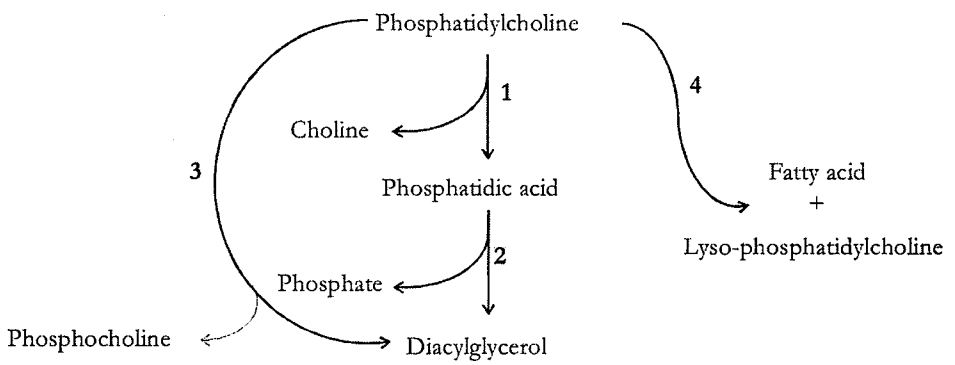

Figure 1.2 Different enzymes can convert phosphatidylcholine into other lipids. Phospholipase D (1) activity results in choline and phosphatidic acid that is converted into diacylglycerol and phosphate by the phosphatidate phosphohydrolase (2). Alternatively, phosphatidylcholine can be converted in diacylglycerol and phosphocholine by phospholipase C (3). Phospholipase A_2 convert the phosphatidylcholine in a molecule of fatty acid and one of lyso-phosphatidylcholine.

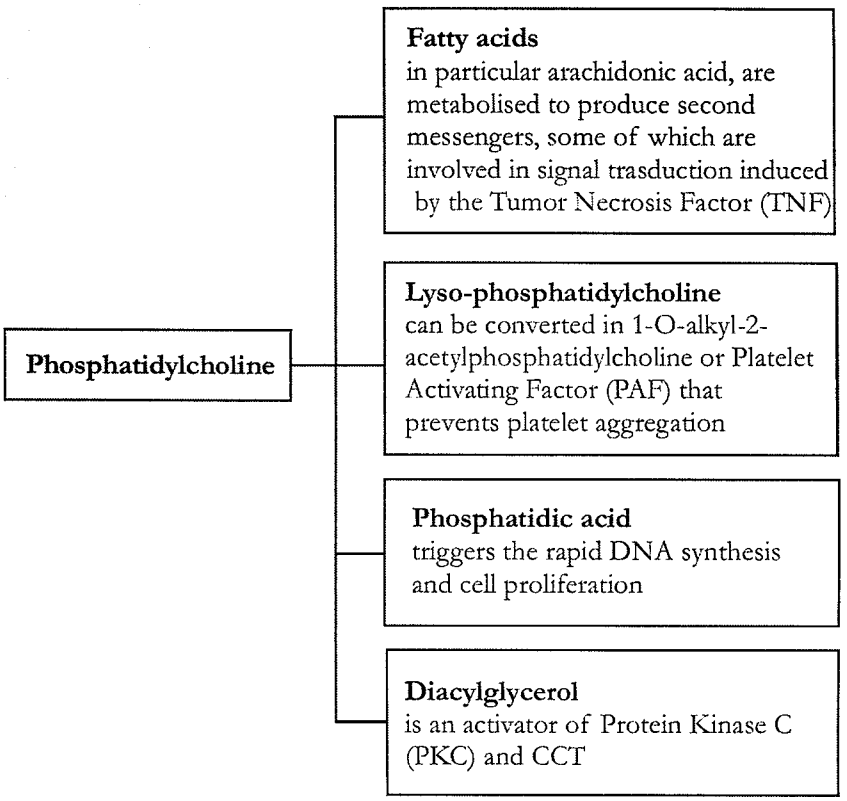

Figure 1.3 PtdCho hydrolysis products are involved in the regulation of several cell events. The PAF is synthesised through two different routes: the de novo pathway and the remodelling pathway, which starts from the 1-O-alkyl-*sn*-glycero-3-phosphocholine (lyso-phosphatidyl-choline). TNFs are molecules having systemic effects, which can cause systemic or endotoxic shock in high doses [5-7].

Phosphatidic acid, diacylglycerol, lyso-phosphatidylcholine and fatty acids are all secondary messengers that trigger different cellular events, some of which are shown in Figure 1.3 . Moreover, as the PtdCho is the most abundant membrane phospholipid, the homeostatic maintenance of its composition in membranes is essential for cell growth and survival [8].

No hereditary disease depending on the biosynthesis of PtdCho is known. CCT inhibition or inactivation, due to genetic mutation of the CCT gene or to the presence of inhibitors, arrests the cell growth and eventually leads to cell death[b].

[b] 1-*O*-octadecyl-2-*O*-methyl-*rac*-glycero-3-phosphocholine (ET-18-CH_3) is an antineoplastic ether-linked phospholipid analogue that inhibits CCT activity and leads the cell to death by triggering its apoptosis [8, 9].

Platelet Activating Factor (PAF) is a lipid mediator whose activity hinges on its proinflammatory, haemostatic and vasoactive properties. The intracellular and extracellular concentration of PAF is related to physiological and pathological events in nervous tissues [10]. CCT plays a key role in the synthesis of PAF in two ways: directly and indirectly. CCT acts indirectly through lyso-phosphocholine that has been reported (Figure 1.3) as one alternative source of PAF. CCT acts directly through the de novo pathway, in which a dithiothreitol-insensitive isozyme of the choline-phosphotransferase catalyses the transfer of the phosphocholine moiety from CDP-choline to 1-alkyl-2-acetyl-*sn*-glycerol [10].

The photoreceptor cells in the retina are permanent cells that do not divide and undergo a rapid turnover of their components, proteins and membranes. The rod outer segments (ROS) of photoreceptors contain disks of photoreceptive membrane that convert light to electric impulse, Figure 1.4. Due to the absorption of the light, ROS are susceptible to photoreactive oxidative stress and undergo a renewal process during which the apical tips are shed daily and phagocytised by retinal pigment epithelial (RPE) cells. Because of the daily shedding, the synthesis of new membrane is fundamental and photoreceptor cell analysis has revealed decreased phagocytosis and membrane renewal as a consequence of decreased activity of CCT and CTP: phosphoethanolamine cytidylyltransferase (CET) [11].

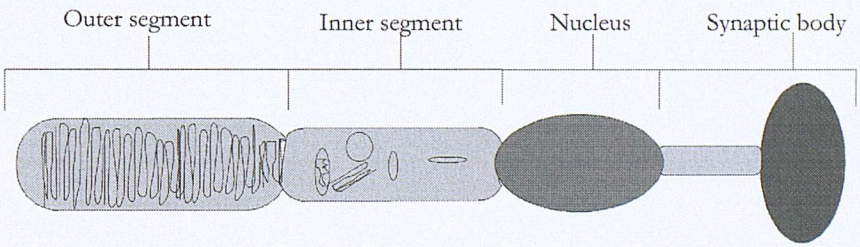

Figure 1.4 Rod photoreceptor structure. The disks of photoreactive membranes are contained in the rod outer segmenr (ROS).

Mouse embryos exposed to ET-18-CH_{3b} displayed abnormal development, such as cranofacial hypoplasia and open neural tube defects in the forebrain, midbrain, and hindbrain regions [12]. In humans, chronic Cadmium-exposure causes severe

damage in nervous, endocrine, and immune systems, and is linked to enhanced aging processes as well as cancer. Mice induced to chronic Cd-exposure show a wide range of pathologies: damage of tissues and cells caused by oxidative stress, decreasing of PtdCho and phosphatidylglycerol, increasing of phosphatidyl-ethanolamine (PtdEtn) and decreased CCT activity [13].

Studies of brain injury revealed reduced CCT activity [14, 15]. It has also been demonstrated that in cases such as Alzheimer's disease (AD), Parkinson's disease, stroke, brain injury or forebrain ischemia, the effects of the brain damage was slowed down by increasing the CCT activity [16-19]. In all these cases it was demonstrated that the administration of CDP-choline or its precursors, choline, cytidine, or uridine[c] had positive effects on the treatment of stroke and brain injury [20, 21].

1.2 Bibliography

[1] Borkenhagen, L. F., and Kennedy, E.P., "The enzymatic synthesis of cytidine diphosphate choline," in *Journal of Biological Chemistry*, vol. 227, 1957, pp. 951-962.

[2] Clement, J. M., and Kent, C., "CTP: phosphocholine cytidylyltransferase: insights into regulatory mechanisms and novel functions," in *Biochemical and Biophysical Research Communications*, vol. 257, 1999, pp. 643-650.

[3] Cornell, R., and Northwood, I. C., "Regulation of CTP: phosphocholine cytidylyltransferase by amphitropism and relocalization," in *TIBS*, vol. 25, 2000, pp. 441-447.

[4] Bishop, W. R., and Bell, R.M., "Assembly of phospholipids into cellular membranes: biosynthesis, transmenbrane movement and intracellular translocation," vol. 4, 1988, pp. 479-610.

[5] Stryer, L., *Biochimica*, Fourth Edition ed. Bologna: Zanichelli, 1996.

[6] Thain, M., and Hickman, M., *The penguin dictionary of biology*, Tenth edition ed. London: Penguin Books Ltd, 2000.

[c] Uridine, after crossing the blood barrier, is converted in uridine monophosphate (UMP), then in uridine triphosphate (UTP) and finally in CTP.

[7] Tronchere, H., Record, M., Terce, F., and Chap, H, "Phosphatidylcholine cycle and regulation of phosphatidylcholine biosynthesis by enzyme translocation," in *Biochimica et Biophysica Acta*, vol. 1212, 1994, pp. 137-151.

[8] Boggs, K. P., Rock, C.O., and Jackowski, S., "Lysophosphatidylcholine attenuates the cytotoxic effects of the antineoplastic phospholipid 1-O-octadecyl-2-O-methyl-rac-glycero-3-phosphocholine," in *Journal of Biological Chemistry*, vol. 270, 1995, pp. 11612-11618.

[9] Attard, G. S., Templer, R.H., Smith, W.S., Hunt, A.N., and Jackowski, S., "Modulation of CTP: phosphocholine cytidylyltransferase by membrane curvature elastic stress," in *Proceedings of the National Academy of Sciences of the United States of America*, vol. 97, 2000, pp. 9032-9036.

[10] Giménez, R., and Aguilar, J., "Cytidine(5')diphosphocholine-induced decrease in celebral platelet activating factor is due to inactivation of its synthesizing enzyme choline phosphotransferase in aged rats," in *Neuroscience Letters*, vol. 299, 2001, pp. 209-212.

[11] Ikemoto, A., Fukuma, A., Fujii, Y., and Okuyama, H., "Diurnal rhythms of retinal phospholipid synthetic enzymes are retained but their activities are decreased in rats under a-linolenic acid deficiency.," in *Archives of Biochemistry and Biophysics*, vol. 383, 2000, pp. 108-113.

[12] Fisher, M. C., Zeisel, S.H., Mar, M-H., and Sadler, T.W., "Inhibitors of choline uptake and metabolism cause developmental abnormalities in neurulating mouse embryos," in *Teratology*, vol. 64, 2001, pp. 114-122.

[13] Ramirez, D.C., and Gimenez, M.S., "Lipid modification in mouse peritoneal macrophages after chronic cadmium exposure," in *Toxicology*, vol. 172, 2002, pp. 1-12.

[14] Vivekananda, J., Smith, D., and King, R.J., "Sphingomyelin metabolites inhibit sphingomyelin synthase and CTP:phosphocholine cytidylyltransferase," vol. 281, 2001, pp. L98-L107.

[15] Awasthi, S., Vivekananda, J., Awasthi, V., Smith, D., and King, R.J., "CTP:phosphocholine cytidylyltransferase inhibition by ceramide via PKC-a, p38 MAPK, cPLA$_2$, and 5-lipoxygenase," vol. 281, 2001, pp. L108-L118.

[16] Xiong, Y., Liu, X.-I., Wang, Y., and Du, Y., "Cloning of cytidine triphosphate: phosphocholine cytidylyltransferase mRNA upregulated by a neuropeptide arginine-vasopressin$_{(4-8)}$ in rat hippocampus," in *Neuroscience Letters*, vol. 283, 2000, pp. 129-132.

[17] Ross, B. M., Mamalias, N., Moszczynska, A., Rajput, A.H., and Kish, S.J., "Elevated activity of phospholipid biosynthetic enzymes in substantia nigra of patients with Parkinson's disease," in *Neuroscience*, vol. 102, 2001, pp. 899-904.

[18] Wurtman, R. J., Regan, M., Ulus, I., and Yu, L., "Effect of oral CDP-choline on plasma choline and uridine levels in humans," in *Biochemical Pharmacology*, vol. 60, 2000, pp. 989-992.

[19] Rao, A. M., Hatcher, J.F., and Dempsey, R.J., "Does CDP-choline modulate phospholipase activities after transient forebrain ischemia?," in *Brain Research*, vol. 893, 2001, pp. 268-272.

[20] Friedrich, A., George, R.L., Bidges, C.C., Prasad, P.D., and Ganapathy, V., "Transport of choline and its relationship to the expression of the organic cation transporters in a rat brain microvessel endothelial cell line (RBE4)," in *Biochimica et Biophysica Acta*, vol. 1512, 2001, pp. 299-307.

[21] Plataras, C., Tsakiris, S., and Angelogianni, P., "Effect of CDP-choline on brain acetylcholinesterase and Na^+, K^+-ATPase in adult rats," in *Clinical Biochemistry*, vol. 33, 2000, pp. 351-357.

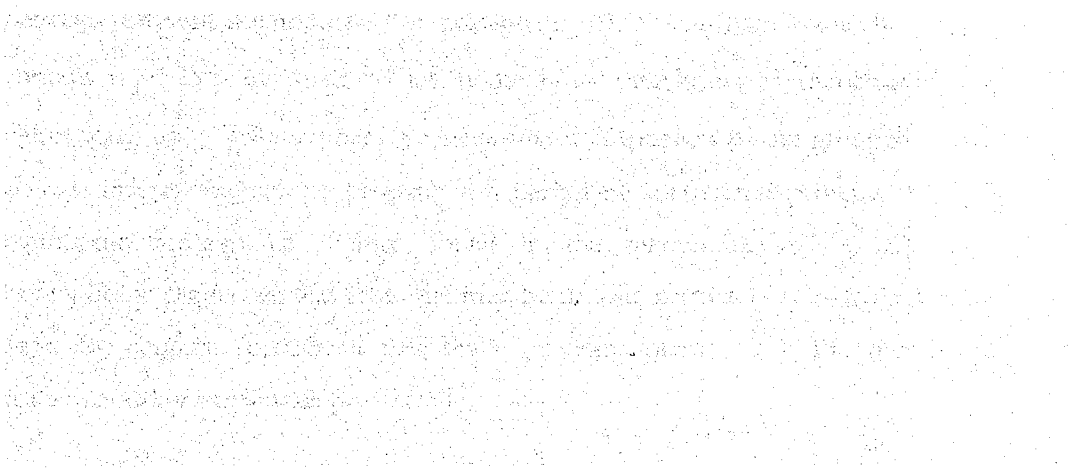

2 Cellular membranes

2.1 The structure of biological membranes

Cellular membranes are fundamental to the organisation of both prokaryotes and eukaryotes. Figure 2.1 shows the type of organization that may be found inside an eukaryotic cell. The internal compartmentalisation results in a number of organelles that usually differ in their lipid and protein composition.

Figure 2.2 shows a simple representation of a biological membrane constituted entirely by phospholipids, which are amphipathic molecules with hydrophobic and hydrophilic characters distinct within the same molecule. The amphipathic nature of the phospholipids determines the structure of the lipid bilayer in which the hydrophilic moiety remains in contact with the water while the hydrophobic chains associate creating a hydrophobic space that stands apart from the aqueous environment.

Although Figure 2.2 exemplifies the structure of biological membranes, it does not include one of its fundamental components: proteins. The average percentage of protein in membranes is ~ 50% of the lipid mass, but this percentage can change between different membranes. For example, in the myelin membrane the protein content is ~ 25% by mass, whilst in the inner membrane of mitochondria or chloroplast it is ~ 75% by mass. Proteins found in membranes are grouped in two classes: integral membrane proteins and peripheral membrane proteins. Integral membrane proteins are tightly bound to the membrane and usually have hydrophobic sequences that cross the membrane and interact with its hydrophobic core. By contrast, peripheral membrane proteins interact with the membrane surface or other membrane proteins [1].

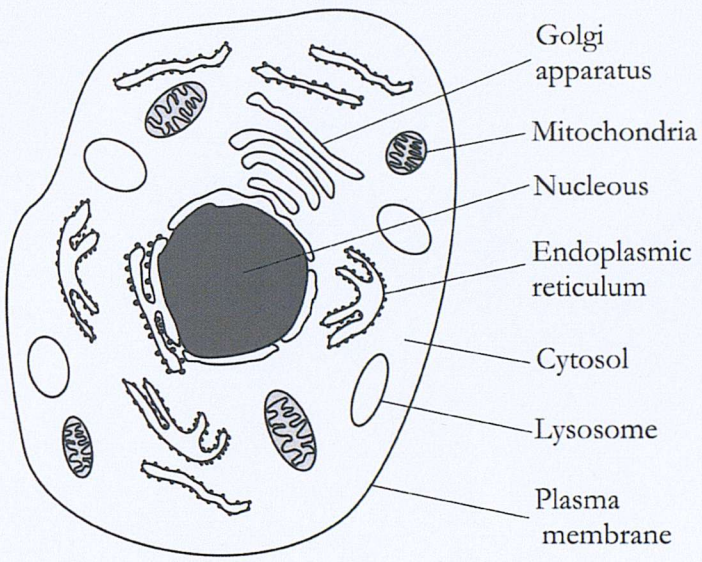

Figure 2.1 Eukaryote cells use membranes for the separation of the cellular space from the surrounding environment and for the maintenance of the internal compartmentalisation, through organelles which internal space is delimited by one or two membranes.

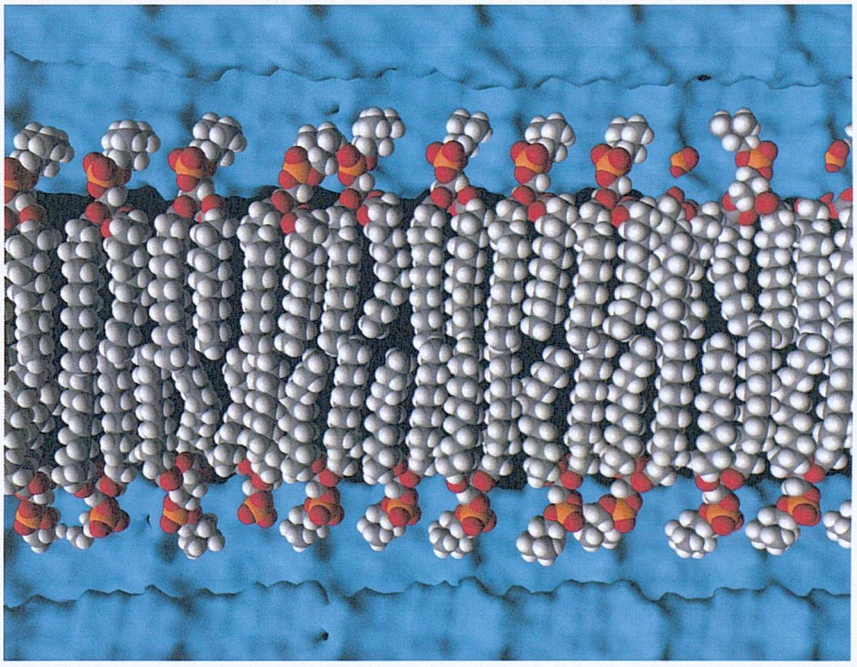

Figure 2.2 Section of a phospholipid bilayer. The hydrophobic core in the bilayer separates the two aqueous regions at the two sides of the membrane. Spheres having different color represent different atoms: carbon in gray, hydrogen in white, oxygen in red and phosphorous in orange. the molecules of water are represented in a simple way by the two blue surfaces at the top and at the bottom of the lipid bilayer.

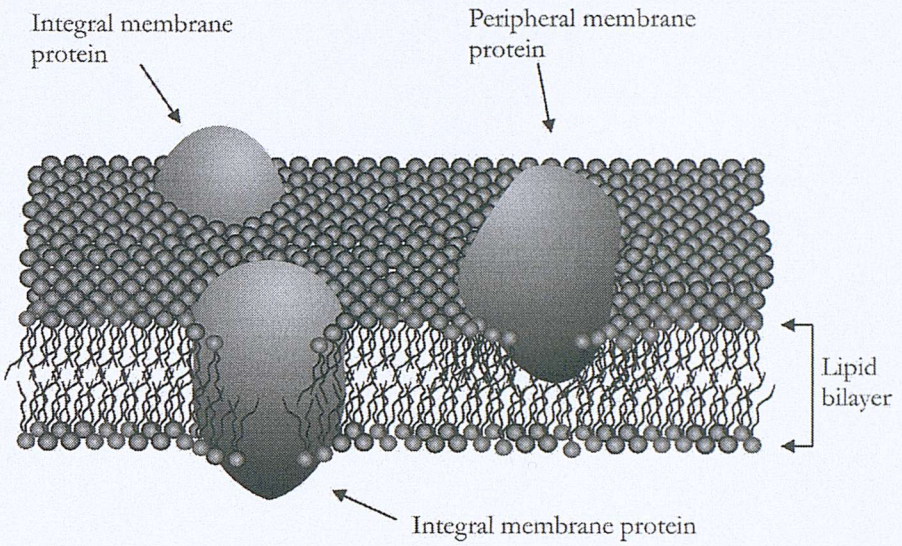

Figure 2.3 Simplified representation of the fluid mosaic model, which is currently the accepted structure that best describes most biological membranes.

By X-ray crystallography, freeze-fracture electron microscopy, radiolabelling, fluorescence, and other techniques, it was found that proteins and lipids are closely associated in the biological membrane. The fluid mosaic model, proposed by Singer and Nicholson in 1972, is currently the accepted structure that describes the tight protein/lipid association in most biological membranes, Figure 2.3 [1, 2].

2.2 Cell organelles

Different organelles inside the cell play different roles and may differ in both protein and lipid composition of their membranes. Some of the organelles and cell membranes shown in Figure 2.1 are discussed below:

- Plasma membrane (plasmalemma). This is a barrier between the inner and outer part of the cell. The closed space inside the plasma membrane, the cytoplasm, enables the cell to survive chemical and physical changes in the external environment and contains the biosynthetic apparatus necessary for the cell's survival. Because of the membrane's hydrophobic core, the spontaneous passage of charged molecules is prevented, as well as the passage of most polar molecules. Usually, the passage of polar and charged molecules

through the membrane is mediated by carrier proteins or by channel proteins. While carrier proteins specifically recognise some molecules and shuttle them through the membrane; channel proteins, intrinsic membrane proteins, create slots in the membrane and regulate the passage of charged species through it. Large molecules, which cannot cross the membrane by either channels or carrier proteins, and even solid particles can enter the cellular space by endocytosis (pinocytosis and phagocytosis) and leave the cellular space by exocytosis. Specific proteins on the membrane surface usually mediate endocytosis and exocytosis.

- Nuclear membrane. This membrane is an envelope constituted by two membranes and surrounds the nucleus in which the cell's genetic material (DNA) is stored and protected, Figure 2.4. A number of biosynthetic apparatus are present in the nucleus and the nuclear membrane is subjected to molecule trafficking mediated by carrier proteins and channels, called nuclear pores.

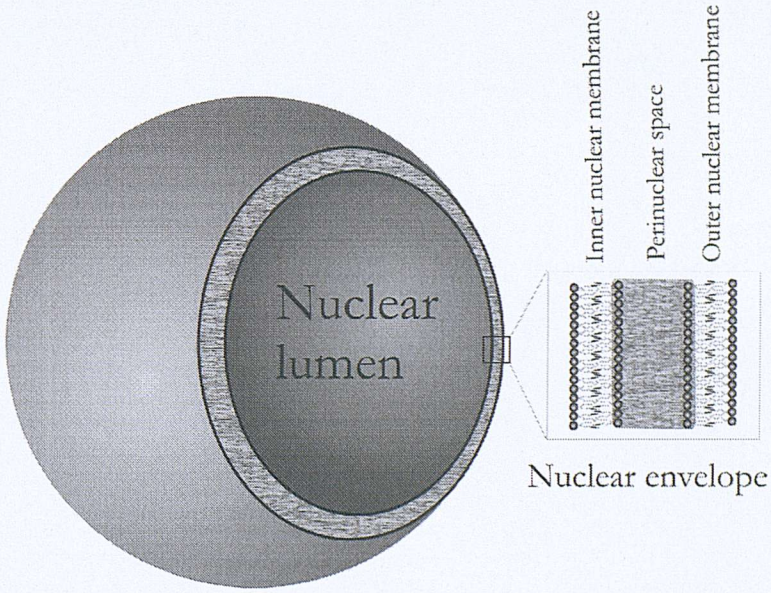

Figure 2.4 The nuclear envelope is constituted by a double membrane. The genetic material is contained in the nuclear lumen; the molecule trafficking between the nuclear lumen and the cytoplasm is mediated by carrier protein and channels.

- Lysosomes. These are closed spaces surrounded by membranes used by the cell for storing metabolites, proteins, ions, or for the removal of toxic secondary products present in the cytoplasm.

- Endoplasmic reticulum (ER) and Golgi apparatus. These are complex membrane structures that have a number of functions. Two of the functions in which the ER is involved are the synthesis of proteins and phospholipids (in eukaryote cells). Functions of the Golgi apparatus concern protein functionalisation, compartmentalisation and secretion.

- Mitochondria. These are the sites of chemical reactions for the production of energy. Mitochondria make use of membrane impermeability to charged species for the conversion of electric potential, between the two sides of the membrane, into ATP, the form in which the energy is transported all over the cell. The electrical potential between the two sides of the membrane is generated by the creation of a gradient in the ion concentration between the two sides of the membrane.

2.3 Lipids

The class of lipids is constituted by amphipatic molecules such as fatty acids, glycerides, phosphoglycerides, sphingolipids (or glycolipids) and steroids. Lipid compositions of different cell membranes are compared in Table 2.1.

Fatty acids are aliphatic carboxylic acids that often contain an even number of carbon atoms and may have one or more *cis*-double bonds, Figure 2.5. Mono-, di- and tri-glycerides are obtained from the condensation of one, two or three molecules of fatty acids with one molecule of glycerol.

Phosphoglycerides are a class of lipids that are derived from di- and monoglycerides (the latter also called lyso-phosphoglycerides), in which the hydroxyl group at the C-3 of the glycerol is linked through an ester bond to the phosphate group. Different phosphoglycerides take their name from the group that is linked through an ester

bond to the phosphatidic function, Table 2.2. Phosphoglycerides present in the cell may differ for both the head-group function and the fatty acid groups (the unsaturated fatty acid is usually esterified with the hydroxyl at the C-2 of the glycerol).

Table 2.1 Approximate lipid compositions of different cell membranes [1].

	Percentage of total lipid by weight					
Lipids	Liver plasma membrane	Erythrocithes plasma membrane	Myeline	Mitochondria (inner and outer membranes)	Endoplasmic reticulum	*E. coli*
Cholesterol	17	23	22	3	6	0
PtdSer	4	7	9	2	5	trace
PtdEtn	7	18	15	35	17	70
PtdCho	24	17	10	39	40	0
Sphingomyelin	19	18	8	0	5	0
Glycolipids	7	3	28	trace	0	0
Others	22	13	8	21	27	30

The glycerol-ether-phospholipids are similar to the phosphoglycerides but differ in the nature of the bond at the C-1 of the glycerol: an ether bond instead of ester bond, Figure 2.6. PAF, mentioned in the previous chapter, is an important member of the ether-phospholipid family and its presence is required to prevent platelet aggregation. Glycerol-ether-phospholipids are converted by a desaturase enzyme into plasmalogens, which contains an α,β-unsaturated ether at the C-1 of the glycerol.

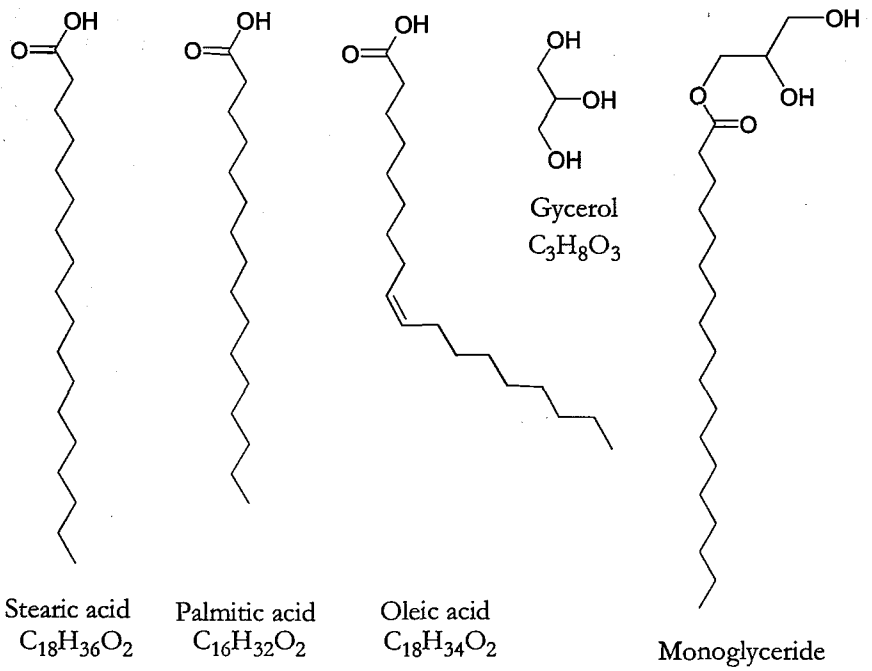

Figure 2.5 Three fatty acids that may be found in biological membranes are stearic, palmitic and oleic acid. The oleic acid is an unsaturated fatty acid with one *cis* double bond. Other fatty acids may have longer chains and more than one *cis* double bond (all double bond found in fatty acids are *cis*-double bond). Mono-, di- and tri-glycerides are obtained by linking one, two or three fatty acids to the glycerol moiety through an ester bond.

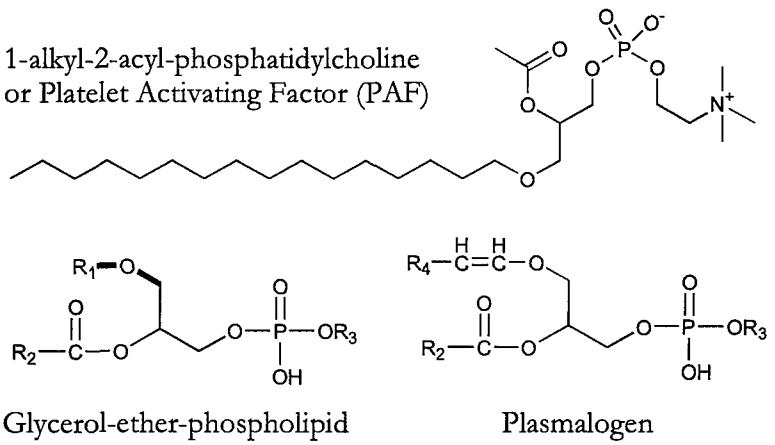

Figure 2.6 Glycerol-ether-phospholipids are very similar to phosphoglycerides, although synthesised through a different biosynthetic pathway. The platelet activating factor (1.1) plays a fundamental role in preventing the platelet aggregation. The glycerol-ether-phospholipid is converted by a desaturase in plasmalogen, a glycerol-ether-phospholipid having an α-β unsaturation at the C-1 of glycerol.

Table 2.2 Different phospholipids present in membranes. R_1 and R_2 are two acyl chains; only chain R_2 normally contains one or more double bonds.

Head group	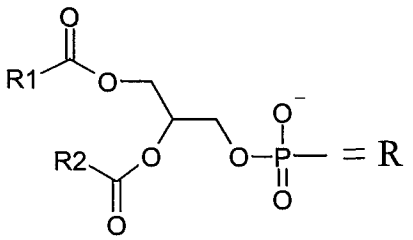
R-OH	Phosphatidic acid (PtdOH)
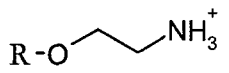	Phosphatidylethanolamine (PtdEtn)
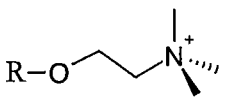	Phosphatidylcholine (PtdCho)
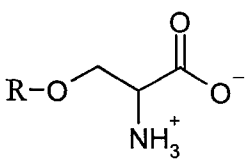	Phosphatidylserine (PtdSer)
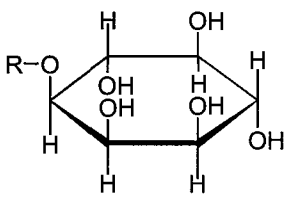	Phosphatidylinositol (PtdIns)
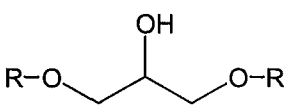	Diphosphatidylglycerol (diPtdGly)

Another class of lipids comprises molecules that derives from sphingosine: sphingomyeline and glycosphingolipids (glycolipids), Figure 2.7. These lipids are present at high percentage in the myelin sheath, a multi-layered membrane surrounding the nerve axon in a tight spiral to prevent any leakage of current across the axon membrane.

Cholesterol is an uncharged lipid that differs in the chemical structure from all the lipids listed above and is present especially in the plasma membrane of eukaryotes, Figure 2.8.

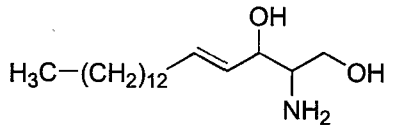

Sphingosine

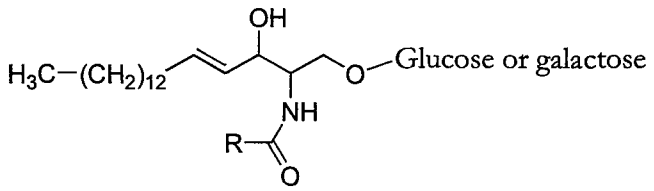

Cerebroside (Sphingolipid or glycolipid)

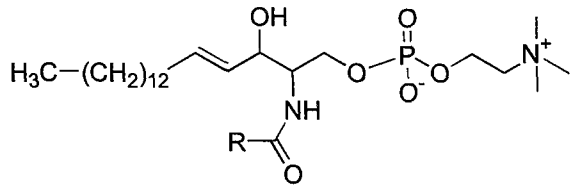

Sphingomyelin

Figure 2.7 Sphingomyelin and sphingolipids are two classes of lipids showing the sphingosine moiety. Sphingolipids, or glycolipids, are lipids in which one molecule of sugar or branched sugar is bound to the sphingosine. Galactocerebroside is largely contained in the myelin sheath.

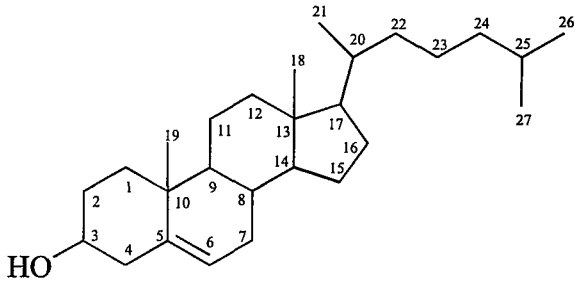

Figure 2.8 Cholesterol is present only in eukaryotes and has no charge. The only polar group in the molecule is the hydroxyl function at the C-3.

2.4 Phosphatidylcholine biosynthetic pathways

The lipid demand of a eukaryotic cell is mostly provided in the ER membrane and in particular in the cytosolic side of the ER. After the synthesis of the lipids, head-group specific enzymes (phospholipid translocators) regulate their asymmetric distribution between the two leaflets of the membrane.

As CCT is involved in the PtdCho synthesis, only the phosphatidylcholine biosynthetic pathways are shown and described in Figure 2.9 . Although more than one biosynthetic route brings to the PtdCho synthesis, those routes are not accessible to all kind of eukaryote organisms; in particular:

1. Animals and unicellular organisms can synthesise PtdCho through two pathways: the CDP-choline pathway, from choline to PtdCho (lecithin in the schemes), and through the methylation of PtdEtn, deriving either from the CDP-ethanolamine pathway or from the decarboxylation of PtdSer.
2. PtdSer is synthesised only in unicellular eukaryotic organisms (e.g. Saccharomyces cerevisiae).

2.5 Saccharomyces cerevisiae

Saccharomyces cerevisiae (yeast) can synthesise PtdCho using all three pathways shown in Figure 2.9; the availability of appropriate precursors determines the contribution of those pathways to the overall synthesis of PtdCho. Differently from mammals and in absence of exogenous choline, the preferred route for the PtdCho synthesis is via the decarboxylation of PtdSer, and the CDP-choline pathway accounts approximately for the 1% of the total synthesis of PtdCho. Because the CDP-choline pathway is not the preferential one, all the required enzymes are expressed at a lower level than the enzymes involved in the PtdSer pathway. McMaster *et al.* demonstrated that the synthesis of PtdCho is regulated at the gene level. The gene repression of some of the enzymes involved in the PtdSer synthesis was achieved

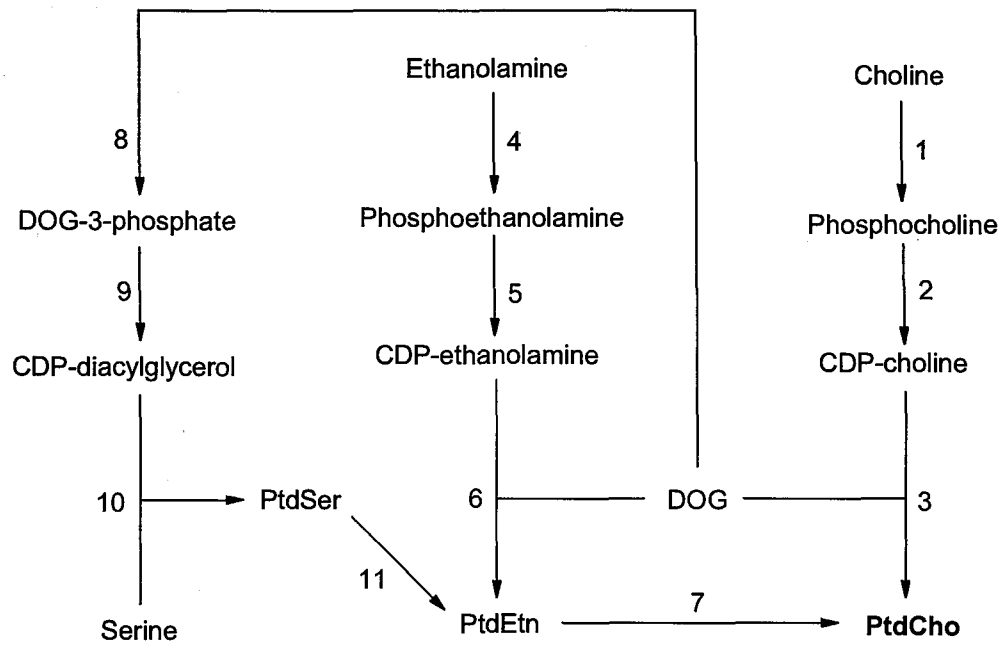

1) Choline kinase	Choline + ATP ⇄ phosphocholine + ADP
2) CTP:phosphocholine cytidylyltransferase	Phosphocholine + CTP ⇄ CDP-choline + PPi
3) Choline phosphotransferase	CDP-choline + DOG ⇄ PtdCho + CMP
4) Ethanolamine kinase	Ethanolamine + ATP ⇄ phosphoethanolamine + ADP
5) CTP: phosphoethanolamine transferase	Phosphoethanolamine + CTP ⇄ CDP-ethanolamine + Ppi
6) Ethanolamine phosphotransferase	CDP-ethanolamine + DOG ⇄ PtdEtn + CMP
7) Phosphatydylethanolamine and phosphatidyl-N-methyl-ethanolamine methyltransferase	PtdEtn +S-adenosyl methionine ⇄ N-methyl-PtdEtn + S-adenosyl homocysteine
	N-methyl-PtdEtn + S-adenosyl methionine ⇄ N,N-dimethyl-PtdEtn + S-adenosyl homocysteine
	N,N-dimethyl-PtdEtn + S-adenosy lmethionine ⇄ PtdCho + S-adenosyl homocysteine
8) Diacylglycerol kinase	DOG + ATP ⇄ DOG-3-phosphate + ADP
9) CTP: phosphatidate cytidylyltransferase	DOG-3-phosphate + CTP ⇄ CDP-diacylglycerol + PPi
10) CDP-diacylglycerol serine phosphatidyltransferase	CDP-diacylglycerol + serine ⇄ PtdSer + CMP
11) Phosphatidylserine decarboxylase	PtdSer ⇄ PtdEtn + CO_2

Figure 2.9 Eukaryote accessible routes for the synthesis of phosphatidylcholine [2, 3].

by adding inositol to the culture medium and resulted in an increased activity of both the choline transporter and choline kinase[a] [4]. Moreover, it was shown that by increasing the CTP cellular concentration 2.4 times[b] the amount of PtdCho synthesised through the CDP-choline pathway increased of a factor 1.4 [5].

2.6 CCT in mammals

Mammals are multicellular organisms that undergo cellular differentiation and specialisation during their development, from the egg phase to the maturity. The role of the PtdCho synthetic pathways in mammals will be described in more details in the next sections. However, it is important to notice that::

- Eukaryotes can synthesise choline exclusively through the hydrolysis of PtdCho, which is produced through the methylation of PtdEtn.
- The CDP-choline pathway is the preferred route in mammals.
- In mammals, the PtdCho synthesis through the ethanolamine pathway occurs exclusively in the liver.

Consequently, the liver is in mammals the only source of choline for all the other cells and tissues [6, 7].

2.6.1 CDP-choline pathway and phosphatidylethanolamine methylation pathway

Cellular differentiation and the role of the two PtdCho synthetic pathways in mammals are still a subject of study. Using male Wistar rats, early studies have shown that the CDP-choline and the ethanolamine pathways are both active in adults and that each pathway can compensate the inhibition of the other. For example, it was observed that the PtdCho synthesis via the CDP-choline pathway

[a] The choline transporter and the choline kinase increased the uptake of choline from the culture medium, making it available for the CDP-choline pathway.

[b] The increase of the CTP cellular concentration was achieved using cells over-expressing the CTP synthetase.

increased 2-3 times when the enzymes involved in the N-methylation of PtdEtn (Figure 2.9) where inhibited by 3-deazaadenosine (DZA) [8].

The study of the CDP-choline and CDP-ethanolamine pathways interconnection in embryo developmental stages has improved the knowledge of the role and the complex regulation of CCT. Studies on liver from embryos of Wistar female rats have shown that three classes of enzyme involved in the metabolism PtdCho are under regulation during the embryo developmental stages: phosphatidyl-ethanolamine methyltransferase (PEMT), CCT and protein kinase C (PKC) isozymes (α, β, δ and ζ[c]). The tests showed that:

- CCT gene expression and activity in rat liver during developmental growth (~3 days before and ~10 days after the birth) was higher than in the rat adult liver.
- PEMT gene expression and activity in rat liver during developmental growth was much lower than in adult rat liver.
- PKC α, β and ζ were approximately two-fold more active in foetal and newborn liver than in adult rat liver. On the contrary, PKC δ was less active in the foetus than in the adult rat liver, but was even higher in the newborn liver.

Hence, the CDP-choline route is preferred during cell proliferation in the embryo developmental stages, when new membrane is required, whilst the PEMT route is the preferential one during cellular differentiation in the first days after birth [9].
However, CCT regulation is not driven exclusively by the need for new membrane. Analysis of the fatty acid of the PtdCho produced through the two pathways has shown differences in composition. In particular, it was found that the ethanolamine pathway seems to be preferred for the synthesis of unsaturated PtdCho, while the choline pathway seems to be preferred for the synthesis of saturated PtdCho. Using RH7777 cells, it was found that PtdCho from the CDP-choline pathway had a fatty

[c] Even if PKC isozymes are not directly involved in the synthesis of PtdCho, they act on the homeostasis of membrane phospholipids through the regulation of the enzymes involved in phospholipids hydrolysis.

acid composition rich in saturated species: 16:0/18:1[d], 18:0/18:2 and 18:1/18:1; PtdCho from PtdEtn methylation, on the contrary, was rich in unsaturated fatty acids: 18:1/18:1, 18:0/18:2, 18:2/20:4, 18:1/20:4, 18:0/20:4, 18:0/22:6 and 18:1/22:5 [10].

2.6.2 CDP-choline pathway and the secretion of lipoproteins

Lipoproteins are micellar complexes of proteins and lipids. These protein/lipid mixtures play a fundamental role in the transport of highly insoluble lipids or molecules involved in signalling in the extracellular spaces. Lipoproteins are classified according to their size and to the lipids they transport: chylomicrons, very low-density lipoproteins (VLDL), intermediate-density lipoproteins (IDL), low-density lipoproteins (LDL), and high-density lipoproteins (HDL). Studies conducted in cultured hepatocytes from female Wistar rats revealed that the CDP-choline pathway is the preferred route for the synthesis of PtdCho used for assembling the different lipoproteins [11-14].

2.6.3 CCT localization inside the cell

CCT cellular localization was a subject of controversy, and the enzyme association with different organelles in the cell was shown to be affected by the method of purification (differential centrifugation, percoll density gradient fractionation and sucrose gradient centrifugation). While in early studies CCT was found prevalently associated with the endoplasmic reticulum [15], it was revealed later that CCT was associated with the outer membrane of the nuclear envelope [16, 17].

Further studies have revealed that all the enzymes involved in the PtdCho synthesis through the CDP-choline pathway are present inside the nucleus, in which the PtdCho metabolism plays a fundamental role [18]. Using human neuroblastoma LA-N-1 cells the effect of D609 (tricyclodecan-9-yl xanthogenate) and TPA (12-O-

[d] The two acyl chains present in the phospholipids are indicated using the format X:x/Y:y, where X and Y correspond to the chain lengths, in unit of number of carbon atoms in the main chain, and x and y indicate the number of double bonds present in the chains X and Y, respectively.

tetradecanoylphorbol-13-acetate) on both CCT activity and PtdCho synthesis was investigated. TPA is a tumour promoter that increases the nuclear production of diacylglycerol, through the activation of a PLC and/or PLD/PPH (phospholipase D/phosphatidate phosphohydrolase). On the contrary, D609 is a selective PtdCho-PLC inhibitor. TPA was shown to increase the synthesis of PtdCho in the nucleus, confirming the presence of an active PtdCho cycle. Furthermore, these results were confirmed by the inefficiency of TPA on cells pre-treated with D609, demonstrating that the PtdCho cycle can be inhibited and that TPA stimulates the synthesis of DAG, which triggers the activation of CCT and the cellular proliferation [19].

Although CCT was localised in the nucleus, extensive studies have shown the possibility of a different CCT localization in different cells[e], leaving open the possibility that the nucleus could act as reservoir of CCT.

2.7 References

[1] B. Alberts, Bray, D., Lewis, J., Raff, M., Roberts, K., and Watson, J.D., *Molecular biology of the cell*, Third ed. New York: Garland Publishing, 1994.

[2] L. Stryer, *Biochimica*, Fourth Edition ed. Bologna: Zanichelli, 1996.

[3] M. Gerhard, "Biochemical pathways, part 1," Third ed: Roche, 1992.

[4] C. R. McMaster, and Bell, R.M., "Phosphatidylcholine biosynthesis via CDP-choline pathway in *Saccharomyces cerevisiae*," in *Journal of Biological Chemistry*, vol. 269, 1994, pp. 14776-14783.

[5] V. M. McDonough, Buxeda, R.J., Bruno, M.E.C., Ozier-Kalogeropoulos, O., Adeline, M.-T., McMaster, C.R., Bell, R.M., and Carman, G.M., "Regulation

[e] Nuclear CCT localization was found in primary hepatocytes, rat hepatoma cells (RH7777), baby hamster kidney cells, human hepatoma cells (Hep G2), sheep choroids plexus, rat embryo fibroblast, human lung cells (MRC-9), and human mammary gland (MCF-10A) [20]. However, studies on human pulmonary epithelial cells (A549) and mouse lung epithelial cells (MLE-15) have revealed that CCT is prevalently localised in the cytosol. Moreover, primary fetal rat lung epithelial cells (FRLE) showed a stronger CCT cytosolic localization without any signal in the nucleus [21].

of phospholipid biosynthesis in *Saccharomices cerevisiae* by CTP," in *Journal of Biological Chemistry*, vol. 270, 1995, pp. 18774-18780.

[6] A. G. Howe, and McMaster, C.R., "Regulation of vesicle trafficking, transcription, and meiosis: lessons learned from yeast regarding the disparate biologies of phosphatidylcholine," in *Biochimica et Biophysica Acta*, vol. 1534, 2001, pp. 65-77.

[7] B. A. Bladergroen, Wensing, T., Golde, L. M. G. van, and Geelen, M. J. H., "Reversible translocation of CTO: phosphocholine cytidylyltransferase from cytosol to membranes in the adult bovine liver around parturition," in *Biochimica et Biophysica Acta*, vol. 1391, 1998, pp. 233-240.

[8] P. H. Pritchard, Chiang, P.K., Cantoni, G.L., and Vance, D.E., "Inhibition of phosphatidylethanolamine N-methylation by 3-deazaadenosine stimulates the synthesis of phosphatidylcholine via the CDP_choline pathway," in *Journal of Biological Chemistry*, vol. 257, 1982, pp. 6362-6367.

[9] E. Sesca, Perletti, G. P., Binasco, V., Chiara, M., and Tessitore, L., "Phosphatidylethanolamine N-Methyltransferase 2 and CTP-phosphocholine cytidylyltransferase expression are related with Pritein Kinase C isozymes in developmenal liver growth," in *Biochemical and Biophysical Research Communications*, vol. 229, 1996, pp. 158-162.

[10] C. J. DeLong, Shen, Y.J., Thomas, M.J., and Cui, Z., "Molecular distinction of phosphatidylcholine synthesis between the CDP-choline pathway and phosphatidylethanolamine methylation pathway," in *Journal of Biological Chemistry*, vol. 274, 1999, pp. 29683-29688.

[11] J. E. Vance, and Vance, D.E., "Specific pools of phospholipids are used for lipoprotein secretion by cultured rat hepatocytes," in *Journal of Biological Chemistry*, vol. 261, 1986, pp. 4486-4491.

[12] Z. Yao, and Vance, D.E., "The active synthesis of phosphatidylcholine is required for Very Low Density Lipoprotein secretion from rat hepatocytes," in *Journal of Biological Chemistry*, vol. 263, 1988, pp. 2998-3004.

[13] Z. Yao, and Vance, D.E., "Head-group specificity in the requirement of phosphatidylcholine biosynthesis for very low density lipoprotein secretion from cultured hepatocytes," in *Journal of Biological Chemistry*, vol. 264, 1989, pp. 11373-11380.

[14] J. E. Vance, and Vance, D.E., "Does rat liver golgi have the capacity to synthesize phospholipids for lipoprotein secretion?," in *Journal of Biological Chemistry*, vol. 263, 1988, pp. 5898-5909.

[15] F. Tercè, Record, M., Ribbes, G., Chap, H., Douste-Blazy, L., "Intracellular processing of cytidylyltransferase in Krebs II cells during stimulation of phosphatidylcholine synthesis," in *Journal of Biological Chemistry*, vol. 263, 1988, pp. 3142-3149.

[16] J. N. Morand, and Kent, C., "Localization of the membrane-associated CTP: phosphocholine cytidylyltransferase in Chinese Hamster Ovary cells with an altered membrane composition," in *Journal of Biological Chemistry*, vol. 264, 1989, pp. 13785-13792.

[17] J. D. Watkins, and Kent, C., "Immunolocalization of membrane-associated CTP:phosphocholine cytidylyltransferase in phosphatidylcholine-deficient Chinese hamster ovary cells," in *Journal of Biological Chemistry*, vol. 267, 1992, pp. 5686-5692.

[18] A. N. Hunt, Clark, G.J., Attard, G.S., and Postle, A.D., "Highly saturated endonuclear phosphatidylcholine is synthesized in situ and colocated with CDP-choline pathway enzymes," in *Journal of Biological Chemistry*, vol. 276, 2001, pp. 8492-8499.

[19] P. Antony, Farooqui, A.A., Harrocks, L.A., and Freysz, L., "Effect of D609 on phosphatidylcholine metabolism in the nuclei of LA-N-1 neuroblastoma cells: a key role for diacylglycerol," in *FEBS Letters*, vol. 509, 2001, pp. 115-118.

[20] C. J. DeLong, and Cui, Z., "Nuclear localization of enzymatically active green fluorescent protein-CTP: phosphocholine cytidylyltransferase a fusion protein is independent of cell cycle conditions and cell types," in *Journal of Biological Chemistry*, vol. 275, 2000, pp. 32325-32330.

[21] R. Ridsdale, Tseu, I., Wang, J., and Post, M., "CTP:phosphocholine cytidylyltransferase a is a cytosolic protein in pulmonary epithelial cells and tissues," in *Journal of Biological Chemistry*, vol. 276, 2001, pp. 49148-49155.

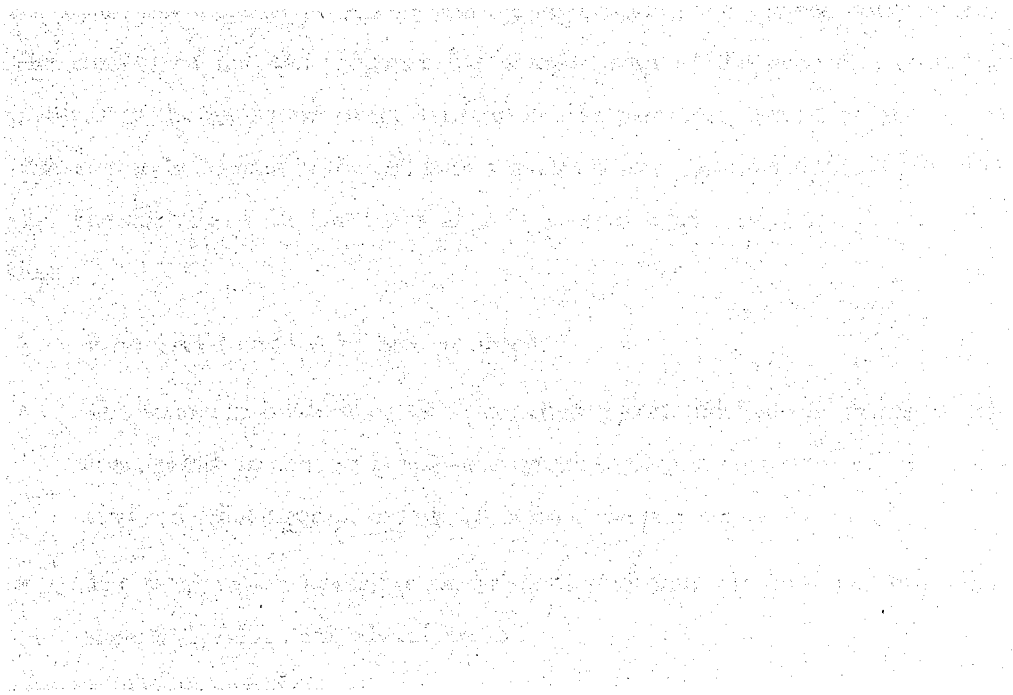

3 CCTα

3.1 CCTα: gene structure[a]

The most common and widely studied CCT isoform is CCTα; the other two known isoforms are CCTβ1 and CCTβ2, which will be described later.

CCTα cDNA was completely sequenced and characterized for its exon/intron structure. The gene structure reported here is referred to the Murine *ctpct* gene, encoding for the CCTα [1]. The gene encoding for CCTα is constituted of nine exons, which encodes for the different domains of the protein (Table 3.1 and Figure 3.1).

The CDP-choline pathway, which is the major route for the synthesis of PtdCho in extrahepatic tissues, has shown a complex regulation exerted through both the modulation of the enzyme activity and the regulation of the enzyme transcription. The analysis of the *ctpct* sequence has revealed sites of the gene that could be involved in the regulation of its transcription. In particular, regulatory features of *ctpct* seem to be located in the 600 base segment before the transcriptional initiation site. The analysis of the 600 bases of the upstream regulatory region has revealed that:

- Both TATA and CAAT box are absent.
- The sequence possesses a G+C enriched region and five GC boxes, which corresponds to consensus Sp1-binding site present in promoters of numerous viral and cellular genes, and typical of housekeeping genes.
- The same region possesses several consensus transcriptional factor-binding sites: AP1, AP2, AP3, TFIIIA and Y1.

---

[a] In accordance with the Biochemistry format, genes are named in italics with no capitalisation of the first letter, whilst gene product are named in normal character with the first letter capitalised.

Table 3.1 Gene/domain structure of CCT obtained from the comparing of the Murine *ctpct* sequence with the protein amino acid sequence [1].

Murine Ctptc gene structure	
Exon 1	This exon is untraslated, like in other genes involved in lipid biosynthesis and metabolism, such as PEMT2, apolipoproteins A-I, A-II, C-II, C-III, E, and phospholipid transfer protein
Exon 2	This exon encodes the first 39 amino acids of CCTα, which include the nuclear signal sequence composed by the amino acids from residue 8 to 28.
Exon 3	This exon encodes for residues 40 to 72. Even if this amino acid sequence is encoded by a proper exon, no specific functional role has been reported.
Exon 4, 5, 6 and 7	These exons encode for the catalytic domain, from residue 73 to residue 236; in particular, exon 4 contains the codons for HSGH motif, residues 89 to 92.
Exon 8	This exon encodes for the amino acid sequence from residue 237 to residue 299. In particular, this exon encodes for the 58 residues constituting the hydrophobic α-helix (256-288), the membrane binding domain of CCTα. The binding domain was extensively studied because of its role in the enzyme activation. Besides the binding domain, exon 8 encodes for a highly positively charged sequence from residue 248 to residue 254. This seven residue sequence contains 5 lysines whose role is still not well understood.
Exon 9	This exon encodes for the C-terminal domain of CCTα from residue 300 to residue 367. This sequence contains two main domains: a second α-helix having high hydrophobic character and a domain rich in serine and threonine, residues often involved in enzyme activity modulation mediated by phosphorylation and dephosphorylation. If the role of the second α-helix is not still well understood, the phosphorylation/ dephosphorylation domain was object of several studies, as well as the binding domain.

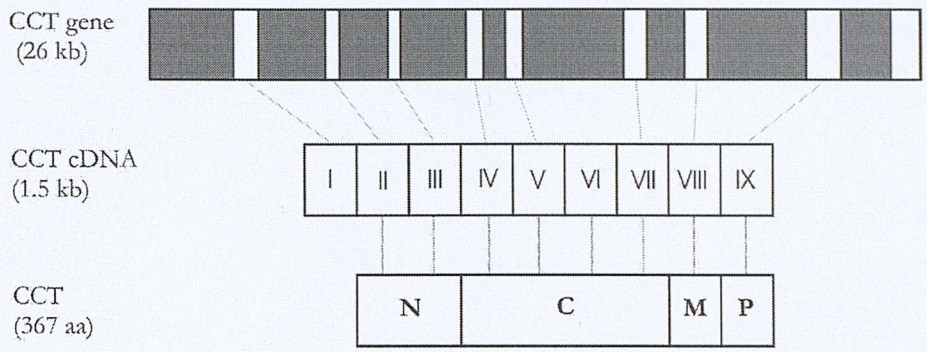

Figure 3.1 Structure of the Murine *ctpct* encoding for CCT. The entire CCT gene is ~ 26 kb long, while the CT cDNA is only ~ 1.5 kb [1]. Exons from II to IX (the first exon is not translated) are translated into the 367 amino acid sequence long CCTα. Domain N (residues 1-72) contains the nuclear localisation sequence; domain C (residues 73-236) contains the residues involved in the catalysis; domain M (residues 237-299) contains the lipid-binding domain; domain P (residues 300-367) contains the residues involved in phosphorylation/dephosphorylation.

It has been hypothesised that these transcriptional factor-binding sites could be involved in the basal transcription of the gene or in its transcriptional regulation [1, 2]. Further investigations of promoters in *ctpct* were focused on the upstream regulatory region, and four motifs were found for the binding of SP1- and/or Ap1-related nuclear factors. The most important part of this regulatory region is the similarity between the *ctpct* promoter and the regulatory regions of several other genes involved in the lipid metabolism (e.g. in Acetyl-CoA carboxylase, in fatty acid synthase and in low density lipoprotein receptor) [3].

3.2 CCTα: protein structure

The characterization of CCTα started with the advent of molecular biology. The over-expression of CCTα allowed the isolation of large amount of reasonably pure protein. CCTα was found to be not easy to handle, as reported by a number of papers that appeared in the 1980s. For example, the purification of this enzyme from not over-expressing cells often yielded impure CCT, contaminated with other proteins found to be responsible for the observed heterodimeric and multimeric structure of CCT in solution. Further experiments demonstrated that CCT is

normally present as a homodimer and that the co-purified proteins were the cause of the observed etherodimeric and multimeric structures. It was also reported that oxidising conditions could induce the formation of covalently bound CCT monomers originating homodimeric and multimeric structures [4].

The first experiments of CCTα cDNA expression were attempted using *E. coli.*, but failed because the bacterium proved to be an unsuitable organism. Successful expression was instead achieved in eukaryote cells, whose DNA normally encodes for CCT [5].

The availability of CCTα cDNA made possible the determination of its amino acid sequence, which is shown in Table 3.2. The entire sequence is divided in four big domains: N, C, M and P. Domain N is constituted by the first 72 residues and contains the nuclear localization sequence. Domain C is constituted by the residues from 73 to 236 and corresponds to the catalytic sequence. Domain M, corresponding to the sequence from residue 237 to residue 299 and contains the lipid-binding region. Domain P, constituted by the residues from 300 to 376, contains the phosphorylation domain, Figure 3.1.

Different approaches were attempted to identify the four CCTα domains and to determine their role in the enzyme's regulation [6-9]. One of the most widely applied methods involves the use of truncated mutants (enzymes lacking one or more amino acid sequences) to investigate the role of a particular sequence on the enzymatic activity. Investigating CCTα truncated mutants it was found that:

- The N domain is involved in the nuclear localization of the enzyme. In the previous chapter CCTα localization was described in a number of different organisms and it was shown that the nucleus is the place for PtdCho synthesis. CCTα mutants lacking the nuclear localization sequence were found in the cytosol and not in the nucleus [6].
- The M domain is fundamental for enzyme translocation from the cytosol to the membrane surface. CCTα is an amphitropic enzyme that becomes active when it translocates from the soluble inactive form to the surface-bound

active form. Using different mutants it was demonstrated that this sequence is fundamental for the binding and that the mutants could be partially active or completely inactive depending on the extent of truncation [10].

- The P domain is involved in enzyme regulation. Mutants lacking this sequence are more active than the wild type. However, further studies on those mutants revealed the possibility that some proteins inside the nucleus might interact with this domain [11].

Table 3.2 CCTα amino acid sequence obtained from CCTα cDNA.

10	20	30	40
MDAQSSAKVN	SRKRRKEVPG	PNGATEEDGI	PSKVQRCAVG
50	60	70	80
LRQPAPFSDE	IEVDFSKPYV	RVTMEEACRG	TPCERPVRVY
90	100	110	120
ADGIFDLFHS	GHARALMQAK	NLFPNTYLIV	GVCSDELTHN
130	140	150	160
FKGFTVMNEN	ERYDAVQHCR	YVDEVVRNAP	WTLTPEFLAE
170	180	190	200
HRIDFVAHDD	IPYSSAGSDD	VYKHIKEAGM	FAPTQRTEGI
210	220	230	240
STSDIITRIV	RDYDVYARRN	LQRGYTAKEL	NVSFINEKKY
250	260	270	280
HLQERVDKVK	KKVKDVEEKS	KEFVQKVEEK	SIDLIQKWEE
290	300	310	320
KSREFIGSFL	EMFGPEGALK	HMLKEGKGRM	LQAISPKQSP
330	340	350	360
SSSPTHERSP	SPSFRWPFSG	KTSPSSSPAS	LSRCKAVTCD
367			
ISEDEED			

The amino acid sequence HSGH, contained in the catalytic domain, is essential for the catalytic activity of CCTα. Studies on this four amino acid-long sequence revealed that to remain functional that sequence requires the conservation of H and GH. Therefore a general sequence HXGH, were X is an undefined amino acid, is still active but even the exchange of one amino acid, especially glycine, would result in a decrease/loss of activity [12].

The importance and the role of the M domain were demonstrated using [^{125}I]TID (3-(trifluoromethyl)-3-(m[^{125}I]iodophenyl)diazirine). [^{125}I]TID is a radioactive and photoreactive hydrophobic molecule that partitions into the hydrophobic core of lipid membranes. When present in a membrane, [^{125}I]TID can be phoactivated producing a highly reactive carbene species able to react non-selectively with any molecules in the vicinity in the hydrophobic core of the membrane. Experiments made in presence of CCTα, vesicles and [^{125}I]TID have shown the α-helix in the M domain was the only sequence involved in the photoreaction [13]. Further experiments involved synthetic peptides whose sequence derived from the M domain of CCTα. These peptides showed a random coil conformation in solution and a α-helical structure in presence of SDS micelles. The two different conformations were determined by NMR and proved that CCTα M domain is in a α-helical conformation when the enzyme translocates on the membrane surface [14]. In other similar experiments four different peptides, whose sequences were deduced from the α-helical domain of CCTα, were used to investigate their partitioning between aqueous buffer and vesicles. The four peptides showed high partition coefficients in favour of the vesicles, confirming that the M domain is involved in the binding to the membrane [15].

3.3 CCT isoforms: α, β1 and β2

Molecular biology and the increasing amount of data on gene sequencing have made possible to discover that CCT is present in more than one isoform. Human

CCTβ was the second CCT isoform found and its amino acid sequence is very similar to the CCTα one. Differently from CCTα, CCTβ lacks the nuclear localization sequence and is expressed at lower level. Hypothesises advanced for the CCTβ role suggest that the expression of CCTβ could be related to specific tissues and/or to specific developmental stages [16].

After one year from the discovery of CCTβ, it was found that the human DNA encodes more than two isoforms of CCT: α, β1 and β2. CCTα was found to be localized in the nucleus while CCTβ1 and CCTβ2 were found to be localized in the ER. CCTβ1 and CCTβ2 differ essentially for the total length of the amino acid sequence, being both the product of different splicing of the same gene. The different isoforms were localized in different human tissues and it was found that CCTα and CCTβ1 were ubiquitous, CCTβ2 was mainly present in brain and in HeLa cells, poorly present in liver and foetal lung, and almost absent in placenta and adult lung. Unfortunately, even if the CCT isoform distribution is known, the exact role of the CCTβ isoforms has not been elucidated yet [17].

3.4 CCTα: activity modulation

Modulation of CCTα activity was demonstrated to occur at different levels:

- Phosphorylation/dephosphorylation of the P domain.
- Membrane lipid composition effect of on the translocation from the soluble to the membrane bound form.
- CTP and phosphocholine concentration.
- Enzyme expression and digestion.

As CTP and phosphocholine are CCTα substrates, studies were carried out to determine the effect of their concentration on CCTα activity. The effect of CTP

was tested using HeLA cells infected with poliovirus, which increased the cellular synthesis of CTP. The experiments showed a positive effect of CTP on CCTα activity [18, 19]. Unfortunately, experiments of phosphocholine over-expression are not reported, probably because PtdCho is the only source available inside the cell.

The analysis of the gene structure of CCTα has revealed several transcriptional factor-binding sites present in the upstream region of the gene, suggesting the possibility that the regulation of CCTα expression is similar to that of other proteins involved in lipid metabolism. Investigating the CCTα turnover, it was demonstrated that CCTα is digested inside the cell by the cytosolic calcium-activated proteases (calpains) and through the ubiquitin-proteasome pathway [20], suggesting a possible way to control the concentration of CCTα inside the cell.

3.4.1 Phosphorylation/dephosphorylation

The phosphorylation/dephosphorylation of the P domain has been discussed in a number of papers [21-28]. The P domain is rich in serine and threonine and is often subjected to phosphorylation or dephosphorylation as a regulatory mechanism. This kind of regulation appears to be linked to the availability of energetic resources, e.g. glucose, and it is a regulatory mechanism shared by other different enzymes and related to low energy level inside the cell [21]. cAMP is a second messenger synthesised by adenylyl cyclase when the energetic resources are low. This molecule activates protein kinase A (PKA) that phosphorylates residues of serine and threonine of different proteins sensitive to this mechanism of regulation. cAMP effects on CCT were studied and it was shown that high levels of cAMP were correlated to high levels of phosphorylated CCT and to a subsequent decrease in activity [22-24, 28, 29].

Even if it was demonstrated that phosphorylation/dephosphorylation of the P domain can be used by the cell for modulating CCT activity, the role of the P domain, the effect of different levels of phosphorylation, and the mechanism of inhibition remain unclear [25-27].

3.4.2 *Lipid modulation of CCTα activity*

Studies on CCTα have shown that the presence of lipid membranes is essential for the enzyme activation and that the membrane lipid composition can modulate the enzyme activity. Figure 3.2 shows that CCTα is essentially inactive in solution and active when bound to the membrane. However, although it has been demonstrated that the enzyme's activation is mediated by its translocation from the cytosol to the surface of the membrane, it was hypothesised that both inactive and active forms could be bound to the membrane and that some other parallel mechanism could modulate the enzyme activity [30].

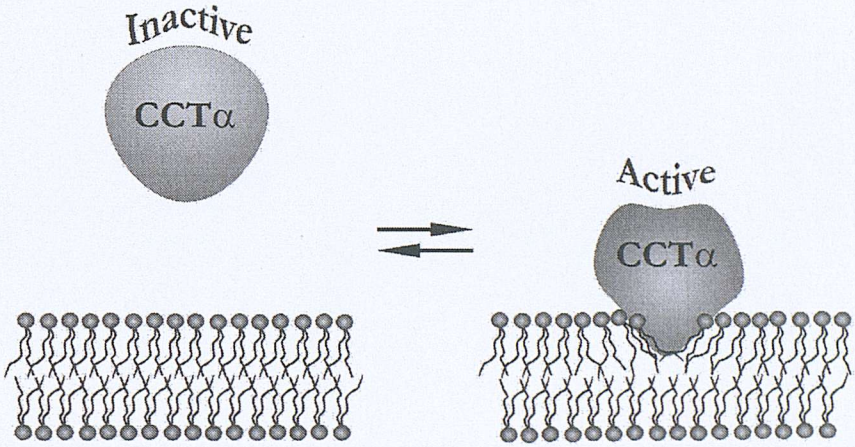

Figure 3.2 CCTα is essentially inactive when in solution and becomes active when bound to the membrane. The membrane-binding domain M seems to be involved in the interaction with the lipid membrane.

Fatty acids or lipid were added to the culture medium in *in vivo* studies, or to purified CCTα in *in vitro* studies, to investigate the effect on the enzymatic activity [31-33]. Other studies, instead, tested the effect of a de-lipidated culture medium on CCTα activity [34]. All those experiments showed that lipid membrane properties, e.g. surface density charge or torque tension, were able to activate the enzyme. Subsequent work was directed to investigate how the degree of lipid oxidation [35,

36], surface density charge [37, 38], and other surface and bulk properties [39-45] affected the enzyme activity. It was finally found that the torque tension and the surface charge of the membrane were the only properties affecting CCTα activity. Other studies focused on the effect that some lipids have on the transcription of *cctα*. In particular, it was demonstrated that the gene transcription of CCTα was sensitive to the sterol concentration in the culture medium. Experiments on macrophages showed that they are susceptible to the free-cholesterol (FC) in the medium. In particular, macrophages lacking *cctα* were easily subjected to free cholesterol-induced death while wild type macrophages increased the post-translational activation of CCTα as response to the presence of FC, probably to minimise the cytotoxic effect of this substance on the membrane and on the integral membrane-proteins [46]. Moreover, other studies showed that SREBP (Sterol Regulatory Element-Biding Protein) trans-activates the CCTα gene, in a way similar to other related lipogenic genes involved in the fatty acids, triacylglycerol and cholesterol biosynthesis [47-49].

3.5 CCTα and cell signalling

CCTα plays a fundamental role not only in the synthesis of PtdCho, but also in the cell cycle, in cell signalling and in cell survival: "Phosphatidylcholine seems to be essential to mammalian life, since no hereditary disease in the biosynthesis of this lipid is known" [50]. Phosphatidylinositol (PtdIns), 4-phosphate-phosphatidyl-inositol, PtdIns(4)P, and 4,5-diphosphate-phosphatidylinositol, PtdIns(4,5)P_2, are intermediates involved in cell signalling and are converted one into the other in the phosphatidylinositol cycles (Figure 3.3).

PtdCho cycle (Figure 3.4) and the phosphatidylinositol cycle have DAG as common intermediate and it has been hypothesised that the PtdCho cycle is important for the cell signalling [50]. Two observations can give credit to the above hypothesis:

- The PtdCho pool is greater than the PtdIns one.

- DAG can be reconverted in PtdCho through one step only, instead of the five required for the reconversion into PtdIns(4,5)P_2.

As CCTα controls the rate at which PtdCho is synthesised, the concentration of DAG in the membranes can be regulated by the modulation of CCTα activity. Several studies have investigated the effect of CCTα inhibition on the cellular signalling and have shown that CCTα inhibition triggered cell apoptosis, the specific pathway of programmed cell death [52-54].

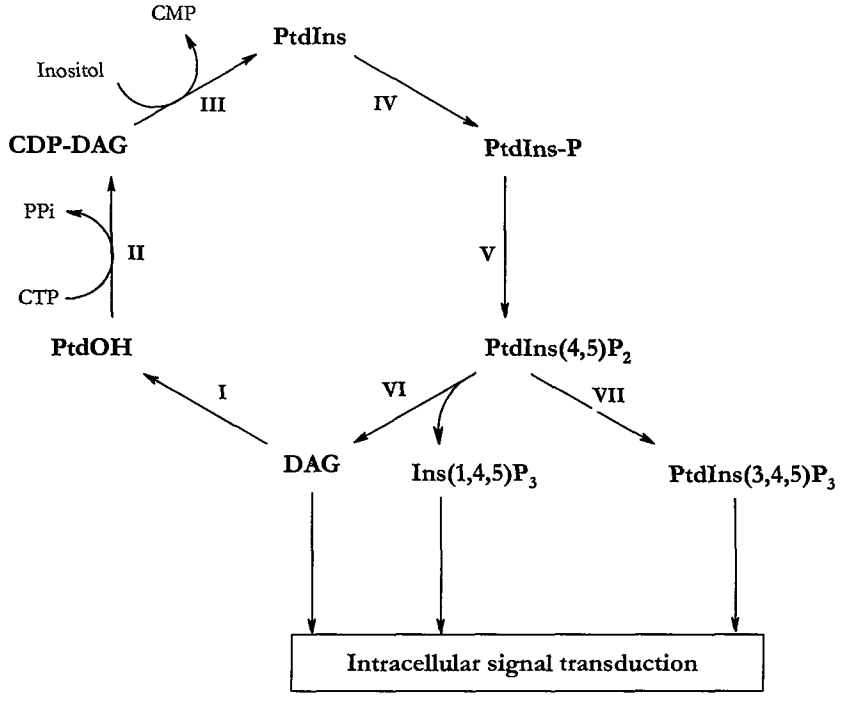

Figure 3.3 Metabolic cycle of regeneration of PtdIns(4,5)P_2. I) DAG kinase; II) CDP-DAG synthase; III) PtdIns synthase; IV) PtdIns kinase; V) PtdInsP kinase; VI) PLC; VII) PtdInsP_2 kinase [51].

3.6 CCTα and cell cycle

The different phases of the cell cycle are shown in Figure 3.5. Studies on phospholipidic mass accumulation during the cell cycle have been reported in the literature [55, 56] and have shown that CCTα was maximally active during the G_1

phase and essentially inactive during the mitosis[b]. However, due to the rapid PtdCho turnover during the G_1 phase, the net phospholipid mass accumulation occurred during the S phase, when the rate of PtdCho synthesis was higher than the rate of its degradation.

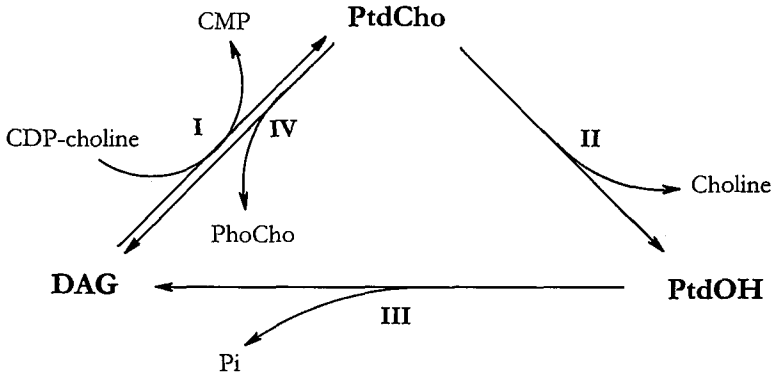

Figure 3.4 PtdCho cycle. I) choline phosphotransferase; II) PLD; III) phosphatidate sphosphohydrolase; IV) PLC.

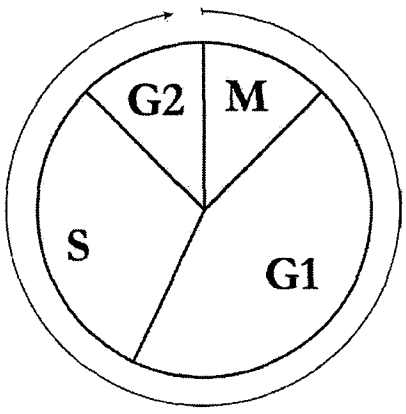

Figure 3.5 The four phases of a typical eukaryotic cell. G_1, S and G_2 phases form the interphase, during which the cell continues to grow. New DNA is synthesised during S phase and cell division occurs in M phase [51].

[b] mRNA quantification demonstrated that CCTα gene is highly expressed during the mid-G_1 phase and poorly expressed in the S and G_2/M phases [55, 56]. Further experiments of immunofluorescence localisation have shown that CCTα is located in the nucleus when the cell requires low level of activity. CCTα was translocated to the cytosol during the high rate PtdCho turnover in the G_1 phase [57], strengthening the possibility that the nucleus acts as reservoir of CCTα.

3.7 References

[1] W. Tang, Keesler, G.A., and Tabas, I., "The structure of the gene for murine CTP: phosphocholine cytidylyltransferase, Ctpct," in *Journal of Biological Chemistry*, vol. 272, 1997, pp. 13146-13151.

[2] H. Sugimoto, Bakovic, M., Yamashita, S., and Vance, D.E., "Identification of transcriptional enhancer factor-4 as a transcriptional modulator of CTP: phosphocholine cytidylyltransferase," in *Journal of Biological Chemistry*, vol. 276, 2001, pp. 12338-12344.

[3] M. Bakovic, Waite, K., Tang, W., Tabas, I., and Vance, D.E., "Transcriptional activation of the murine CTP: phosphocholine Cytidylyltransferase gene (Ctpct): combined action of upstream stimulatory and inhibitory cis-acting elements," in *Biochimica et Biophysica Acta*, vol. 1438, 1999, pp. 147-165.

[4] R. Cornell, "Chemical cross-linking reveals a dimeric structure for CTP: phosphocholine cytidylyltransferase," in *Journal of Biological Chemistry*, vol. 264, 1989, pp. 9077-9082.

[5] J. I. S. MacDonald, Kent, C, "Baculovirus-mediated expression of rat liver CTP: phosphocholine cytidylyltransferase," in *Protein Expression and Purification*, vol. 4, 1993, pp. 1-7.

[6] C. J. DeLong, and Cui, Z., "Nuclear localization of enzymatically active green fluorescent protein-CTP: phosphocholine cytidylyltransferase α fusion protein is independent of cell cycle conditions and cell types," in *Journal of Biological Chemistry*, vol. 275, 2000, pp. 32325-32330.

[7] J. A. Friesen, Campbell, H. A., and Kent, C., "Enzymatic and cellular characterization of a catalytic fragment of CTP: phosphocholine cytidylyltransferase α," in *Journal of Biological Chemistry*, vol. 274, 1999, pp. 13384-13389.

[8] A. Lykidis, Jackson, P., and Jackowski, S., "Lipid activation of CTP: phosphocholine cytidylyltransferase α: characterization and identification of a second activation domain," in *Biochemistry*, vol. 40, 2001, pp. 494-503.

[9] W. Yang, Boggs, K.P., and Jackowski, S., "The association of lipid activators with the amphipathic helical domain of CTP: phosphocholine cytidylyltransferase accelerates catalysis by increasing the affinity of the enzyme for CTP," in *Journal of Biological Chemistry*, vol. 270, 1995, pp. 23951-23957.

[10] J. Yang, Wang, J., Tsen, I., Kuliszewski, M., Lee, W., and Port, M., "Identification of an 11-residue portion of CTP: phosphocholine cytidylyltransferase that is required for enzyme-membrane interaction," in *Biochemical Journal*, vol. 325, 1997, pp. 29-38.

[11] W. Tang, Walsh, A., and Tabas, I., "Macrophages-targeted CTP: phosphocholine cytidylyltransferase (1-314) transgenic mice," in *Biochimica et Biophysica Acta*, vol. 1437, 1999, pp. 301-316.

[12] D. P. Veitch, and Cornell, R.B., "Substitution of Ser for Glycine-91 in the HXGH motif of CTP: phosphocholine cytidylyltransferase implicayes this motif in CTP binding," in *Biochemistry*, vol. 35, 1996, pp. 10743-10750.

[13] J. E. Johnson, Aebersold, R., and Cornell, R.B., "An amphiphatic α-helix is the principle membrane-embedde region of CTP: phosphocholine cytidylyltransferase. Identification of the 3-(trifluoromethyl)-3-(m-[^{125}I]iodophenyl)diaziridine photolabeled domain," in *Biochimica et Biophysica Acta*, vol. 1324, 1997, pp. 273-284.

[14] S. J. Dunne, Cornell, R.B., Johnson, J.E., Glover, N.R., and Tracey, A.S., "Structure of the membrane binding domain of CTP: phosphocholine cytidylyltransferase," in *Biochemistry*, vol. 35, 1996, pp. 11975-11984.

[15] J. E. Johnson, Rao, N.M., Hui, S.W., and Cornell, R.C, "Conformation and lipid binding properties of four peptides derived from the membrane-binding domain of CTP: phosphocholine cytidylyltransferase," in *Biochemistry*, vol. 37, 1998, pp. 9509-9519.

[16] A. Lykidis, Murti, K.G., and Jackowski, S., "Cloning and characterization of a second human CTP:phosphocholine cytidylyltransferase," in *Journal of Biological Chemistry*, vol. 273, 1998, pp. 14022-14029.

[17] A. Lykidis, Barburina, I., and Jackowski, S., "Distribution of CTP: phosphocholine cytidylyltransferase (CCT) isoforms," in *Journal of Biological Chemistry*, vol. 274, 1999, pp. 26992-27001.

[18] D. E. Vance, Trip, E.M., and Paddon, H.B., "Poliovirus increases phosphatidylcholine biosynthesis in HeLa cells by stimulation of the rate-limiting reaction catalyzed by CTP: phosphocholine cytidylyltransferase," in *Journal of Biological Chemistry*, vol. 255, 1980, pp. 1064-1069.

[19] P. C. Choy, Paddon, H.B., and Vance, D.E., "An increase in cytoplasmic CTP accelerates the reaction catalyzed by CTP: phosphocholine cytidylyltransferase in poliovirus-infected HeLa cells," in *Journal of Biological Chemistry*, vol. 255, 1980, pp. 1070-1073.

[20] R. K. Mallampalli, Ryan, A.J., Solome, R.G., and Jackowski, S., "Tumor necrosis factor-α inhibits expression of CTP: phosphocholine cytidylyltransferase," in *Journal of Biological Chemistry*, vol. 275, 2000, pp. 9699-9708.

[21] Z. H. Beg, Stonik, J.A., and Brewer, H.B. jr, "In vitro and in vivo phosphorylation of rat liver 3-hydroxy-3-methylglutaryl coenzyme A reductase and its modulation by glucagon," in *Journal of Biological Chemistry*, vol. 255, 1980, pp. 8541-8545.

[22] S. L. Pelech, Pritchard, P.H., and Vance, D.E., "cAMP analogues inhibit phosphatidylcholine biosynthesis in cultured rat hepatocytes," in *Journal of Biological Chemistry*, vol. 256, 1981, pp. 8283-8286.

[23] S. L. Pelech, and Vance, D.E., "Regulation of Rat liver cytosolic CTP: phosphocholine cytidylyltransferase by phosphorylation and dephosphorylation," in *Journal of Biological Chemistry*, vol. 257, 1982, pp. 14198-14202.

[24] J. S. Sanghera, and Vance, D.E., "CTP: phosphocholine cytidylyltransferase is a substrate for cAMP-dependent protein kinase in vitro," in *Journal of Biological Chemistry*, vol. 264, 1989, pp. 1215-1223.

[25] J. D. Watkins, and Kent, C., "Phosphorylation of CTP:phosphocholine cytidylyltransferase *in Vivo*," in *Journal of Biological Chemistry*, vol. 265, 1990, pp. 2190-2197.

[26] H. Jamil, Utal, A.K., and Vance, D.E., "Evidence that cyclic AMP-induced inhibition of phosphatidylcholine biosynthesis is caused by a decrease in cellular diacylglycerol levels in cultured rat hepatocytes," in *Journal of Biological Chemistry*, vol. 267, 1992, pp. 1752-1760.

[27] M. Houweling, Jamil, H., Hatch, G.M., and Vance, D.E., "Dephosphorylation of CTP-phosphocholine cytidylyltransferase is not required for binding to membrane," in *Journal of Biological Chemistry*, vol. 269, 1994, pp. 7544-7551.

[28] M. Wieprecht, Wieder, T., Paul, C., Geilen, C.C., and Orfanos, C.E., "Evidence for phosphorylation of CTP: phosphocholine cytidylyltransferase by multiple proline-directed protein kinases," in *Journal of Biological Chemistry*, vol. 271, 1996, pp. 9955-9961.

[29] M. Houweling, Klein, W., and Geelen, M.J.H., "Regulation of phosphatidylcholine and phosphatidylethanolamine synthesis in rat

hepatocytes by 5-aminoimidazole-4-carboxamide ribonucleoside (AICAR)," in *Biochemical Journal*, vol. 362, 2002, pp. 97-104.

[30] P. A. Weinhold, and Barrett, D., "Studies on the regulation of CTP: phosphocholine cytidylyltransferase using permeabilized HEP G2 cells: evidence that both active and inactive enzyme are membrane-bound," in *Biochimica et Biophysica Acta*, vol. 1391, 1998, pp. 307-319.

[31] S. L. Pelech, Pritchard, P.H., Brindley, D.N., and Vance, D.E., "Fatty acids promote translocation of CTP: phosphocholine cytidylyltransferase to the endoplasmic reticulum and stimulate rat hepatic phosphatidylcholine synthesis," in *Journal of Biological Chemistry*, vol. 258, 1983, pp. 6782-6788.

[32] P. A. Weinhold, Rounsifer, M.E., and Feldman, D.A., "The purification and characterization of CTP: phosphocholine cytidylyltransferase from rat liver," in *Journal of Biological Chemistry*, vol. 261, 1986, pp. 5104-5110.

[33] D. A. Feldman, and Weinhold, P.A., "CTP: phosphocholine cytidylyltransferase from rat liver," in *Journal of Biological Chemistry*, vol. 262, 1987, pp. 9075-9081.

[34] A. J. Ryan, McCoy, D. M., Mathur, S. N., Field, F. J., and Mallampalli, R. K., "Lipoprotein deprivation stimulates transcription of the CTP: phosphocholine cytidylyltransferase gene," in *Journal of Lipid Research*, vol. 41, 2000, pp. 1268-1277.

[35] A. E. Drobnies, Ende, B. van der, Thewalt, J.L., and Cornell, R.B., "CTP: phosphocholine cytidylyltransferase activation by oxidized phosphatidylcholines correlates with a decrease in lipid order: a ^{2}H-NMR analysis," in *Biochemistry*, vol. 38, 1999, pp. 15606-15614.

[36] A. E. Drobnies, Davies, S.M.A., Kraayenhof, R., Epand, R.F., Epand, R.M, and Cornell, R.B., "CTP:phosphocholine cytidylyltransferase and protein

kinase C recognize different physical features of membrane: differential responses to an oxidized phosphatidylcholine," in *Biochimica et Biophysica Acta*, vol. 1564, 2002, pp. 82-90.

[37] P. S. Sohal, and Cornell, R.B., "Sphingosine inhibits the activity of rat liver CTP: phosphocholine cytidylyltransferase," in *Journal of Biological Chemistry*, vol. 265, 1990, pp. 11746-11750.

[38] R. B. Cornell, "Regulation of CTP: phosphocholine cytidylyltransferase by lipids. 1. Negative surface charge dependence for activation," in *Biochemistry*, vol. 30, 1991, pp. 5873-5880.

[39] R. Cornell, and Vance, D.E., "Binding of CTP: phosphocholine cytidylyltransferase to large unilamellar vesicles," in *Biochimica et Biophysica Acta*, vol. 919, 1987, pp. 37-48.

[40] R. B. Cornell, "Regulation of CTP: phosphocholine cytidylyltransferase by lipids. 2 Surface curvature, acyl chain length, and lipid-phase dependence for activation," in *Biochemistry*, vol. 30, 1991, pp. 5881-5888.

[41] H. Jamil, Yao, Z., and Vance, D.E., "Feedback regulation of CTP: phosphocholien cytidylyltransferase translocation between cytosol and endoplasmic reticulum by phosphatidylcholine," in *Journal of Biological Chemistry*, vol. 265, 1990, pp. 4332-4339.

[42] R. S. Arnold, and Cornell, R.B., "Lipid regulation of CTP: phosphocholine cytidylyltransferase: electrostatic, hydrophobic, and synergistic interactions of anionic phospholipids and diacylglycerol," in *Biochemistry*, vol. 35, 1996, pp. 9917-9924.

[43] R. S. Arnold, DePaoli-Roach, A.A., and Cornell, R.B., "Binding of CTP: phosphocholine cytidylyltransferase to lipid vesicles: diacylglycerol and enzyme dephosphorylation increase the affinity for negatively charged membranes," in *Biochemistry*, vol. 36, 1997, pp. 6149-6156.

[44] G. S. Attard, Templer, R.H., Smith, W.S., Hunt, A.N., and Jackowski, S., "Modulation of CTP: phosphocholine cytidylyltransferase by membrane curvature elastic stress," in *Proceedings of the National Academy of Sciences of the United States of America*, vol. 97, 2000, pp. 9032-9036.

[45] S. M. A. Davies, Epand, R.M., Kraayenhof, R., and Cornell, R.B., "Regulation of CTP: phosphocholine cytidylyltransferase activity by the physical properties of lipid membranes: an important role for store curvature strain energy," in *Biochemistry*, vol. 40, 2001, pp. 10522-10531.

[46] D. Zhang, Tang, W., Yao, M.P., Yang, C., Xie, B., Jackowski, S., and Tabas, I., "Macrophages deficient in CTP: phosphocholine cytidylyltransferase-α are viable under normal culture conditions but are highly susceptible to free cholesterol induced death," in *Journal of Biological Chemistry*, vol. 275, 2000, pp. 35368-35376.

[47] T. A. Lagace, Storey, M.K., and Ridgway, N.D., "Regulation of phosphatidylcholine metabolism in Chinese Hamster Ovary cells by the sterol regulatory element-binding protein (SREBP)/SREBP cleavage-activating protein pathway," in *Journal of Biological Chemistry*, vol. 275, 2000, pp. 14367-14374.

[48] H. R. Kast, Nguyen, C.M., Anisfeld, A.M., Ericsson, J., and Edwards, P.A., "CTP:phosphocholine cytidylyltransferase, a new sterol- and SREBP-responsive gene," in *Journal of Lipid Research*, vol. 42, 2001, pp. 1266-1272.

[49] R. K. Mallampalli, Ryan, A.J., Carroll, J.L., Osborne, T.F., and Thomas, C.P., "Lipid deprivation increases surfactant phophatidylcholine synthesis via a sterol-sensitive regulatory element within the CTP:phosphocholine cytidylyltransferase promoter," in *Biochemical Journal*, vol. 362, 2002, pp. 81-88.

[50] H. Tronchere, Record, M., Terce, F., and Chap, H, "Phosphatidylcholine cycle and regulation of phosphatidylcholine biosynthesis by enzyme translocation," in *Biochimica et Biophysica Acta*, vol. 1212, 1994, pp. 137-151.

[51] G. Krauss, *Biochemistry of signal trasduction and regulation*, Second Edition ed: Wiley-VCH, 2001.

[52] J. D. Esko, Wermuth, M.M., and Raetz, R.H., "Thermolabile CDP-choline synthetase in an animal cell mutant defective in lecithin formation," in *Journal of Biological Chemistry*, vol. 256, 1981, pp. 7388-7393.

[53] Z. Cui, Houweling, M., Chen, M.H., Record, M., Chap, H., Vance, D.E., and Terce, F., "A genetic defect in phosphatidylcholine biosynthesis triggers apoptosis in chinese hamster ovary," in *Journal of Biological Chemistry*, vol. 271, 1996, pp. 14668-14671.

[54] K. P. Boggs, Rock, C.O., and Jackowski, S., "The antiproliferative effect of hexadecylphosphocholine toward HL60 cells is prevented by hexogenous lysophosphatidylcholine," in *Biochimica et Biophysica Acta*, vol. 1389, 1998, pp. 1-12.

[55] S. Jackowski, "Coordination of membrane phospholipid synthesis with the cell cycle," in *Journal of Biological Chemistry*, vol. 269, 1994, pp. 3858-3867.

[56] S. Jackowski, Wang, J., and Barburina, I., "Activity of the phosphatidylcholine biosynthetic pathway modulates the distribution of fatty acids into glycerolipids in proliferating cells," in *Biochimica et Biophysica Acta*, vol. 1483, 2000, pp. 301-315.

[57] I. C. Northwood, Tong, A.H.Y., Crawford, B., Drobnies, A.E., and Cornell, R.B., "Shuttling of CTP: phosphocholine cytidylyltransferase between the nucleus and endoplasmic reticulum accompanies the wave of

phosphatidylcholien synthesis during G_0 to G_1 transition," in *Journal of Biological Chemistry*, vol. 274, 1999, pp. 26240-26248.

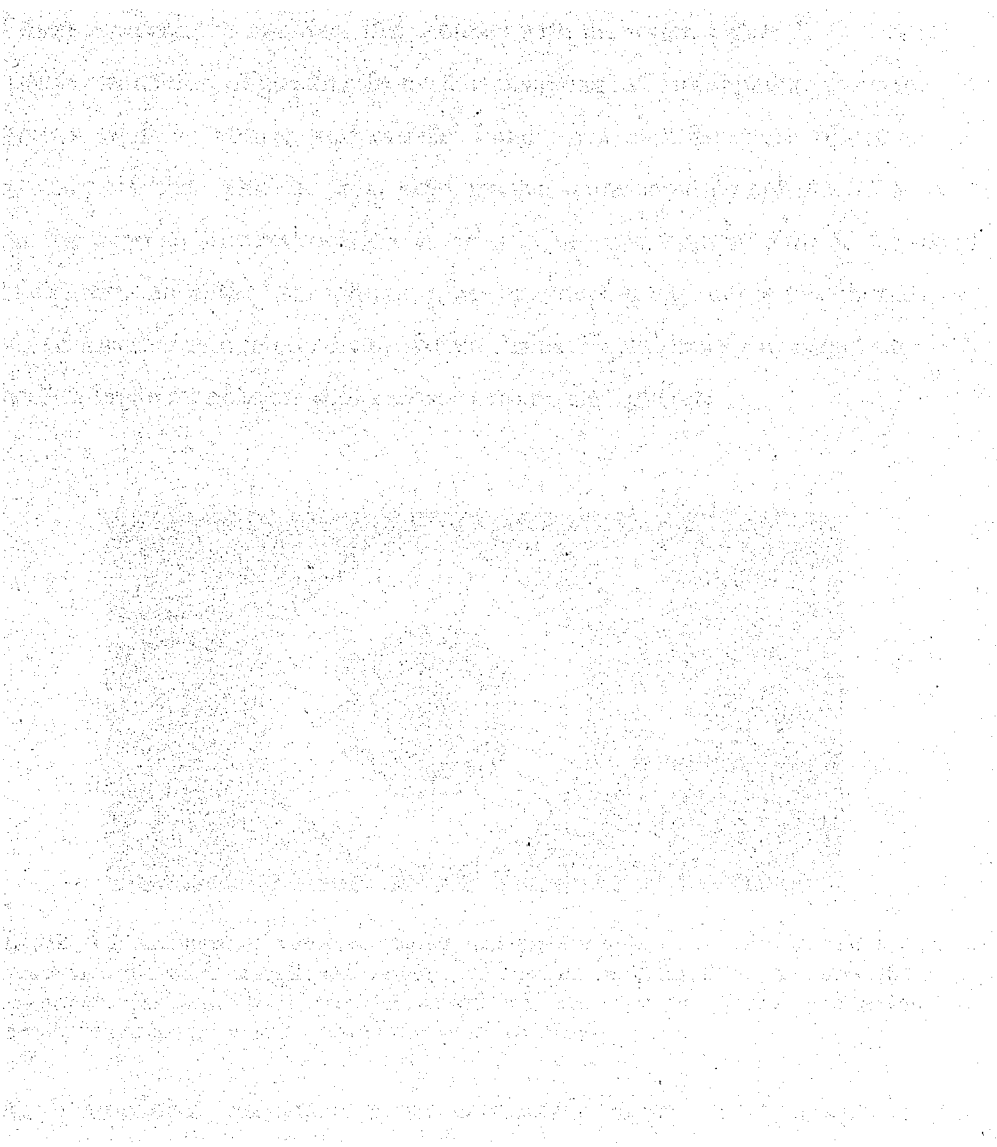

4 Physical chemistry of membranes

4.1 The hydrophobic effect

When either nonpolar or amphipathic molecules are mixed with water, the hydrophobic effect, also called hydrophobic interaction, gives rise to the clustering of these molecules to minimise their contact with the water. Figure 4.1 shows three possible structures originating from the clustering of amphipathic molecules in water: monolayer, vesicle, and micelle. Lipids in a monolayer are placed at the air/water interface with the polar head groups, represented by spheres, in contact with the water and the hydrophobic acyl chains, the tails, turning to the air. Lipids in vesicles respond to the hydrophobic effect by grouping together in two monolayers stacked together through the hydrophobic chains. Finally, lipids can also cluster into micelles, single monolayers with a closed surface, e.g. spheres.

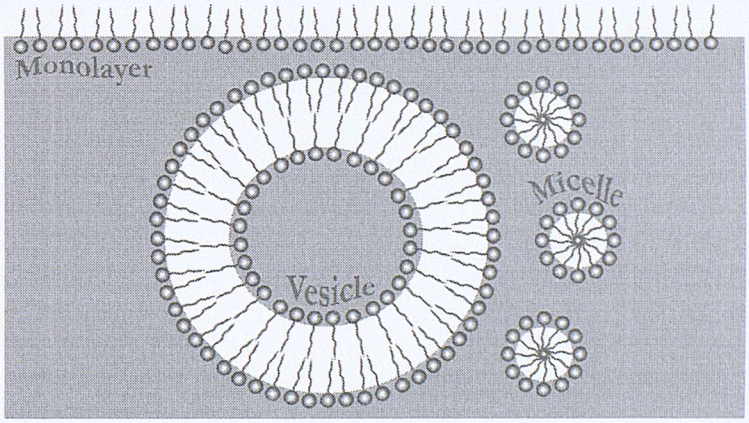

Figure 4.1 Amphipathic molecules cluster into three different structures to minimise their contact with the water: monolayers, vesicles and micelles. In all the three structures, the polar head-groups, represented by spheres, interact with the water while the acyl chains, represented by the tails, turn to the air or get in contact with other acyl chains.

The hydrophobic interaction is an entropically driven effect caused by the formation of ordered structures of water molecules, referred to as clathrates, around

the apolar molecules (Figure 4.2 is an example of water structure surrounding methane) [1]. Therefore there are two contributions to the hydrophobic effect: one derives from the restoration of H-bonds, broken during the dissolving process of the nonpolar molecule, in the new clathrate structure (ΔH for the dissolution can consequently be either positive or negative); the second contribution derives fom the decrease in the entropy of the system, caused by the formation of the clathrates (ΔS is negative). Examples of both the enthalpic and the enthropic effects for the transfer of organic molecules to water are given in Table 4.1 [1].

Table 4.1 Thermodynamic quantities for the transfer of non polar solutes from cyclo-hexane to water at 25 °C. n-hexane was transferred from n-hexane. Table from reference [1].

Organic molecule	ΔH ($kJ \cdot mol^{-1}$)	ΔS ($J \cdot K^{-1}$)	ΔG ($kJ \cdot mol^{-1}$)
Methane	-11.7	-75.8	10.9
Ethane	-9.2	-83.6	15.7
n-Hexane	0.0	-95.3	28.4
Cyclo-hexane	0.0	-57.7	17.2

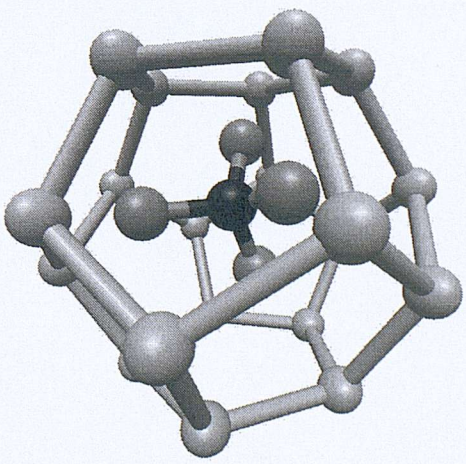

Figure 4.2 Probable structure for methane hydrate. Clathrate cage model of water molecules surrounding a molecule of methane. The ordered structure of the water reduces the entropy of the system and drives the phenomenon of immiscibility of nonpolar molecules with water [1].

An estimation of the molar free energy δ_μ for transferring a hydrocarbon chain from oil to water is given by:

Eq. 4.1 $$\delta_\mu \approx 10.2 + 3.7n \left(kJmol^{-1}\right)$$

where n is the number of carbon atoms in the hydrocarbon chain [2].

4.2 Surfaces: forces, energy and topology

4.2.1 Geometric and thermodynamic variables

Each surface is characterised by geometric and thermodynamic variables. The surface geometry is described by an area, A, and two principal radii of curvature, r_1 and r_2, Figure 4.3.

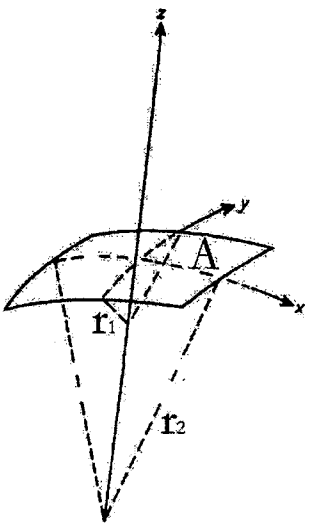

Figure 4.3 The two radii of curvature, r_1 and r_2, correspond to the radius of the two arcs of circumference defined by the two orthogonal planes xz and yz, being z perpendicular to the surface.

Four geometric elements are related to the two radii of curvature: the two principal curvatures, c_1 and c_2, the mean curvature H and the Gaussian curvature K [3, 4].

The two principal curvatures, c_1 and c_2, correspond to the inverse of the two radii r_1 and r_2:

Eq. 4.2 $$c_1 = \frac{1}{r_1} \quad \text{and} \quad c_2 = \frac{1}{r_2}$$

H and K correspond to the combination of the two principal curvatures and are given by:

Eq. 4.3 $$H = \frac{1}{2}(c_1 + c_2)$$

Eq. 4.4 $$K = c_1 c_2$$

The thermodynamic variables of the surface consist of the surface entropy, S^S, the absolute temperature, T, the number of components in the surface, n_i^S, and their chemical potentials, μ_i. There are parameters depending on the geometrical variables: the Gibbs surface tension, γ_G, and the moments C_1 and C_2. Hence, the change in the internal energy of an interface, dU^S, is given by:

Eq. 4.5 $$dU^S = TdS^S + \sum_i \mu_i dn_i^S + \gamma_G dA + C_1 dc_1 + C_2 dc_2$$

where $\gamma_G = \left(\partial U^S / \partial A\right)$ is the work involved in the surface extension-compression of an unit area, $C_1 = \left(\partial U^S / \partial c_1\right)$ and $C_2 = \left(\partial U^S / \partial c_2\right)$ are the work involved in the surface bending per unit of curvature [3].

4.2.2 Forces between lipids in monolayers

Figure 4.4 shows the forces acting between lipids that, in water, are grouped together in structures similar to those shown in Figure 4.1. The interfacial tension of the water tends to reduce the surface at the lipid/water interface and results in the attractive force F_γ; in contrast, lipids constrained to stay too close are subjected to two repulsive forces due to the hindrance effect: F_c from the acyl chains, and F_h

from the head-groups. Because F_h, F_γ and F_c may differ in magnitude, the lipid monolayer will tend to assume a curvature that minimises the imbalance of the forces across it. The three spontaneous mean curvatures of a lipid monolayer are shown in Figure 4.5. Lipids having positive, zero and negative spontaneous mean curvature are also called Type I, 0 and II amphiphiles, respectively.

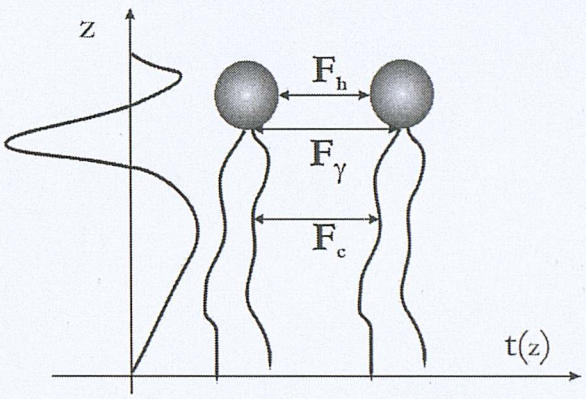

Figure 4.4 The force t(z) acting between lipids grouped together in an aqueous environment is function of the position z across the lipid molecule. F_h is the force acting between the lipid head-groups and derives from both electrostatic and hydrational effect; F_γ is the force acting at the water/acyl-chains interface and depends on the water interfacial tension tending to minimise the interfacial area; finally, F_c is the force acting between the acyl-chains.

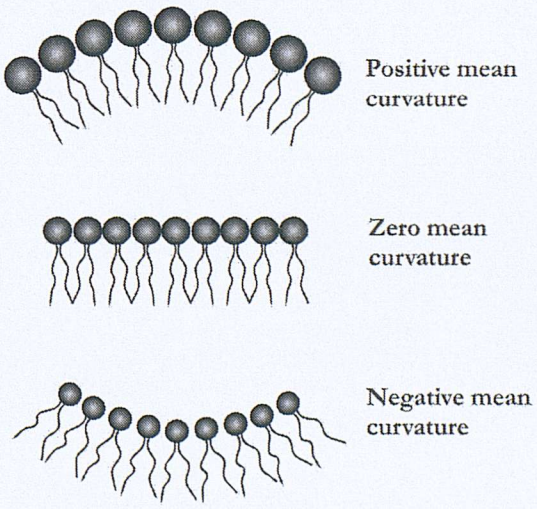

Figure 4.5 The imbalance between the forces across a lipid monolayer determine the spontaneous mean curvature.

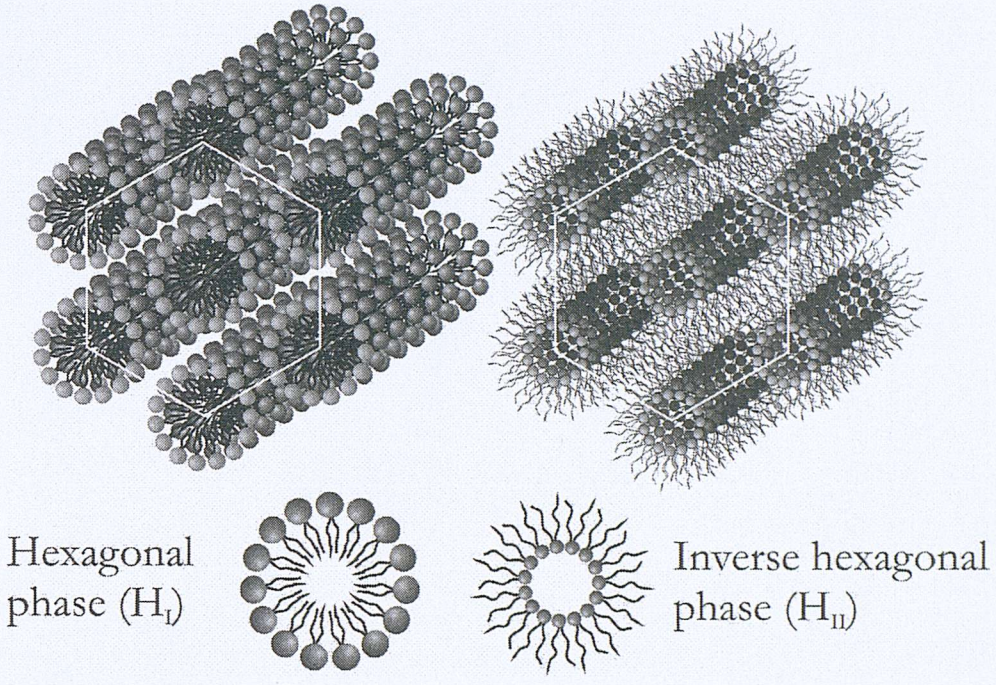

Figure 4.6 Hexagonal (H_I) and inverse hexagonal (H_{II}) phase are two simple examples of normal and inverse topology phases, respectively.

Depending on the content of water, different types of amphiphiles can aggregate in normal topology phases, characterised by $H > 0$, or inverse topology phases, characterised by $H < 0$; two examples of normal and inverse phases are the hexagonal (H_I) and inverse hexagonal phase (H_{II}) respectively (Figure 4.6).

4.3 Energies in monolayers and bilayers: lateral expansion and bending

4.3.1 The surface chemical potential

The first step to analysing the forces and energies in a surface is to consider the chemical potential term (μ) given by Eq. 4.5. It is assumed that the system is composed of lipids that are present in water either as monomers or as aggregates. If only one lipid species is present, the chemical potential μ can be represented as the sum of hydrophobic and hydrophilic terms [4]

Eq. 4.6 $$\mu = \mu_N^0(\Gamma) - \mu_1^0 = f_h(\Gamma) + f_c(\Gamma)$$

where $\mu_N^0(\Gamma)$ is the standard potential energy per molecule of lipid in the aggregate and "Γ" means that the potential energy is dependent upon the geometry of the aggregate

μ_1^0 is the standard free energy per molecule of lipid in the monomeric form

$f_h(\Gamma)$ is the surface term arising from the lipid head-group region

$f_c(\Gamma)$ is a core term arising from the hydrocarbon chain region.

The interfacial term can be represented in its simplest form as

Eq. 4.7 $$f_h(\Gamma) = \gamma A_h + \left(\frac{C}{A'}\right)$$

where C is a constant

A_h is the area per lipid molecule at the hydrocarbon/water interface,

A' is the area per molecule at the centre of the head-group repulsion [4].

The hydrocarbon region term, $f_c(\Gamma)$, is rather difficult to calculate as it is not easy to predict the force distribution across the acyl chains. The potential energy can be calculated by solving the integral given by:

Eq. 4.8 $$f_c(\Gamma) = -\int \pi(z) A(z) dz$$

where $A(z)$ is the molecular area at the distance z from the interface and $\pi(z)$ is the lateral pressure existing at the same distance [4]. Attempts to solve Eq. 4.8 have been done by calculating the geometry-dependent part given by:

Eq. 4.9 $$\pi(z)dz = -\delta f_c / \delta A(z)$$

The above expression has been evaluated for minimising the free energy per chain by using the statistical thermodynamic treatment of the conformational probability distribution function for the hydrocarbon chains [4].

Lipids in Figure 4.5 and Figure 4.6 are aggregated in structures having different geometries. The preferred geometry corresponds to the one that minimise Eq. 4.6.

Lipid molecular structure, temperature, pressure, water content and its ionic strength are variables affecting in different ways f_h, f_c, A_h and A_c, the last two corresponding to the optimal area per interfacial and chain packing region, respectively.

4.3.2 *Surface elastic energy: extension and bending*

A surface can be subjected to two different kinds of deformation: lateral expansion, involving change in the surface area, and surface bending, involving change in the surface curvature, as shown in Figure 4.7.

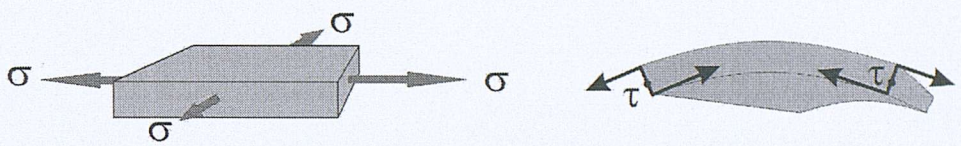

Figure 4.7 Surfaces can undergo two different types of deformation: extension of the surface area, under the lateral tension σ, and bending of the surface under the torque tension τ.

The energy per unit area involved in the deformation of a surface having area A is given by

Eq. 4.10 $$g_{el} = \left(\frac{G_{el}}{A} \right) = g_A + g_{curv}$$

where g_A is the elastic energy for any expansion or compression of the surface, and g_{curv} is the elastic energy involved in any bending of the surface [4]. The function defining the expansion energy is given by

Eq. 4.11 $$g_A = \frac{1}{2} \kappa_A \left(\frac{A}{A_0} - 1 \right)^2$$

where the isothermal lateral compression modulus κ_A is defined as

Eq. 4.12 $$\kappa_A = A\left(\frac{\delta\sigma}{\delta A}\right)_T$$

where σ, the isotropic lateral expansion, is given by

Eq. 4.13 $$\sigma = \left(\frac{\delta G_{el}}{\delta A}\right)_T$$

G_{el} can be equated to the free energy per molecule $(f_c + f_h)$ and, if estimates for the form of the free energy are known, then κ_A can be obtained from the second derivative with respect to the area [4].

Usually g_A is much larger than g_{curv} and deformations involving a stretching requires more energy than those involving a bending. However, because the primary interest herein is the relationship between surface curvature and CCTα activity, g_A will be ignored in the following statements.

The elastic energy per unit area of a surface with principal curvature c_1 and c_2 is given by

Eq. 4.14 $$g_{curv} = g_M + g_G = \frac{1}{2}\kappa_M (c_1 + c_2 - 2c_0)^2 + \kappa_G c_1 c_2$$

where c_0 is the spontaneous curvature of the surface, κ_M and κ_G are the elastic moduli for the mean and the Gaussian curvatures, respectively [4]. A typical value for the elastic modulus of the fluid lipid bilayer is represented by the calculated one for egg-PtdCho: $\kappa_M \approx 2 \cdot 10^{-19}$ J. The approximate value of the modulus for a lipid monolayer is given by [4]:

Eq. 4.15 $$\kappa_M^{bilayer} \approx 2\kappa_M^{monolayer}$$

The value for κ_M decreases strongly with increasing equilibrium area per molecule and increases with decreasing chain-length of the lipid or when mixed chain-length lipids are present in the same layer.

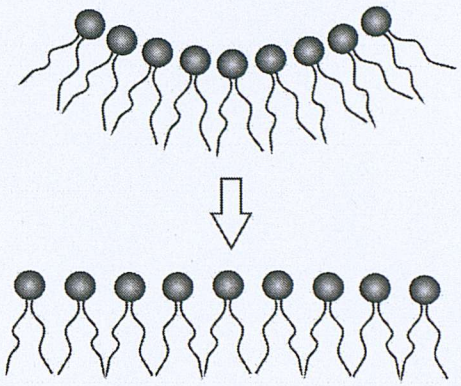

Figure 4.8 A monolayer constituted by type II lipids and in contact with the water through the polar head-groups can be free to bend (monolayer on the top) or can be constrained to remain flat (monolayer on the bottom). The flat monolayer is more stressed than the curved one and the increased exposure of the hydrophobic core to the water is one of the origins of the stress.

The Gaussian elastic modulum, κ_G, controls the tendency of the membrane to form structures of non-zero Gaussian curvature: $\kappa_G > 0$ favours saddle-like surfaces, while $\kappa_G < 0$ favours elliptic surfaces, e.g. spheres. The shape and the curvatures of a surface depend on the distribution of the forces between the molecules. For a flat monolayer at equilibrium, the net lateral tension must be equal to zero [4]:

Eq. 4.16 $$\int t(z)dz = 0$$

If the positive and negative stresses are not symmetric about the mid-plane of the molecules, there will be a spontaneous tendency of the layer to curve away from a planar geometry. The tendency to bend corresponds to the torque tension τ that is given by [4]:

Eq. 4.17 $$\tau = \int zt(z)dz = -\kappa_M 2c_0$$

Lipid monolayers are frustrated when constrained to maintain a position that is far from the equilibrium one, as shown in Figure 4.8, where a type II lipid monolayer is constrained to remain flat. The torque tension is a good indication of the amount of stress in a monolayer or a bilayer under frustration.

4.4 References

[1] R. Chang, *Physical Chemistry for the chemical and biological sciences*, 3rd ed. Sausalito, CA 94965: University Science Books, 2000.

[2] C. Tanford, *The hydrophobic effect: formation of micelles and biological membranes.*, 2nd Edition ed. New York: John Wiley, 1980.

[3] M. M. Kozlov, and Markin, V.S., "Definition of the force factors for an interface with non-uniform curvature," in *Journal of the Chemical Society, Faraday Transactions 2*, vol. 85, 1989, pp. 261-276.

[4] J. M. Seddon, "Structure of the inverted hexagonal (H_{II}) phase, and non-lamellar phase transitions of lipids," in *Biochimica et Biophysica Acta*, vol. 1031, 1990, pp. 1-69.

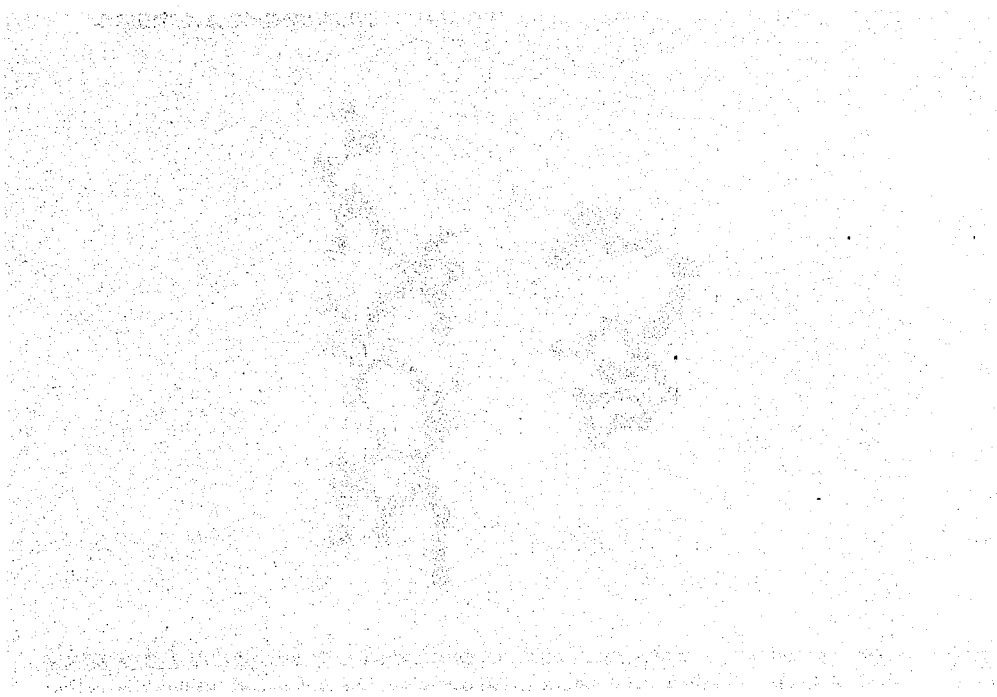

5 Protein folding and energy

5.1 Folding and structures of proteins

The structural description of a protein requires knowledge of the spatial distribution of its amino acids. Protein structure can be reported in four different ways by using the primary, secondary, tertiary or the quaternary structures. The definition of the four structures is given below [1-3]:

- Primary structure corresponds to the sequence of the amino acids of a protein. Usually, the left side of the sequence correspond to the amino function of the chain, while the right side to the carboxylic one.
- Secondary structure defines the regular local structure of a polypeptide chain due to hydrogen bonding. The secondary structures most commonly found in proteins are known as α-helix and β-sheet, shown in Figure 5.1 and Figure 5.2, respectively.

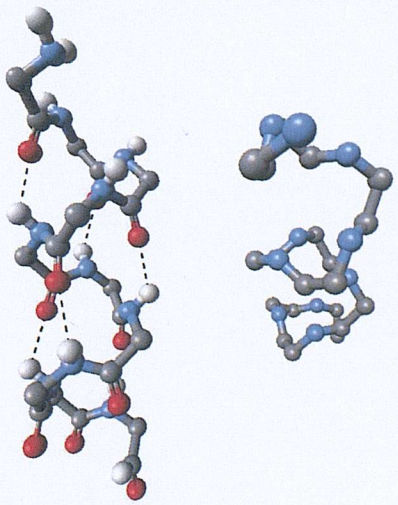

Figure 5.1 Polyglycine in α-helix structure. The representation on the left shows only those hydrogens (white balls), bound to the amide nitrogen (blue balls), involved in H-bond (dashed black lines) with the carbolic oxygen (red balls). The structure on the right shows only nitrogen and carbon (grey balls) atoms to highlight the backbone of the α-helix structure

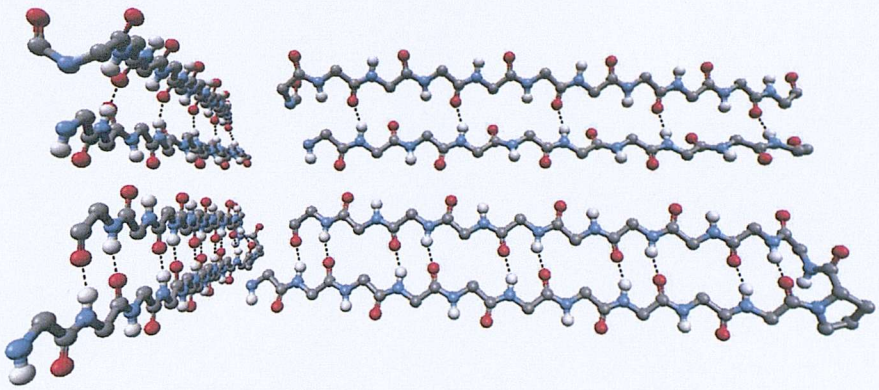

Figure 5.2 Polyglycines arranged in parallel (up chains) and anti-parallel (down chains) β-sheets. The two structures show only those hydrogens (white balls) bound to the amide nitrogens (blue balls). The two β-sheets differ for the orientation of the chains and for the number of H-bonds (dashed black lines) between the shown hydrogen and the carbolic oxygen (red balls). Grey balls represent carbon atoms. The projections on the left show that β-sheets are flat structures.

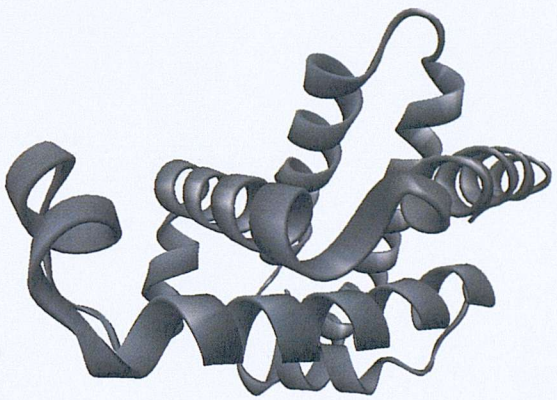

Figure 5.3 Schematic representation of a haemoglobin molecule. The haemoglobin tertiary structure corresponds to the spatial diposition of all the amino acids that are not part of the same segment. Alternatively, the tertiary structure corresponds to the spatial diposition of the different secondary structures.

- Tertiary structure defines the overall folding of a polypeptide chain (Figure 5.3 and Figure 5.4) due to disulphide bonds and noncovalent forces as electrostatic and van der Waals forces, and hydrogen bonds.

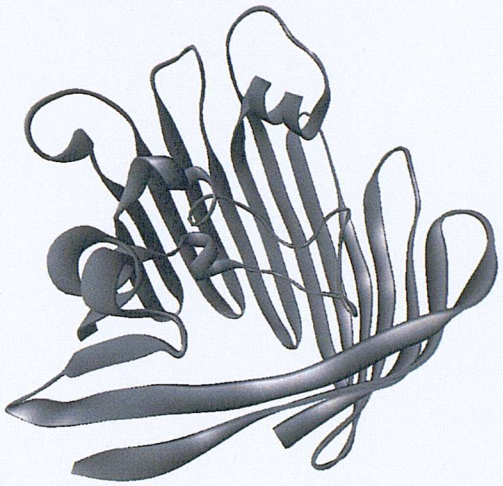

Figure 5.4 Schematic representation of a porin molecule. The tertiary structure corresponds to the spatial diposition of all the amino acids that are not part of the same segment. Alternatively, the tertiary structure corresponds to the spatial position of the different secondary structures.

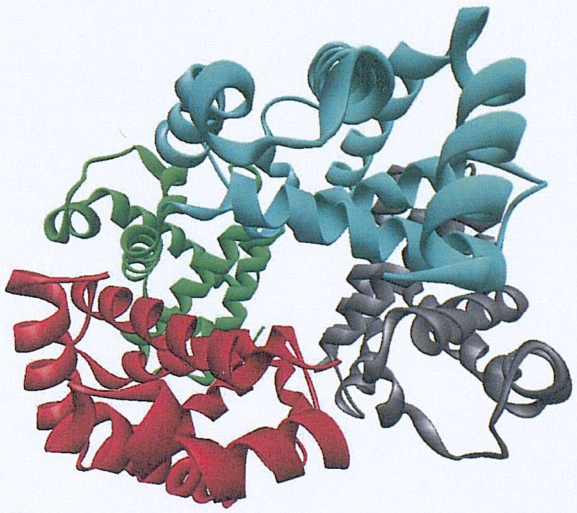

Figure 5.5 Quaternary structure of the haemoglobin complex. The four identical units, singularly shown in Figure 5.3, are represented with different colours.

- Quaternary structure describes the relative spatial position of identical or different polypeptide chains (referred to as subunits) in an oligomeric structure, stabilised by electrostatic and van der Waals forces, hydrogen bonds and occasionally disulphide bonds. Figure 5.5 is an example of the quaternary structure of four haemoglobin units assembled in a tetramer.

5.1.1 *α-helix and β-sheets*

α-helix and β-sheets (Figure 5.1 and Figure 5.2) are characterised by a periodical spatial disposition of amino acids. The structural analysis of an α-helix revels that:

- L-amino acids form right-handed helices, which are more stable than left-handed helices [1].
- 3.6 amino acid residues are required for a complete helix turn.
- The distance between two successive turns, the pitch, is 5.4 Å.
- The polypetide chains are stabilised in the helical structure by hydrogen bonds (perpendicular to the helix axis) occurring between the amide hydrogen and the carbonyl oxygen on the following third residue.

Crystallographic structures have shown that the hydrogen bond is not necessarily restricted to groups separated by three residues; also amino acids 2 or 4 residues apart, in the same chain, can form hydrogen bonds adapting to the environmental conditions in which the helix is placed [4].

β-sheets, parallel and anti-parallel, have a planar structure with hydrogen bonds between amide hydrogens and carbonyl oxygens of residues located in different chains inside the protein, as shown in Figure 5.2 and Figure 5.4. Parallel and anti-parallel β-sheets differ in the direction of the two chains.

5.1.2 *Protein folding*

Protein folding defines the mechanism by which the primary sequence of a polypeptide chain gives rise to the three-dimensional structure of the protein active form (the three-dimensional structures of haemoglobin and porin, resolved by X-ray crystallography, give a fixed representation of the amino acid position in space). However, protein structural studies (by NMR, fluorescence, CD, temperature and pressure jump, AFM) have shown that environmental conditions can cause conformational changes in protein tertiary structure occurring in a few

microseconds as well as in hours [1, 5]. Moreover, these studies have shown that intermediate states, called *molten globule* (MG), are characterised by the presence of secondary but not tertiary structure [1].

5.2 Cytosolic and membrane proteins

A number of rules and algorithms have been developed to predict some of the properties of polypeptide sequences: hydrophobicity, charge, solubility and membrane affinity. A number of polypeptide sequences have been studied and several algorithms developed to combine their properties with their tendency to bind to membranes or remain in solution [6, 7]. All these correlations, used to predict unknown protein features, are often based on algorithms that assign the protein sequences scores based on scales that discriminate among the twenty common amino acids. Table 5.1 shows seven different scales that have been obtained in different ways: KDE, GES, WIF and WOCT from the analysis of amino acid partitioning from water to an apolar solvent, ARH, VHE and EIS from statistical analysis of residues occurrence in transmembrane protein segments as reported in data bases.

Statistical studies of amino acid distribution, especially in bacterial proteins, have shown that the content of arginine and lysine is higher in peripheral or integral membrane proteins, known as the positive-inside rule [8, 9]. In particular, von Heijne suggested, as a possible mechanistic implication for the role of segments rich in positive residues, that these segments could function as hairpins for the insertion of neighbouring segments into the membrane. However, the positive-inside rule is not adequate to discriminate between cytosolic and membrane proteins, even if it becomes useful when combined with other methods of sequence analysis. Two algorithms are particularly useful when scoring sequences to discriminate between membrane and cytosolic proteins, the average hydropathy $\langle H \rangle$ and the hydrophobic moment μ_H, both discussed in the next section.

Table 5.1

Amino acid	KED	GES	ARH	VHE	EIS	WIF	WOCT
Ala	1.8	1.6	1.6	0.267	0.25	0.17	0.50
Cys	2.5	2.0	1.2	1.806	0.04	-0.24	-0.02
Asp	-3.5	-9.2	0.1	-2.303	-0.72	1.23	3.64
Glu	-3.5	-8.2	0.2	-2.442	-0.62	2.02	3.63
Phe	2.8	3.7	2.0	0.427	0.61	-1.13	-1.71
Gly	-0.4	1.0	0.6	0.160	0.16	0.01	1.15
His	-3.2	-3.0	0.3	-2.189	-0.40	0.96	2.33
Ile	4.5	3.1	1.7	0.971	0.73	-0.31	-1.12
Lys	-3.9	-8.8	0.2	-2.996	-1.10	0.99	2.80
Leu	3.8	2.8	2.9	0.623	0.53	-0.56	-1.25
Met	1.9	3.4	3.0	0.136	0.26	-0.23	-0.67
Asn	-3.5	-4.8	0.3	-1.988	-0.64	0.42	0.85
Pro	-1.6	-02	0.8	-0.451	-0.07	0.45	0.14
Gln	-3.5	-4.1	0.5	-1.814	-0.69	0.58	0.77
Arg	-4.5	-12.3	0.5	-2.749	-1.80	0.81	1.81
Ser	-0.8	0.6	0.8	-0.119	-0.26	0.13	0.46
Thr	-0.7	1.2	0.9	-0.083	-0.18	0.14	0.25
Val	4-2	2.6	1.1	0.721	0.54	0.07	-0.46
Trp	-0.9	1.9	1.1	-0.875	0.37	-1.85	-2.09
Tyr	-1.3	-0.7	0.7	-0.386	0.02	-0.94	-0.71

Hydrophobicity scales buit to determine the amino acid hydrophobic character. KED scale was determined studying the amino acid partition from water to ethanol [6]; GES scale was determined measuring the amino acid partition from water to oil [7]; ARH scale gives the membrane-buried preference parameters calculated from a 1125-residue data base [10]; VHE scale gives the membrane-buried preference parameters based of 135 transmembrane segments from 24 bacterial inner membrane proteins [8]; EIS scale is based on the analysis of five other scales [11]; WIF and WOCT scales were obtained from the amino acid partition from water to POPC, and from water to octanol, respectively [12].

5.2.1 *Average hydropathy and hydrophobic moment*

The analysis of protein affinity for biological membrane has been calculated using the average hydropathy, which provides a protein profile reflecting its hydrophobic or hydrophilic character, moving from the amino to the carboxy terminus of the protein. The average hydropathy along the protein sequence is given by:

Eq. 5.1 $$\langle H \rangle = \left(\sum_n r_i / n \right)$$

Where n is the number of residues and r_i is the hydrophobic value of the i^{th} residue of the sequence for which the average hydropathy is calculated. r_i is obtained from one of the scales reported in Table 5.1. The analysis of the hydropathy of a number of proteins has revealed that, generally, membrane-penetrating segments are more hydrophobic than segments from cytosolic globular proteins [6, 7, 9, 10]. However, sometimes the hydrophobic character is not sufficient to discriminate between membrane and globular proteins; in fact, Kyte and Doolittle showed that the globular protein dogfish lactate dehydrogenase contains sequences more hydrophobic than those found in several known membrane-associated proteins [6]. The fundamental limit of $\langle H \rangle$ is the lack of any relationship between the hydrophobic/hydrophilic character of a protein and its secondary structures, thus preventing any prediction of potential co-operativity between the protein segments. The algorithm for the hydrophobic moment, μ_H, was developed to correlate protein hydrophobicity and secondary structure (α-helix) [11]. Eisenberg's algorithm for the hydrophobic moment μ_H is given by

Eq. 5.2 $$\mu_H = \left\{ \left[\sum_{n=1}^{N} H_n \sin(n\delta) \right]^2 + \left[\sum_{n=1}^{N} H_n \cos(n\delta) \right]^2 \right\}^{1/2}$$

where H_n is the hydrophobicity of the n^{th} residue, obtained from one of the scales reported Table 5.1, and δ is 100°, the angle between two consecutive residues defined on the plane perpendicular to the α-helix axis, Figure 5.6.

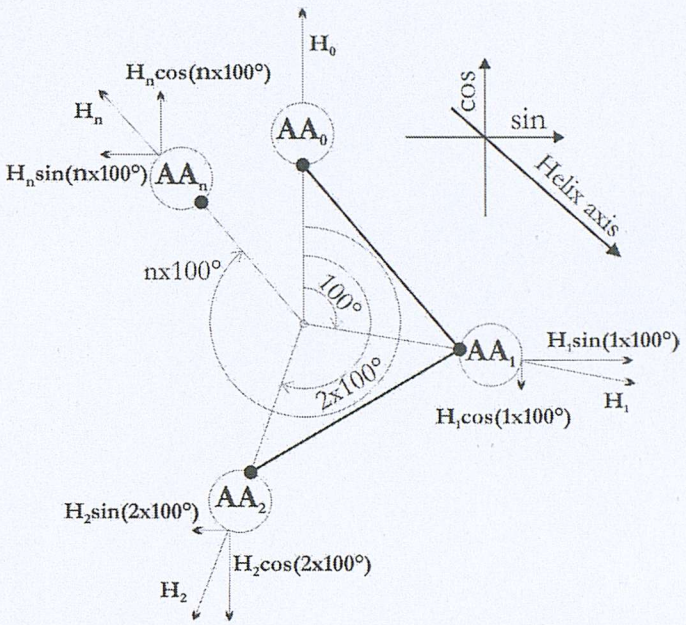

Figure 5.6 Four residues in a α-helix structure. Three consecutive amino acids are separated by 100°, whilst the n^{th} residue by **n**x100° from the first one. H_0, H_1, H_2 and H_n are the hydrophobicities of the four residues AA_0, AA_1, AA_2 and AA_n respectively. The hydrophobicity of each residue is resoluted by the sin and cos functions in two orthogonal components and perpendicular to the helix axis.

The hydrophobicity of each residue is represented in Eq. 5.2 as a vector perpendicular to the helix axis; each vector is resoluted in two orthogonal components, as shown in Figure 5.6, by the sine and cosine functions. Using the μ_H function it is possible to find out if the disposition of the amino acids in an helix structure generates an hydrophobic strip (Figure 5.7).

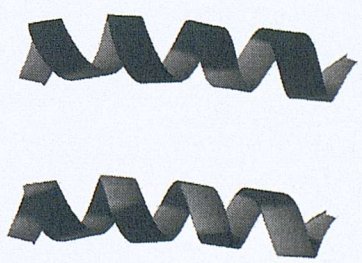

Figure 5.7 The above α-helices have the same hydrophilic (in grey) and hydrophobic (in black) residues and, consequently, the same hydrophobicity. The residues in the upper helix are ordered to form a hydrophobic strip, resulting in a high hydrophobic moment; the random disposition of the residues, in the lower helix, results in a low hydrophobic moment.

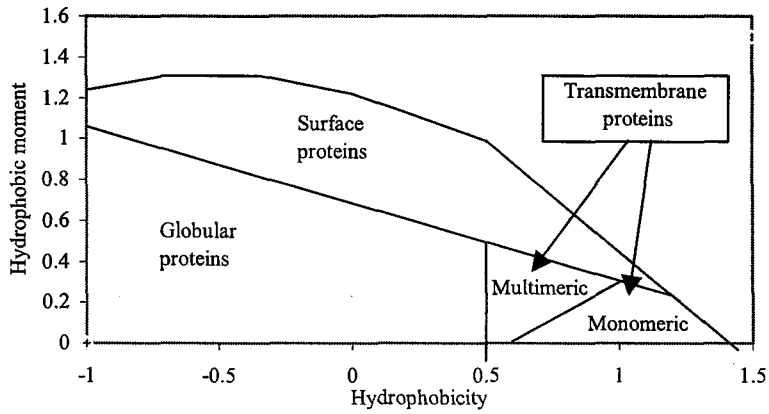

Figure 5.8 Protein classification as a function of their hydrophobic moment and hydrophobicity. Figure re-drawn from reference [11].

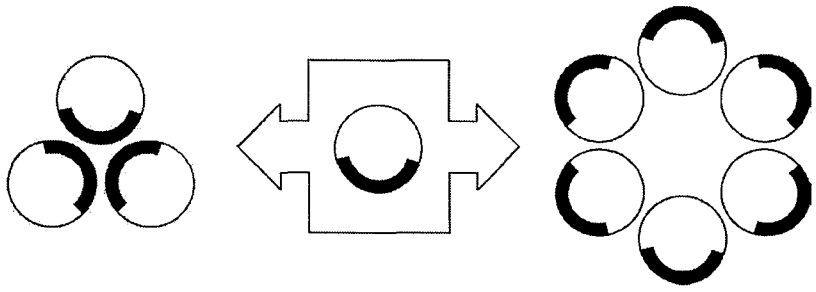

Figure 5.9 α-helices with low hydrophobicity and high hydrophobic moments (a single α-helix is shown in the middle with the hydrophobic residues represented by the thick arc) can bundle in two different ways: through the polar (on the left) or through the apolar (on the right) residues. The structure on the left exposes to the environment only the polar residues (decreasing the affinity for the membrane hydrophobic core), while the structure on the right exposes only the apolar residues (increasing the affinity for the membrane hydrophobic core).

The correlation between μ_H and <H> of several protein segments reveals that both <H> and μ_H have a role in discriminating between membrane and cytosolic proteins (Figure 5.8). In particular, Eisenberg observed that sequences with higher values of <H> and smaller values of μ_H are generally monomeric transmembrane anchors; helices with high μ_H and small <H> are generally paired or are bundled together in membranes (Figure 5.9); helices from surface seeking proteins have a higher value of μ_H and a medium value of <H> [11].

However, Eisenberg reported three cases in which the predictions from the analysis of both the hydrophobicity and the hydrophobic moment failed: 1) respiratory NADH dehydrogenase from *E. coli*, 2) gene product P from histidine transport operon of *Salmonella typhimurium* and 3) a matrix protein from the outer membrane of *E. coli*. All three proteins were identified as membrane-associated proteins while the previous algorithms identified no membrane-associated segment [11].

5.3 Energy of partition

The process of protein partitioning between cytosol and membranes can occur through two different paths, as reported by White and Wimley and by Popot and Engelman [4, 13]. The free energy for the partition process can be considered as the sum of different energetic terms as represented in Eq. 5.3

Eq. 5.3 $$\Delta G^0 = \Delta G^0_{np} + \Delta G^0_{elc} + \Delta G^0_{qE} + \Delta G^0_{con} + \Delta G^0_{imm} + \Delta G^0_{lip}$$

where ΔG^0_{elc} is the effect of changing the dielectric constant (from water to the hydrophobic core) on the hydrogen- bonded peptides

ΔG^0_{np} is the non-polar interaction between the helix and the membrane acyl chains[a], in which the hydrophobic effect is the driving force

ΔG^0_{qE} is the electrostatic interaction between basic residues and anionic lipids

ΔG^0_{con} is the energy involved in the conformational changes caused by the binding of the protein or peptide, to the membrane

ΔG^0_{imm} is the energy from the decreased degrees of freedom caused by the immobilisation of the protein or peptide, on the membrane

[a] H-bond effect on the partitioning of peptide bonds between water and an alkane, or water and POPC, have been studied. It has been reported that the free energy for the partition of H-bonded peptide between water and an alkane is 17 kJmol^{-1} lower than the partition of not H-bonded peptide [14]. Other studies have shown that the free energy decreases of about 3.0 kJmol^{-1} when the partition occurs between the water and the POPC interface [13].

ΔG^0_{lip} is the energy coming from the perturbation of the acyl chain structure of the membrane core.

The effects of the change in the solvation state of the peptide, or protein, can be grouped into one term

Eq. 5.4 $$\Delta G^0_{sol} = \Delta G^0_{np} + \Delta G^0_{elc}$$

and then

Eq. 5.5 $$\Delta G^0 = \Delta G^0_{sol} + \Delta G^0_{qE} + \Delta G^0_{con} + \Delta G^0_{imm} + \Delta G^0_{lip}$$

The immobilisation and conformational components, often referred to as ***non-classical hydrophobic effect***, and ΔG^0_{lip} are strictly dependent on the bilayer nature and are included in one term

Eq. 5.6 $$\Delta G^0_{bilayer} = \Delta G^0_{con} + \Delta G^0_{imm} + \Delta G^0_{lip}$$

Hence, the free energy of partitioning can be simplified into a two-component function

Eq. 5.7 $$\Delta G^0 = \Delta G^0_{sol} + \Delta G^0_{qE} + \Delta G^0_{bilayer}$$

Eq. 5.7 splits the free energy of partition in three components depending prevalently on the peptide and on the bilayer. White and Wimley refer to the possible involvement of both the bilayer compressibility and bilayer bending moduli effects on $\Delta G^0_{bilayer}$ [13].

5.4 References

[1] R. Chang, *Physical Chemistry for the chemical and biological sciences*, 3rd ed. Sausalito, CA 94965: University Science Books, 2000.

[2] B. Alberts, Bray, D., Lewis, J., Raff, M., Roberts, K., and Watson, J.D., *Molecular biology of the cell*, Third ed. New York: Garland Publishing, 1994.

[3] K. Wilson, and Walker, J., *Principles and techniques of practical biochemistry*, Fifth ed. Cambridge: Cambridge University Press, 2000.

[4] J. L. Popot, and Engelman, D.M., "Helical membrane protein folding, stability, and evolution," in *Annual Review of Biochemistry*, vol. 69, 2000, pp. 881-922.

[5] J. K. Myers, and Oas, T.G., "Mechanisms of fast protein folding," in *Annual Review of Biochemistry*, vol. 71, 2002, pp. 783-815.

[6] J. Kyte, and Doolittle, R.F., "A simple method for displaying the hydropathic character of a protein," in *Journal of Molecular Biology*, vol. 157, 1982, pp. 105-132.

[7] D. M. Engelman, Steitz, T.A., Goldman, A., "Identifying nonpolar transbilayer helices in amino sequences of membrane proteins," in *Annu. Rev. Biophys. Biophys. Chem.*, vol. 15, 1986, pp. 321-353.

[8] G. v. Heijne, "Membrane protein structure prediction," in *Journal of Molecular Biology*, vol. 225, 1992, pp. 487-494.

[9] L. Sipos, and Heijne, G. von, "Predicting the topology of eukaryotic membrane proteins," in *European Journal of Biochemistry*, vol. 213, 1993, pp. 1333-1340.

[10] P. Argos, Rao, J.K., and Hargrave, P.A., "Structural prediction of membrane-bound proteins," in *European Journal of Biochemistry*, vol. 128, 1982, pp. 565-575.

[11] D. Eisenberg, Schwarz, E., Komaromy, M., and Wall, R., "Analysis of membrane and surface protein sequences with the hydrophobic moment plot," in *Journal of Membrane Biology*, vol. 179, 1984, pp. 125-142.

[12] S. H. White, and Wimley, W.C., "Hydrophobic interaction of peptide with membrane interfaces," in *Biochimica et Biophysica Acta*, vol. 1376, 1998, pp. 339-352.

[13] S. H. White, and Wimley, W.C., "Membrane protein folding and stability: physical principles," in *Annual Review in Biophysical and Biomolecular Structure Antimicrobial Agents and Chemotherapy*, vol. 28, 1999, pp. 319-365.

[14] N. Ben-Tal, Sitkoff, D., Topel, I.A., Yang, A-S., Burt, S.K., and Honig, B., in *Journal of Physical Chemistry B*, vol. 101, 1997, pp. 450-457.

6 Vesicles and monolayers

6.1 Lipid monolayers

Lipid monolayers are often used as model systems of biological membranes because their easy preparation allows the measurement of interfacial properties such as electrical potential, dipole moment or lipid density. Monolayers are usually prepared at the air/water interface[a], even if an alternative option is offered by the oil/water interface.

Lipids in monolayers can undergo phase changes as illustrated by the isotherm of Figure 6.1. Lipids can be in gaseous, liquid and solid phases by changing either the head-group area[b] or the temperature. The collapse pressure, π_c, and the collapse head-group area, A_c are the pressure and the head-group area corresponding to the loss of monolayer integrity, as shown in Figure 6.2.

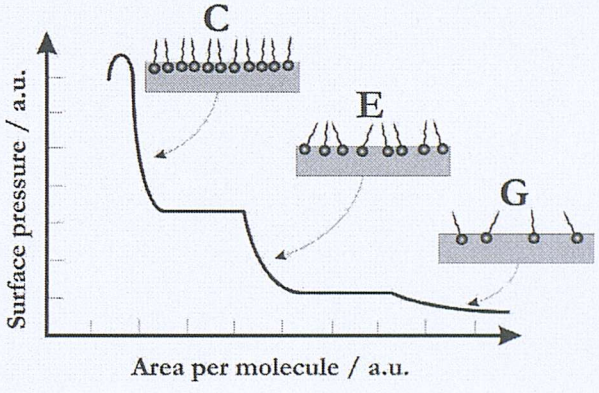

Figure 6.1 Surface pressure versus area per molecule isotherm for a long-chain organic compound. The surface pressure and the area per molecule are given in arbitrary units, a.u. G= gaseous phase, E= expanded liquid phase, C= condensed liquid phase [1].

---

[a] Lipid monolayers are easily prepared by dropping a lipid solution (using a water immiscible volatile solvent) on the surface of the water and allowing the solvent to evaporate. The lipid molecules will spontaneously spread on the surface with the polar head-group in contact with the water and the hydrocarbon chains on the opposite side.

[b] Head-group area is defined as the air/water or oil/water interface area occupied by each molecule in the monolayer. Conversely, lipid density is the number of lipid molecules per unit area.

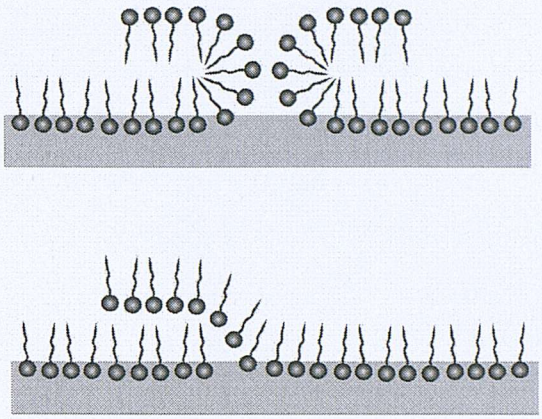

Figure 6.2 Two possible ways in which monolayers collapse when the pressure between the lipids overcomes the collapsing pressure π_c. Alternatively, the monolayer structure can evolve into micelles or vesicles.

When the lipid molecules in the monolayer interact with the water surface, the free energy of both the monolayer and the water surface change from those of the two components to those of the mixed monolayer/water system. The free energy is then defined as in Eq. 6.1

Eq. 6.1 $$G_m^{'} = G_S^{'} - G_0^{'}$$

where $G_m^{'}$ is the free energy of the monolayer, $G_S^{'}$ is the free energy of the water surface in the presence of the monolayer, that is the monolayer/water interface, and $G_0^{'}$ is the free energy of the clean air/water interface [2]. Maintaining temperature and lipid moles constant, the partial derivatives of Eq. 6.1 with respect to the total area of the monolayer gives

Eq. 6.2 $$\pi_m = \gamma_{a/w} - \sigma_m$$

Where $\pi_m = -\left(\partial G_m^{'}/\partial A\right)_{N,T}$, $\gamma_{a/w} = -\left(\partial G_0^{'}/\partial A\right)_{N,T}$ and $\sigma_m = -\left(\partial G_S^{'}/\partial A\right)_{N,T}$ are the lateral pressure of the monolayer, the water tension and the monolayer/water interfacial tension respectively [2]. The lateral pressure of the monolayer is the pressure that is experimentally measured and shown in the isotherm of Figure 6.1 as a function of the head-group area.

In contrast to monolayers, vesicles are closed surfaces in which the lipid density results from the equilibrium between forces acting between the lipid molecules and the aqueous environment, as discussed in 4.1. One of the forces that maintain the closed structure of the vesicles comes from the tendency of the bilayer to reduce the exposure of the hydrophobic chains to the aqueous environment, the so called hydrophobic effect. Differently from vesicles, the hydrophobic effect does not act on the close packing of the lipids but on the maintenance of the monolayer structure, with the polar head-group in contact with the aqueous phase and the acyl chains placed into the air. Figure 6.3 shows a bilayer and three monolayers having different lipid density and, consequently, different distribution of the forces along the molecules. Figure 6.3 suggests that monolayers can be used as model system of biological membranes only if the lipid density, and consequently the lateral pressure, resembles the one present in one leaflet of a lipid bilayer.

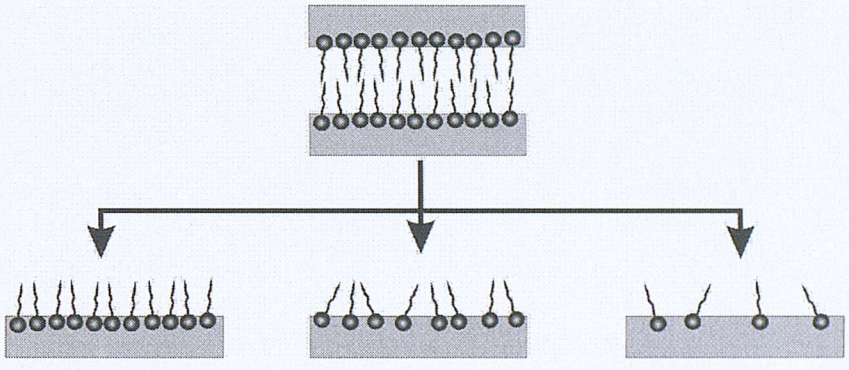

Figure 6.3 Lipids in vesicles and in monolayers may differ in their density. The hydrophobic effect is principally responsible for the close lipid packing in vesicles; on the contrary, lipid density in monolayer is not affected by the hydrophobic effect and can be changed reducing the total area available for the monolayer.

6.2 The bilayer/monolayer correspondence

The measurement of the lateral pressure in a lipid bilayer has been attempted experimentally (measuring the pressure of lipid vesicles spread at the air/water interface,) and calculated theoretically (developing equations of state to describe the force distribution for a monolayer or bilayer, or by computer simulations) resulting

in values ranging from 15 mN/m to collapse pressure [2-7]. The bilayer/monolayer correspondence discussed below is based on a theoretical approach and is divided in two sections: the first one describes the correlation between the mechanochemical properties of the two systems and the second one describes the correlation in terms of free energy and chemical potential.

6.2.1 Intrinsic pressure and surface tention

The systems discussed below are monolayers and bilayer composed of the same kind of lipids. For simplicity, both leaflets of the bilayer are hypothesised to be equivalent and, consequently, these demonstrations are based exclusively on one leaflet. The interface refers to the region of contact between water and monolayer, or water and one leaflet of a bilayer. The free energy, G, for both the systems is then defined as

Eq. 6.3 $$G_m = G_{phob} + G_{phil} + G_{\text{int}} + G_{a/o}$$

Eq. 6.4 $$G_b = G_{phob} + G_{phil} + G_{\text{int}}$$

where:

G_m and G_b are the free energies of the monolayer and one leaflet of a bilayer respectively

G_{phob} is the free energy due to the hydrophobic interaction between the hydrocarbon chain region, of both the monolayer and the bilayer, and the water

G_{phil} is the free energy due to the interaction between the polar head groups of the monolayer or the bilayer and the water

G_{int} is the free energy due to the interaction between the hydrocarbon chains of the lipids in the monolayer or in the bilayer

$G_{a/o}$ is the free energy due to the interaction between the air and the hydrocarbon chains of a monolayer at the air/monolayer interface [2].

If both the temperature and the amount of lipids in the monolayer and in one leaflet of the bilayer are kept constant, the partial derivative with respect to the area, $(\partial/\partial A)_{N,T}$, of both G_m and G_b gives the surface tension:

Eq. 6.5 $$\sigma_m = \gamma_{o/w} - \pi_{phil} - \pi_{\text{int}} + \gamma_{a/o}$$

Eq. 6.6 $$\sigma_b = \gamma_{o/w} - \pi_{phil} - \pi_{\text{int}}$$

Where:

$\sigma_m = (\partial G_m/\partial A)_{N,T}$ is the surface tension of the monolayer

$\sigma_b = (\partial G_b/\partial A)_{N,T}$ is the surface tension of one leaflet of the bilayer

$\gamma_{o/w} = (\partial G_{phob}/\partial A)_{N,T}$ is the interfacial tension between the hydrophobic layer and the water

$\pi_{phil} = (\partial G_{phil}/\partial A)_{N,T}$ is the bilayer leaflet and monolayer component pressure due to the hydrophilic interaction; the forces acting between the head-groups are usually repulsive (repulsive stress)

$\pi_{\text{int}} = (\partial G_{\text{int}}/\partial A)_{N,T}$ is the bilayer leaflet and monolayer component pressure due to the hydrocarbon chains; the forces acting between the hydrocarbon chains, as for the head-groups, are usually repulsive (repulsive stress)

$\gamma_{a/o} = (\partial G_{a/o}/\partial A)_{N,T}$ is the interfacial tension between the air and the hydrophobic layer of the monolayer [2].

For monolayers and bilayers with the same density, the pressures in the head-group and in the hydrocarbon regions can be combined in the same way for both the bilayer and the monolayer to give the intrinsic pressure π, defined as [2]

Eq. 6.7 $$\pi = \pi_{phil} + \pi_{\text{int}} = \pi_m = \pi_b$$

The intrinsic pressure in Eq. 6.7 corresponds to the lateral pressure showed in the isotherm of Figure 6.1. Using Eq. 6.7, Eq. 6.5 and Eq. 6.6 can be rewritten in the form of Eq. 6.8 and Eq. 6.9 [2]

Eq. 6.8 $$\sigma_b = \gamma_{o/w} - \pi_b$$

Eq. 6.9 $$\sigma_m = \gamma_{a/o} + \gamma_{o/w} - \pi_m$$

The combination of Eq. 6.5, Eq. 6.6 and Eq. 6.7 shows the difference between the intrinsic pressure between the monolayer and that of one leaflet of the bilayer [2]

Eq. 6.10 $$\pi_m - \pi_b = \gamma_{a/w} - \left(\gamma_{a/o} - \gamma_{o/w}\right)$$

Experimental observations have demonstrated that

Eq. 6.11 $$\gamma_{a/w} \cong \gamma_{o/w} + \gamma_{a/o}$$

at least for the system n-octane/water [2]. For this system the experimental values were $\gamma_{a/w} = 72$ mN/m, $\gamma_{o/w} = 49$ mN/m and $\gamma_{a/o} = 23$ mN/m [2]. The intrinsic pressure equivalence deduced from Eq. 6.10 and Eq. 6.11 is apparently independent from the aqueous phase. Consequently, the pressure in both a monolayer and a leaflet of a bilayer depends exclusively on the temperature and lipid density, the latter being inversely proportional to the lipid head-group area a. If T and a are the same, the intrinsic pressure is the same for both the monolayer and one leaflet of a bilayer [2]

Eq. 6.12 $$\pi_m(a,T) = \pi_b(a,T)$$

Unlike the case of the intrinsic pressure, monolayers and bilayers differ in surface tensions. Defining the surface tension as a function of the temperature and of the head-group area, the comparison of monolayer and bilayer results gives

Eq. 6.13 $$\sigma_m(a,T) = \sigma_b(a,T) + \gamma_{a/o}$$

Eq. 6.13 shows that the difference between a monolayer and a leaflet of a bilayer differ for $\gamma_{a/o}$, taking into account the additional surface at the air/oil interface present in the monolayer [2]. The surface tension corresponds to the work required to create a unit area of surface and for the case of a monolayer $\gamma_{a/o}$ represents the work required to create the surface at the air/hydrocarbon chain interface. The presence of $\gamma_{a/o}$ results in a force acting on the monolayer that tries to reduce or increase the area at the air/hydrocarbon chain interface. This additional force indicates that a monolayer at the air/water interface is intrinsically mechanochemically different from a bilayer.

At constant temperature and number of moles in one leaflet of a bilayer, the head-group area of the lipid is an equilibrium value, meaning that the first derivative with respect to the area of the free energy function is zero. If temperature and number of moles in one leaflet of a bilayer are constant, it follows that the value of the derivative of Eq. 6.8, done with respect to the head-group area, is

Eq. 6.14 $$\sigma_b\left(a^0\right)=\frac{1}{N_b}\left(\frac{\partial G_b}{\partial a}\right)_{N_b,T,a=a^0}=\gamma_{o/w}\left(a^0\right)-\pi\left(a^0\right)=0$$

where a^0 is the molecular area at the equilibrium [2]. If the bending energy and the trans-membrane osmotic pressure are negligible, the result of Eq. 6.14 means that one leaflet of a bilayer is in a tension-free state and that the intrinsic pressure at the equilibrium head-group area is [2]

Eq. 6.15 $$\pi^0=\pi_b^0=\pi_b\left(a^0\right)=\gamma_{0/w}^0$$

Because the intrinsic pressure is equal for both the monolayer and the bilayer under the same lipid density, it follows that at the same equilibrium area a^0, the equilibrium intrinsic pressure for a monolayer is [2]

Eq. 6.16 $$\pi^0=\pi_m^0=\gamma_{0/w}^0$$

If the monolayer is slowly compressed, the collapse pressure π_c for the monolayer is considered to be close to π^0.

6.2.2 *Free energy and chemical potential*

If the temperature T is constant, then the free energy for a lipid molecule can be considered as a function of its molecular area; either the free energy for a monolayer or one leaflet of a bilayer can then be defined as

Eq. 6.17 $$G_b = N_b \phi(a)$$

Eq. 6.18 $$G_m = N_m \phi(a) + \gamma_{a/o} A_m$$

in which N_b and N_m are the number of molecules in the bilayer and monolayer respectively, a is the lipid head-group area, A_m is the total monolayer area, which is maintained constant, and $\phi(a)$ is the free energy per lipid molecule dependent exclusively from the lipid head-group area The partial derivative with respect to the number of moles of the two functions in Eq. 6.17 and Eq. 6.18 gives the chemical potential per molecule of lipid

Eq. 6.19 $$\mu_b = \left(\frac{\partial G_b}{\partial N_b}\right)_a = \phi(a)$$

Eq. 6.20 $$\mu_m = \left(\frac{\partial G_m}{\partial N_m}\right)_{A_m} = \phi(a) - a\phi'(a)$$

in which $\phi'(a) = d\phi(a)/da$ is the first derivative with respect to the head-group area [2]. When the monolayer and one leaflet of the bilayer are in equilibrium and under the same condition of temperature and density, their head-group area is a^0 and the chemical potential becomes

Eq. 6.21 $$\mu(a^0) = \mu_b(a^0) = \mu_m(a^0)$$

and $\phi'(a^0) = 0$ because the free energy function is in a minimum when $a = a^0$ [2].

The head-group area, the number of molecules and the total area of one monolayer and one leaflet of a bilayer are correlated, according to

Eq. 6.22 $A_m = N_m a$ and $A_b = N_b a$

in which A_m, A_b are the total respective areas and N_m, N_b are the number of molecules in the monolayer and in the bilayer leaflet, respectively [2].

The surface tension of the lipid layer can then be calculated deriving Eq. 6.17 with respect to the total area, giving [2]

Eq. 6.23 $$\sigma_b(a) = \left(\frac{\partial G_b}{\partial A_b}\right)_{N_b} = \phi'(a)$$

The intrinsic pressure in one leaflet of a bilayer is obtained by combining Eq. 6.8 and Eq. 6.23 [2]

Eq. 6.24 $$\pi_b(a) = \gamma_{o/w} - \phi'(a)$$

The surface tension for the lipid monolayer can be calculated deriving Eq. 6.18 with respect to the total area, giving [2]

Eq. 6.25 $$\sigma_m(a) = \left(\frac{\partial G_m}{\partial A_m}\right)_{N_m} = \gamma_{a/o} + \phi'(a)$$

The monolayer intrinsic pressure, obtained by combining Eq. 6.9 and Eq. 6.25, is given by [2]

Eq. 6.26 $$\pi_m(a) = \gamma_{o/w} - \phi'(a)$$

Eq. 6.24 and Eq. 6.26 show that the intrinsic pressure $\pi(a)$ is the same for both the systems. The differential equation for $\phi(a)$ can be recast in terms of intrinsic pressure substituting Eq. 6.16 into Eq. 6.24 or Eq. 6.26 [2]

Eq. 6.27 $$\phi'(a) = \pi(a^0) - \pi(a)$$

The calculation of $\phi(a)$ from $\phi'(a)$ makes it possible to estimate the value for the surface tension of a monolayer and for a leaflet of a bilayer. The change in the chemical potential of the lipid in the bilayer can be calculated by integrating Eq. 6.27 between the equilibrium area, a^0, and any other specific value of the head-group area [2]:

Eq. 6.28 $$\mu_b(a) - \mu_b(a^0) = \phi(a) - \phi(a^0) = \int_{a^0}^{a} [\pi(a^0) - \pi(a)]da$$

The same procedure can be applied for calculating the change in the chemical potential of the lipids in the monolayer, integrating between the equilibrium area a^0 and any other specific value of the head-group area [2]:

Eq. 6.29 $$\mu_m(a) - \mu_m(a^0) = \int_{a^0}^{a} [\pi(a^0) - \pi(a)]da - a[\pi(a^0) - \pi(a)]$$

Eq. 6.28 and Eq. 6.29 are then combined to give the difference in terms of chemical potential between the lipid in one leaflet of a bilayer and in a monolayer [2]

Eq. 6.30 $$\mu_b(a) - \mu_m(a) = a\left[\pi(a^0) - \pi(a)\right]$$

Eq. 6.30 shows that the lipids in a monolayer and in a bilayer have the same potential only when they have the same intrinsic pressure, which happens when they have the same density.

6.3 References

[1] M. C. Petty, *Langmuir-Blodgett films*. Cambridge: Cambridge University Press, 1996.

[2] S.-s. Feng, "Interpretation of mechanochemical properties of lipid bilayer vesicles from the equation of state or pressure-area measurement of the monolayer at the air-water or oil-water interface," in *Langmuir*, vol. 15, 1999, pp. 998-1010.

[3] R. Maget-Dana, "The monolayer technique: a potent tool for studying the interfacial properties of antimicrobial and membrane. Lytic peptide and their

interactions with lipid membranes," in *Biochimica et Biophysica Acta*, vol. 1462, 1999, pp. 109-140.

[4] D. Marsh, "Lateral pressure in membranes," in *Biochimica et Biophysica Acta*, vol. 1286, 1996, pp. 183-223.

[5] H. Brockman, "Lipid monolayers: why use half a membrane to characterize protein-membrane interaction," in *Current Opinion in Structural Biology*, vol. 9, 1999, pp. 438-443.

[6] D. H. Wolfe, and Brockman, H.L., "Regulation of the surface pressure of lipid monolayers and bilayers by the activity of water: derivatization and application of an equation of state," in *Proceedings of the National Academy of Sciences of the United States of America*, vol. 85, 1988, pp. 4285-4289.

[7] M. V. Aguilella, Mafè, S., and Manzanares, J.A., "Double layers potential and degree of dissociation in charged lipid monolayers," in *Chemistry and Physics of Lipids*, vol. 105, 2000, pp. 225-229.

7 Lipid monolayer and pressure/area isotherms

7.1 Phospholipids and monolayer isotherms

The metabolism of phosphatidylcholine (PtdCho) and phosphatidylethanolamine (PtdEtn) has been discussed previously in 2.3. PtdCho and PtdEtn monolayers have been studied extensively because they are the most aboundant lipids in biological membranes [1-4]. Figure 7.1 shows pressure/area isotherms of phosphatidylcholines differing in the composition of the acyl chains. It should be noted that saturated PtdCho are not oxygen sensitive; however, phospholipids with one or more unsaturations are readily oxidised. Hence, the preparation and study of monolayers of unsaturated phospholipids requires an oxygen-free environment [4-6].

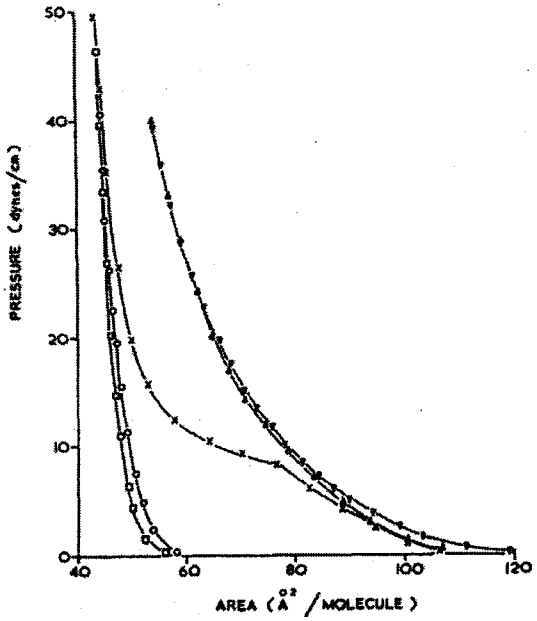

Figure 7.1 Pressure/area isotherms for saturated phosphatidylcholines on 0.1 M NaCl at 22°C. □, dibenheoylphosphocholine (C_{22}); O, distearoylphosphocholine (C_{18}); ×, dipalmitoyl-phosphocholine (C_{16}); Δ, dimyristoylphosphocholine (C_{14}); ∇, dicaprylphosphocholine (C_{10}). Figure from reference [2].

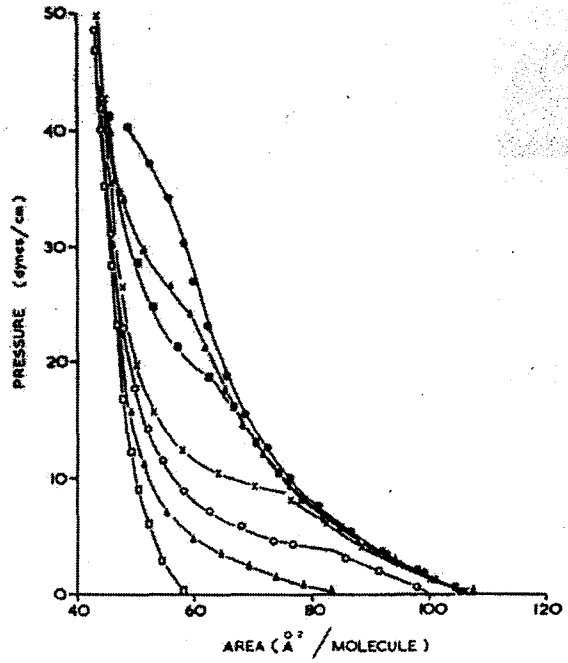

Figure 7.2 Pressure-area isotherms for L-α-dipalmitoylphosphatidyl-choline on 0.1 M NaCl at various temperatures. •, 34.6 °C; Δ, 29.5 °C; ■, 26.0 °C; ×, 21.1 °C; ○, 16.8 °C; ▲, 12.4 °C ; □, 6.2 °C. Figure from reference [2].

The effect of temperature on the monolayer properties depends on the nature of the constituting lipid molecules. A number of equations are available in the literature that describe the monolayer pressure/area curve. The simplest equation considers a general monolayer as a gas, and correlates the lateral pressure, Π, the head-group area, a, the Boltzmann's constant k and the absolute temperature, T, using an equation similar to the equation of state valid for an ideal-gas [7]:

Eq. 7.1 $$\Pi a = kT$$

As for gases, Eq. 7.1 cannot be used to derive pressure/area isotherms when the temperature of lipid monolayers is close to that of the lipid phase change. Figure 7.2 shows the effect of different temperatures on the isotherms of DPPC, whose phase transition from the gel phase, L_β, to the liquid crystalline phase, L_α, occurs at 41.3 °C [8]. The schematic representation of lipid gel phases is shown in Figure 7.3 [8].

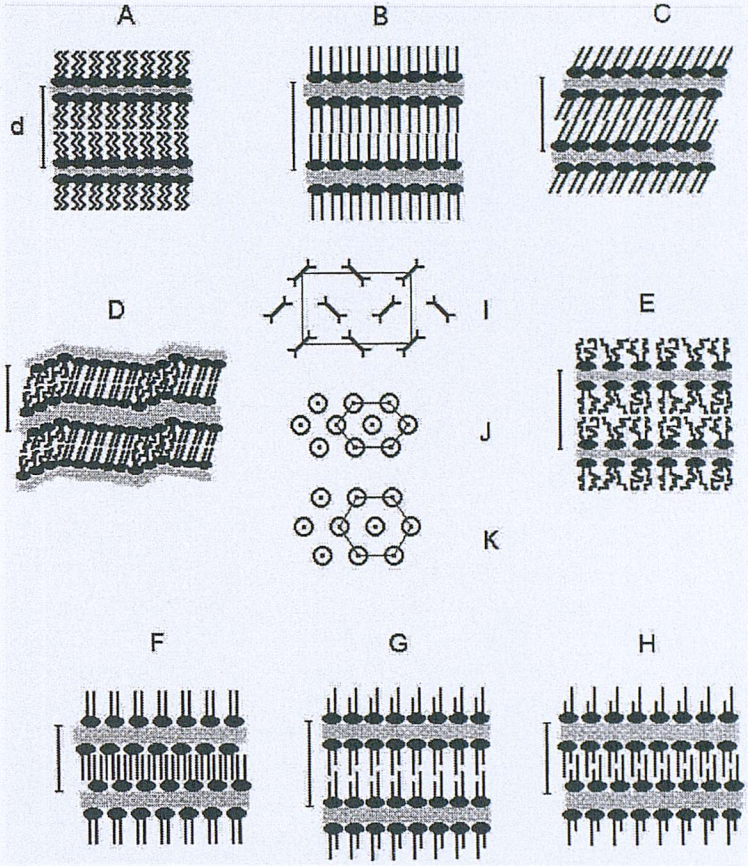

Figure 7.3 Schematic representation of various lamellar phases found in PtdCho/water systems: (A) subgel, L_c; (B) gel (untilted chains) , L_β; (C) gel (tilted chains), $L_{\beta'}$; (D) rippled gel, $P_{\beta'}$; (E) liquid crystalline, L_α; (F) fully interdigitated gel, L_β^{int}; (G) partially interdigitated gel; (H) mixed. Cross-sectional view of the hydrocarbon chain arrangement in various chain packing modes (view is down the long axis of the chains): (I) orthorhombic; (J) quasi-hexagonal; (K) hexagonal. Figure and legend from reference [8].

7.2 Materials and methods

7.2.1 *Materials*

1,2-dimyristoyl-*sn*-glycero-3-phosphocholine (DMPC), 1,2-dioleoyl-*sn*-glycero-3-phosphocholine (DOPC), 1,2-dioleoyl-*sn*-glycero-3-ethanolamine (DOPE) were purchased from Fluka or Avanti Polar Lipids. Tris(hydroxymethyl)aminomethane (Tris), NaCl, $MgCl_2$, dimethyldichlorosilane, toluene, chloroform and ~ 26 % HCl were purchased from Sigma Aldrich. Water was deionised using an Elga Purelab

deionisator system. All aqueous solutions were filtered using Nylon66 filter disks 0.45 μm (Supelco) prior to use. Isotherms were recorded using a Langmuir film balance Type 601 with PS4 sensor (NIMA Technology, UK) and paper (Filter paper Whatman n° 1) or platinum (NIMA Technology, UK) Wilhelmy plate.

7.2.2 Pressure/area isotherms

Monolayers were prepared by spreading a phospholipid solution (30-100 μl, 0.8 $mg \cdot ml^{-1}$ in chloroform) on 50-250 ml of 0.1 M NaCl or of buffer A (0.1 M Tris-HCl, pH 7.2 at 37 °C, 0.1 M NaCl and 10 mM $MgCl_2$). After 5-10 minutes, to allow the chloroform to evaporate, pressure/area isotherms were recorded at 20 or 37 °C. Monolayers were normally compressed at 10 or 120 cm^2min^{-1}.

7.2.3 Head-group area measurement of mixed phospholipid monolayers

Phospholipid mixtures were prepared as chloroform solution (~0.8 $mg \cdot ml^{-1}$) and spread on buffer A. After 5-10 minutes to allow the chloroform evaporation, isocycle pressure/area isotherms were recorded at 37 °C. Monolayers were subjected from three to seven isocycles of compression to 25 mNm^{-1} and decompression to 15 mNm^{-1} at 10 cm^2min^{-1}.

7.2.4 Monolayer stability

Monolayer stability was investigated by spreading phospholid solutions (0.05-0.8 $mg \cdot ml^{-1}$ in chloroform) on 0.1 M NaCl using the Nima trough, 550 cm^2, or on buffer A, using either the Nima trough or a smaller glass trough (30 cm^2 fixed surface area mounting the Nima PS4 sensor with platinum Wilhelmy plate) silanised using 5% (w/v) dimethyldichlorosilane in toluene. The fixed area trough was contained in a chamber filled with nitrogen to prevent the oxidation of the monolayer lipids.

7.3 Results

7.3.1 Pressure/area isotherms

Figure 7.4 shows two DMPC isotherms recorded in two different conditions (7.2.2). The DMPC isotherm recorded at 20 °C showed the phase transition, from the rippled gel phase $P_{\beta'}$ to the liquid crystalline phase L_{α} (occurring at 23.6 °C [8]) and the collapse pressure π_c and collapse head-group area A_c at 60 mN/m and ~41-42 Å^2, respectively. Whilst the isotherm recorded at 37 °C showed no phase transition and collapse occurring at around 50 mN/m when A_c was ~50 Å^2.

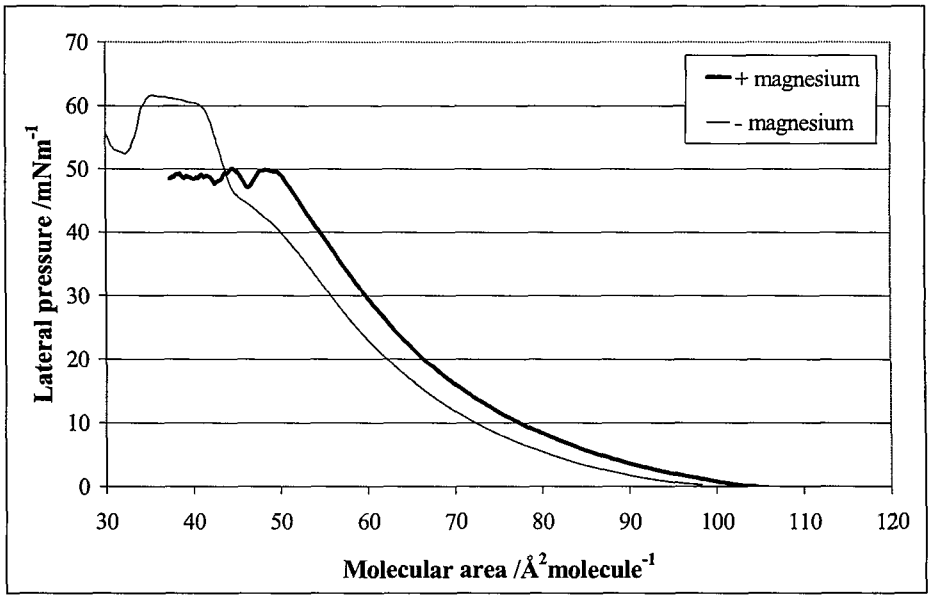

Figure 7.4 DMPC isotherms recorded in two different conditions: 20 °C on 0.1 M NaCl (- magnesium) and 37 °C on 0.1 M NaCl, 0.1 M Tris-HCl, pH 7.2, 10 mM $MgCl_2$ (+ magnesium).

Figure 7.5 shows two DOPC monolayer isotherms recorded following the conditions described in 7.2.2. No phase transition was observed for the DOPC monolayers (phase transition from the lamellar gel to the liquid crystalline is reported to occur at –18.3 °C [8]). Furthermore, in our study, the DOPC monolayers showed the same collapse pressure, ~47-48 mN/m at 20 and 37 °C, corresponding to different head-group areas of ~52 and ~59 Å^2, respectively.

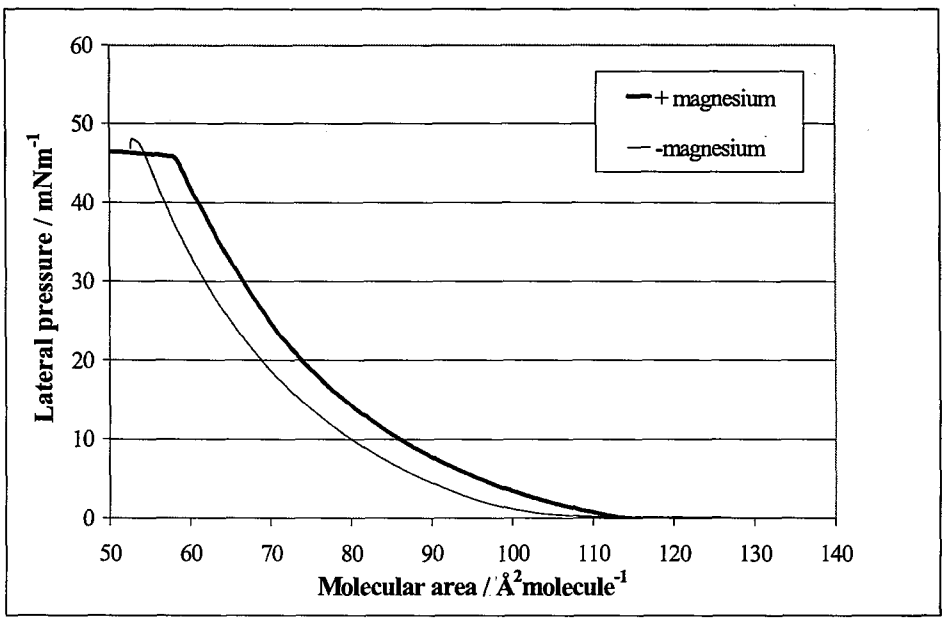

Figure 7.5 DOPC isotherms were recorded in two different conditions. One isotherm was recorded at 20 °C on 0.1 M NaCl (- magnesium). The second isotherm was recorded at 37 °C on 0.1 M NaCl, 0.1 M Tris-HCl at pH 7.2, and 10 mM $MgCl_2$ (+ magnesium).

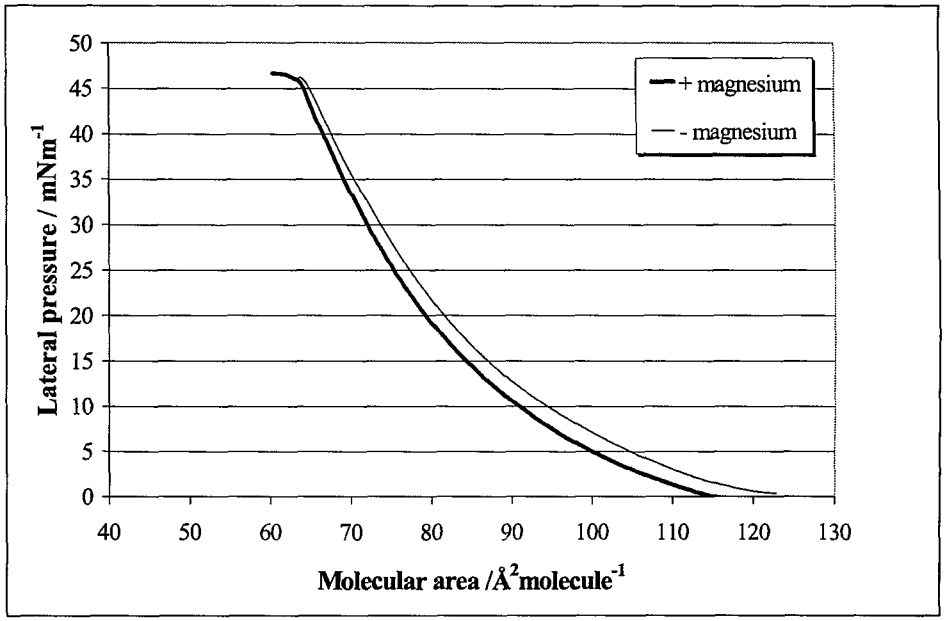

Figure 7.6 DOPE isotherms were recorded in two different conditions. One isotherm was recorded at 20 °C on 0.1 M NaCl (- magnesium). The second isotherm was recorded at 37 °C on 0.1 M NaCl, 0.1 M Tris-HCl at pH 7.2 and 10 mM $MgCl_2$ (+ magnesium).

Similarly to DOPC, DOPE monolayers did not show any phase transition (Figure 7.6). Differently from DMPC and DOPC, DOPE isotherms collapsed at ~46 mN/m and at the same head-group area, 63-64 $Å^2$, in both conditions.

7.3.2 Head-group area in mixed DMPC/DOPC and DOPC/DOPE monolayers

Lipid binary mixtures of DMPC/DOPC and DOPC/DOPE were prepared and the head-group area of the mixtures was measured at different lateral pressures (7.2.3). The 15-25 mN/m range of pressures was choosen because 20 mN/m has been reported as the lateral pressure in membranes [9], even if different values can also be found as discussed in 6.2.

The first set of results was obtained using paper Wilhelmy plates. Lipid molecules in the monolayer were compressed and decompressed (isocycle) three times between 15 and 25 mN/m. The lipid head-group area versus DOPC molar fraction for the DMPC/DOPC mixtures is plotted in Figure 7.7; Table 7.1 reports head-group areas measured at 15 and 25 mN/m during the first and the third isocycle.

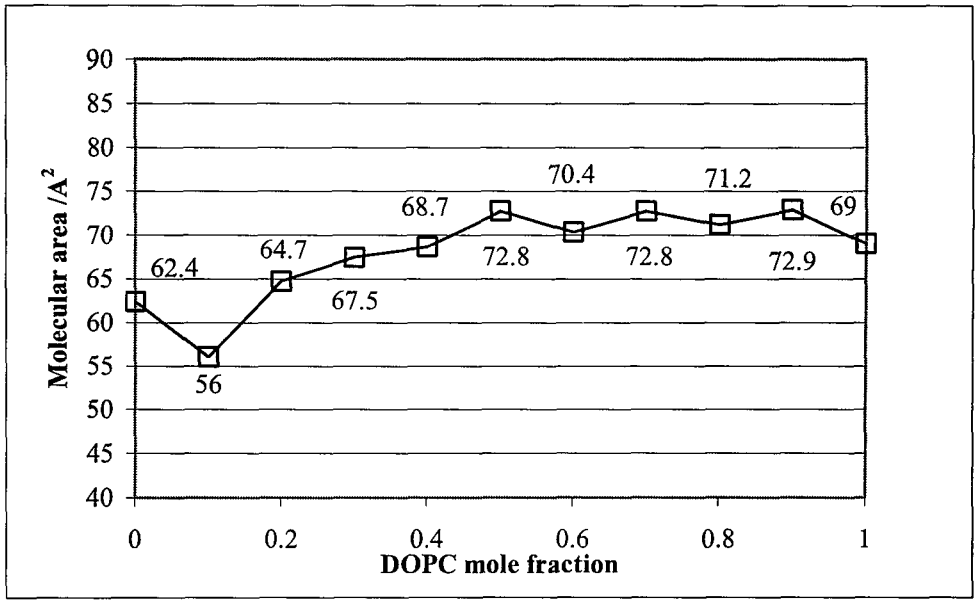

Figure 7.7 Head-group areas measured for mixtures with different DMPC/DOPC ratio. The head-group areas shown in this graph were measured after the third isocycle at 25 mM/m. Experimental conditions are reported in 7.2.2. The indicated values are reported in Table 7.1

Table 7.1 Head-group areas for the DMPC/DOPC mixtures. $A_{15}(1)$ and $A_{25}(1)$ are the head-group areas measured at 15 and 25 mN/m, respectively, during the first compression; $A_{15}(3)$ and $A_{25}(3)$ correspond to the head-group areas at 15 and 25 mN/m, respectively, after three cycles of compression and decompression.

DOPC (mole fraction)	$A_{15}(1)$ (Å^2)	$A_{25}(1)$ (Å^2)	$A_{15}(3)$ (Å^2)	$A_{25}(3)$ (Å^2)
0	72.7	63.3	70.5	62.4
0.1	64.3	56.2	63.5	56
0.2	75.8	66.2	73.6	64.7
0.3	79.6	69.3	76.8	67.5
0.4	78.4	69.1	77.4	68.7
0.5	83.3	73.4	82	72.8
0.6	80.2	70.6	79.2	70.4
0.7	83.5	73.7	82.4	72.8
0.8	85	74.5	81.7	71.2
0.9	87.6	76.4	83.7	72.9
1	81.1	70.2	77.9	69

Linear regression analysis was applied to calculate the trend for the curve in Figure 7.7 and the head-group areas for DMPC and DOPC. In particular, the calculated areas were 62.0 and 74.1 Å^2 for DMPC and DOPC, respectively[a]. As expected, the presence of oleyl chains in DOPC causes an increase of the head-group area proportional to the phospholipid molar fraction.

Head-group areas for the DOPC/DOPE mixtures are shown in Figure 7.8, whilst the areas at 15 and 25 mN/m, for the first and the third isocycle, are reported in Table 7.2. Because the ethanolamine group is smaller than the choline one, a decrease of the head-group area was expected to be proportional to the DOPE molar fraction. Differently from what was expected, it was instead found that the head-group area increased by increasing the molar fraction of DOPE.

[a] The linear trend was calculated using the method of least squares. The equation obtained from the analysis was: $y = 12.04 \cdot x + 62.02$ with $r^2 = 0.58$, where y is the head-group area for the DMPC/DOPC mixture when the DOPC molar fraction is x.

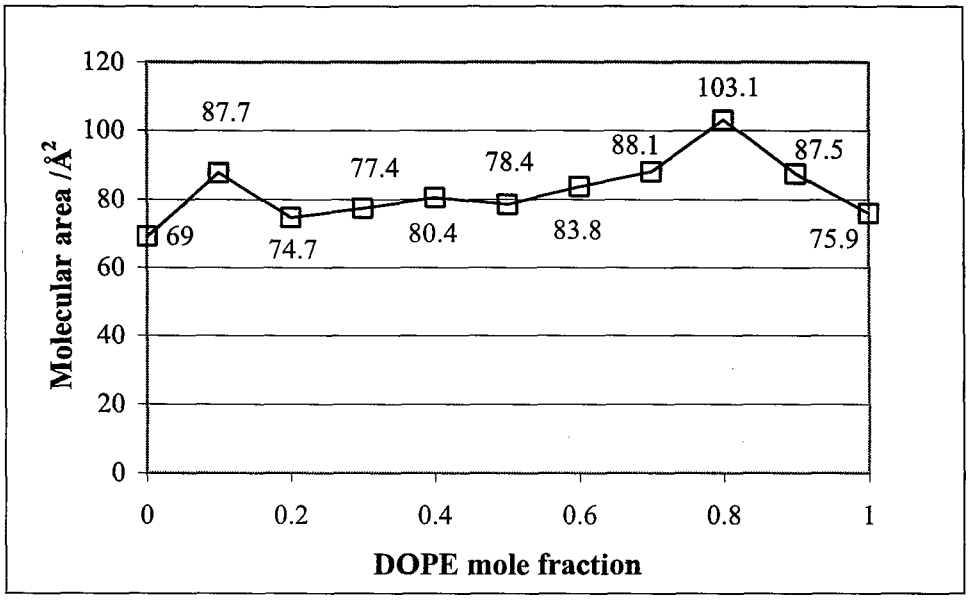

Figure 7.8 Head-group areas measured for different DOPC/DOPE mixtures. The head-group areas shown were measured at 25 mN/m after the third isocycle. Experimental conditions are reported in 7.2.2. The indicated values are reported in Table 7.2

Table 7.2 Head-group area for the DOPC/DOPE mixtures. $A_{15}(1)$ and $A_{25}(1)$ are the head-group areas measured at 15 and 25 mN/m, respectively, after one monolayer compression; $A_{15}(3)$ and $A_{25}(3)$ correspond to the head-group areas at 15 and 25 mN/m, respectively, after three cycles of compression and decompression.

DOPE (mole fraction)	$A_{15}(1)$ (Å^2)	$A_{25}(1)$ (Å^2)	$A_{15}(3)$ (Å^2)	$A_{25}(3)$ (Å^2)
0	81.1	70.2	77.9	69
0.1	100.8	88.5	98.1	87.7
0.2	90.8	78.8	86.5	74.7
0.3	90.3	78.8	87.6	77.4
0.4	92.5	81.4	91.3	80.4
0.5	91.7	80.3	89.6	78.4
0.6	97	85	94.3	83.8
0.7	100.5	88.6	98.7	88.1
0.8	120.6	104.7	116.3	103.1
0.9	100.6	88.5	98.9	87.5
1	89.7	78.5	85.3	75.9

As for DMPC/DOPC, linear regression analysis was applied to calculate the linear trend of the head-group areas measured for the DOPC/DOPE mixtures. The calculated areas were 75.8 and 88.9 Å^2 for DMPC and DOPC, respectively[b].

A second set of data was obtained by repeating each experiment twice. Conditions used for the head-group area measurement are reported in 7.2.2. Figure 7.9 shows the average head-group area for each DMPC/DOPC mixture measured during the first isocycles at 15 and 25 mN/m; the same data and the standard deviations are listed in Table 7.3 and Table 7.4. The head-group areas were found to be 64.4 and 82.2 Å^2 for DMPC and DOPC, respectively, by linear regression analysis[c].

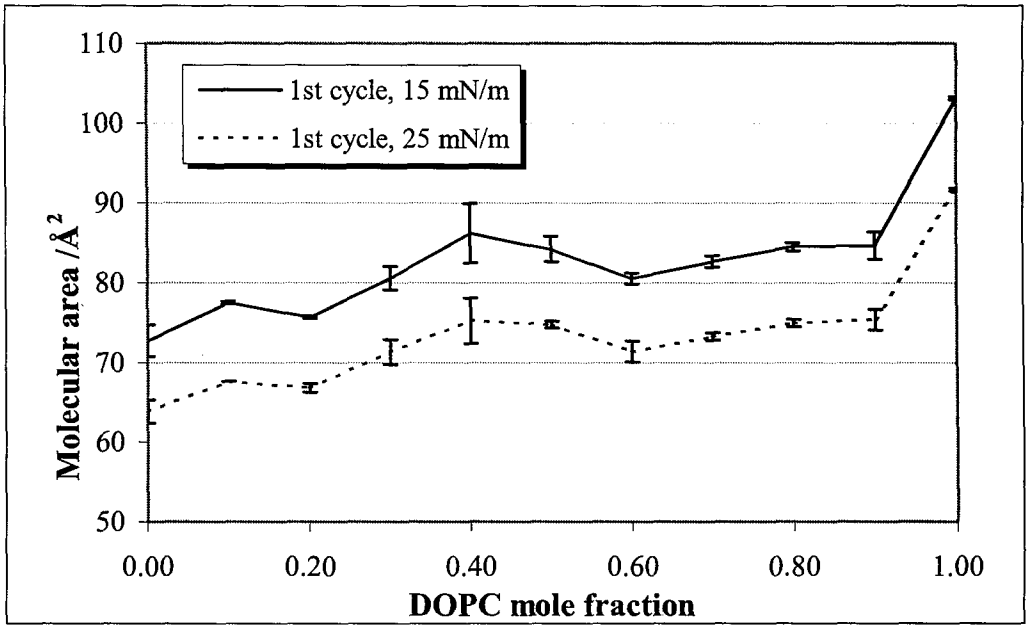

Figure 7.9 DMPC/DOPC head-group areas measured during the 1st cycle at 15 and 25 mN/m. The error bars correspond to ± the standard deviations calculated on two measurements.

[b] The equation obtained from the data analysis using the method of least squares was: $y = 13.06 \cdot x + 75.83$ with $r^2 = 0.22$, where y is the head-group area for the DOPC/DOPE mixture when the DOPE molar fraction is x.

[c] The linear trend was calculated using the method of least squares. The equation obtained from the analysis was: $y = 17.72 \cdot x + 64.44$ with $r^2 = 0.66$, where y is the head-group area for the DMPC/DOPC mixture when the DOPC molar fraction is x.

Table 7.3 DMPC/DOPC head-group areas measured at 15 mN/m during the first isocycle.

DOPC (mole fraction)	A(1) (Å^2)	A(2) (Å^2)	<A> (Å^2)	Std. Dev. (Å^2)
0.0	74.1	71.3	72.7	2.0
0.1	77.6	77.4	77.5	0.2
0.2	75.8	75.5	75.7	0.2
0.3	81.6	79.5	80.7	1.5
0.4	88.9	83.6	86.3	3.7
0.5	85.4	83.1	84.2	1.6
0.6	80.0	81.0	80.5	0.7
0.7	83.2	82.1	82.7	0.7
0.8	84.2	84.9	84.6	0.5
0.9	85.9	83.4	84.6	1.7
1.0	103.0	103.3	103.2	0.2

Table 7.4 DMPC/DOPC head-group areas measured at 25 mN/m during the first isocycle.

DOPC (mole fraction)	A(1) (Å^2)	A(2) (Å^2)	<A> (Å^2)	Std. Dev. (Å^2)
0.0	64.9	62.8	63.9	1.5
0.1	67.6	67.7	67.7	0.02
0.2	66.4	67.2	66.8	0.5
0.3	72.4	70.2	71.3	1.5
0.4	77.3	73.2	75.3	2.9
0.5	74.5	75.1	74.8	0.4
0.6	70.5	72.3	71.4	1.3
0.7	73.6	72.9	73.3	0.5
0.8	74.6	75.3	74.9	0.5
0.9	76.3	74.5	75.4	1.3
1.0	91.6	91.9	91.7	0.2

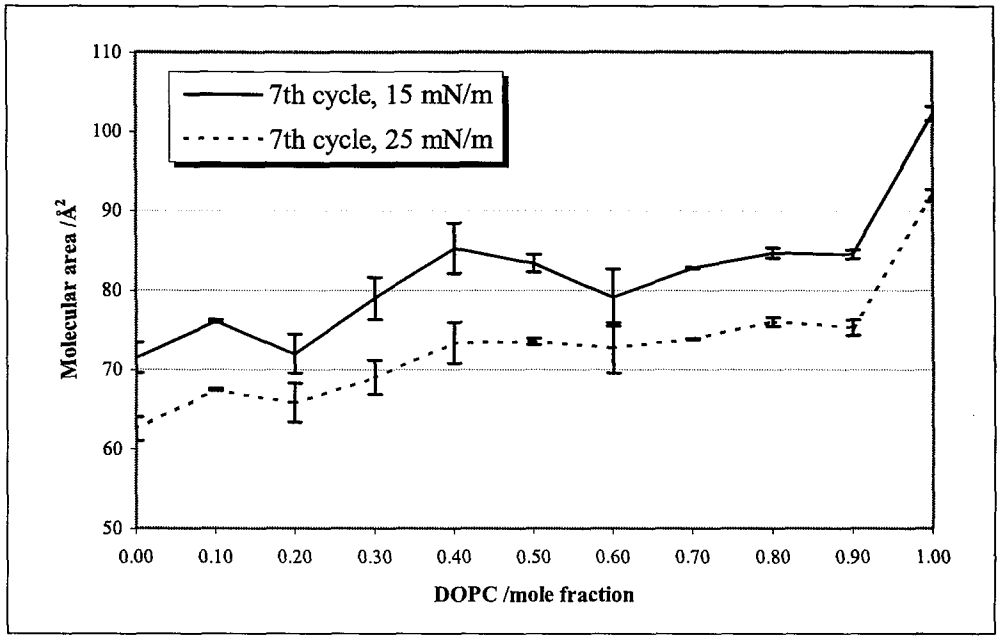

Figure 7.10 DMPC/DOPC head-group areas measured at 15 and 25 mN/m after seven isocycles. The values plotted are the average of two separate measurements.

The average of the head-group areas measured during the seventh isocycle are shown in Figure 7.10, whilst the single measurements, the averages and the standard deviation are reported in Table 7.5 and Table 7.6. The head-group areas were found to be 63.0 and 82.8 $Å^2$ for DMPC and DOPC, respectively[d]. As expected, the head-group area increased as DOPC molar fraction increased. Differently from the previous set, the difference in the head-group areas between DMPC and DOPC was 12 and 19.8 $Å^2$ for the first and the second set respectively. Furthermore, the DOPC head-group area result was higher than expected from the trend of the molar fraction/head-group area curve. Figure 7.11 and Figure 7.12 show head-group areas for DOPC/DOPE mixtures during the first and the seventh isocycle, respectively. The values for the single measurements, average and standard deviation for the data plotted in Figure 7.11, are reported in Table 7.7 and Table 7.8.

[d] The equation obtained from the data analysis using the method of least squares was: $y = 19.83 \cdot x + 62.96$ with $r^2 = 0.74$, where y is the head-group area for the DMPC/DOPC mixture when the DOPC molar fraction is x.

Table 7.5 DMPC/DOPC head-group areas measured at 15 mN/m after seven isocycles.

DOPC (mole fraction)	A(1) (Å^2)	A(2) (Å^2)	<A> (Å^2)	Std. Dev. (Å^2)
0.0	72.8	70.1	71.5	1.9
0.1	76.2	76.0	76.1	0.2
0.2	70.3	73.8	72.0	2.5
0.3	80.9	77.2	79.0	2.6
0.4	87.5	83.0	85.2	3.5
0.5	84.1	82.5	83.3	1.1
0.6	76.5	81.6	79.1	3.6
0.7	82.8	82.7	82.8	0.1
0.8	84.2	85.1	84.7	0.6
0.9	84.9	84.1	84.5	0.5
1.0	101.6	102.9	102.2	0.9

Table 7.6 DMPC/DOPC head-group areas measured at 25 mN/m after seven isocycles.

DOPC (mole fraction)	A(1) (Å^2)	A(2) (Å^2)	<A> (Å^2)	Std. Dev. (Å^2)
0.00	64.60	62.50	63.55	1.48
0.10	67.32	67.47	67.40	0.11
0.20	62.36	65.84	64.10	2.46
0.30	72.06	69.03	70.55	2.14
0.40	77.00	73.38	75.19	2.56
0.50	74.12	73.54	73.83	0.41
0.60	68.27	72.74	70.51	3.16
0.70	73.78	73.89	73.84	0.08
0.80	75.26	76.06	75.66	0.57
0.90	76.66	75.31	75.99	0.95
1.00	90.85	91.91	91.38	0.75

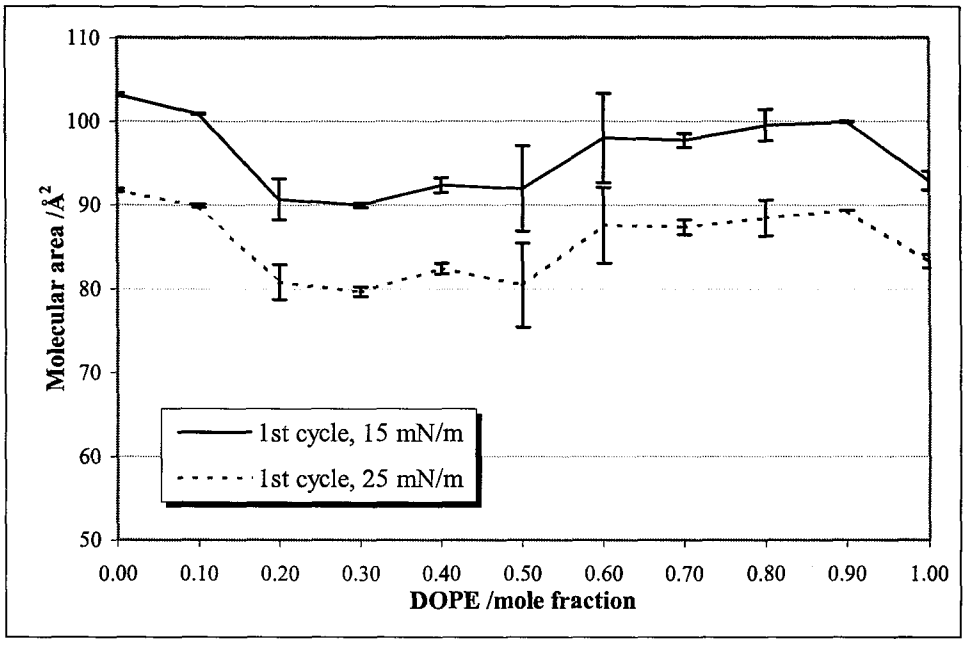

Figure 7.11 DOPC/DOPE head-group areas measured at 15 and 25 mN/m after one isocycle. The areas plotted correspond to the average of two separate measurements.

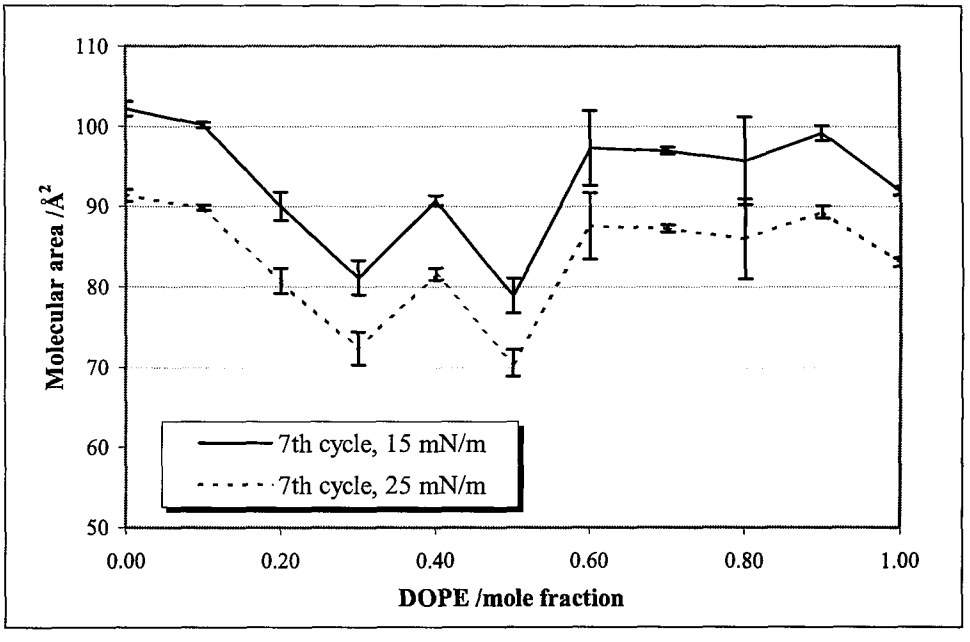

Figure 7.12 DOPC/DOPE head-group areas measured at 15 and 25 mN/m after seven isocycles. The plotted areas are the average of two separate measurements.

Table 7.7 DOPC/DOPE head-group areas measured at 15 mN/m after one isocycle.

DOPE (mole fraction)	A(1) (Å^2)	A(2) (Å^2)	<A> (Å^2)	Std. Dev. (Å^2)
0.0	103.0	103.3	103.2	0.2
0.1	100.8	101.0	100.9	0.1
0.2	92.4	88.9	90.7	2.5
0.3	89.8	90.1	90.0	0.3
0.4	93.0	91.7	92.4	0.9
0.5	88.3	95.5	91.9	5.1
0.6	101.7	94.2	98.0	5.3
0.7	98.3	97.1	97.7	0.8
0.8	98.2	100.9	99.5	1.9
0.9	99.9	100.0	99.9	0.1
1.0	92.1	93.7	92.9	1.1

Table 7.8 DOPC/DOPE head-group areas measurement at 25 mN/m after one isocycle

DOPE (mole fraction)	A(1) (Å^2)	A(2) (Å^2)	<A> (Å^2)	Std. Dev. (Å^2)
0.0	91.6	91.9	91.7	0.2
0.1	89.8	90.0	89.9	0.2
0.2	82.3	79.4	80.8	2.1
0.3	79.3	80.1	79.7	0.6
0.4	82.9	82.0	82.4	0.6
0.5	76.9	83.9	80.4	5.0
0.6	90.8	84.3	87.6	4.5
0.7	88.0	86.7	87.3	0.9
0.8	86.9	90.0	88.5	2.2
0.9	89.3	89.3	89.3	0.01
1.0	82.8	83.8	83.3	0.7

Table 7.9 DOPC/DOPE head-group areas measured after seven isocycles at 15 mN/m.

DOPE (mole fraction)	A(1) (Å^2)	A(2) (Å^2)	<A> (Å^2)	Std. Dev. (Å^2)
0.0	101.6	102.9	102.2	0.9
0.1	99.9	100.4	100.2	0.4
0.2	91.3	88.8	90.0	1.8
0.3	79.7	82.7	81.2	2.2
0.4	90.3	91.2	90.7	0.6
0.5	77.4	80.5	78.9	2.2
0.6	100.6	94.0	97.3	4.7
0.7	97.3	96.7	97.0	0.4
0.8	91.9	99.6	95.7	5.5
0.9	99.9	98.6	99.2	0.9
1.0	91.6	92.4	92.0	0.6

Table 7.10 DOPC/DOPE head-group area measured at 25 mN/m after seven isocycles.

DOPE (mole fraction)	A(1) (Å^2)	A(2) (Å^2)	<A> (Å^2)	Std. Dev. (Å^2)
0.0	90.9	91.9	91.4	0.8
0.1	89.6	90.1	89.8	0.4
0.2	81.8	79.6	80.7	1.6
0.3	70.9	73.8	72.3	2.1
0.4	81.1	82.1	81.6	0.7
0.5	69.4	71.7	70.5	1.7
0.6	90.5	84.7	87.6	4.1
0.7	87.6	87.0	87.3	0.5
0.8	82.5	89.5	86.0	5.0
0.9	89.9	88.8	89.3	0.8
1.0	82.7	83.4	83.1	0.5

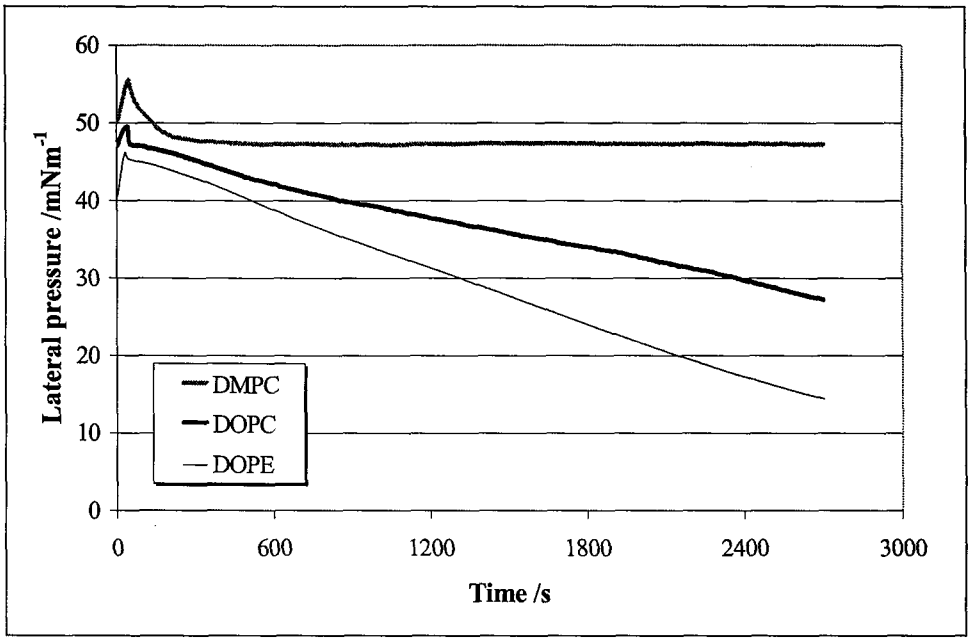

Figure 7.13 DMPC, DOPC and DOPE monolayer stability.

Linear regression analysis of the data from the first isocycle gave very similar values for DOPC and DOPE head-group areas, 85.6 and 85.7 Å^2 respectively[e]. Data for the curves of Figure 7.12 are reported in Table 7.9 and Table 7.10. The regression analysis consistently gave 83.2 and 84.0 Å^2 for the head-group areas of DOPC and DOPE, respectively[f].

7.3.3 Monolayer stability

Monolayer stability was investigated to verify the possibility of obtaining data in conditions of high lateral pressure and for long experiment times. DMPC, DOPC and DOPE monolayers were prepared as reported in 7.2.4, and were compressed to the collapse point (Figure 7.13).

---

[e] The equation obtained from the data analysis using the method of least squares was: $y = -0.094 \cdot x + 85.58$ with $r^2 = 0.0001$, where y is the head-group area for the DOPC/DOPE mixture when the DOPE molar fraction is x.

[f] The linear trend was calculated using the method of least squares. The equation obtained from the analysis was: $y = 0.74 \cdot x + 83.22$ with $r^2 = 0.0013$, where y is the head-group area for the DMPC/DOPC mixture when the DOPC molar fraction is x.

DMPC monolayers appeared to be the most stable, as shown in Figure 7.13; after the monolayer collapsed, the pressure decreased reaching and stabilising at the value corresponding to the change of phase (Figure 7.4) for at least 40 minutes.

DOPC and DOPE mixtures showed a completely different behaviour. In fact, after the monolayer collapse, both monolayers were characterised by a continuous pressure decrease, bringing the lateral pressure close to zero. Whilst DMPC is a type 0 lipid, DOPC and DOPE are type II lipids, meaning that they have a negative radius of curvature, and the force distribution along the molecules makes them bend towards the water phase. The collapse of a monolayer usually involves the displacement of part of the monolayer from the air/water interface, slipping on the surface of the monolayer portion remaining at the interface or a possible reorganisation of the monolayer structures (7.1). Because of the bending energy stored in the flat monolayer of both DOPC and DOPE, it is possible that the collapse starts a process of monolayer structural re-organization, able to release the excess of stored bending energy. The DOPE bending modulus and radius of curvature are respectively higher and smaller than the corresponding DOPC values. Consequently, the bending energy stored in the DOPE monolayer is higher than the one store in the DOPC monolayers. The bending moduli and the radius of curvature for DOPC are $9k_BT$ and –160 Å while the ones for DOPE are 13 k_BT and –53 Å [10]. The energy stored in a flat monolayer[g], per unit area, is then ~17.6×10^{-6} k_BT Å^{-2} for DOPC and ~2.31×10^{-3} k_BT Å^{-2} for DOPE. Figure 7.13 shows that the pressure decreases more rapidly for DOPE than for DOPC, in apparent agreement with the bending energy stored in their flat monolayers.

Figure 7.14 shows the DOPE pressure/time isotherm recorded when the starting lateral pressure was close to zero (7.2.4). After two hours of pressure recording, the monolayer was compressed to the minimum of the trough area; Figure 7.15 shows that the lateral pressure was ~11 mN/m when the head-group area was ~15 Å^2.

---

[g] The bending energy g_{curv} was calculated using a simplified form of **Eq. 4.14**: $g_{curv} = \frac{1}{2}\kappa_M (c_1 + c_2 - 2c_0)^2$

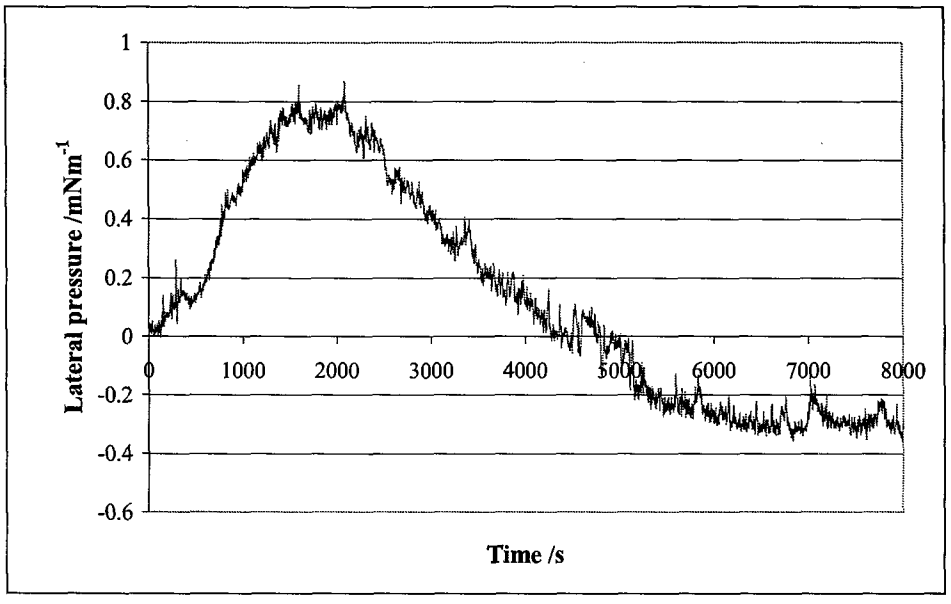

Figure 7.14 DOPE monolayer pressure/time isotherm was recorded on 0.1 M NaCl at 37 °C. The lipid chloroform solution was spread on the aqueous phase and the pressure monitored for more than two hours without any compression.

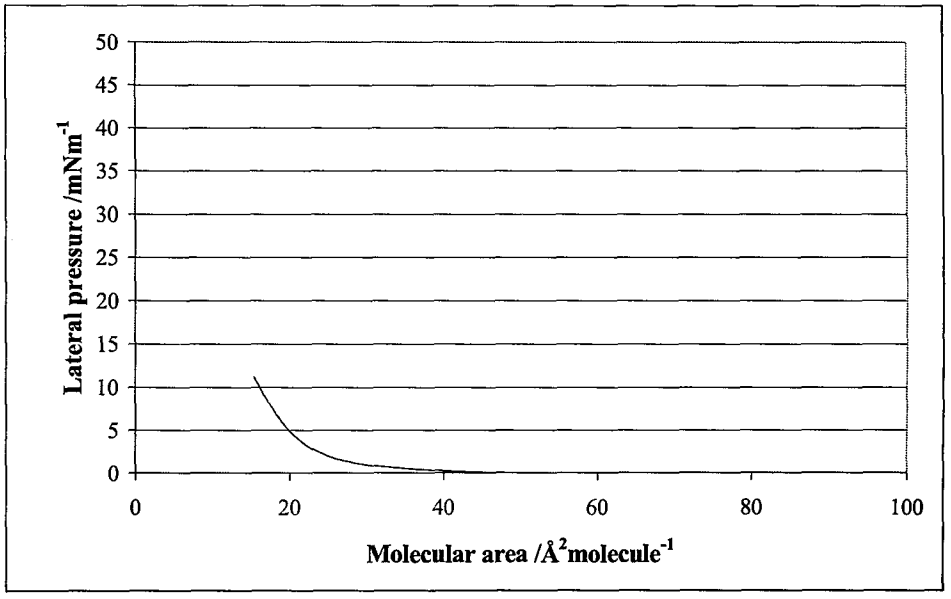

Figure 7.15 DOPE pressure/area isotherm of the monolayer whose pressure was monitored for two hours as shown in Figure 7.14

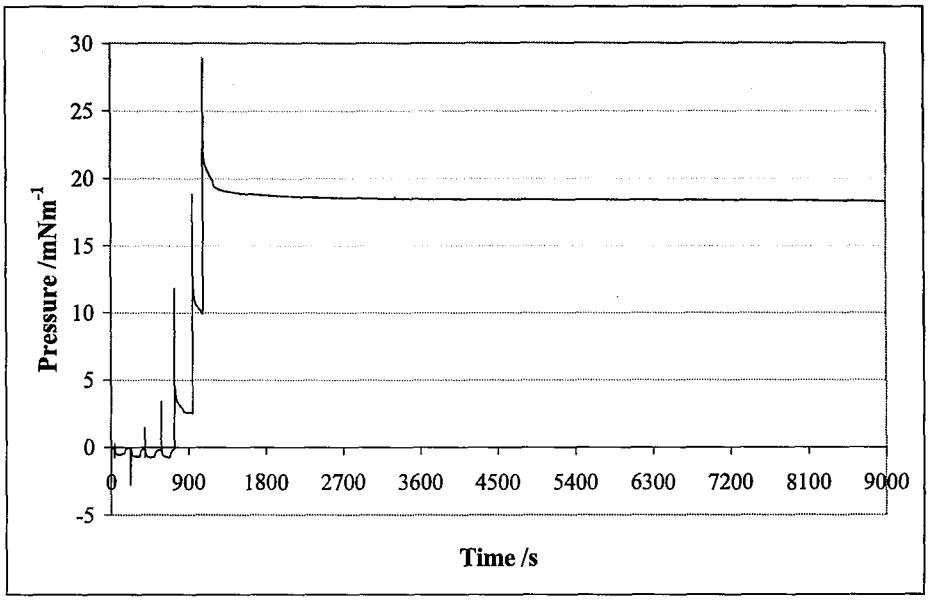

Figure 7.16 DOPC monolayer stability on a fixed area trough.

Differently from DOPE, DOPC monolayers are stable if the monolayer is not compressed over the collapse point, as shown in Figure 7.16. The spikes in the figure are due to the addition of the DOPC chloroform solution to the water surface. It should be noted that the DOPC monolayer remained stable at ~19 mN/m for at least two hours after the preparation.

7.4 Discussion

7.4.1 Pressure/area isotherms

Figure 7.17 and Figure 7.18 show the different isotherms for DMPC, DOPC and DOPE (7.3.1) recorded under the same conditions. The head-group area increased, as expected, going from DMPC to DOPC, due to the higher area in the oleyl chain region. Rather unexpectedly, the head-group area increased going from DOPC to DOPE, even if the ethanolamine group is smaller than the choline one. It could be possible that oleyl chains prevailed in determining the head-group area or that a particular monolayer structure formation increased the area occupied by DOPE at the air/water interface.

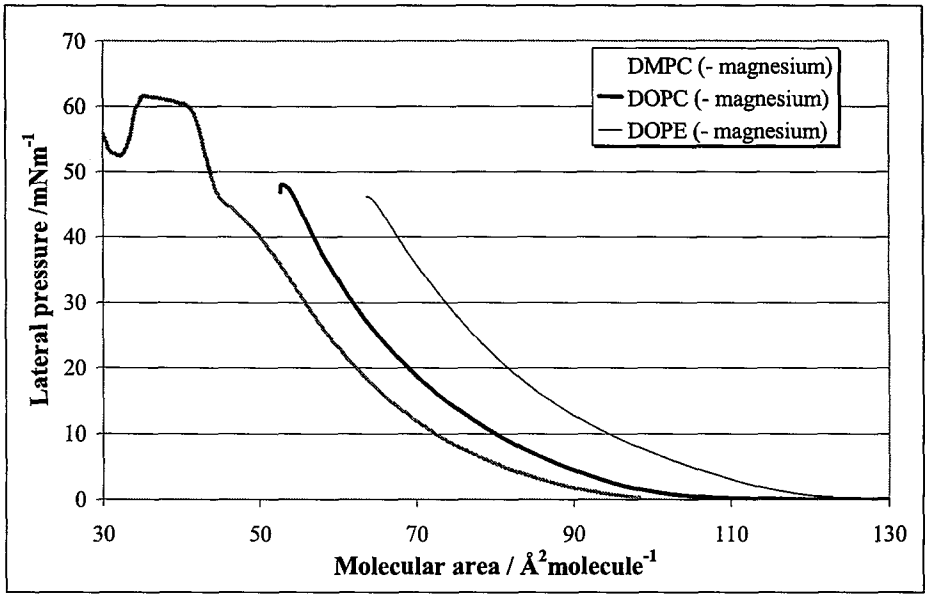

Figure 7.17 DMPC, DOPC and DOPE pressure/area isotherms recorded on 0.1 M NaCl at 20 °C (7.3.1).

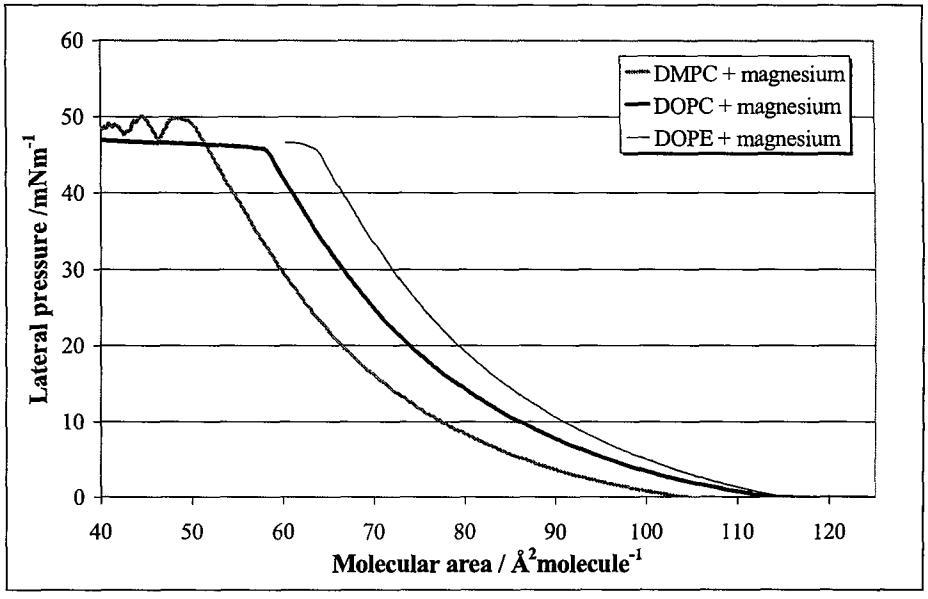

Figure 7.18 DMPC, DOPC and DOPE pressure/area isotherms recorded on 0.1 M NaCl, 0.1 M Tris-HCl at pH 7.2, and 10 mM $MgCl_2$ (7.3.1).

7.4.2 *Head-group area of DMPC/DOPC and DOPC/DOPE mixtures*

The head-group areas for the DMPC/DOPC mixtures, even if slightly different for the two reported set of experiments, were still in agreement with what was expected. DOPC/DOPE mixtures have shown different results for the two sets of experiments. It is possible that monolayers of DOPC/DOPE mixtures have particular structures that could result in higher head-group areas.

7.4.3 *Monolayer stability*

DOPE behaved differently from the DMPC and DOPC, especially when their monolayer stability was investigated. Even if DOPC and DOPE are both type II amphiphiles, DOPE monolayers were found to be unstable even when the lateral pressure was close to zero, while DOPC ones remained stable even when compressed to 20 mN/m. The bending energy stored in a flat monolayer could justify the observed instability and it could also justify the different behaviour of DOPC and DOPE monolayers, being the bending energy for DOPE being almost 130 times higher than the one for DOPC monolayers.

In the previous discussion it was suggested that different monolayer structures could be the cause of the differences observed amongst the monolayers of the three phospholipids. A hypothetical mechanism of monolayer reorganisation is shown in Figure 7.19. The intermediate structure B, with the formation of the domains "d", could explain the increase in the lateral pressure observed for the DOPE pressure/time isotherm (Figure 7.14); C and D structures could be responsible for the observed decreased lateral pressure and for the extremely low molecular area observed in the DOPE pressure/area isotherm (Figure 7.15). Because of the smaller bending energy, it is possible that DOPC monolayers can reorganise the structure only if the process is triggered by the monolayer collapse.

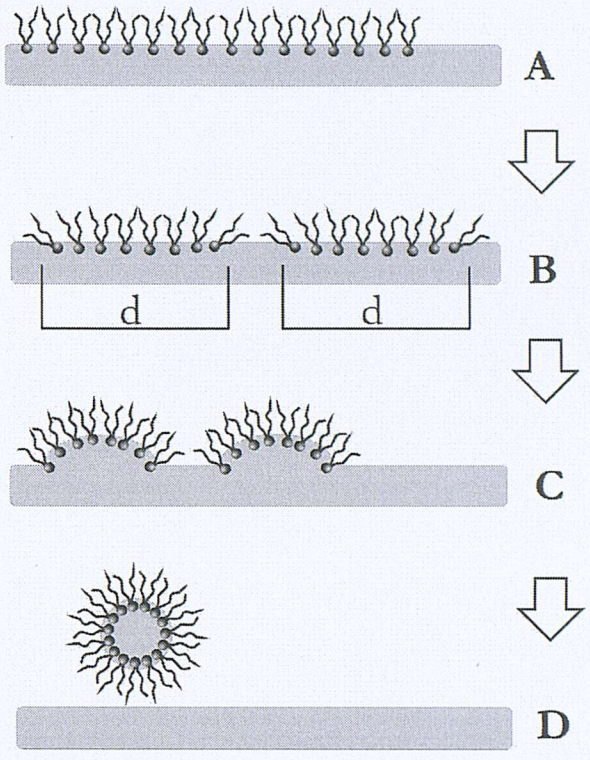

Figure 7.19 The monolayer structure A could be reorganised to the final structure D through the intermediate B and C. The monolayer A, constituted by type II lipids, is under stress when constrained in a flat position. The first step in the reorganisation, B, could involve the formation of expanded domains "d" causing the initial increase of the monolayer area or alternatively, if the area is fixed, the increase of the lateral pressure. The following structure, C, corresponds to a structure halfway between the monolayer and the inversed phase showed in the structure D.

7.5 Conclusions

The aims of the experiments discussed in this chapter were to gain a better understanding of the possibility and the limit of applicability of lipid monolayers as a model system of biological membranes. Several considerations follow the analysis of the result previously discussed:

- DOPC and DOPE, both type II lipids, are unstable after the collapse of their monolayers. On the contrary, DMPC, a type 0 lipid, remained stable after the collapse, which occurred when the lateral pressure reached the value correspondent to the passage from the expanded to the condensed liquid phase.

- Monolayer instability seems to be related to the bending energy of the lipid constituting the monolayer; a DOPE monolayer is less stable than a DOPC one because of the higher bending energy (almost 130 fold bigger than the DOPC one) stored.

The conclusion is that monolayers cannot be used if their constituents are subjected to excessive stress[h].

7.6 References

[1] Phillips, M. C., Ladbrooke, B.D., and Chapman, D., "Molecular interactions in mixed lecithin systems," in *Biochimica et Biophysica Acta*, vol. 196, 1970, pp. 29-34.

[2] Phillips, M. C., and Chapman, D., "Monolayer characteristic of saturated 1,2-diacyl-phosphatidylcholines (lecithin) and phosphatidylethanolamines at the air-water interface," in *Biochimica et Biophysica Acta*, vol. 163, 1968, pp. 301-313.

[3] Joos, P., and Demel, R.A., "The interaction energies of cholesterol and lecithin in spread mixed monolayers at the air-water interface," in *Biochimica et Biophysica Acta*, vol. 183, 1969, pp. 447-457.

[4] Chapman, D., Owens, N.F., Walker, D.A., "Monolayer studies of some synthetic 2,3-diacyl-dl-phosphatidylethanolamines and phosphatidylcholines containing trans double bonds," in *Biochimica et Biophysica Acta*, vol. 120, 1966, pp. 148-155.

[5] Smaby, J. M., and Brockman, H.L., "Miscibility, chain packing, and hydration of 1-palmitoyl-2-oleyl-phosphatidylcholine and other lipids in surface phases," in *Biophysical Journal*, vol. 48, 1985, pp. 701-708.

[6] Smaby, J. M., and Brockman, H.L., "Surface dipole moments of lipids at the argon-water interface," in *Biophysical Journal*, vol. 58, 1990, pp. 195-204.

[7] Petty, M. C., *Langmuir-Blodgett films*. Cambridge: Cambridge University Press, 1996.

[h] Even if Type I amphiphiles were not investigated, it is a reasonable hypothesises that stressed monolayers can reorganise the structure in micelles going from the air/water interface to the water phase (7.1) as a consequence of the monolayer collapse.

[8] Koynova, R., and Caffrey, M., "Phases and phase transitions of phosphatidylcholines," in *Biochimica et Biophysica Acta*, vol. 1376, 1998, pp. 91-145.

[9] Beitinger, V., Mobius, D., and Rahmann, H., "Surface potentials and electric dipole moments of ganglioside and phospholid monolayers: contribution of the polar head-group ate the air/water interface," in *Biochimica et Biophysica Acta*, vol. 984, 1989, pp. 293-300.

[10] Attard, G. S., Templer, R.H., Smith, W.S., Hunt, A.N., and Jackowski, S., "Modulation of CTP: phosphocholine cytidylyltransferase by membrane curvature elastic stress," in *Proceedings of the National Academy of Sciences of the United States of America*, vol. 97, 2000, pp. 9032-9036.

8 Peptide adsorption onto monolayers

8.1 Adsorption of proteins at interface

Analysis of protein or peptide adsorption at the air/water interface can be used to obtain information about protein hydrophobic or hydrophilic character, secondary structure or the thermodynamics of folding/unfolding [1].

Proteins in solution are free to move from the bulk solution to the air/water interface, forming a monolayer. The phenomenon by which proteins or peptides reach the air/water interface is called "adsorption". An equation describing the adsorption phenomenon is given by

Eq. 8.1 $$n = 2C_b\left(\frac{Dt}{\pi}\right)^{\frac{1}{2}}$$

where n is the number of molecules per unit area, C_b is the bulk concentration of the protein and D is its diffusion coefficient [2]. If the surface pressure is kept constant and the increase of surface area at the interface is measured, the rate of adsorption can be given by the equation

Eq. 8.2 $$\frac{dn}{dt} = \frac{1}{A}\frac{dA}{dt}n$$

where $(1/A)(dA/dt)$ is the fractional rate of the increase of surface area and n is the concentration (mg/m^2) of surfactant at the constant pressure at which the area is measured [2]. If the adsorption occurs at constant area, the relationship between adsorption and pressure is given by

Eq. 8.3 $$\left(\frac{dn}{dt}\right)_\pi = \left(\frac{d\pi}{dt}\right)_\pi\left(\frac{dn}{d\pi}\right)_\pi$$

where $(d\pi/dt)_\pi$ and $(dn/d\pi)_\pi$ are obtained from the adsorption curves and the monolayer compression curves, respectively [2]. Combining Eq. 8.1, Eq. 8.2, and Eq. 8.3, the rate of adsorption is shown to be dependent on the protein concentration C_b and on the monolayer pressure π [2]

Eq. 8.4 $$\frac{dn}{dt} = f(C_b, \pi)$$

If the adsorption is carried out at constant pressure, π, then the adsorption of the protein at the interface causes an increase in the monolayer area. If ΔA is the increase in area, the work required for this process is $\pi \cdot \Delta A$. Using the Boltzmann's distribution function, the reversible adsorption process at different values of π is given by

Eq. 8.5 $$\frac{dn}{dt} = k_1 a_b \exp\left(\frac{-\pi\Delta A}{kT}\right) - k_2 a_m \exp\left(\frac{\pi\Delta A}{kT}\right)$$

where k_1 and k_2 are the first-order rate constants for the adsorption and desorption process, and a_b and a_m are the activities of the solute in the bulk and at the surface, respectively [3]. If the adsorption process is irreversible and the activity coefficient is replaced by the concentration, the natural logarithm of Eq. 8.5 gives

Eq. 8.6 $$\ln\left(\frac{dn}{dt}\right) = \ln(k_1 C_b) - \frac{\pi\Delta A}{kT}$$

where $k_1 C_b$ is the rate of collision of a molecule with the surface [3].

If the molecule if charged and if ψ is the potential at the interface, electric work has to be spent to reach the interface from the bulk solution. Using the Debye-Hückel theory, the concentration of charged molecules close to the surface will be given by

Eq. 8.7 $$C = C_b \exp\left(\frac{-Q\,\psi}{kT}\right)$$

where C_b is the corresponding concentration at remote distance from the surface and Q is the charge carried by the molecule [4]. Consequently, the effect of electrical potential on the adsorption rate is given by [4]

Eq. 8.8 $$\frac{dn}{dt} = k_1 C_b \exp\left(\frac{-Q\psi}{kT}\right)$$

Combining Eq. 8.5, Eq. 8.7 and Eq. 8.8, the irreversible adsorption is given by [4]

Eq. 8.9 $$\frac{dn}{dt} = k_1 C_b \exp\left(\frac{-\pi\Delta A}{kT}\right)\exp\left(\frac{-Q\psi}{kT}\right)$$

or, in the logarithmic form

Eq. 8.10 $$\ln\left(\frac{dn}{dt}\right) = \ln(k_1 C_b) - \frac{\pi\Delta A + Q\psi}{kT}$$

The generalisation of the above equation for different kinds of work W (protein unfolding or folding could be required for the adsorption) gives [4]

Eq. 8.11 $$\ln\left(\frac{dn}{dt}\right) = \ln(k_1 C_b) - \frac{\pi\Delta A + Q\psi + W}{kT}$$

8.2 PPF2

PPF2 is a peptide whose sequence is similar to a portion of the M-domain (segment 251-268) of CCTα (**Table 3.2**) apart from the substitution of D-255 with E, of F-263 with V and of Q-265 with S:

```
                    251                     268
                     |                       |
CCTα(251-268)   KKVKDVEEKSKEFVQKVE
                      ↓       ↓ ↓
PPF2            KKVKEVEEKSKEVVSKVE
```

The hydrophobic moment profile of CCTα (Figure 8.1) shows that the highest hydrophobic moment corresponds to the M-domain, as expected for the role that this segment plays in binding to the membrane.

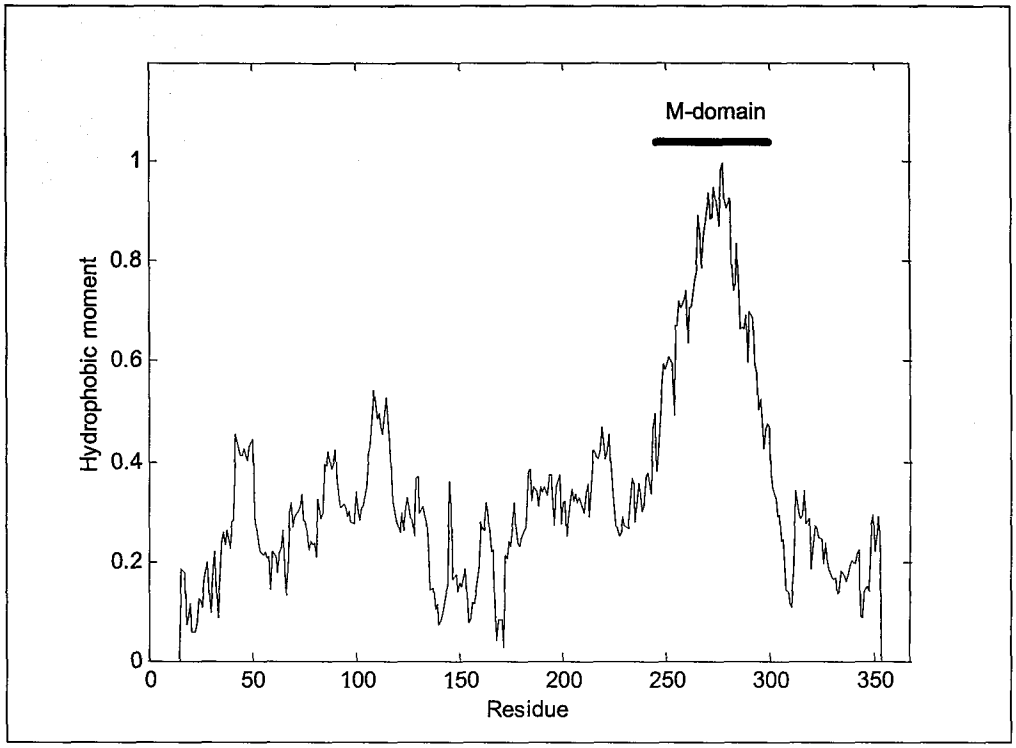

Figure 8.1 Hydrophobic moment profile of CCTα was calculated using the WIF scale (Table 5.1) and the Eisenberg algorithm (Eq. 5.2). The local hydrophobic moment (representing the average of a 31 residues window) has been normalized to the maximum value in the graph.

Table 8.1 Hydrophobic moment and hydrophobicity were calculated for CCTα(251-268) and for PPF2 using the WIF scale (Table 5.1) and the Eisenberg algorithm (Eq. 5.2). The hydrophobic moment per residue is indicated in brackets.

	Hydrophobicity	**Hydrophobic moment**
M-domain (237-299)	0.6	21.2 (0.34)
CCTα(251-268)	0.8	6.4 (0.36)
PPF2	0.9	5.6 (0.31)

The hydrophobic moments calculated for the M-domain, CCTα(251-268) and for PPF2 (the latters shown as α-helices in Figure 8.2) are reported in Table 8.1. Although the hydrophobicity values for CCTα(251-268) and PPF2 are higher than that determined for the M-domain, the hydrophobic moment per residue (value in brackets in Table 8.1) is similar for all three sequences. This allows the use of PPF2

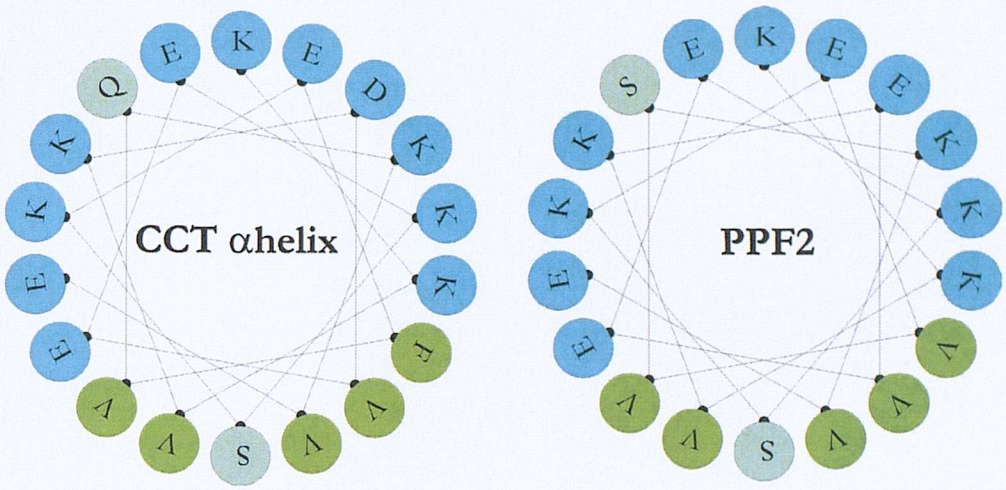

Figure 8.2 α-helical representation of the CCTα M-domain (segment 251-268) and PPF2. Charged residues are light blue, polar residues are sea-green and apolar residues are green. The hydrophobic strip formed by the apolar residues of the CCTα helix are involved in the binding to the membrane interface. PPF2 was used as model system of CCTα in the study of the torque tension effect on the partitioning of the enzyme on the lipid membrane.

to investigate the effects of the membrane surface properties on the partitioning of CTα onto monolayers or bilayers.

8.3 Material and methods

8.3.1 *Materials*

1,2-dimyristoyl-*sn*-glycero-3-phosphocholine (DMPC) and 1,2-dioleoyl-*sn*-glycero-3-phosphocholine (DOPC) were purchased from Fluka or Avanti Polar Lipids. Tris(hydroxymethyl)aminomethane (Tris), NaCl, $MgCl_2$, dimethyldichlorosilane, toluene, chloroform and ~ 26 % HCl were purchased from Sigma Aldrich. Water was deionised using an Elga Purelab deionisator system. Buffer A (0.1 M Tris-HCl, pH 7.2 at 37 °C, 0.1 M NaCl, 10.0 mM $MgCl_2$), buffer B (0.1 M Tris-HCl, pH 7.4 at 37 °C, 0.1 M NaCl, 10.0 mM $MgCl_2$) and water were filtered using Nylon66 filter disks 0.45 μm (Supelco) prior to use. pH was adjusted using a Hanna pHTester 3 metre. Isotherms were recorded using a glass trough (30 cm^2 fixed surface area)

mounting a PS4 sensor with platinum Wilhelmy plate (NIMA Technology, UK), silanised using a 5% (w/v) dimethyldichlorosilane in toluene. The fixed area trough was contained in a chamber filled with nitrogen to prevent oxidation of the monolayer lipids. *N*-α-Fmoc-*L*-glutamine, *N*-α-Fmoc-*L*-valine, Fmoc-*O*-*t*-butyl-*L*-serine, *N*-α-Fmoc-*N*-ε-*t*-Boc-*L*-Lysine and Rink amide MBHA resin were obtained from NovaBiochem. 1-hydroxybenzotriazole (HOBt), triethylamine acetate and acetonitrile were purchased from Acros Organics. Trifluoroacetic acid, piperidine, dichloromethane and N,N'-diisopropylcarbodiimide were obtained from Fluka.

8.3.2 PPF2 synthesis, purification and characterisation

PPF2 was synthesised by the Fmoc method [5] and purified by RP-chromatography, using a Perkin Elmer Prep-10 column (Octyl 20 μm, 250x10 mm) connected to a Gilson 321 Pump HPLC system; the purification method is given in Table 8.2. PPF2 was eluted in 13 minutes. PPF2 sequence was analysed by positive MS-MS ES. The molecular weight of the peptide and its amino acid sequence were confirmed by analysis of its fragmentation pathway shown in the MS spectrum, Figure 8.3 and Table 8.3. The fragmentation of an idealised peptide is reported in Figure 8.4.

Table 8.2 Method used for the purification of PPF2. Aqueous solvent: H_2O with 0.1% TFA; organic solvent: CH_3CN with 0.1% TFA.

Time (min)	Aqueous solvent (%)	Organic solvent (%)	Devices
0	100	0	UV/vis detector: 230 nm Flow: 3.0 ml/min
7	80	20	
20	60	40	
25	30	70	
30	30	70	
35	100	0	
45	100	0	

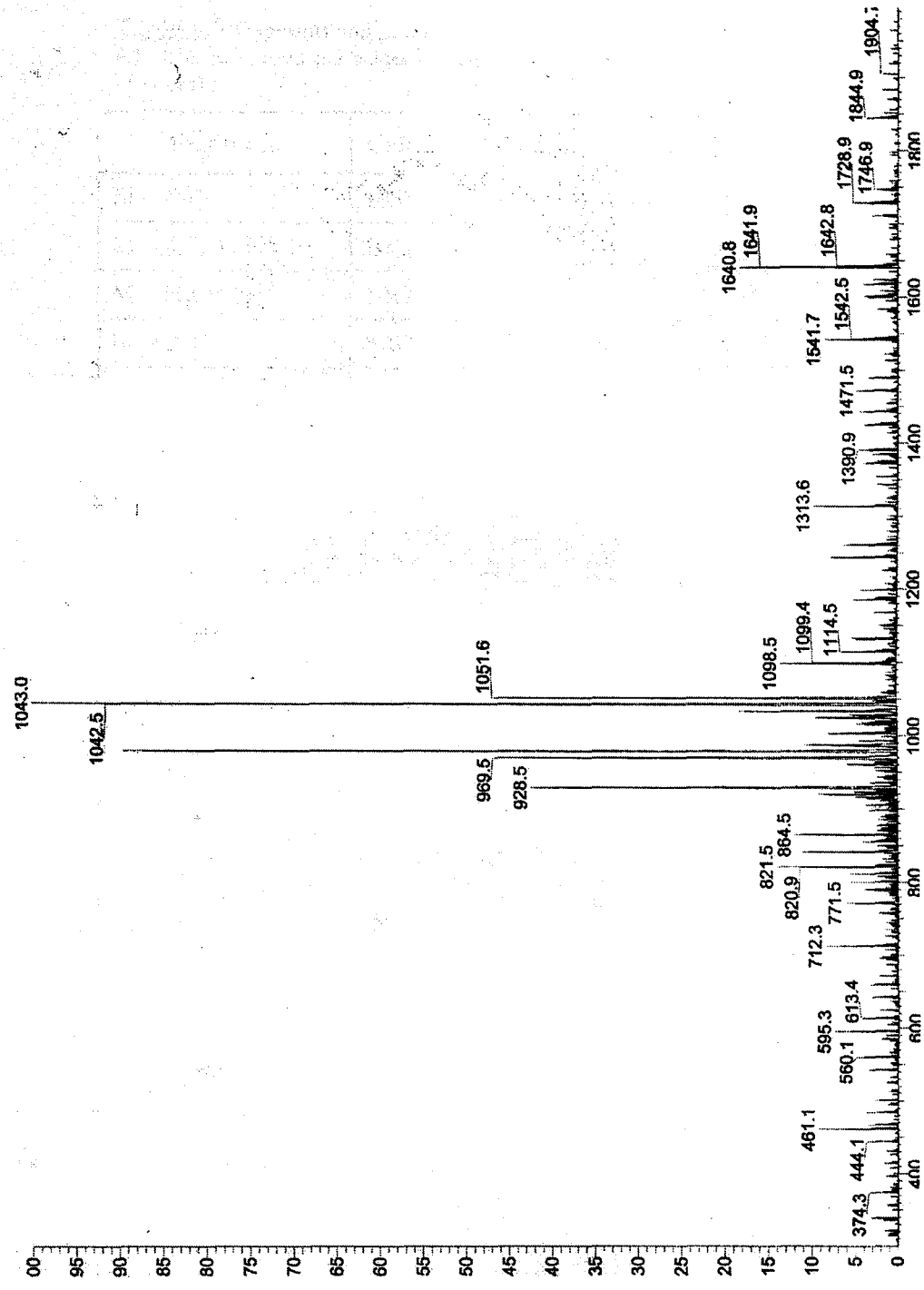

Figure 8.3 MS-MS ES spectrum of PPF2. The spectrum represent the secondary fragmentation of the peak at m/z 1051.1 ($[M+2H]^{2+}$).

Table 8.3 Fragments and peaks for the MS-MS analysis of PPF2 (Figure 8.3). The two calculated values correspond to the M and to the isotopic M+1 peaks.

Fragment	Calculated (m/z)	Found (m/z)
$M+2H^+$	1051.1/1051.6	1051.6
$M-NH_3+2H^+$	1042.6/1043.1	1043.0
$M-H_2O+2H^+$	1042.1/1042.6	1042.5
$b_{17}+2H^+$	978.1/978.6	978.5
$b_{17}-H_2O+2H^+$	969.6/970.1	969.5
$b_{16}+2H^+$	928.5/929.0	928.5
$b_{15}+H^+$	1728.0/1729.0	1728.9
$b_{15}+2H^+$	864.5/865.0	864.5
$b_{14}+H^+$	1641.0/1642.0	1640.8 and 1641.9
$b_{14}+2H^+$	821.0/821.5	820.9 and 821.5
$b_{13}+H^+$	1541.9/1542.9	1541.7 and 1542.5
$b_{13}+2H^+$	771.4/771.9	771.5
$b_{11}+H^+$	1313.8/1314.8	1313.6
b_9+H^+	1098.7/1099.7	1099.4
b_6+H^+	712.5/713.5	712.3
$y_{16}+H^+$	1845.0/1846.0	1844.9
$y_{15}+H^+$	1746.0/1747.0	1746.9
$y_{11}+H^+$	1389.8/1390.8	1390.9
y_5+H^+	560.3/561.3	560.1
y_4+H^+	461.3/462.3	461.1
y_3+H^+	374.2/375.2	374.3

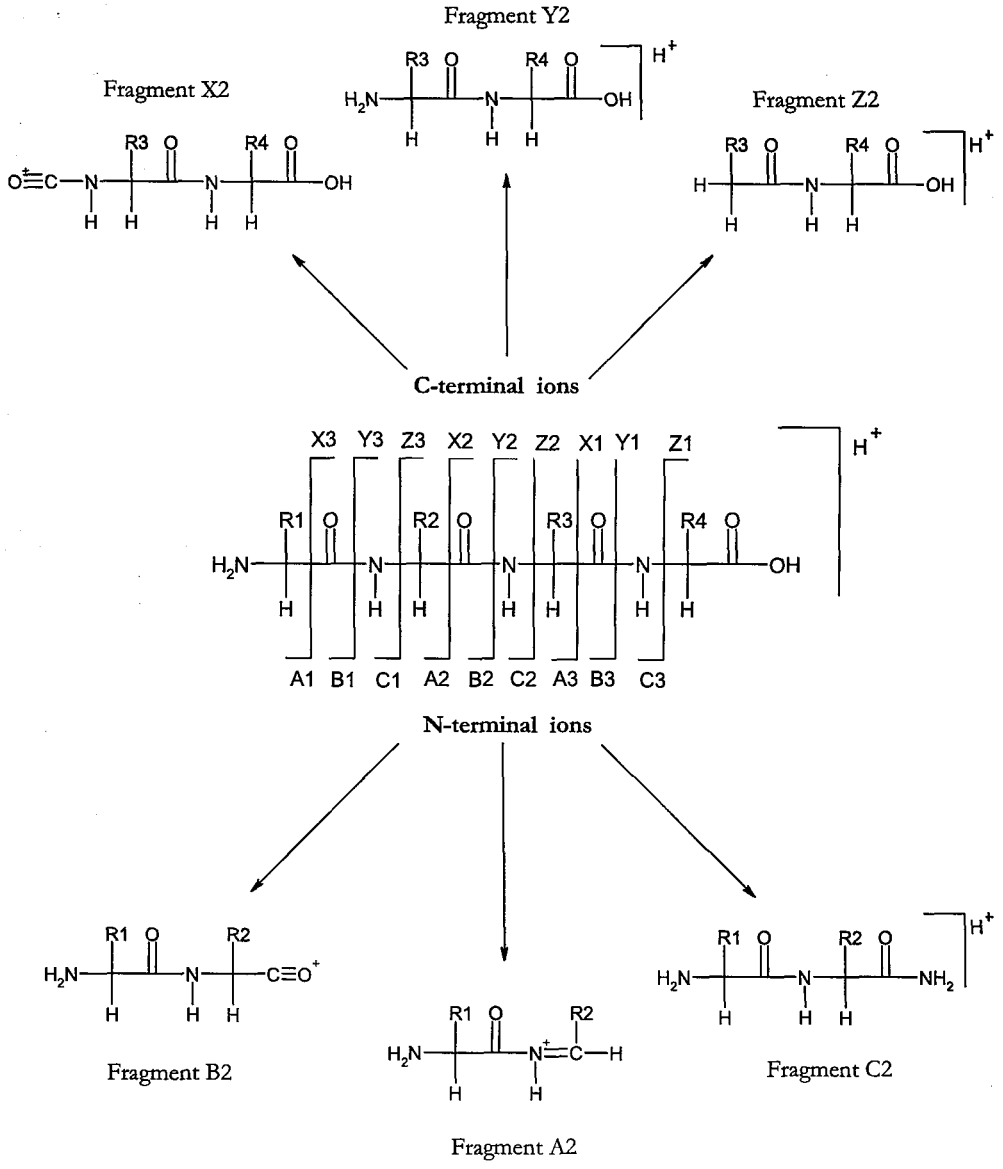

Figure 8.4 Fragmentation of an idealised peptide (protonated) in the ionizing chamber of a mass spectrometer. R1, R2, R3 and R4 refer to the lateral chain of the residues.

8.3.3 PPF2 adsorption at the air/water interface

Adsorption experiments were carried out using the glass trough filled with 40 ml of buffer A or B. 25-250 µl of 2.37 mM PPF2 were injected beneath the air/water interface and the pressure monitored for ~ 2 hours at 37°C.

8.3.4 PPF2 adsorption into DMPC and DOPC monolayers

DMPC or DOPC monolayers were prepared by spreading their solutions (20-80 µl, 0.05-0.8 $mg \cdot ml^{-1}$ in chloroform) on the surface of 40 ml of buffer A or B. After 5-10 minutes to allow the chloroform evaporation, 25-250 µl of 2.37 mM PPF2 were injected beneath the air/water interface and the pressure monitored for ~ 2 hours at 37°C

8.4 Results

8.4.1 PPF2 adsorption at the air/water interface

PPF2 adsorption at the air/water interface is shown in Figure 8.5 to Figure 8.9. Peptide adsorption was studied using the same buffer at two different pH values: curves shown from Figure 8.5 to Figure 8.7 were recorded at pH 7.2, while the curves in Figure 8.8 and Figure 8.9 were recorded at pH 7.4[a]. The adsorption curves at pH 7.2 differ from those at pH 7.4 both in the shape and in the pressure recorded at the end of the measurement.

8.4.2 PPF2 adsorption into DMPC and DOPC monolayers

PPF2 adsorption into phospholipid monolayers was tested using DMPC, type 0 lipid, and DOPC, type II lipid. Figure 8.10 and Figure 8.11 show the adsorption recorded in presence of DMPC at pH 7.2. Figure 8.12 shows the adsorption recorded at pH 7.4. PPF2 adsorption into DOPC monolayer is shown in Figure 8.13. Differently from the adsorption into DMPC monolayer, DOPC, stable without PPF2 (**Figure 7.16**), shows a pressure decrease caused by the presence of PPF2.

[a] A magnetic stirrer was used in all the experiments at pH 7.2.

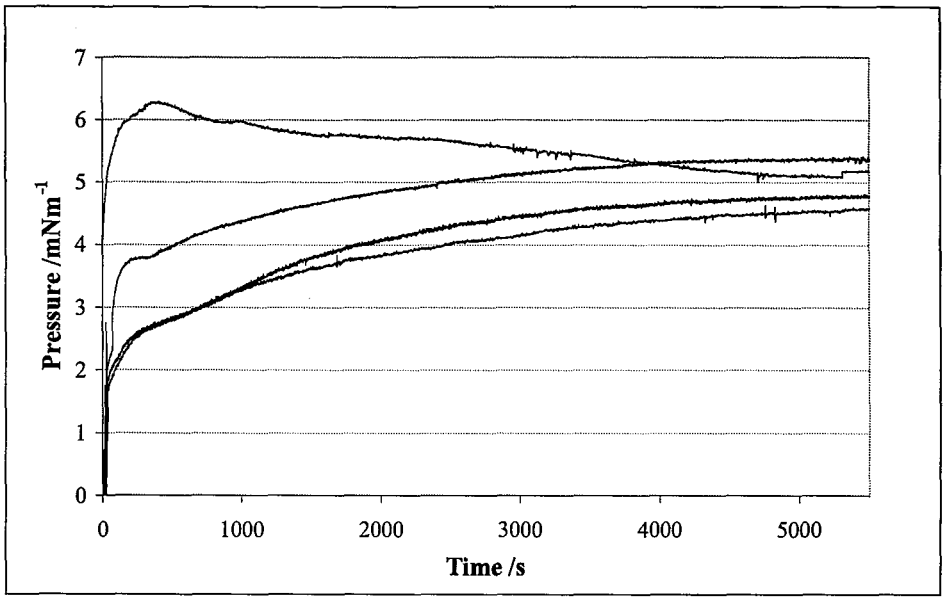

Figure 8.5 PPF2 adsorption at the air/water interface. 250 µl of 2.37 mM PPF2 where injected in 60 ml of buffer A. A magnetic stirrer was switched on for 20s after the injection of the PPF2 solution.

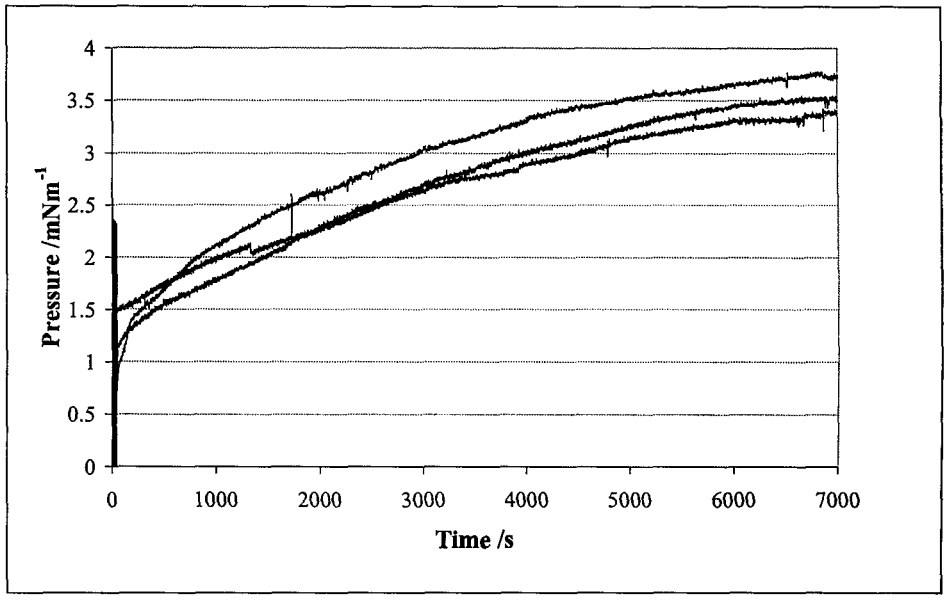

Figure 8.6 PPF2 adsorption at the air/water interface. 125 µl of 2.37 mM PPF2 where injected in 60 ml of buffer A. A magnetic stirrer was switched on for 20s after the injection of the PPF2 solution.

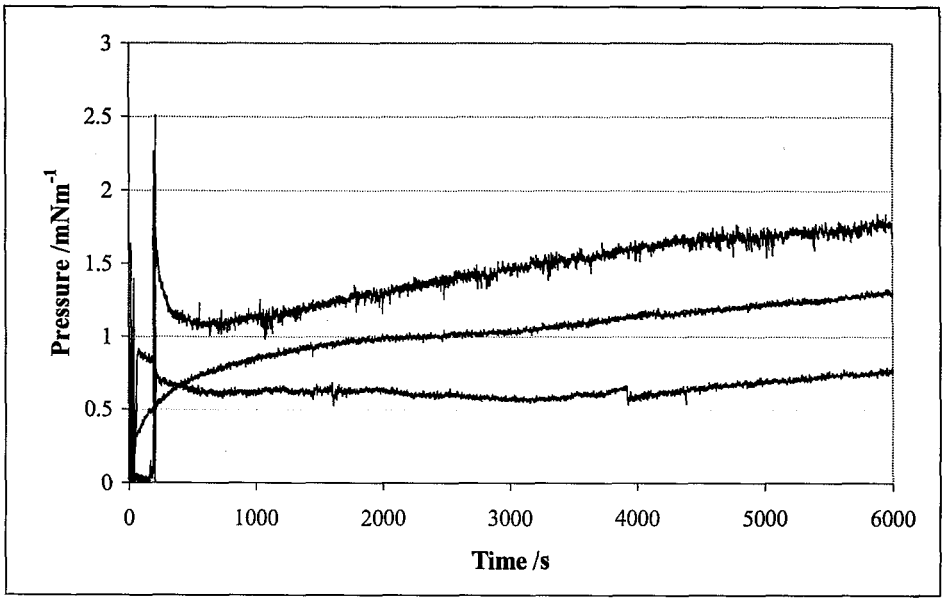

Figure 8.7 PPF2 adsorption at the air/water interface. 25 µl of 2.37 mM PPF2 where injected in 60 ml of buffer A. A magnetic stirrer was switched on for 20s after the injection of the PPF2 solution.

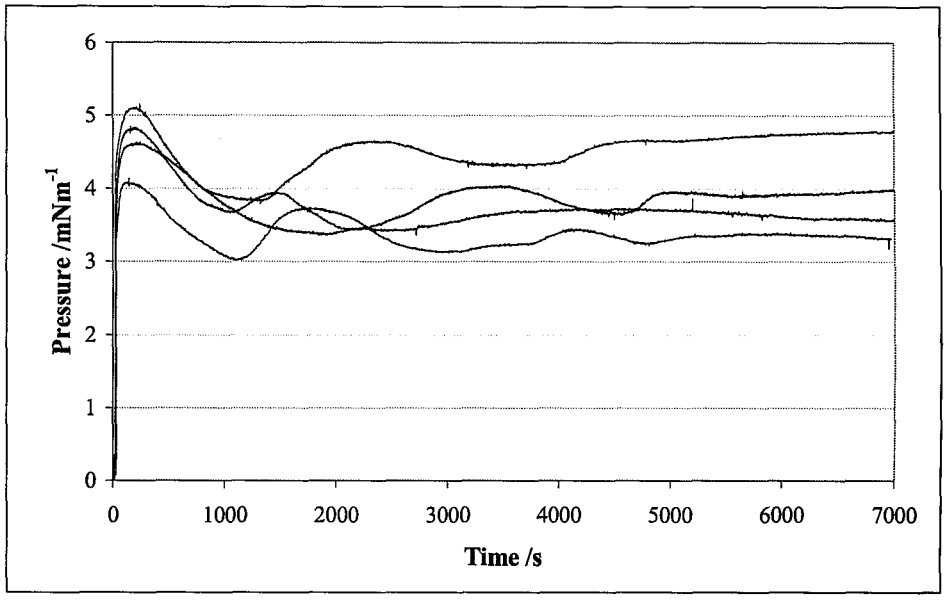

Figure 8.8 PPF2 adsorption at the air/water interface. 200 µl of 2.37 mM PPF2 where injected in 60 ml of buffer B

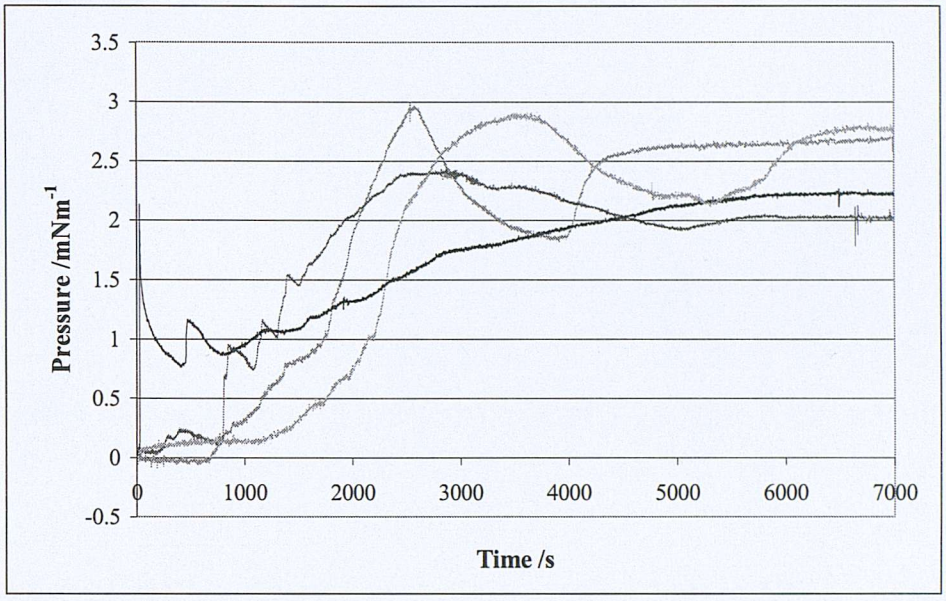

Figure 8.9 PPF2 adsorption at the air/water interface. 100 µl of 2.37 mM PPF2 where injected in 60 ml of buffer B. Magnetic stirrer was used for the black curves.

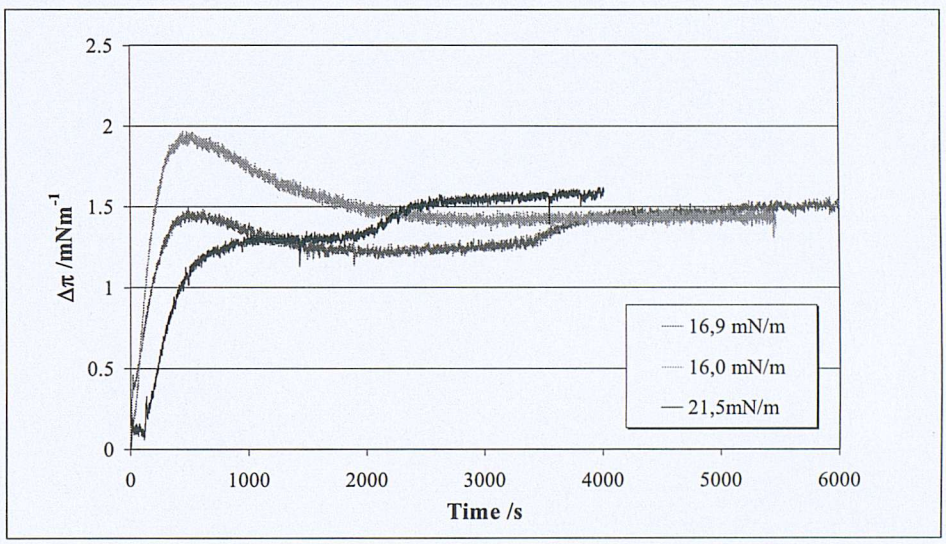

Figure 8.10 PPF2 adsorption into DMPC monolayer. 200 µl of 2.37 mM PPF2 where injected in 50 ml of buffer A (pH 7.2). The pressures in the figure legend correspond to the monolayer pressure measured before the addition of PPF2.

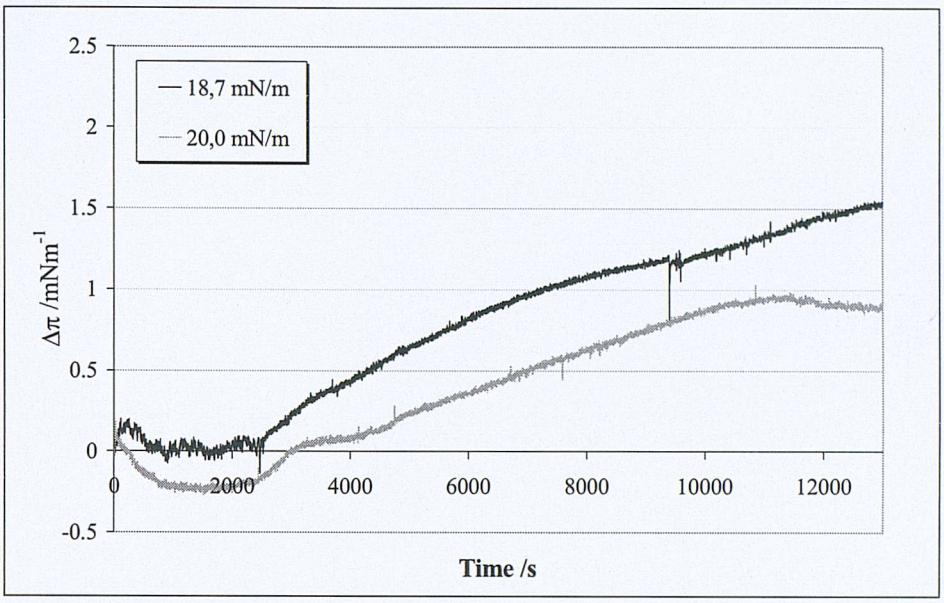

Figure 8.11. PPF2 adsorption into DMPC monolayers. 100 μl of 2.37 mM PPF2 where injected in 50 ml of buffer A (pH 7.2). The pressures in the legend correspond to the monolayer pressure measured before the addition of PPF2.

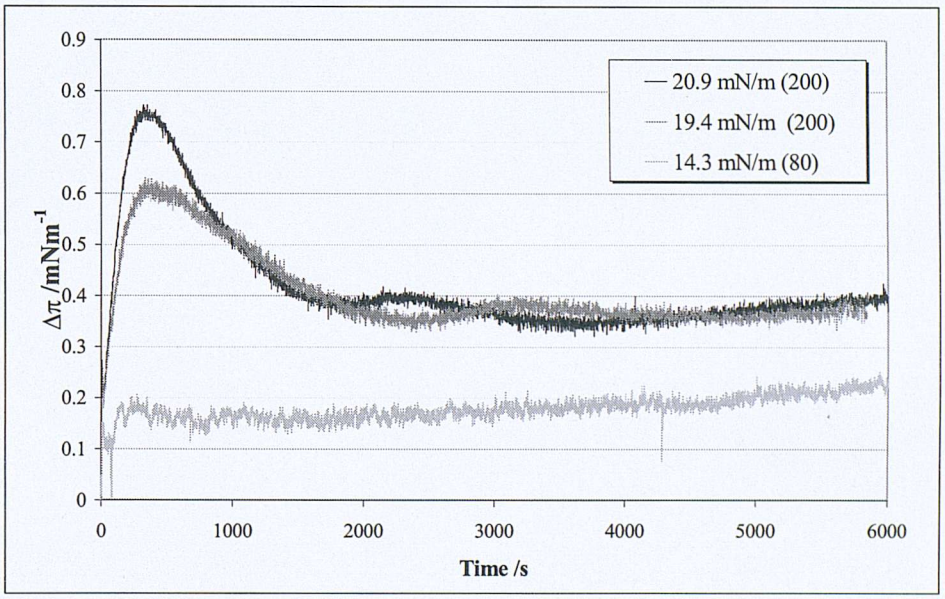

Figure 8.12 PPF2 adsorption into DMPC monolayers. 80-200 μl of 2.37 mM PPF2 were injected in 50 ml of buffer B (pH 7.4). The pressures in the legend correspond to the monolayer pressure measured before the addition of PPF2 (the values in brackets).

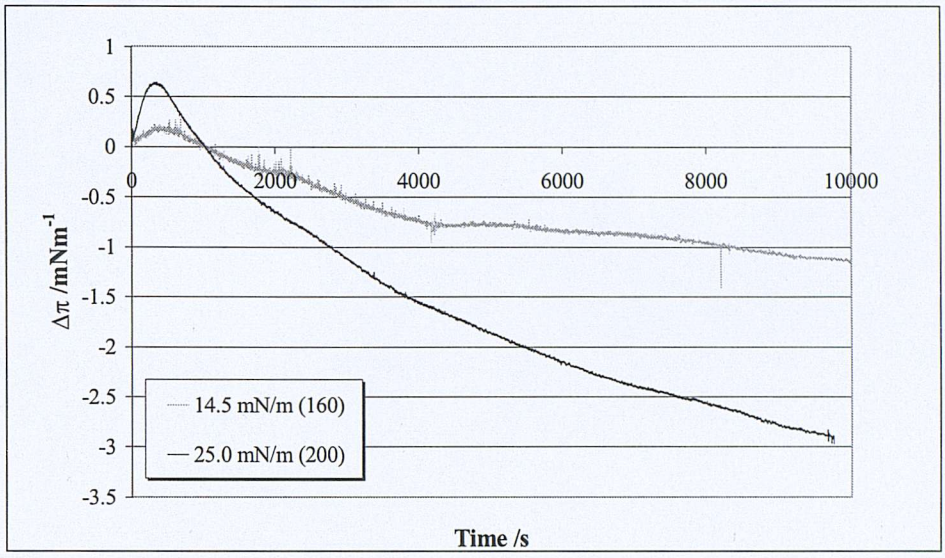

Figure 8.13 PPF2 adsorption into DOPC monolayers. 200 or 160 μl of 2.37 mM PPF2 where injected in 50 ml of buffer A (pH 7.2). The pressures in the legend correspond to the monolayer pressure measured before the addition of PPF2, whilst the number in brackets refer to the volume of PPF solution injected beneath the monolayer.

8.5 Conclusions

8.5.1 PPF2 adsorption at the air/water interface

The adsorption of PPF2 at the air/water interface was sensitive to both the concentration of the peptide beneath the interface and the pH of the buffer. Unfortunately, it was not possible to determine the molecular area of the peptide at the air/water interface and consequently the partition coefficient. However, the increase of the pressure measured in the absence of a monolayer suggests that PPF2, and then the α-helix of CCTα, could form an α-helix featuring distinct hydrophilic and hydrophobic character. It is reasonable to assume that the different pH has affected the peptide charge (acting on the protonation of the lysines) and then both the hydrophilic/hydrophobic character or the formation of an α-helix[b]. Howevere, because of the limited number of experiments and because no data have been collected about PPF2 folding at different pH, it is not possible to give a

[b] Analysis of pH effect on the peptide folding could have been done by circular dichroism spectrospy.

rationale explanation of the observed variation in the absorptin ate the air/water interface.

8.5.2 PPF2 adsorption into DMPC or DOPC monolayer

PPF2 adsorption into DOPC monolayers was significantly different from the adsorption into a DMPC monolayer. The small increase in the DMPC monolayer suggest that PPF2 interact probably with the interface of the monolayer and that PPF2 could be particular sensitive to the component of the monolayer pressure featured in the hydrophilic region of the monolayer.

The DOPC monolayer, stable in the absence of PPF2 (Figure 7.16) became unstable after the addition of the PPF2 solution. The pressure decrease was discussed for DOPC and DOPE monolayers in 7.4.3 and 7.5, and the reorganisation of the monolayer structure was hypothesised as a cause of the drop in the pressure. Although one could reasonably hypothesise that PPF2 acts as a catalyst in the monolayer reorganisation, the experimental data are not sufficient to suggest any reasonable explanation of the observed phenomenon.

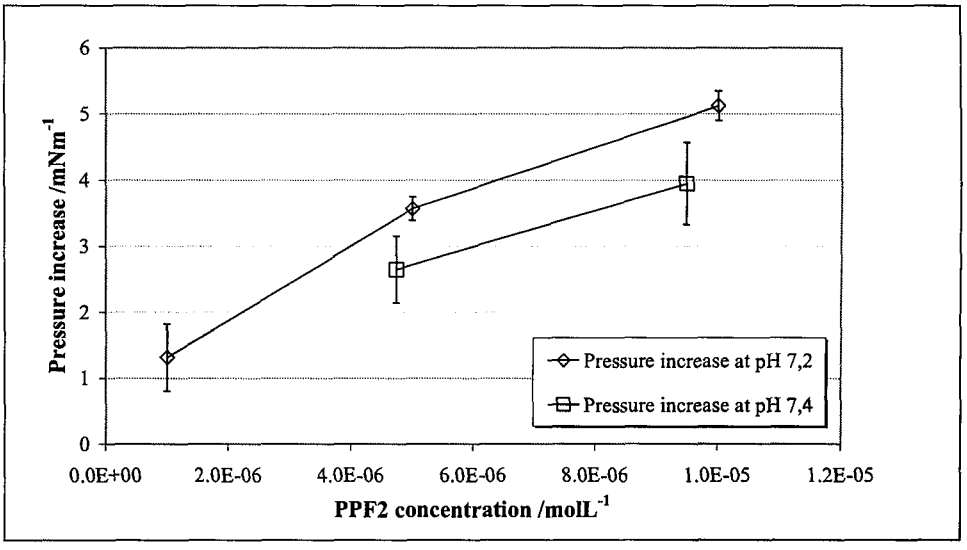

Figure 8.14 Pressure increases as a function of the PPF2 concentration in solution. Each point is the average of the highest pressures reached during the adsorption experiments at the air/water interface shown from Figure 8.5 to Figure 8.9.

8.6 References

[1] L. Razumovsky, and Damodaran, S., "Surface activity-compressibility relationship of proteins at the air-water interface," in *Langmuir*, vol. 15, 1999, pp. 1392-1399.

[2] F. MacRitchie, and Alexander, A.E., "Kinetics of adsorption of proteins at the interfaces. Part I. The role of bulk diffusion in adsorption," in *Journal of Colloid Science*, vol. 18, 1963, pp. 453-457.

[3] F. MacRitchie, and Alexander, A.E., "Kinetics of adsorption of proteins at the interface. Part II. The role of pressure barriers in adsorption," in *Journal of Colloid Science*, vol. 18, 1963, pp. 458-463.

[4] F. MacRitchie, and Alexander, A.E., "Kinetics of adsorption of proteins at the interface. Part III. The role of electrical barriers in adsorption," in *Journal of Colloid Science*, vol. 18, 1963, pp. 464-469.

[5] W. C. Chang, and White, P.D., *Fmoc solid phase peptide synthesis: a practical approach*. Oxford: Oxford University Press, 2000.

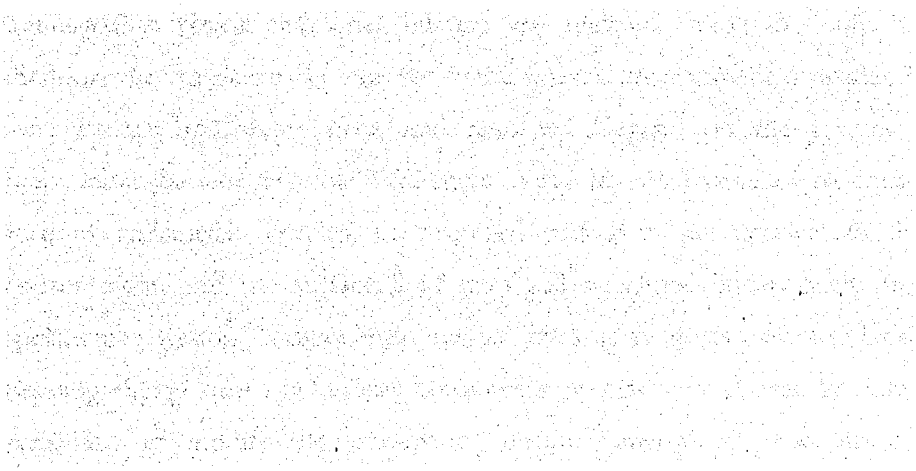

9 Unilamellar vesicles

9.1 Large Unilamellar Vesicles (LUVs)

Lipid LUVs are essential components of all the enzymatic assays reported in this thesis. This kind of vesicle was chosen as model system of biological membranes for two of its properties: the size and the unilamellarity.

Figure 9.1 shows the bending energy stored in the two leaflets of a bilayer vesicle, expressed in units independent from the lipid bending modulus, head-group area and spontaneous curvature. Vesicles having a diameter close to or smaller than the spontaneous radius of curvature have a stored bending energy higher than the one stored in a flat monolayer, with positive contributions to it from the geometric stress, both functions of the vesicle diameter. On the contrary, vesicles with big diameter (8-10 times bigger than the spontaneous curvature) store an amount of bending energy close to that found in flat monolayers and independent from the vesicle diameter.

Vesicle unilamellarity is the second fundamental assumption in all the hypotheses and experiments discussed in this thesis. Figure 9.2 shows the difference between a unilamellar vesicle (on the right) and a multilamellar vesicle (on the left). In a multilamellar vesicle the inner bilayers are enclosed inside the outer bilayers, therefore the vesicle surface exposed to the external environment is smaller than the total surface and the surface/lipid ratio will depend on the specific vesicle preparation (because possible differences in the degree of vesicle inclusion). In the case of unilamellar vesicles, the exposed surface is proportional to the lipid concentration and the surface/lipid ratio will be almost independent from the specific preparation. Consequently, because the studies discussed herein involve the bending energy stored in vesicles, unilamellar vesicles were chosen because of the possibility to modify the amount of bending energy by changing the lipid concentration.

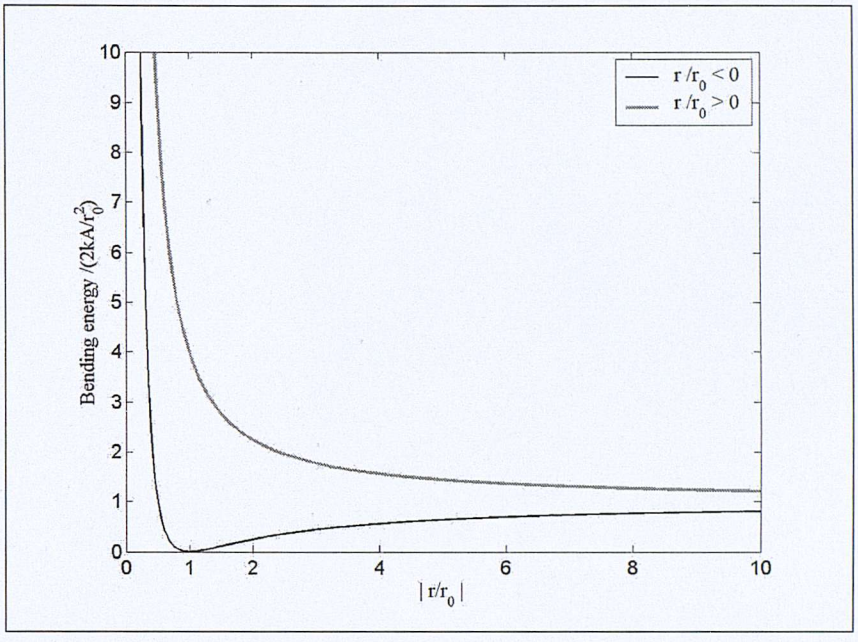

Figure 9.1 Bending energy in unit of $2kA/r_0^2$ as a function of the $|r/r_0|$ ratio, where k is the bending moduli, A is the head-group area, r_0 is the spontaneous radius of curvature and r is the vesicle radius of curvature. The bending energy has been calculated using the simplified version of Eq. 4.14: $g_{curv}=(1/2)k_M(c_1+c_2-2c_0)^2$, where $c_1=c_2=1/r$ and $c_0=1/r_0$.

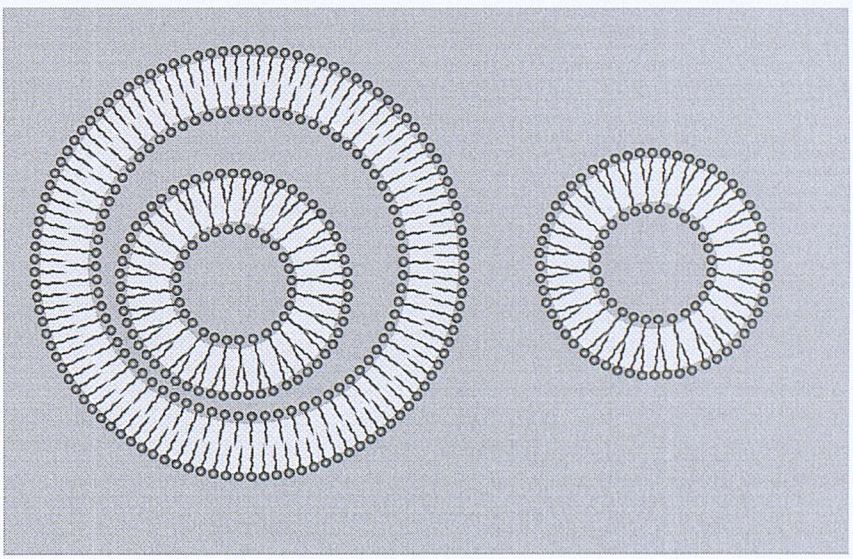

Figure 9.2 A multilamellar vesicle, resembling the onion layer structure, is represented on the left, while a unilamellar vesicles is represented on the right. Clearly, the lipid area exposed to the external solution is larger for a unilamellar than for a moltilamellar vesicle.

9.2 Light scattering and particle sizing

9.2.1 Light scattering

The fundamental principle of particle sizing is the correlation between particle size and diffusion. If a light beam crosses a solution containing particles in motion, a fraction of the total light will be scattered. Due to the continuous random movement of the particles in solution, the intensity of the light scattered will oscillate in a way that is correlated to the brownian motion of the particles.

The motion of solute molecules in a fluid depends on the nature of the solute, the physical properties of the fluid and the temperature, as proposed by Einstein:

Eq. 9.1 $$D = \frac{k_B T}{f}$$

where D is the diffusion coefficient of the solute in the fluid, k_B is the Boltzmann constant, and f is the frictional coefficient of the solute [1]. Further studies conducted by Stokes showed that there is a correlation between the frictional coefficient, the solvent viscosity and the radius of the particles. Under the hypothesis of a spherical particle, Stokes demonstrated that

Eq. 9.2 $$f = 6\pi r \eta$$

where r is the radius of the molecule and η is the viscosity of the solvent [1]. The combination of Eq. 9.1 and Eq. 9.2 gives the Stokes-Einstein equation

Eq. 9.3 $$D = \frac{k_B T}{3\pi d \eta}$$

where the radius of the particle is replaced by the diameter, d [1]. The mean-square distance traveled by a particle, $\overline{x^2}$, during the time t is linked to the diffusion coefficient by the following relationship [1]

Eq. 9.4 $$\overline{x^2} = 2Dt$$

Due to the dependency of the fluctuation time on the random motion of the particles, it is possible to calculate the particle size by determining the fluctuation time of the scattered light. The light fluctuation is then correlated to the particle size and the diffusion coefficient by mathematical transformation of the light intensity signal, resulting in an autocorrelation function (ACF) having the form

Eq. 9.5 $$A(\tau) = \langle I(t) \times I(t+\tau) \rangle$$

where $A(\tau)$ is the autocorrelation function, $I(t)$ and $I(t+\tau)$ are the light intensity at time t and $t+\tau$ respectively, τ is the delay time and $\langle\ \rangle$ means that the product is time averaged [2]. The analysis of different delay times results in the measurement of the time scale in which the intensity fluctuations occur, that is the *decay time* for the system and is dependent on the brownian motion. The inverse of the decay time is the decay constant Γ that is related to the ACF and the brownian motion through the functions

Eq. 9.6 $$A(\tau) \propto e^{-2\Gamma\tau}$$

Eq. 9.7 $$\Gamma = DK^2 = D\left(\frac{4\pi n}{\lambda}\right)^2 \sin^2\left(\frac{\theta}{2}\right)$$

Eq. 9.8 $$K = \left(\frac{4\pi n}{\lambda}\right)\sin\left(\frac{\theta}{2}\right)$$

where n is the refractive index of the solvent, λ is the laser wavelength in vacuum and θ is the angle at which the scattered light is measured [2]. The particle diameter d can then be obtained by Eq. 9.3 and Eq. 9.7 [2]

Eq. 9.9 $$d \propto \frac{n^2 T}{\eta\Gamma}$$

Eq. 9.9 clearly shows that the diameter determined by the light scattering depends on the absolute temperature, the square of the refractive index, the solvent viscosity and the decay constant. Due to the variability of the particle size, the diameter will be a distribution of values around one or more central values.

9.2.2 *Particle sizing*

All the above theories about diffusion and diameter of particles are applicable to hypothetically perfect spheres having the same size. Due to the shape and the size variability, each diameter is given with the standard deviation, index of the size variability. If the particle size is distributed around more than one diameter, the standard deviation associated with each diameter will be indicative of the size distribution. The method of analysis applied to the scattering data will give different values for the particle diameters and their standard deviations. Two methods of analysis are discussed in the next sections: Unimodal analysis and Size Distribution Processor (SDP) analysis.

9.2.2.1 *Unimodal analysis*

The unimodal analysis results in an averaged diameter based on the entire size distribution of the sample. When the ACF is calculated, it will result in an expression giving the logarithm of the ACF as an expanded power series in time

Eq. 9.10 $$\ln\left(A(\tau_i) - baseline\right) = a + b\tau_i + \frac{1}{2}c\tau_i^2$$

where b and c are the so called first and second cumulant of the ACF A and τ_i are the delay times at which the autocorrelation function is measured [2]. The first cumulant is correlated to the decay constant [2]

Eq. 9.11 $$b = 2\Gamma$$

and then, as the decay constant is related to the particle diameter, it follows that the correlation between the diameter and the first cumulant is given by [2]

Eq. 9.12 $$\frac{1}{b} = const\frac{1}{\left\langle \frac{1}{d} \right\rangle} = const\langle d \rangle$$

Eq. 9.13 $$const = \frac{1}{2K^2} \cdot \frac{3\pi\eta}{k_B T}$$

The standard deviation (SD) is then calculated using the second cumulant via the polydispersity index (P.I.) and the coefficient of variation (CV) given by [2]

Eq. 9.14 $$P.I. = \frac{2c}{b^2}$$

Eq. 9.15 $$CV = \left(\frac{1}{2 \cdot P.I.} + 4 \right)^{-\frac{1}{2}}$$

Eq. 9.16 $$SD = d \cdot CV$$

The unimodal analysis gives an average of the diameter distribution and the standard deviation. The standard deviation is particularly useful to have an idea of the size distribution of the particles in the sample and to reveal the possible presence of more than one particle diameter.

9.2.2.2 Size Distribution Process (SDP) analysis

The SDP analysis, differently from the unimodal analysis, gives information about the size distribution in terms of number of size peaks and their standard deviation. The determination of the different sizes is obtained by mathematical separation of the different components by an algorithm applied to the ACF to find out the different possible solutions for the sample in terms of particles size. This method calculates the different size of the particles present in the sample and the percentage of light that they scatter. The correlation between the amount of scattered light and particle size can be obtained using the Mie equation or an approximate conversion function, as the Mie equation requires the complex refractive index of the particles.

Because the light scattered by particles made of the same material depends on the percentage and on the size of the particles, the ACF assumes the more complex form given by

Eq. 9.17 $$A(\tau) \propto \sum a_i e^{-2\Gamma_i(d_i)\tau}$$

where a_i, the amplitude factor, corresponds to the contribution to the total scattered light coming from the particles having diameter d_i [2]. The mathematical process used to calculate all the amplitude factors is called 'inversion'. It is based on a mathematical approach called 'least-square fitting' that varies all the a_i systematically to find out the minimum of the function [2]

Eq. 9.18 $$\sum_j \left[A(\tau_j) - B\sum a_i \exp\left(-2\Gamma_i(d_i)\tau_j\right)\right]^2$$

When the function is minimised, the result gives the different sizes calculated for the particles, their standard deviation, and the mean size. The mean diameter $\bar{d}$ is calculated as defined below [2]

Eq. 9.19 $$\bar{d} = \frac{\sum_i d_i a_i}{a_i}$$

The standard deviation (SD) is then calculated using the equation given by

Eq. 9.20 $$SD = \left[\frac{\sum_i a_i\left(\bar{d} - d_i\right)^2}{\sum a_i}\right]^{\frac{1}{2}}$$

The a_i values in Eq. 9.18 and Eq. 9.20 can correspond to the percentage of the total light scattered by a particle having diameter d_i (intensity result) or, alternatively, to the percentage of particle having diameter d_i (weight result) [2]. The intensity of the scattered light and particle size are related to the number of particles in a complex way. The light scattered by two particles that have the same size but are composed of different materials is dependent on factors like shape and refractive index of the particle. It is difficult to properly convert light intensity in number of particles and hence the intensity result, obtained from SDP analysis, is more accurate than the weight result.

9.3 Coagulation of LUVs

The critical coagulation concentration (*ccc*) is defined as the concentration of electrolyte that is required for the coagulation of spherical particles suspended in solution. If the particles have a high surface density charge, then the *ccc* is approximatively given by

Eq. 9.21 $$ccc \propto z^{-6}$$

Vesicles with a negatively charged surface are sensitive to positively charged ions like Na^+, Mg^{2+} and Cr^{3+}. A direct consequence of Eq. 9.21 is that the ratio between the *ccc* of different ions is inversely proportional to the ratio of the ion charge

Eq. 9.22 $$\frac{ccc(z_1)}{ccc(z_2)} = \left(\frac{z_2}{z_1}\right)^6$$

Where z_1 and z_2 are referred to the charge of two different ions.

9.4 Materials and methods

9.4.1 Materials

1,2-dioleoyl-*sn*-glycero-3-phosphocholine (20 mg/ml choroform solution) and 1,2-dioleoyl-*sn*-glycero-3-phosphoethanolamine (10 mg/ml choroform solution) were purchased from Fluka. Hamilton glass syringes (250 and 100 µl) were used to aliquot the lipid solutions. Deionised water for HPLC and 2.0 ml amber glass vials with Teflon septa were purchased from Fisher. Disposable plastic tips (1 ml, 200 µl and 10 µl) were obtained from Radleys or Fisher. Bis-Tris (BT), NaCl, $MgCl_2$, $CrCl_3$ were obtained from Sigma. Vesicles and latex particles were sized using a Coulter N4 Plus Particle Sizer and 1 cm quartz cuvettes. Standard latex particles (100, 200, 300 and 500 nm diameter) were obtained from Coulter Beckman. Water, buffer A (0.25 M BT-HCl, pH 6.5 at 37 °C, 10 mM $MgCl_2$), buffer B (0.25 M BT-HCl, pH 6.5 at 37 °C), buffer C (0.15 M BT-HCl, pH 6.5 at 37 °C), NaCl, $MgCl_2$, and $CrCl_3$

water solutions were filtered using Durapore® membrane filters 0.1 μm VVPP purchased from Fisher.

9.4.2 Sizing of standard latex particles

Standard latex particle suspensions (100, 200, 300 and 500 nm diameter) were diluted in filtered water until the intensity of the light scattered by the sample was in the range 10^5-10^6 count per second. The four standard suspensions were then used to prepare six different samples, Table 9.1.

Sample sizes were measured in the range 10÷2000 nm monitoring the light scattered at 90° for 600 seconds and using automatic sampling time. Data were treated by Unimodal and SDP analysis.

Table 9.1 Sample composition gives the diameter, in nm, of standard latex particles present in each sample.

Sample number	Sample composition
1	100
2	200
3	300
4	500
5	200 and 500
6	100, 200, 300, 500

9.4.3 Preparation of LUV: F-T method

Vesicles preparation was based on the Freeze-Thaw (F-T) method[a] [3-5]. Vesicles were prepared in amber glass vials to avoid any photochemical decomposition of unsaturated lipids. The steps for vesicle preparation are reported in Table 9.2.

[a] Vesicles prepared by F-T method have been reported to have high trapping volume, low ion permeability and high resistance to osmotic shock [3].

Table 9.2 Steps for vesicle preparation by the Freeze-Thaw (F-T) method.

Preparation steps	Procedure
1st	Removal of organic solvent by nitrogen stream
2nd	1.5-2 hrs of vacuum to remove traces of solvent
3rd	Lipids hydration with filtered water (50 µl of water per mg of lipid) by vortexing (1-2 sec.)
4th	Lyophylisation
5th	Suspension of the dry lipids in buffer (volume required to obtain a 15 mM lipid solution)
6th	Vortexing (10-15 min.) and resting (10-20 min.)
7th	Sonication (20 min.) and resting (20-30 min.)
8th (1st F-T cycle)	Flash-freezing, thawing (10 min. at 40 °C) and resting (20 min. at rt)
9th (2nd F-T cycle)	Flash-freezing, thawing (10 min. at 40 °C) and resting (20 min. at rt)
10th (3rd F-T cycle)	Flash-freezing, thawing (10 min. at 40 °C) and resting (20 min. at rt)
11th	Sonication (30 seconds) and resting (20 min.)
12th (4th F-T cycle)	Flash-freezing, thawing (10 min. at 40 °C) and resting (20 min. at rt)

9.4.4 Freeze-Thaw effect on LUVs size

Vesicles were prepared using a DOPC/DOPE mixture (4:6 mole ratio) as described in 9.4.3 and dissolving the lipids in buffer A. The number of F-T cycles was increased as reported in Table 9.3. Vesicles were sized during the preparation; after each step, 30 µl of the vesicle solution were withdrawn, diluted with 3 ml of water in a quartz cuvette and the vesicles sized following the procedure described in 9.4.2.

Table 9.3 Extension of the F-T protocol reported in Table 9.2

Preparation steps	Procedure
13th (5th F-T cycle)	Flash-freezing, thawing (10 min. at 40 °C) and resting (20 min. at rt)
14th (6th F-T cycle)	Flash-freezing, thawing (10 min. at 40 °C) and resting (20 min. at rt)
15th (7th F-T cycle)	Flash-freezing, thawing (10 min. at 40 °C) and resting (20 min. at rt)
16th (8th F-T cycle)	Flash-freezing, thawing (10 min. at 40 °C) and resting (20 min. at rt)
17th (9th F-T cycle)	Flash-freezing, thawing (10 min. at 40 °C) and resting (20 min. at rt)
18th	Sonication (30 seconds) and resting (20 min.)
19th (10th F-T cycle)	Flash-freezing, thawing (10 min. at 40 °C) and resting (20 min. at rt)

9.4.5 Vesicle stability

Vesicles were prepared using DOPC, DOPC/DOPE (1:1) and DOPA. DOPA vesicles were prepared using buffer B, whilst DOPC and DOPC/DOPE (1:1) vesicles were prepared using buffer A. Vesicles were diluted with the same buffer used for their preparation and then sized (9.4.2).

9.4.6 Anionic phospholipids and coagulation

DOPA and DOPS LUVs were prepared using buffer B. Vesicles were prepared as 15 mM stock solutions and diluted to 1 mM in buffer B, for the titration with the solutions of NaCl (0.10 M), $MgCl_2$ (10 mM) or $CrCl_3$ (1.0 mM). Vesicle solutions (2.0 ml total volume) were stirred during the titration; titration was completed when lipid coagula were visible.

9.5 Results

9.5.1 Sizing of standard latex particles

Figure 9.3 and Figure 9.4 show the limits of applicability of the unimodal analysis to samples differing in particle size distribution. The four curves shown in Figure 9.3 were recorded separately using separate dispersions of the four standard latex particles (9.4.2). In this case, the unimodal analysis gave sufficient information about the size distribution of each sample. The two curves shown in Figure 9.4 were obtained by separate sizing of samples 5 and 6 (9.4.2). The results obtained from unimodal analysis were different from the previous case and did not correspond to the real composition of the samples. However, the width of the two peaks was indicative of two possibilities:

1. The curve corresponds to the correct distribution of particles whose size was distributed around an average value, following a gaussian trend.
2. As the unimodal analysis resulted in an average of the different sizes, the curve corresponded to the distribution of the particles around two or more peak sizes.

Consequently, samples 5 and 6 were analysed by the SPD methods and the results, reported as intensity result, are shown in Figure 9.5. SDP analysis of sample 5 resulted in two mean sizes, as expected for this sample, whilst SDP analysis of sample 6 did not result in four mean sizes. However, the curve for sample 6 excluded the possibility that the size of the particles was centred on any mean size, as shown in Figure 9.4.

9.5.2 Freeze-thaw effect on LUV size

The effect of each F-T step during of the vesicle preparation on the vesicle size was investigated. Figure 9.6 shows the effects of vortexing, sonication and the first F-T cycle on the size of the vesicles: the vortexing step resulted in big multilamellar vesicles (black line) that were converted by sonication in small vesicles with a high

level of unilamellarity (red line). The vesicle size increased after the first F-T cycle (green line).

Differently from the protocol described by Pick, the sonication step was shifted from the first to the third F-T cycle. Figure 9.7 shows that the vesicle size increased after the second F-T (black line) and that the sonication step, supposed to reduce the vesicle stress, caused a reduction of the size (red line). The two following F-T cycles (green and blue line for the 4th and the 5th cycle respectively) increased the vesicles size to the same value observed for the 2nd F-T cycle. Figure 9.8 shows the effect of the 6th, the 7th, the 18th step and the 10th F-T cycle on the vesicles size. Vesicles size started to decrease after the 5th F-T cycle, and the decrease continued after the 6th (black line) and the 7th F-T cycle. Vesicles were sonicated at the 18th step, after 9 F-T cycles, hypothetically to reduce the stress but the sonication was ineffective and caused a further size reduction (green line), as did the last F-T cycle, which caused a further decrease of the vesicle size (blue line). All the sizing results and the references to the figures are summarised in Table 9.4.

Table 9.4 Vesicle size during the several steps constituting the Freeze- Thaw method.

Vesicles preparation step	Vesicle size (nm)	Std. Dev. (nm)	Curve location and colour
Vortexing	2039	943	Figure 9.6, black line
Sonication	774	358	Figure 9.6, red line
1st F-T	1445	656	Figure 9.6, green line
2nd F-T	2593	1193	Figure 9.7, black line
3rd F-T and sonication	791	365	Figure 9.7, red line
4th F-T	2593	1252	Figure 9.7, green line
5th F-T	2255	1054	Figure 9.7, blue line
6th F-T	1969	927	Figure 9.8, black line
7th F-T	805	376	Figure 9.8, red line
9th F-T and sonication	294	131	Figure 9.8, green line
10th F-T	240	103	Figure 9.8, blue line

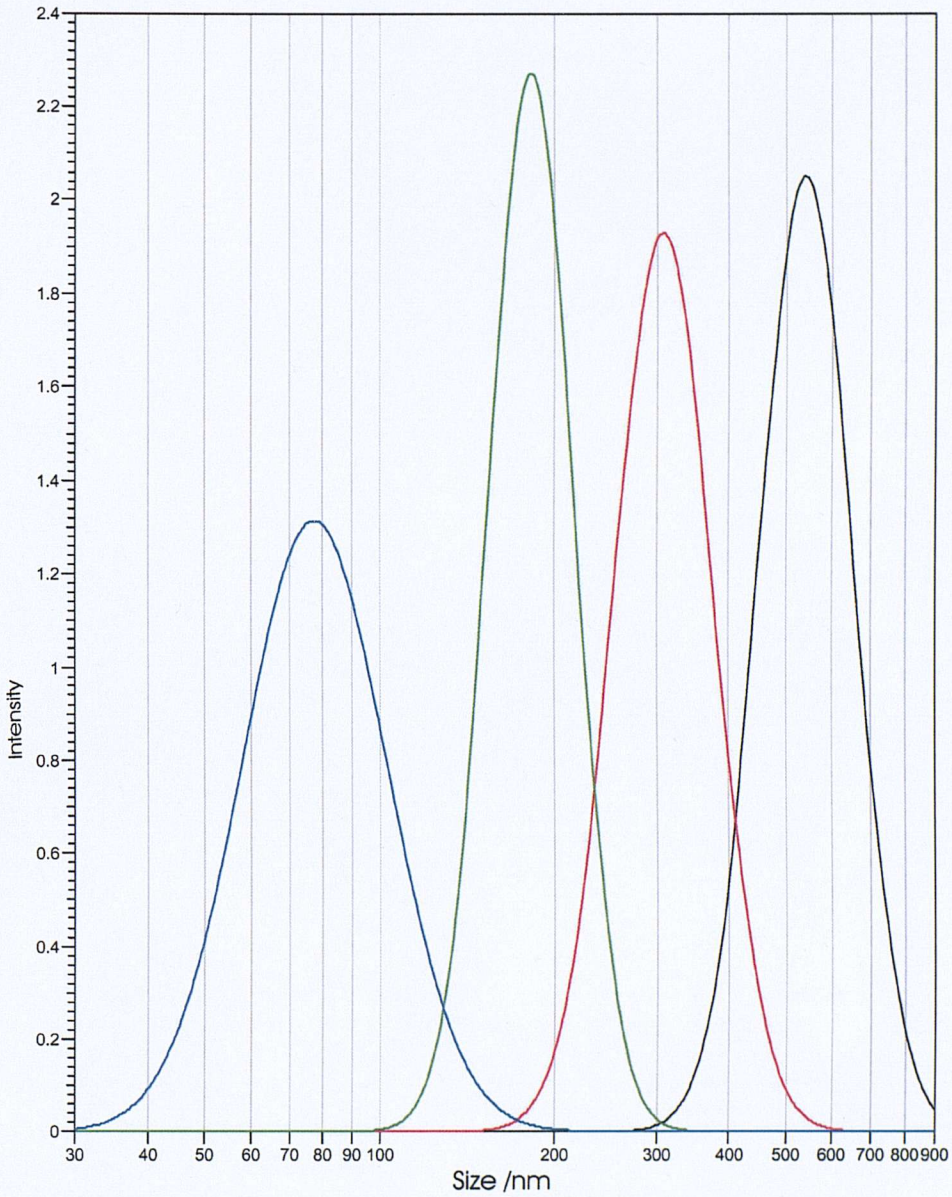

Figure 9.3 Samples from 1 to 4 (9.4.2) were sized separately and analysed by unimodal analysis.

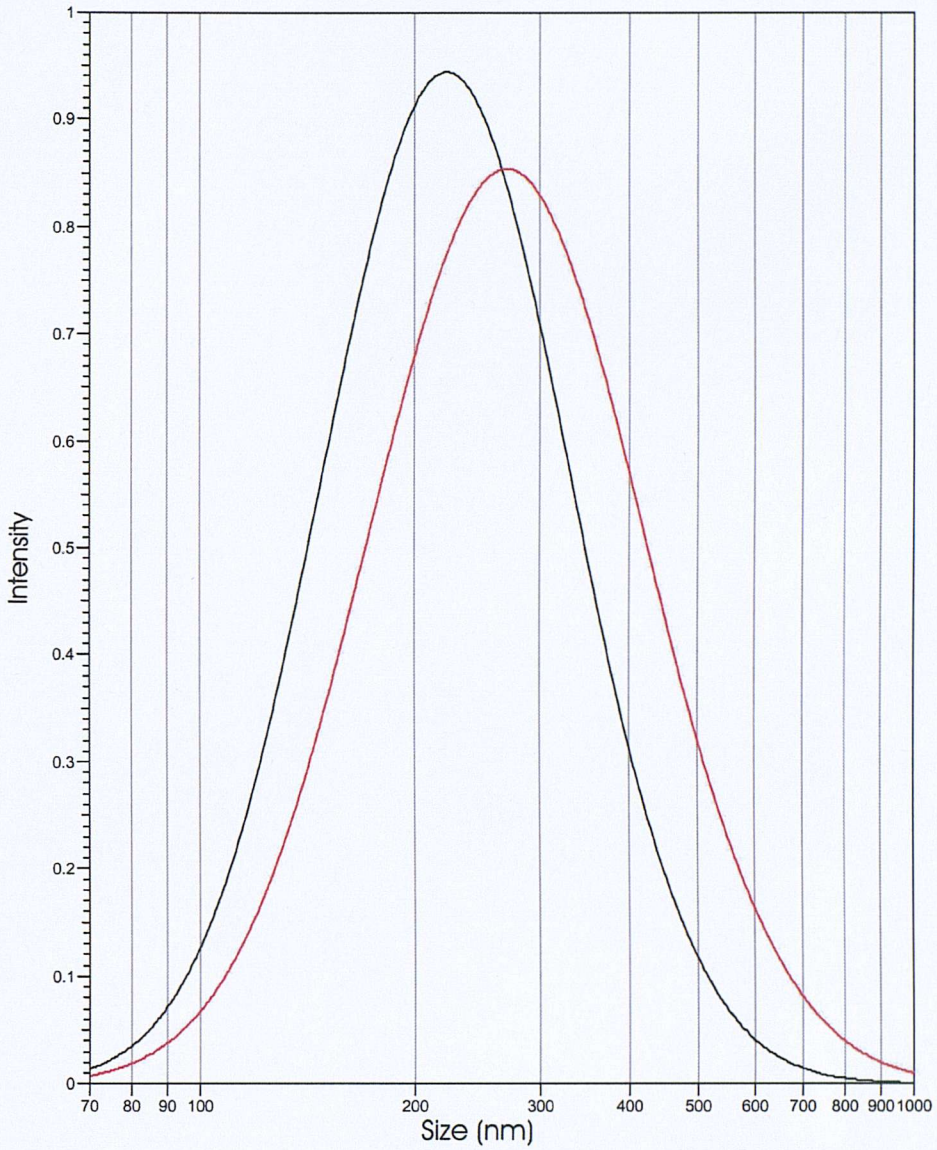

Figure 9.4 Unimodal analysis of sample 5 (black line) and sample 6 (red line)(9.4.2).

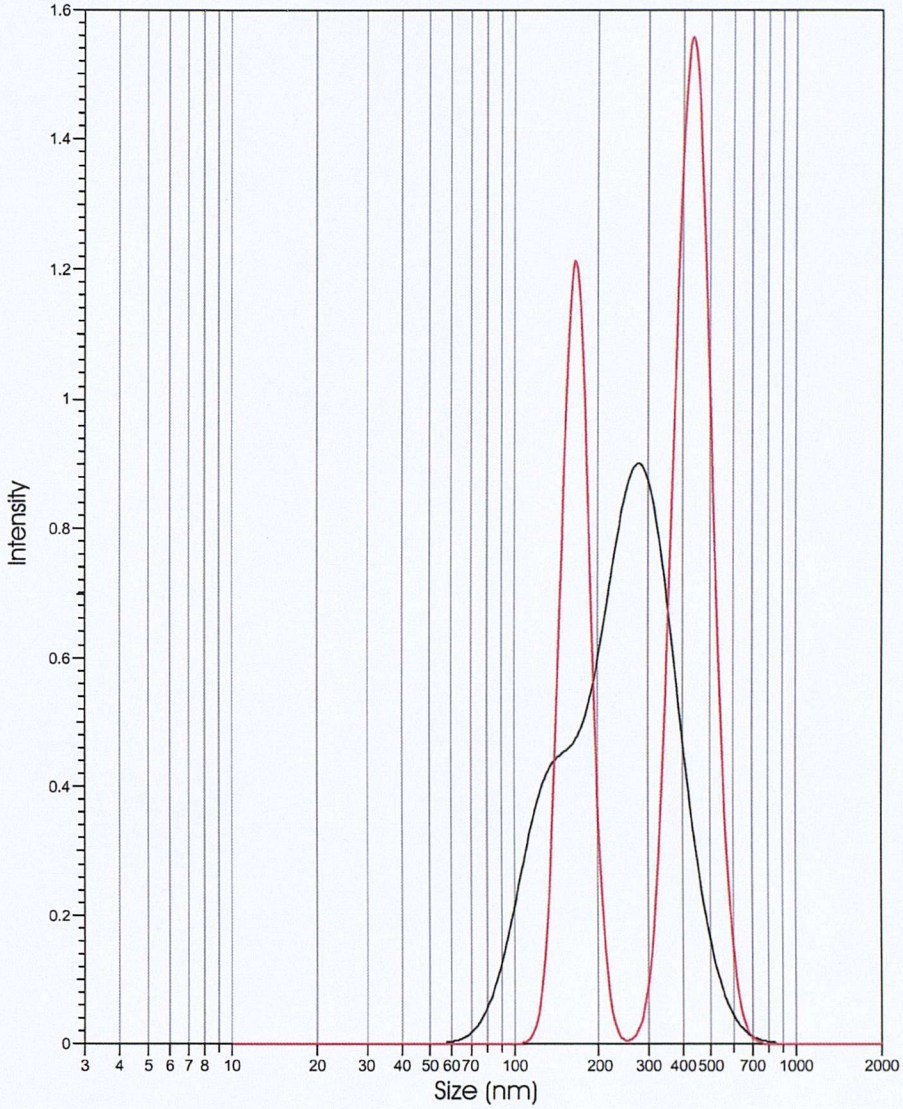

Figure 9.5 Sample 5 (red line) and 6 (black line)(9.4.2), previously sized by unimodal analysis (Figure 9.4), were sized by the SPD analysis and the result shown as intensity result.

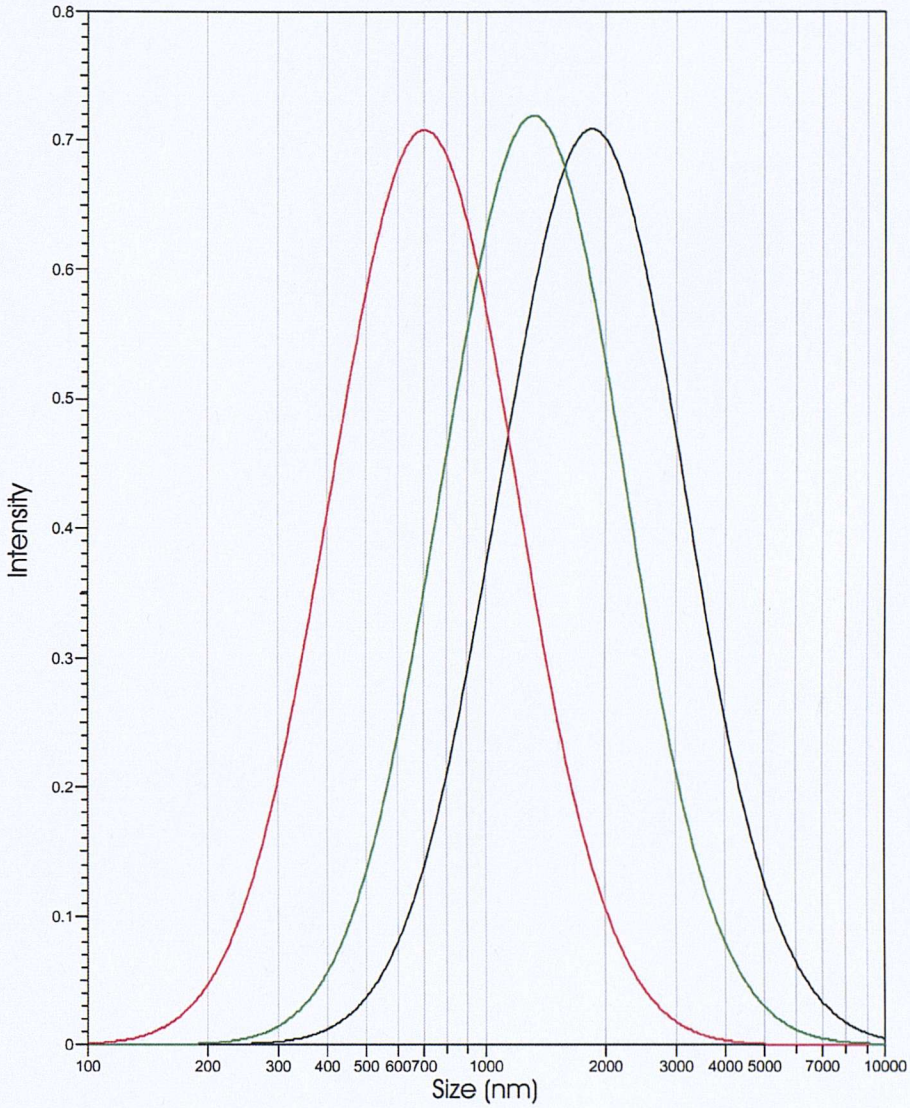

Figure 9.6 Unimodal analysis of vesicles sampled during the step reported in Table 9.2: after the 6th step (black line), after the 7th step (red line) and after the first F-T cycle (green line).

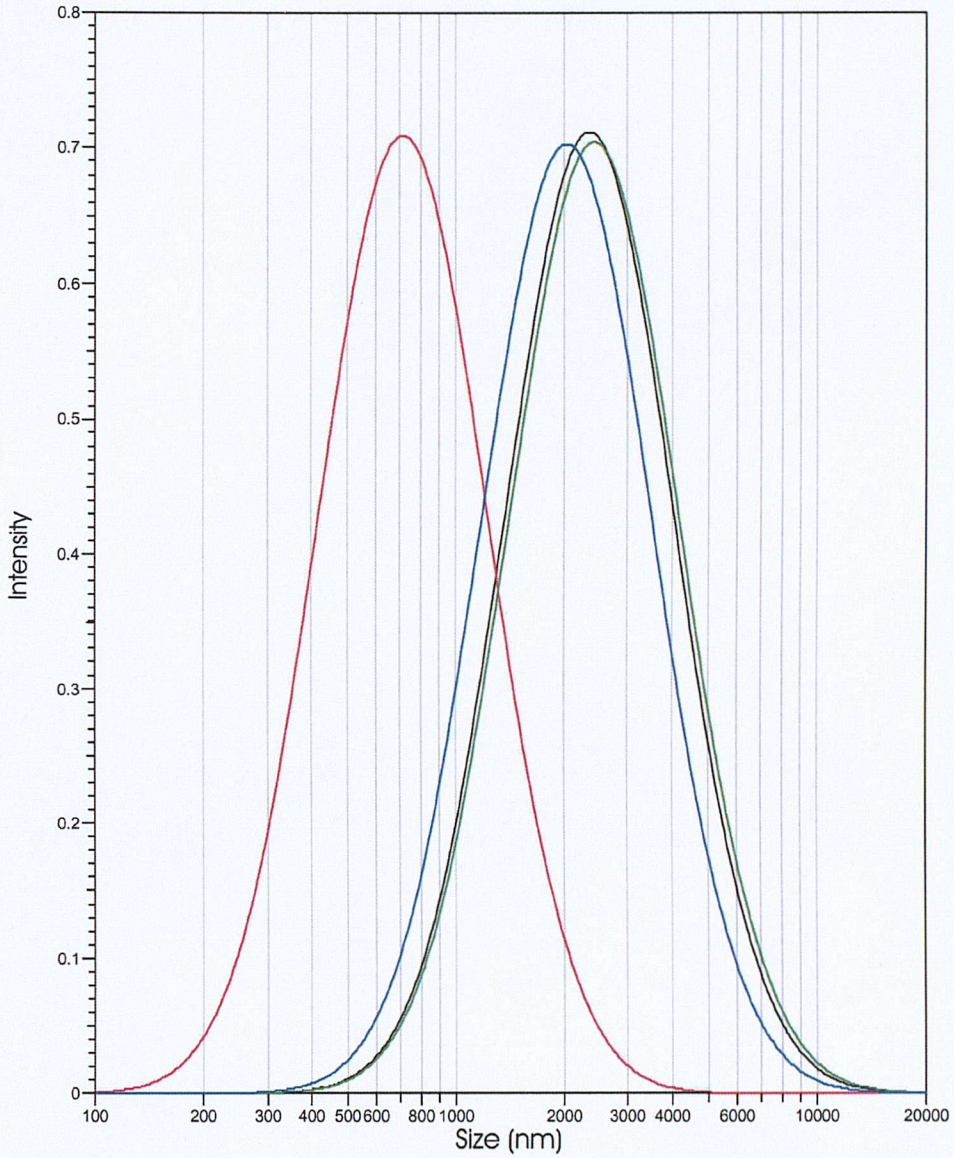

Figure 9.7 Unimodal analysis of vesicles sampled during the steps reported in Table 9.2 and Table 9.3: after the 2nd F-T (black line), the 11th step (red line), the 4th F-T (green line) and the 5th F-T cycle (blue line).

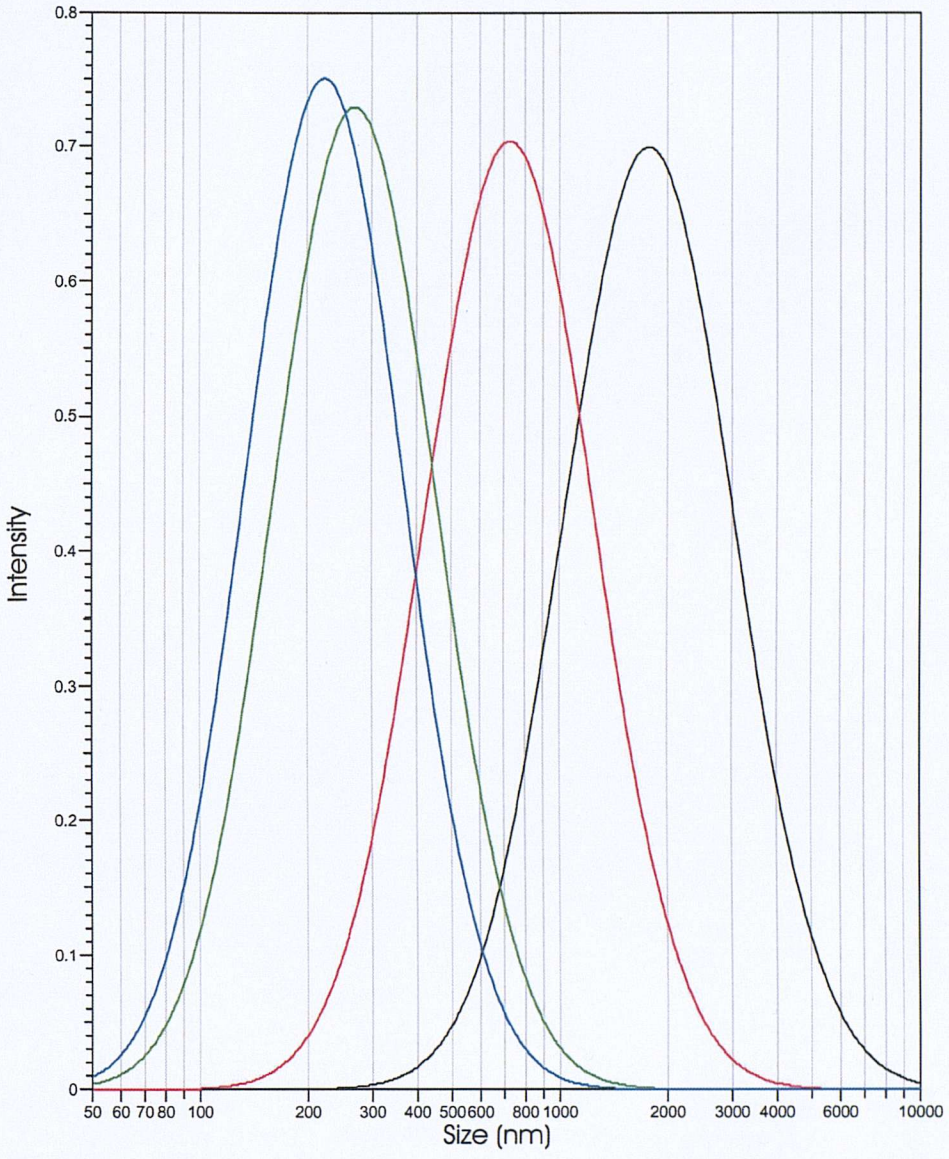

Figure 9.8 Vesicle size after five consecutive F-T cycles following the four showed in Figure 9.7: after the 6th F-T (black line), the 7th F-T (red line), the 9th F-T and 30 second sonication (green line) and the 10th F-T (blue line).

9.5.3 Vesicle stability

DOPC LUVs were monitored for size changes 1.5 hours after the first sizing. The results from the unimodal analysis (Figure 9.9) showed an increase of the vesicle diameter from ~1.3 nm to ~ 1.9 nm in 1.5 hours. Results from SDP analysis are

shown in Figure 9.10 and Figure 9.11, while the size values are reported in Table 9.5.

Table 9.5 Size values for the curves reported in Figure 9.10 and Figure 9.11

Measurement and reference	Mean size and Sdt.Dev. (nm)	Intensity (%)	Size and Sdt. Dev. (nm)
Black line	1916 ±462	95.4	2000 ±137
		4.6	156 ±25
Red line	1946 ±381	97.2	2000 ±137
		2.8	67 ±16

The torque tension effect on vesicle stability was monitored using a DOPC/DOPE (1:1) lipid mixture. Results from unimodal analysis and from SDP analysis (intensity results) are reported in Table 9.6. Results from unimodal analysis are shown in Figure 9.12, whilst intensity results from SDP analyses are shown in Figure 9.13 and Figure 9.14. Unimodal analysis showed that vesicle size increased after 1.5 hours, from ~ 0.85 to ~ 0.98 μm.

Table 9.6 DOPC/DOPE (1:1) LUVs sizing. Intensity results and mean size obtained form SDP analysis.

Measurement and reference	Mean size and Sdt.Dev. (nm)	Intensity (%)	Size and Sdt. Dev. (nm)
Black line	1779 ±715	**87.9**	2000 ±137
		11.9	174 ±22
		0.2	32 ±2
Red line	1713 ±802	84.5	2000 ±137
		15.5	156 ±11

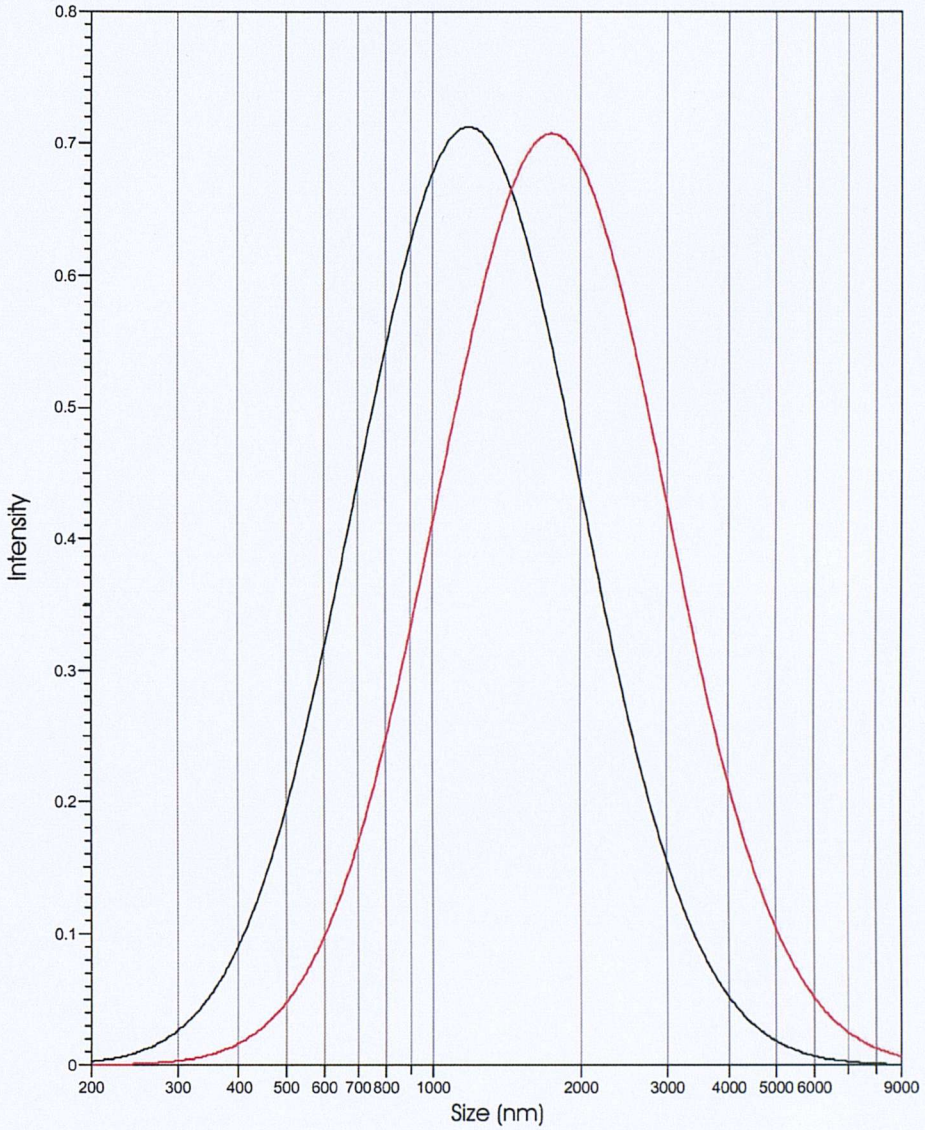

Figure 9.9 DOPC LUVs were sized twice at t = 0 and t = 1.5 h. The size obtained at t = 0 h by unimodal analysis was 1303 ± 598 nm (black line), while at t = 1.5 h it was 1931 ± 895 nm (red line).

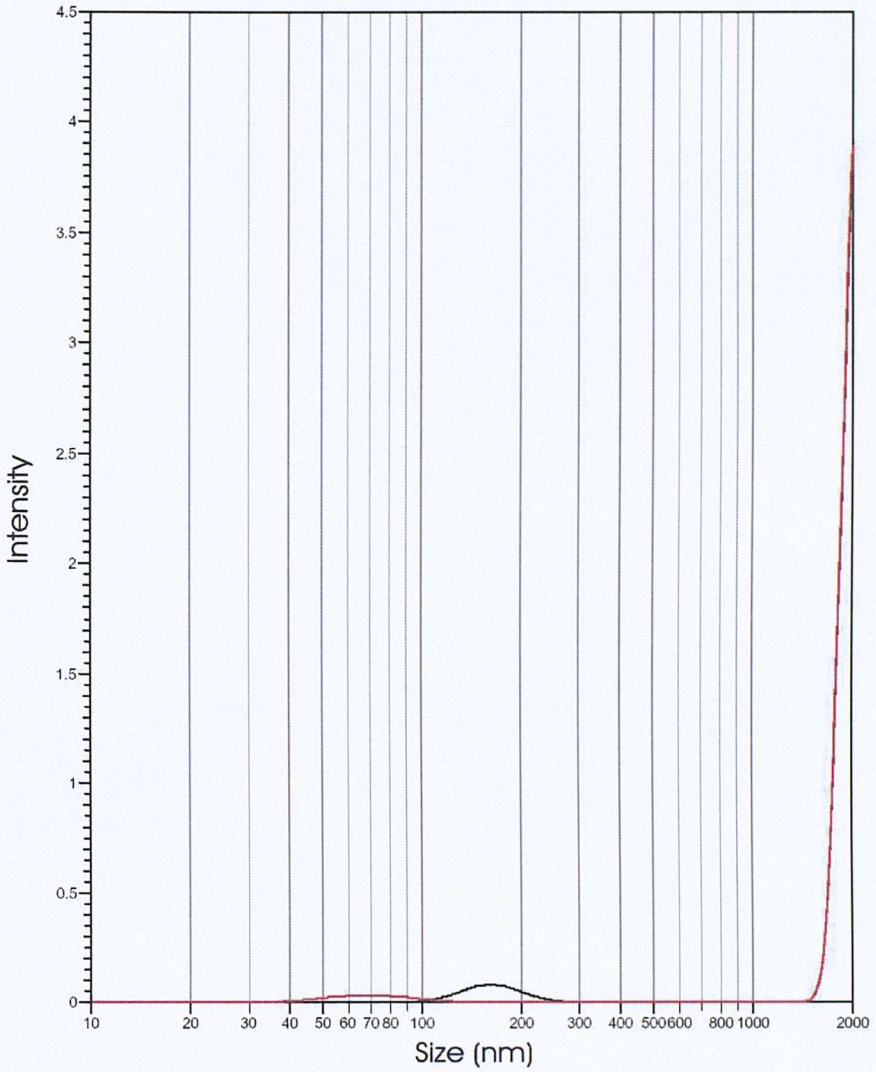

Figure 9.10. Intensity result of SDP analysis of DOPC LUVs sizing. The time gap between the first (black line) and the second measurement (red line) was 1.5 hours.

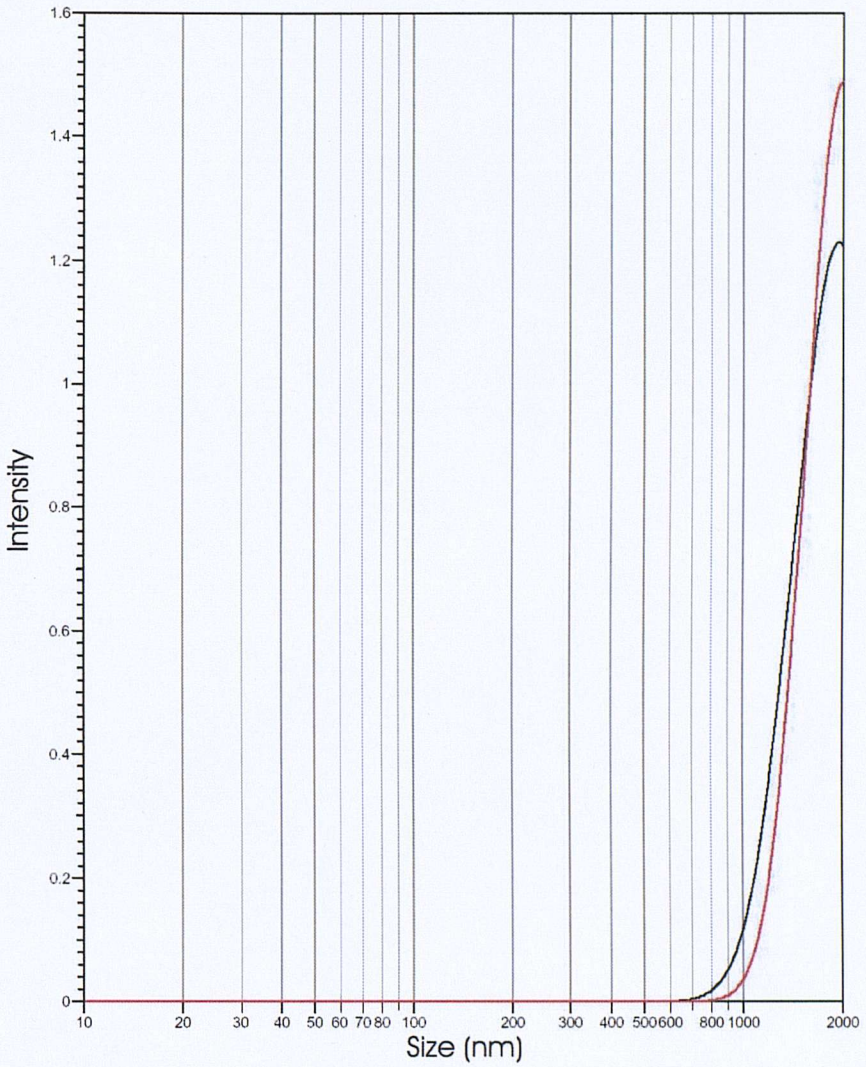

Figure 9.11. Mean peaks for DOPC LUVs size obtained from the intensity results of the SDP analysis, Figure 9.10.

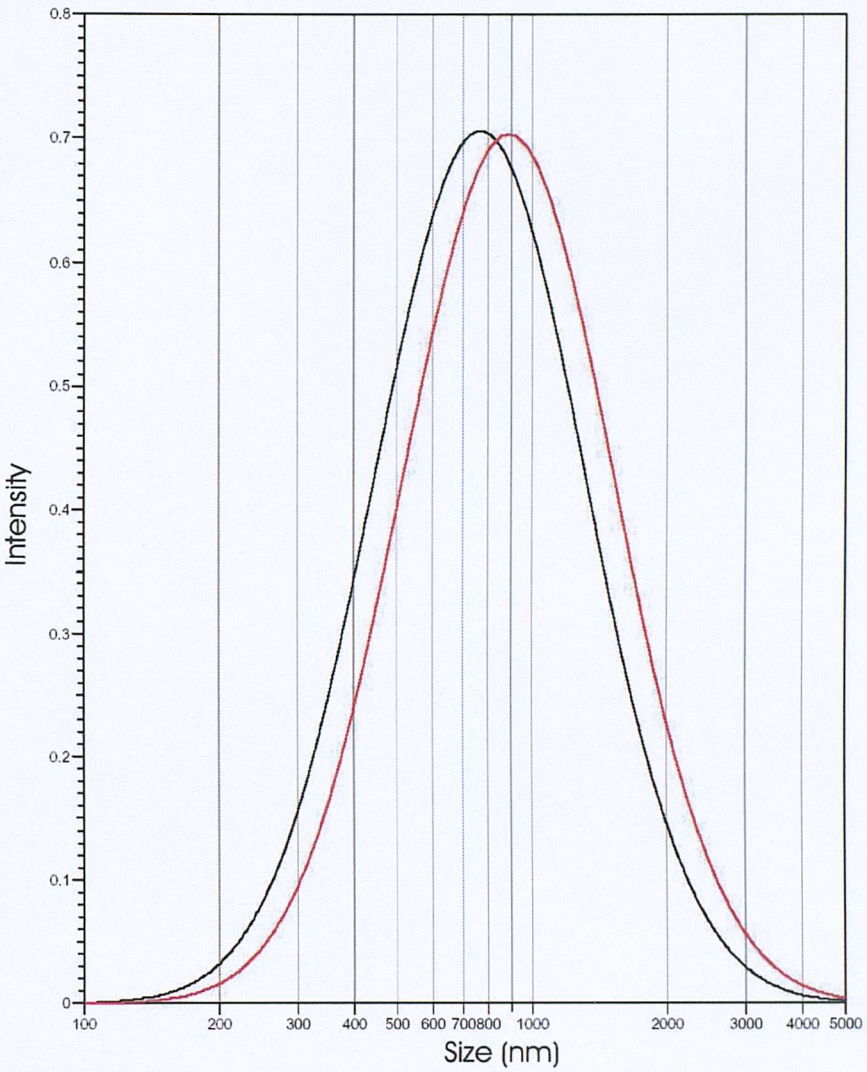

Figure 9.12 DOPC/DOPE (1:1) LUVs were sized at t = 0 and t = 1.5 h. The size at t = 0 h, obtained by unimodal analysis, resulted 849 ± 395 nm (black line), while the size at t = 1.5 h resulted 984 ± 460 nm (red line).

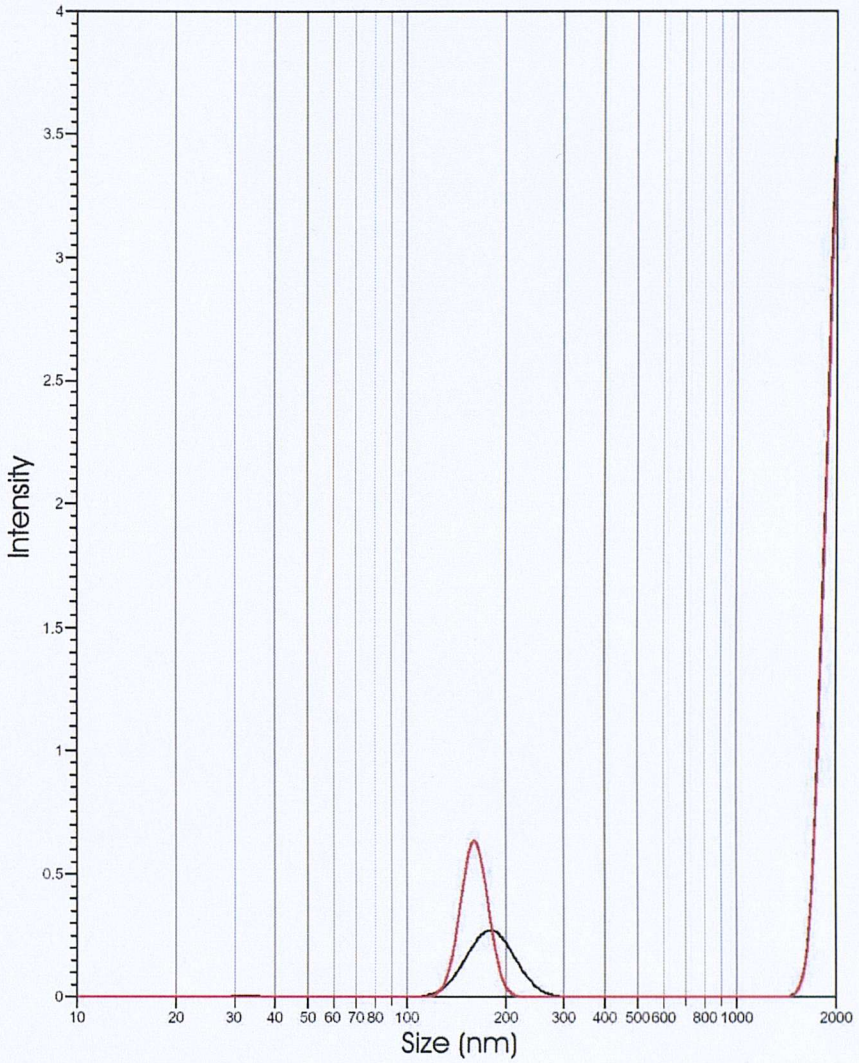

Figure 9.13 DOPC/DOPE (1:1) LUVs were sized at t = 0 and t = 1.5 h. The SDP intensity results are shown as black and red line for t = 0 and t = 1.5 h respectively. All the sizes and standard deviations are reported in Table 9.6.

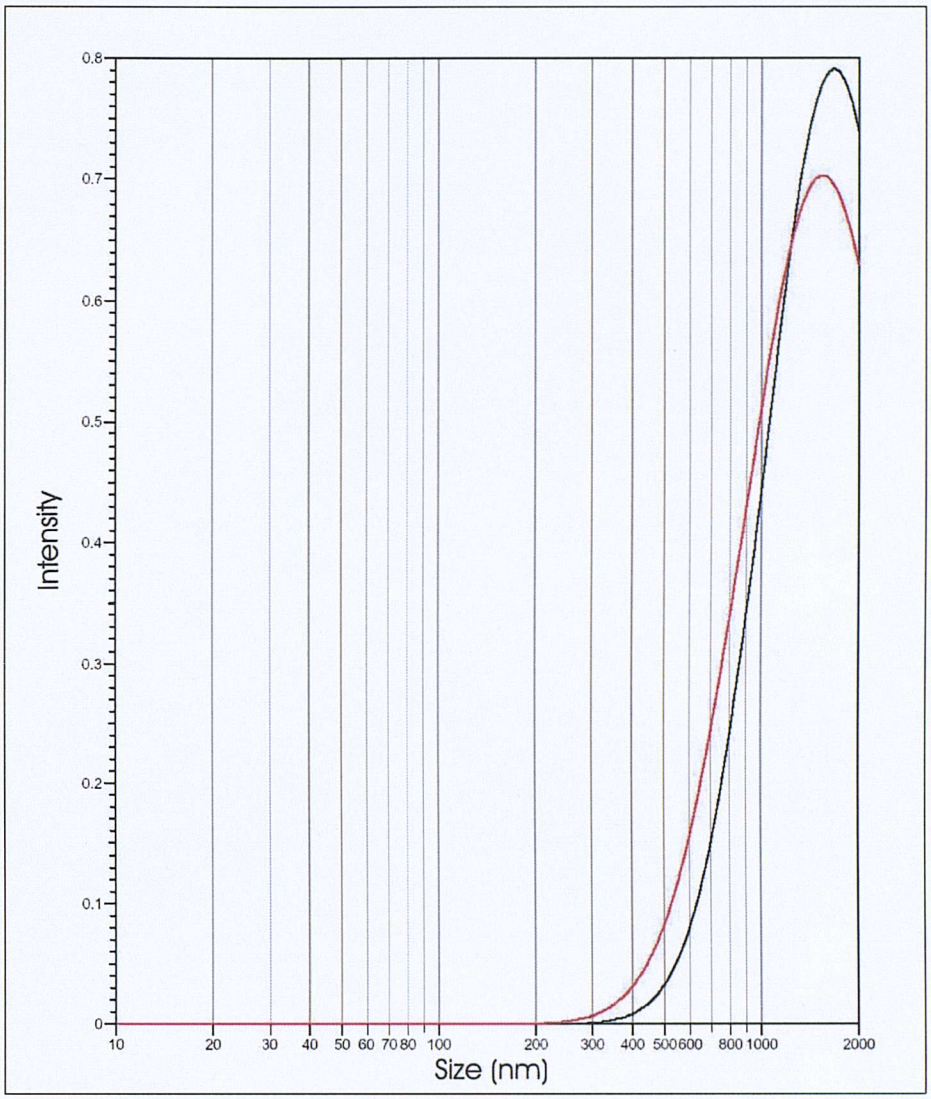

Figure 9.14 Mean size from the SDP analysis of the DOPC/DOPE(1:1) LUVs. The diameters and their standard deviation are reported in Table 9.6

Vesicles stability was monitored by measuring their size every 20 minutes. Scattering data were analysed by both unimodal and SDP methods. Results are reported in Table 9.7 and Table 9.8 for the unimodal and the SDP analysis, respectively. Data from Table 9.7 are plotted in Figure 9.15. SDP analysis (Table 9.8 and Figure 9.16) gave a slightly different result, but all the peaks are in the same region.

Table 9.7 Unimodal results from DOPA LUVs sizing

Measurement	Size (nm)	Std. Dev. (nm)
1	236	88
2	237	88
3	237	88
4	236	88
5	236	89
6	236	87
7	235	88
8	237	88
9	236	89
10	235	87
11	238	89
12	236	86

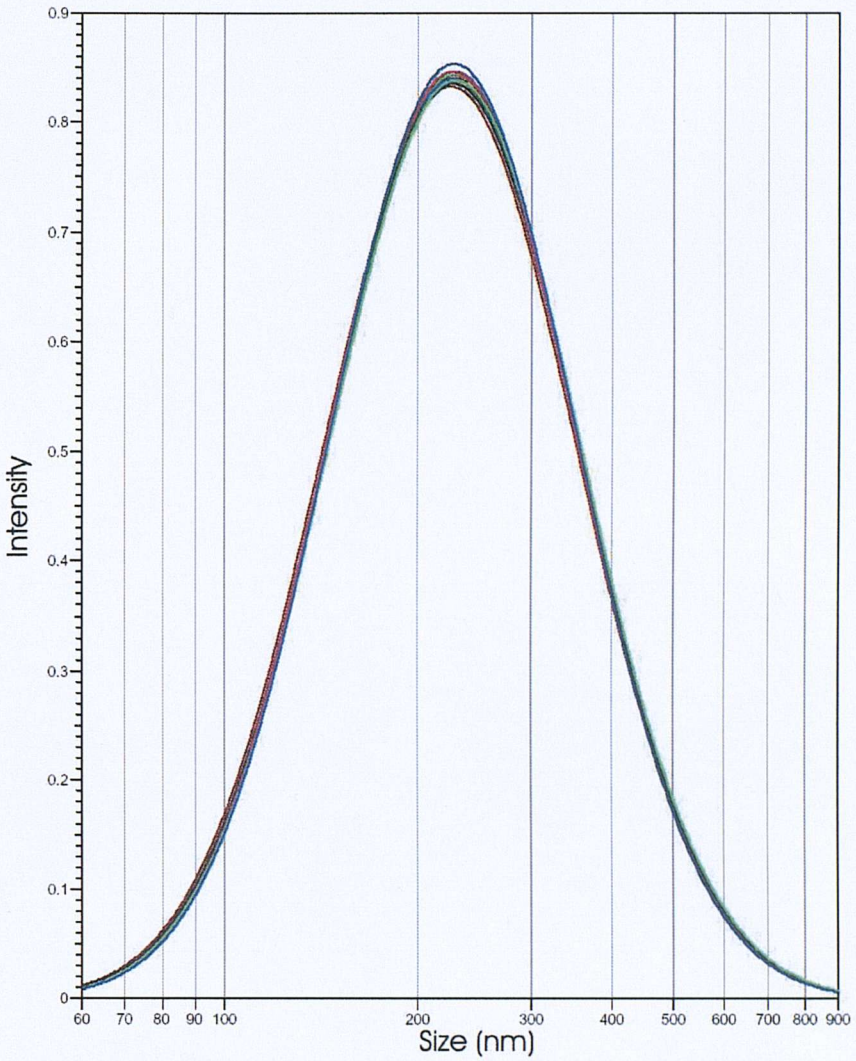

Figure 9.15 Unimodal results from DOPA LUVs sizing. Values for the twelve curves are given in Table 9.7.

Table 9.8 Intensity analysis of the SDP treatment of the data from the 12 sizings of DOPA LUVs.

Measurement	Intensity (%)	Size (nm)	Std. Dev. (nm)
1	74.6	340.9	57.8
	25.4	122.6	22.1
2	62.6	185.6	42.8
	37.4	452.2	59.9
3	62.7	161.5	13.8
	37.3	477.9	47.9
4	71.7	382.4	60.8
	28.3	129.6	21.3
5	62.7	186.6	39.1
	37.3	602.2	87.0
6	67.5	161.4	12.1
	32.5	502.1	34.4
7	68.5	216.6	65.6
	31.5	599.2	112.7
8	75.6	214.2	59.3
	24.4	753.3	88.7
9	69.3	205.6	51.0
	30.7	676.3	116.7
10	58.7	400.6	27.3
	41.3	155.1	17.8
11	72.7	333.2	72.5
	27.3	138.7	31.9
12	87.9	239.0	62.4
	12.1	1133.4	155.5

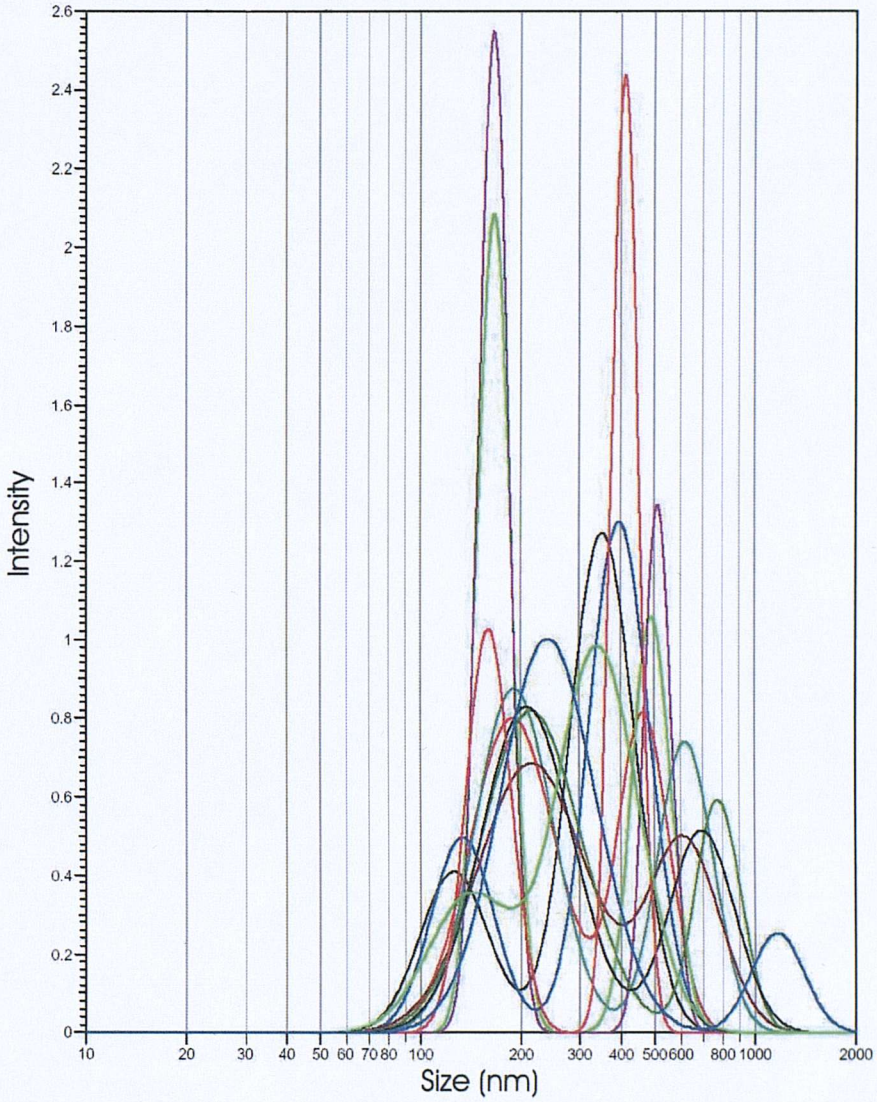

Figure 9.16 SPD intensity analysis of the 12 DOPA LUVs sizing (Table 9.8).

9.5.4 Anionic phospholipids and coagulation

Critical coagulation concentrations for DOPA LUVs, obtained by titration with solutions of NaCl, $MgCl_2$ or $CrCl_3$, are reported in Table 9.9, and Table 9.11 shows theoretical and experimental values obtained using Eq. 9.22. DOPS LUVs coagulation was tested only with NaCl and $MgCl_2$. Titration results are reported

Table 9.10, and Table 9.12 reports the results obtained substituting the values of Table 9.10 in Eq. 9.22. Table 9.9 and Table 9.10 report the cation concentrations from DOPA and DOPS LUVs titrations corrected for the ionic strength of the DOPA and DOPS solutions at the end of the titration. The mean activity coefficients $\gamma_{\pm}$ were calculated applying the Debey-Hückel limiting law

Eq. 9.23 $$\log\gamma_{\pm} = -0.509|z_{+}z_{-}|\sqrt{I}$$

where z_{+} and z_{-} refer to the ionic charge of the electrolyte for which the coefficient is calculated, and I is the ionic strength of the solution at the end of the titration.

Table 9.9 Critical coagulation concentrations for DOPA LUVs

Cation	ccc (mM)	Sdt. Dev. (mM)	$\gamma_{\pm}$	$\gamma_{\pm}$·ccc (mM)
Na^{+}	240	23	0.49	118
Mg^{2+}	2.50	0.04	0.66	1.65
Cr^{3+}	0.25	0.02	0.66	0.165

Table 9.10 DOPS titration using NaCl and $MgCl_2$. The value for Mg^{2+}(a) was obtained using 150 mM BT buffer.

Cation	ccc (mM)	Sdt. Dev. (mM)	$\gamma_{\pm}$	$\gamma_{\pm}$·ccc (mM)
Na^{+}	453	2	0.41	186
Mg^{2+}	5.6	0.1	0.64	3.6
Mg^{2+}(a)	4.9	0.2	0.70	3.4

Table 9.11 Calculated and experimental ccc ratio obtained substituting data from Table 9.9 into Eq. 9.22

	Calculated ratio	Experimental ratio	Experimental ratio for $\gamma_{\pm}$
$\frac{ccc(Na^+)}{ccc(Mg^{2+})}$	64	96	72
$\frac{ccc(Na^+)}{ccc(Cr^{3+})}$	729	960	720
$\frac{ccc(Mg^{2+})}{ccc(Cr^{3+})}$	11.4	10	10

Table 9.12 Calculated and experimental ccc ratio obtained substituting data from Table 9.9 into Eq. 9.22

	Calculated ratio	Experimental ratio	Experimental ratio for $\gamma_{\pm}$
$\frac{ccc(Na^+)}{ccc(Mg^{2+})}$	64	81	52
$\frac{ccc(Na^+)}{ccc(Mg^{2+}(a))}$	64	92	55

9.6 Conclusion

The experimental results showed that it was not possible to increase the vesicle size by increasing the number of F-T cycles and it was found that the sonication step did not relieve the stress stored in the vesicles during the F-T cycles. Experiments indicated that four F-T cycles gave the largest vesicle size and agreement was found between the size of vesicles prepared as described in 9.4.3 and the size of vesicles prepared as reported by Pick (600-700nm).

The stability tests showed that vesicles with different torque tension (DOPC and DOPC/DOPE (1:1)) or different surface charge density (DOPA) are stable for a period longer than 2 or 4 hours.

Finally, the titration of DOPA and DOPS LUVs showed that those vesicles coagulate in the presence of positively charged ions and that the possibility of coagulation can be limiting in the use of those negatively charged lipids.

9.7 References

[1] R. Chang, *Physical Chemistry for the chemical and biological sciences*, 3rd ed. Sausalito, CA 94965: University Science Books, 2000.

[2] C. Coulter, *Coulter® N4 Plus Submicron Particle Sizer, Reference Manual.* Miami, FL 33196, 1995.

[3] U. Pick, "Liposome with a large trapping capacity prepared by freezing and thawing of sonicated phospholipid mixtures," in *Archives of Biochemistry and Biophysics*, vol. 212, 1981, pp. 186-194.

[4] G. S. Attard, Templer, R.H., Smith, W.S., Hunt, A.N., and Jackowski, S., "Modulation of CTP: phosphocholine cytidylyltransferase by membrane curvature elastic stress," in *Proceedings of the National Academy of Sciences of the United States of America*, vol. 97, 2000, pp. 9032-9036.

[5] M. Kasahara, and Hinkle, P.C., "Reconstitution and purification of the α-glucose transporter from human erythrocytes," in *Journal of Biological Chemistry*, vol. 252, 1977, pp. 7384-7390.

10 CCTα activity modulation

10.1 Torque tension, surface charge and CCTα activity

As discussed in 3.4.2, studies conducted on CCTα have shown that both lipid charge and stored bending energy affect the enzyme activity through the enzyme translocation onto the vesicle surface. The modulation of CCTα activity by the torque tension of type II lipid vesicles, outlined in Figure 10.1, has been reported in the literature by Attard *et al.* using DMPC/DOPC and DOPC/DOPE mixtures (Figure 10.2), and by Davies *et al.*, who tested the enzyme activity using DOPC/DOPE mixtures (Figure 10.3)[a] [1, 2]. As discussed in 4.2.2 and 4.3.2, the torque tension arises when the forces acting between the lipids in the aggregate are not in equilibrium. A and B (Figure 10.1) are a representation of the force imbalance arising when a lipid layer is constrained to adopt a curvature (B) different from its spontaneous one (A). The energy spent to adopt the curvature B is stored into the lipid layer as bending energy E. Figure 10.4(b) diagrams the effect on the torque tension τ of the forces acting in a lipid monolayer between the hydrocarbon chains, F_c, and between the polar head-groups, F_h. Figure 10.4(a) shows the phospholipids used by Attard *et al.* and by Davies *et al.* to vary the torque tension. The repulsion in the hydrocarbon region of the lipid monolayer increases as the lipid mole ratio of the DMPC/DOPC mixtures changes: the higher the DOPC mole fraction, the higher the torque tension. The further substitution of the choline head-group (in DOPC) with the smaller ethanolamine (in DOPE) decreases the repulsion between the head-groups of the lipid monolayer, thus causing a further increase in the torque tension of the monolayer. The increase of τ in the mixtures DMPC/DOPC and DOPC/DOPE increases the bending energy stored in those lipid vesicles.

Figure 10.2 is evidence supporting the hypothesis, proposed by Attard *et al.*, that enzyme partitioning is driven by the release of the bending energy stored in a membrane containing type II lipid. In a similar experiment, Arnold and Cornell [3] showed that CCT activation could have been achieved using egg-PtdCho containing up to 15 mol% of diacylglycerol, produced by hydrolysis of the phosphoester bond between the phosphocholine moiety and the glycerol backbone of PtdCho. The removal of the phosphocholine moiety results in a decrease of F_h, an increase of F_c and consequently in an increase of the torque tension and the stored bending energy, which causes a higher enzyme activation [3].

Attard *et al.* also predicted and successfully demonstrated, in accordance with their model, that the addition of type I amphiphiles (Figure 10.5) to type II lipid vesicles resulted in a lower CCT activation [1]. In particular, they showed that even a mole fraction as low as 0.04 was sufficient to decrease of almost 40% the CCT activity measured in presence of DOPC/DOPE (9:1) vesicle.

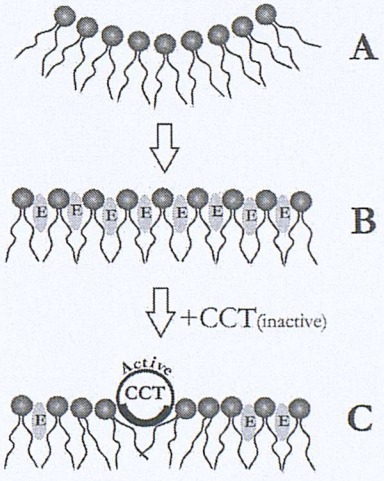

Figure 10.1 Type II lipid monolayer adopting its spontaneous curvature (A) is torque tension free. When the monolayer (A) is constrained in a flat position (B), corresponding to a zero curvature, the torque tension and the bending energy (grey ellipses marked with E) of the monolayer increase. The release of part of the bending energy and reduction of the torque tension are the driving force of CCTα partition onto the monolayer(C)[1].

---

[a] Attard used large unilamellar vesicles of non-homogeneous size with a mean diameter bigger than 0.8 μm, whereas Davies used large unilamellar vesicles of homogeneous size with a ~100 nm mean diameter.

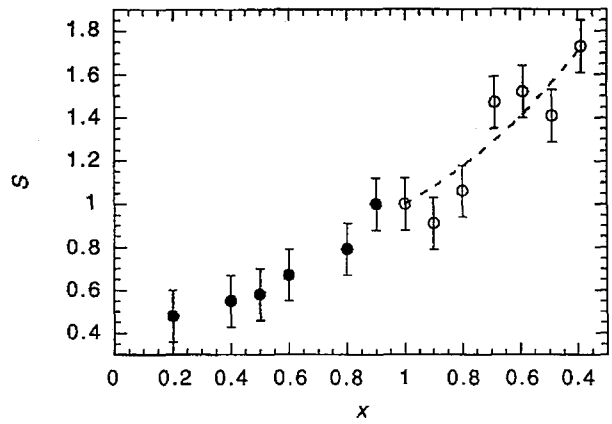

Figure 10.2 CCTα relative activity, S, is plotted as a function of the mole fraction of DOPC, x, in DMPC/DOPC mixtures (solid circles) and in DOPC/DOPE mixtures (open circles). The dotted line represents the theoretical enzyme relative activity as function of DOPE mole fraction [1].

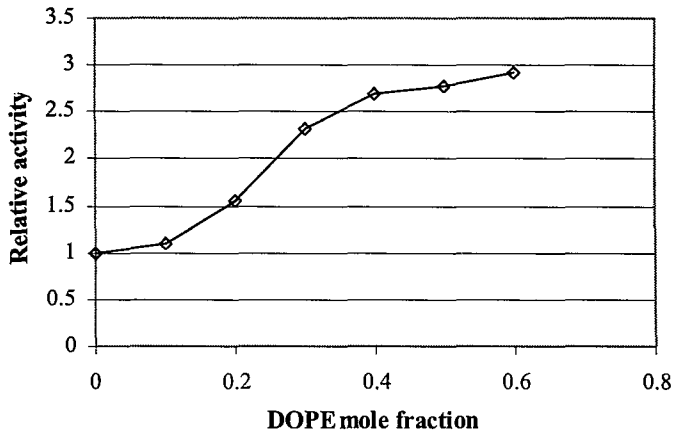

Figure 10.3 CCTα relative activity plotted as a function of the DOPC mole fraction, x, in DOPC/DOPE mixture. Data from Davies et al. [2].

Other than the torque tension, the effect of negatively charged lipids on CCT activity has also been studied and in particular, it has been shown that a dramatic increase in enzyme activity was observed in the presence of negatively charged lipids such as phosphatidic acid, phosphatidylserine, phosphatidylinositol, phosphatidylglycerol or cardiolipin [3-5]. Moreover, Arnold and Cornell showed that there could be a synergistic effect of charge and torque tension on CCT activation by adding diacylglycerol (2.5 mol%) to egg-PtdCho containing 2.5 mol% negative lipids [3].

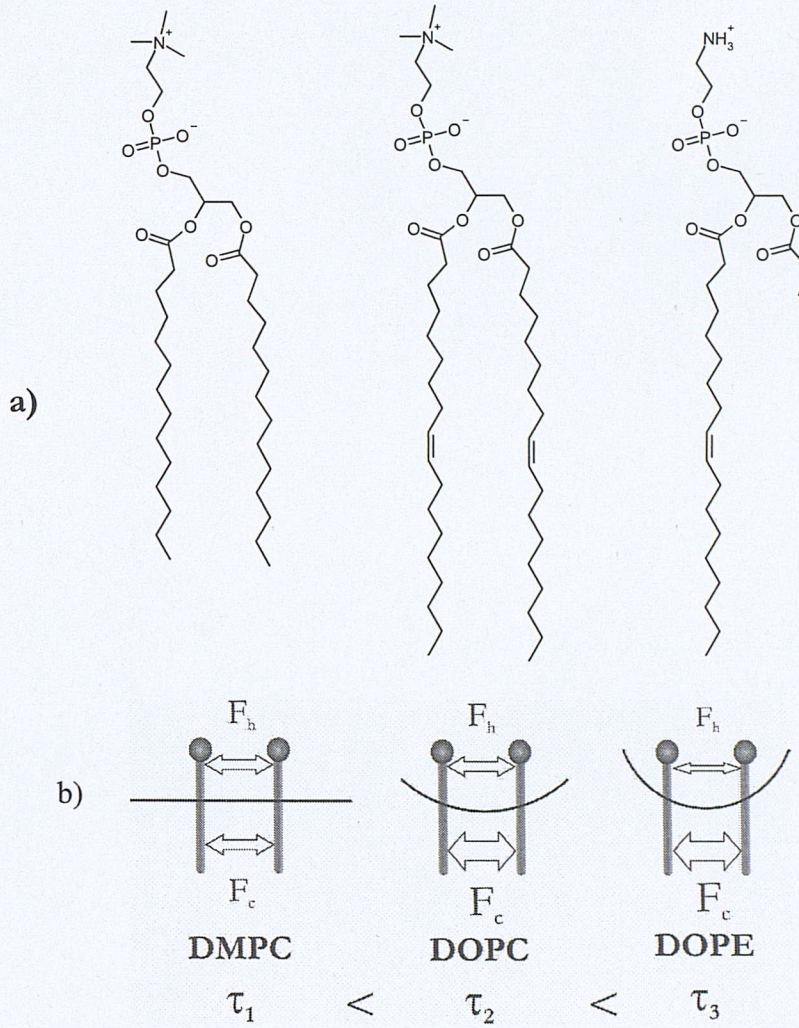

Figure 10.4 a) DMPC and DOPC have the same head-group, choline, but differ in the acyl chains, dimyristoyl and dioleoyl, respectively. DOPC and DOPE have the same hydrocarbon chains but differ in head-groups, choline and ethanolamine respectively. b) Flat monolayers of DMPC, DOPC and DOPE experience different torque tensions due to the different force distribution across the lipid layer. When the force at the hydrocarbon region, F_c, is similar to the force at the head-group region, F_h, the flat monolayer experiences a low tendency to bend (flat line in the middle of two DMPC molecules); the presence of the double bond in the oleoyl chains of DOPC causes an increase of F_c and the flat monolayer experiences a high tendency to bend (curved line in the middle of two DOPC molecules); the substitution of the choline group with the ethanolamine one in DOPE causes a decrease of F_h resulting in a further increase of the tendency to bend (curved line in the middle of two DOPE molecules).

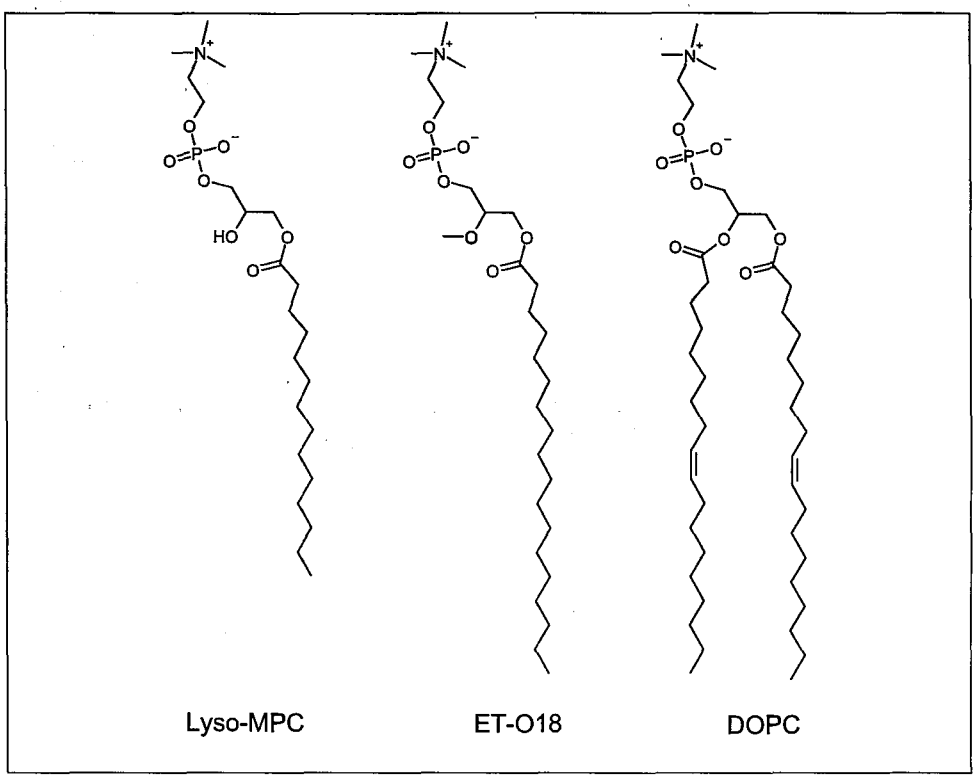

Figure 10.5 Monomyristoylphosphocholine (lyso-MPC) and 1-*O*-octadecyl-2-*O*-methyl-*rac*-glycerophosphocholine (ET-O18) are type I amphipiles, which aggregates experience a reduced force acting across the hydrocarbon region (F_c in Figure 10.4) and in a positive spontaneous curvature (in opposition to the negative one characterising type II lipid such as DOPC).

In a recent paper, Lykidis *et al.* have shown that two possible distinct domains of CCT could be involved in the enzyme sensitivity to either the charge or the stored bending energy of lipid vesicles [6]. Using CCTα truncated mutants, Lykidis *et al.* showed that the M-domain might be the domain sensitive to the bending energy whereas the C-terminal domain might be the domain sensitive to the vesicle charge.

However, the determination of the relative contribution of surface charge and of the bending energy on the partitioning and activation of CCT is not an easy task. No data are available in the literature for the spontaneous curvature, the bending elastic moduli and the surface density charge of charged lipids that have been used. However, the experiments described in this chapter and in chapter 11 were aimed to provide insights into the modulation of CCT activity by charged lipids.

10.2 DOPC mixtures

The activity of CCTα has been subject of considerable interest over the past two decade. Data on the activation of the enzyme by lipids were often based on assaying the enzyme activity in presence of vesicles prepared with egg-PC mixed with other lipids. Egg-PC is a natural mixture of phosphatidylcholines with variable acyl chain composition (the acyl chains may differ in length and in saturation). The variability in the fatty acid composition makes difficult any prediction of the torque tension and bending energy stored in the egg-PC vesicles. Similarly, a number of CCT results were obtained using natural charged or uncharged lipid mixtures, for which the bending energy is unknown and cannot be easily estimated.

In order to avoid variations in enzyme activity resulting from the natural viability of egg-PC, the enzyme assays reported in this thesis were conducted using DOPC and its mixtures with charged and uncharged synthetic lipids. Large unilamellar vesicles (LUVs) of DOPC were employed to determine the standard activity of each batch and aliquot of CCT used throughout these studies. These data provided reference points that could, in principle, be used to compare the activity of different mixtures and enzyme batches. The use of DOPC LUV offers two advantages:

1. The spontaneous curvature and the bending modulus are known and do not change because of the fixed fatty acid composition.
2. DOPC bilayer is in the liquid crystalline phase, resembling the fluid phase of the biological membranes [7, 8].

DOPA, DOPS, OPA, OPS, DPPA, DPPS and OA were chosen as secondary components in the DOPC mixtures attempting to distinguish between the charge and the torque tension effect on the enzyme activation. Unfortunately, as the spontaneous curvature and the bending moduli for the mixtures discussed herein are not known, the discussion of the data reported hereafter will have only a qualitative character.

The literature experiments, which showed CCTα activation by DOPC/DOPE vesicle mixtures, were repeated to verify the assay conditions used for the experiments reported and discussed in this thesis. Phosphatidylserine and phosphatidic acid were used to investigate the effect of lipids with different head-group charge on CCTα activity (nominally phosphatidic acid has two negative charge per molecule whilst phosphatidylserine has two negative and one positive charge per molecule)[b]. The effect of the torque tension in presence of these charged lipids was investigated adopting the same strategy that was used for the DMPC/DOPC system. In particular, maintaining constant the head-group, the decreasing in the forces across the lipid molecules in the hydrophobic region was attempted by changing the type of acyl chains present in the lipids: the two oleoyl chains were substituted with two palmitoyl and then with one oleoyl chain, which are hypothesised to reduce the lateral pressure as result of the reduced chain volume. The expectation is that the enzyme activity decreases in the order DOPC/DOPA ≥ DOPC/DPPA ≥ DOPC/OPA and DOPC/DOPS ≥ DOPC/DPPS ≥ DOPC/OPS.

A common method reported in the literature to determine the maximal activity of CCT involves the use of vesicles comprise of egg-PC/OA (1:1) mixtures. Some instances of the use of DOPC/OA mixtures for this purpose have been reported.

10.3 Enzymatic assay conditions

CCTα, in the presence of vesicles and Mg^{2+}, catalyses the following reaction

$$CTP^{c} + \text{phosphocholine} \rightleftarrows \text{CDP-choline} + PPi$$

[b] The difference in the head-group size between phosphatidylserine and phosphatidic acid will be discussed later in this Chapter.

[c] dCDP-choline and CTP-choline have been found in extracts from microorganisms [9] and mammalian organisms [10]. Moreover, Kennedy et al. have reported that CCT shows the same specificity for both dCTP and CTP[9].

The literature offers a wide range of assays conditions, which differ in the nature and in the concentration of the components required for the enzymatic assay: 0.03-0.1 M TRIS at pH 7.4 [1-3, 5, 11], or 0.12-0.15 M bis-TRIS at pH 6.5 [6, 12, 13], or even a mixture of TRIS/TES/KH_2PO_4 (2 mM/80 mM/9 mM) at pH 5.8-8.3 [3]; 2-20 mM $MgCl_2$ [1-3, 6, 11-15]; 0.8-10 mM CTP or dCTP [1-3, 6, 9, 11-13]; no DTT [6, 11-13] or 5-10 mM DTT [1-3, 5]; 1-3 mM phosphocholine [1, 2, 5, 6, 11-13]; 0.064-1 mM lipids [1-3, 5, 6, 12, 13, 16]; incubation at 20-37 °C for 10-30 min [1-3, 5, 6, 11-13]. Several methods are reported in the literature to stop the enzymatic reaction, either by precipitation or inactivation of the enzyme with trichloroacetic acid [17], methanol/ammonia [18], EDTA [6] or by boiling the samples for 2 minutes [1, 19]. The two most common methods used for the quantification of CDP-choline are: TLC [6, 11, 20] and the charcoal [1, 16, 17].

The assay conditions used for the experiments reported and discussed herein were essentially those used by Attard *et al.* [1] and by Lykidis *et al.* [6]: 150 mM bis-TRIS pH 7.0, 10 mM $MgCl_2$, 3 mM phosphocholine, 3.0 mM dCTP, 1.0 mM lipids and 10 μg/ml CCTα, with a 20 minutes incubation at 37 °C[d]. It is not possible to estimate the percentage of enzyme that is either saturated or active because of the different values for V_{Max} and the K_ms of CTP and phosphocholine reported in the literature[e], and even because no kinetic study was done in the lab to determine V_{Max} and K_ms. The issue of enzyme variability and saturation will be addressed again in the final discussion of this chapter.

Since the principal mechanism of enzyme activation involves only enzyme translocation from the aqueous phase to the vesicle surface, a high lipid/CCTα mole ratio (~ 4200) is used to ensure that adsorption of the enzyme does not lead to gross change in membrane structure and properties. However, the lipid to CCT ratio was also bounded by the need to ensure that all assay were conducted under

[d] In any case the concentration of the species used for the assays was well within the range of those reported in the literature. Because preliminary testes were done using dCTP, this deoxynucleotide was employed in all the assays.

[e] The V_{Max} values reported in the literature extend from 1 to 20 nmol·min^{-1}·mg^{-1} and the KmS range from 0.3 mM to 1.5 mM for CTP and 0.4 mM to 0.9 mM for phosphocholine [12, 21-24]

conditions were not all the enzyme was partitioned onto the membrane. The reason for this latter requirement was that if for some composition all (or virtually all) the enzyme was to be found associated with the membrane, then further changes in composition which introduce higher amount of stored elastic energy would not result in increased enzyme activity. Fixing the lipid to enzyme ratio in this 'compromise' regime provides assays that are potentially more meaningful in relation to physiological processes.

10.4 Materials and methods

10.4.1 Materials

Purified hexahistidine-tagged CCTα[f], referred to as CCTα unless otherwise stated, was shipped as a solution (100-400 μg/ ml in 0.15 M BT, pH 6.5-7.0) in dry ice from the USA and was stored at –70 °C on arrival. Oleic acid, 1,2-dioleoyl-*sn*-glycero-3-phosphocholine (20 mg/ml in chloroform), 1,2-dioleoyl-*sn*-glycero-3-phospho-ethanolamine (10 mg/ml in chloroform) and Lewatit K-2621 cation exchanger resin were obtained from Fluka. 1,2-dioleoyl-*sn*-glycero-3-phosphatidic acid (20 mg/ml in chloroform), 1,2-dioleoyl-*sn*-glycero-3-phosphoserine (20 mg/ml in chloroform), 1,2-dipalmitoyl-*sn*-glycero-3-phosphatidic acid (20 mg/ml in chloroform), 1,2-dipalmitoyl-*sn*-glycero-3-phosphoserine (20 mg/ml in chloroform), 1-oleoyl-*sn*-glycero-3-phosphatidic acid (20 mg/ml in chloroform), 1-oleoyl-*sn*-glycero-3-phosphoserine (20 mg/ml in chloroform) were purchased from Avanti Polar Lipids. Sodium phosphate dibasic, phosphorus reagent kit, Bis-Tris, NaCl, $MgCl_2$, dithiothreitol, EDTA, phosphocholine and dCTP were obtained from Sigma. 2 ml glass ampoules and 8-quinolinol were purchased from Aldrich. Deionised water for HPLC, methanol, 25% HCl, 32% H_2SO_4, Machery-Nagel Polygram® SIL G and SIL G/UV_{254} silica TLC plates, FujiFilm SuperRX (18x24 cm), autoradiogram cassette SQX-112 (14″x17″) (C.B.S. Scientific Company) and

[f] CCTα-histag was a kind gift of Prof. S. Jackowski, St Jude Research Children Hospital, Memphis, Tennesse, USA [6].

4.0 ml polyethylene scintillation vials were purchased from Fisher. Phosphoryl[methyl-^{14}C]choline, Kodak Biomax transcreen LE intensifying screen and BCS-NA scintillation cocktail were obtained from Amersham, UK.

10.4.2 Calcium removal from phosphocholine

Phosphocholine is commercially available as calcium salt, which was found to be an inhibitor of the CCT [16]. Therefore, the following procedure was applied to remove calcium from the phosphocholine prior to its use in the assay reaction. 1 g of Lewatit K-2621 resin was packed in a disposable polyethylene 14 ml column and washed with water (~20 ml), 1.0 M NaCl (~14 ml), water (~10 ml), 1.0 M NH_4Cl (~14 ml) and water (~10 ml). A 83 mM phosphocholine aqueous solution (~15 ml) was then applied onto the column and the column washed with water (~15 ml); the flow through and the washing were pooled and lyophilised. The dry calcium-free phosphocholine, now simply referred to as phosphocholine, was dissolved in water (5.0 ml); 10 µl of this solution were mixed with 6.0 N H_2SO_4 (0.49 ml) in a 2 ml glass ampoule and heated at 180-200 °C for 30 minutes to convert the organic phosphorus in inorganic phosphorus [25]. 10 µl of the resulting inorganic phosphorus solution were mixed with 1.0 ml of phosphorus reagent and the absorbance read at 340 nm. The readings were corrected for the blank (10 µl of 6.0 N H_2SO_4) and the sample concentration estimated using a calibration curve obtained with phosphorus standard solutions. Different volumes of a 1.5 mM commercial phosphocholine solution (1-5 µl) and of a ~150 mM phosphocholine solution (5 µl) were loaded onto a TLC silica plate (not containing fluorophore) to reveal the potential presence of residual calcium. The TLC plate was then sprayed with the quinolinol reagent (8-quinolinol (0.5 g) in H_2O/Ethanol (40:60)) and exposed to UV light (λ = 254 nm): the reagent fluoresces in presence of calcium. The amount of calcium in the phosphocholine solution was estimated to be less than 0.2 mole percent.

10.4.3 Vesicle preparation

Using chloroform solution of the lipid mixtures (~25 mM), Large Unilamellar vesicles (LUVs) were prepared in glass vials following the Freeze-thaw (F-T) method (Table 10.1)[g] [1, 26, 27]. The effect of increasing mole fraction of anionic lipids on the DOPC vesicle size was tested by light scattering using a Coulter N4 Plus Particle Sizer; the size distribution was estimated by intensity SDP analysis (Tables from A19 to A26)[h]. The majority of the preparations resulted in vesicles bigger than 100 nm (diameter of the most commonly used LUVs) and only few samples have shown a low percentage (1-5% of the total scattered light) of vesicles smaller than 100 nm[i]. Moreover, under the conditions used for the sizing, the data collected did not show any increase or presence at all of small vesicles in correspondence to the increase of the second component in mixture with DOPC.

10.4.4 Enzymatic assay

The enzyme activity was tested using CCTα[j] (10 μg/ml) in the presence of 0.15 M BT-HCl (pH 7.0 at 37 °C), 4.0 mM DTT (freshly prepared solution), 3 mM dCTP, 10 mM $MgCl_2$, 1.0 mM lipids (lipid/CCTα mole ratio = 4200) and 3.0 mM radioactive phosphocholine, to a final volume of 50 μl in a 0.6 polypropylene tube. The enzymatic reaction was started by adding the radiolabelled phosphocholine (0.193 μCi) to the assay mixture, kept on ice, and transferring the tube on the water-bath. Samples were incubated at 37 °C for 20 minutes.

---

[g] Lipids were vortexed using a autovortex Stuart SA2 and sonicated using a Bransonic B1210E-MT.

[h] As discussed in 9.2, the conversion of the amount of light scattered by particles having diameter d into the number of particles having the correspondent diameter is based on the Mie approximation; a more exact conversion requires the introduction of parameters (refractive index and density) that are still not available. Hence, the intensity result has been considered more trustworthy than the weight one.

[i] However, as the intensity of the light scattered by the bigger vesicles is lower than the light intensity scattered by the smaller ones, it is reasonable to assume that the real population of small vesicles (<100 nm) is lower than the one reported in Tables from A19 to A26.

[j] The enzyme used for the assays arrived in two separate batches (the first in buffer at pH 6.5 and the second in buffer at pH 7.0) and was obtained from purification of two different cell cultures.

Table 10.1 Steps for the preparation of LUVs by the F-T method

Preparation step	Procedure
1st	Removal of organic solvent by nitrogen stream
2nd	1.5-2 hrs of vacuum to remove traces of solvent
3rd	Lipids hydration with filtered water (50 µl of water per mg of lipid) by vortexing (1-2 sec.)
4th	Lyophilisation
5th	Suspension of the dry lipids in buffer (volume required to obtain a 15 mM lipid solution)
6th	Vortexing (10-15 min.) and resting (10-20 min.)
7th	Sonication (20 min.) and resting (20-30 min.)
8th (1st F-T cycle)	Flash-freezing, thawing (10 min. at 40 °C) and resting (20 min. at rt)
9th (2nd F-T cycle)	Flash-freezing, thawing (10 min. at 40 °C) and resting (20 min. at rt)
10th (3rd F-T cycle)	Flash-freezing, thawing (10 min. at 40 °C) and resting (20 min. at rt)
11th (4th F-T)	Flash-freezing, thawing (10 min. at 40 °C) and resting (20 min. at rt)

The reaction was stopped by flash freezing using liquid nitrogen, followed by the addition of 15 µl of 160 mM EDTA, and by boiling for two minutes. The reaction mixture was then concentrated to 10-20 µl (gyrovapor JOUAN RC1022) and the radioactive products were analysed by TLC (10.4.5) and scintillation counting. All the counting's were corrected for the background using the values obtained from the reactions that did not contained the enzyme. Although the enzyme basal activity (in absence of lipid) was measured, it was not taken into account in the elaboration of the CCT data obtained in presence of lipids. In fact, because in presence of

activating lipids only a fraction of enzyme present in the sample does not bind to the lipids, the contribution of the basal activity was unknown and was not taken into account Using the activity measured in the presence of DOPC LUVs as reference, CCTα relative activity (S) was calculated using Eq. 10.1:

Eq. 10.1 $$S = \frac{CCT\alpha\left(L_1(\chi_1), L_2(\chi_2)\right)}{CCT\alpha\left(L_1(1)\right)}$$

where $CCT\alpha\left(L_1(\chi_1), L_2(\chi_2)\right)$ is the enzyme activity measured in the presence of LUVs constituted by the two lipids L_1 (DOPC) and L_2 (one of the second component lipids), and having mole fractions χ_1 and χ_2, respectively, while $CCT\alpha\left(L_1(1)\right)$ is the enzyme activity in the presence of LUVs constituted by the lipid L_1.

10.4.5 *TLC method*

After the enzymatic reaction and the concentration (10.4.4) the assay samples were loaded onto SIL G TLC plates (10x20 cm) or alternatively on SIL G/UV_{254} TLC plates (10x20 cm). TLC plates were eluted in methanol/14% ammonia (90/10). Photographic films were then exposed to the dry radioactive TLC plates using an intensify screen for 6-12 hours at ~-70 °C and developed (CEATANK developer solution and CEAFIX fixer solution). The radiographs were used to locate CDP-choline and phosphocholine on TLC plates without fluorophore. Spots on plates containing the fluorophore were instead located by exposure to the UV light (λ = 254 nm). CDP-choline and phosphocholine spots were cut from the plate and inserted into scintillation vials filled with scintillation cocktail. The radioactivity was measured by scintillation counting (Beckman LS6500 multi-purpose scintillation counter).

10.5 Results

10.5.1 DOPC/DOPE LUVs

Although the effect of DOPC/DOPE mixtures on CCTα activity has been reported, the experiments were repeated to confirm that the enzyme is sensitive to lipid torque tension under the condition chosen for the assays. CCTα activity was tested under four different conditions, which are summarised in Table 10.2

Table 10.2 Difference between the four sets of experiment employing the DOPC/DOPE lipid mixtures.

Experiments	CCTα batch	DTT (mM)	Vesicle treatment
First	First	0.0	Lipid sonication (30s) between the 10th and the 11th step of Table 10.1
Second	First	0.0	3rd and 4th step of Table 10.1 have been skipped
Third	First	0.0	Thawing in the 11th step of Table 10.1 at 65 °C
Fourth	First	4.0	As in Table 10.1

10.5.1.1 First set of experiments

DOPC/DOPE LUVs used in the enzymatic assays were prepared following the method reported in 10.4.3 and modified by the addition of a 30s sonication step between the 10th and the 11th step[k] (Table 10.1). The enzyme activity (1st batch) was assayed as described in 10.4.4 and 10.4.5 (no DTT was present in the assay mixture). The results of the assays are reported in Table 10.3 and Table A-1, and plotted in Figure 10.6 and Figure 10.7. CCTα relative activity S (Table 10.3) was calculated using Eq. 10.1.

[k] The sonication step was applied as reported in Pick's method [26].

Table 10.3 This tabulation reports CCTα activity and relative activity, S, measured in the presence of DOPC/DOPE LUVs. Relative activity was calculated using Eq. 10.1. All the data reported in the table are plotted in Figure 10.6 and Figure 10.7.

DOPE mole fraction	CCTα activity ($nmol \cdot min^{-1} \cdot mg^{-1}$)	Std. Dev. ($nmol \cdot min^{-1} \cdot mg^{-1}$)	S
No LUVs	29	17	0.08
0	377	49	1.00
0.1	474	57	1.26
0.2	437	86	1.16
0.3	525	35	1.39
0.4	710	35	1.88
0.5	844	28	2.24
0.6	983	77	2.61

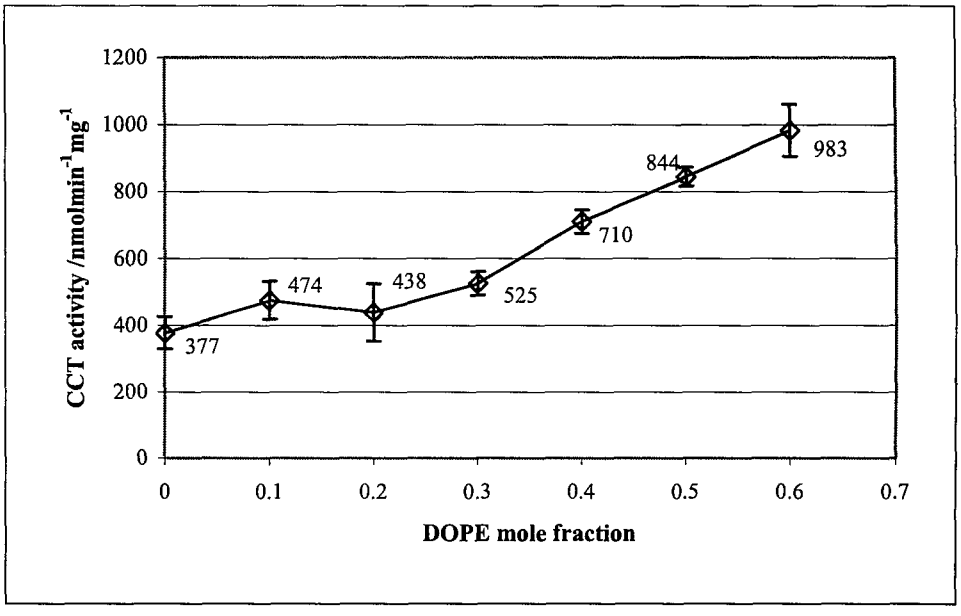

Figure 10.6 CCTα activity is plotted as a function of the mole fraction of DOPE in the DOPC/DOPE mixture. The error bars correspond to ± the standard deviation of three different samples. All data are reported in Table 10.3.

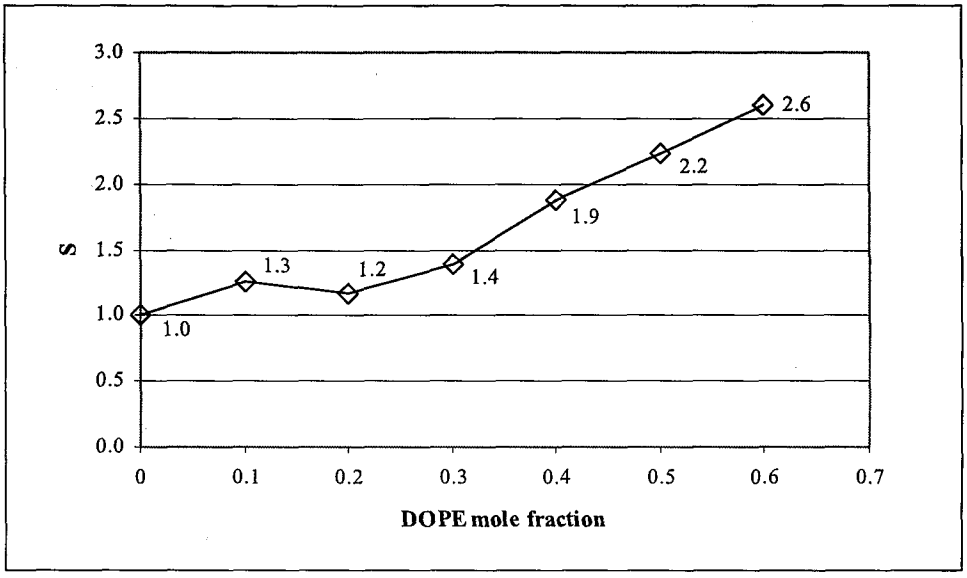

Figure 10.7 CCTα relative activity (S) for the DOPC/DOPE mixtures. Relative activity was calculated using Eq. 10.1. Relative activity data are reported in Table 10.3.

Table 10.4 This tabulation reports CCTα activity and relative activity, S, measured in the presence of DOPC/DOPE LUVs. Relative activity was calculated using Eq. 10.1. All the data reported in the table are plotted in Figure 10.8 and Figure 10.9.

DOPE mole fraction	CCTα activity ($nmol \cdot min^{-1} \cdot mg^{-1}$)	Std. Dev. ($nmol \cdot min^{-1} \cdot mg^{-1}$)	S
No LUVs	15	3	0.11
0	138	13	1.00
0.1	194	25	1.41
0.2	248	42	1.80
0.3	387	49	2.81
0.4	439	165	3.19
0.5	482	83	3.50
0.6	728	134	5.29

10.5.1.2 Second set of experiments

DOPC/DOPE LUVs were prepared following the method reported in 10.4.3 and modified by avoiding the 3rd and 4th step[l]. The enzyme activity (1st batch) was assayed as described in 10.4.4 and 10.4.5 (no DTT was added to the assay mixture, 10.5.1.1). The results of the assays are reported in Table 10.4 and Table A-2, and plotted in Figure 10.8 and Figure 10.9. CCTα relative activity S (Table 10.4) was calculated using Eq. 10.1.

10.5.1.3 Third set of experiments

DOPC/DOPE LUVs used to investigate the CCTα activity were prepared as reported in 10.4.3 and modified by thawing at 65 °C at the 11th step[m]. Enzyme activity (first batch and same aliquot used for the previous set of experiments) was assayed as described in 10.4.4 and 10.4.5 (no DTT was added to the reaction mixture, 10.5.1.1). The assay results are reported in Table 10.5 and Table A-3, and plotted in Figure 10.10 and Figure 10.11. CCTα relative activity S (Table 10.5) was calculated using Eq. 10.1.

10.5.1.4 Fourth set of experiments

DOPC/DOPE LUVs were prepared following the method reported in 10.4.3. The enzyme activity (first batch) was assayed as described in 10.4.4 and 10.4.5. The experimental results are reported in Table 10.6 and Table A-4, and plotted in Figure 10.12 and Figure 10.13. CCTα relative activity S (Table 10.5) was calculated using Eq. 10.1.

---

[l] Using the methods reported in 10.4.3 and 10.5.1.1 small vesicles were observed. The 3rd and the 4th steps were skipped because of the vesicle disruption caused by a high number of F-T and because the role of those steps on the increase of the vesicle size is not known.

[m] The movement of lipids between the two leaflets of a bilayer is a known phenomenon occurring in biological membranes [7, 8]. The increase of the thawing temperature was attempted to test the possibility of an asymmetric distribution of lipids between the two leaflets of the LUVs by assaying the CCTα activity.

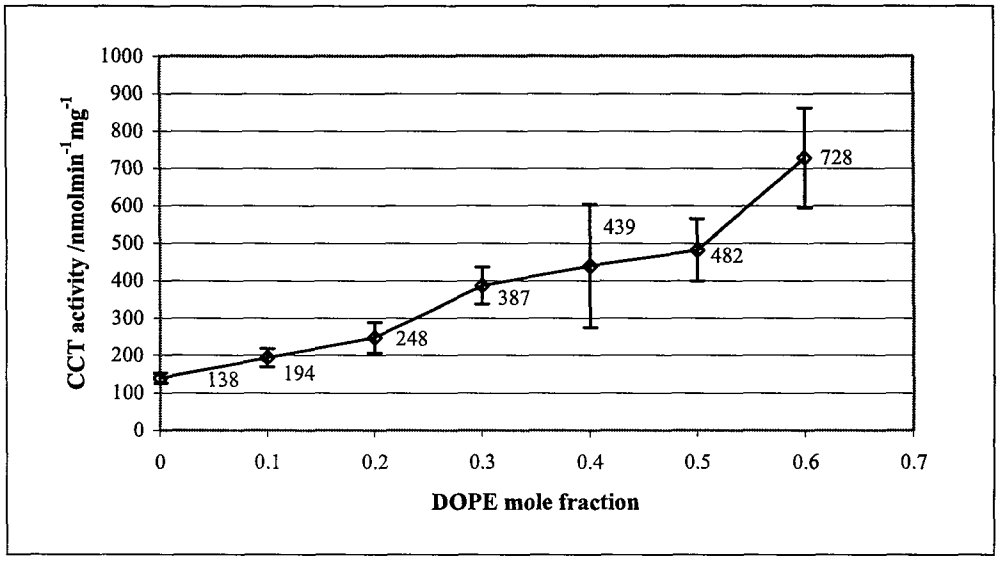

Figure 10.8 CCTα activity is plotted as a function of the mole fraction of DOPE in the DOPC/DOPE mixture. The error bars correspond to ± the standard deviation of three different samples. All data are reported in Table 10.4.

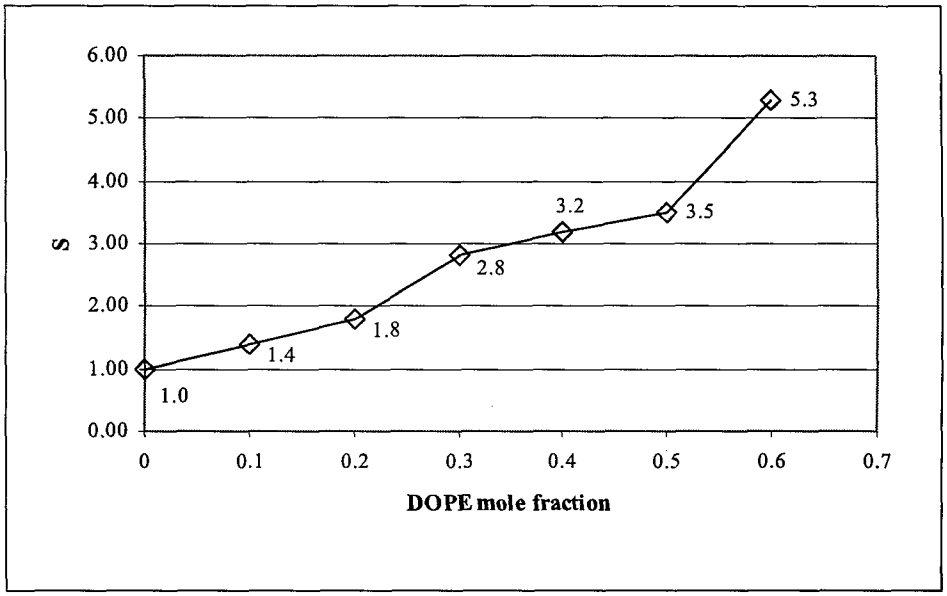

Figure 10.9 CCTα relative activity S for the DOPC/DOPE mixtures. Relative activity was calculated using Eq. 10.1. Relative activity data are reported in Table 10.4.

Table 10.5 This tabulation reports CCTα activity and relative activity, S, measured in the presence of DOPC/DOPE LUVs. Relative activity was calculated using Eq. 10.1. All the data reported in the table are plotted in Figure 10.10 and Figure 10.11.

DOPE mole fraction	CCTα activity ($nmol \cdot min^{-1} \cdot mg^{-1}$)	Std. Dev. ($nmol \cdot min^{-1} \cdot mg^{-1}$)	S
No LUVs	15	3	0.21
0.0	73	8.9	1.00
0.1	90	30	1.23
0.2	131	19	1.78
0.3	178	39	2.42
0.4	221	56	3.01
0.5	245	98	3.33
0.6	234	19	3.18

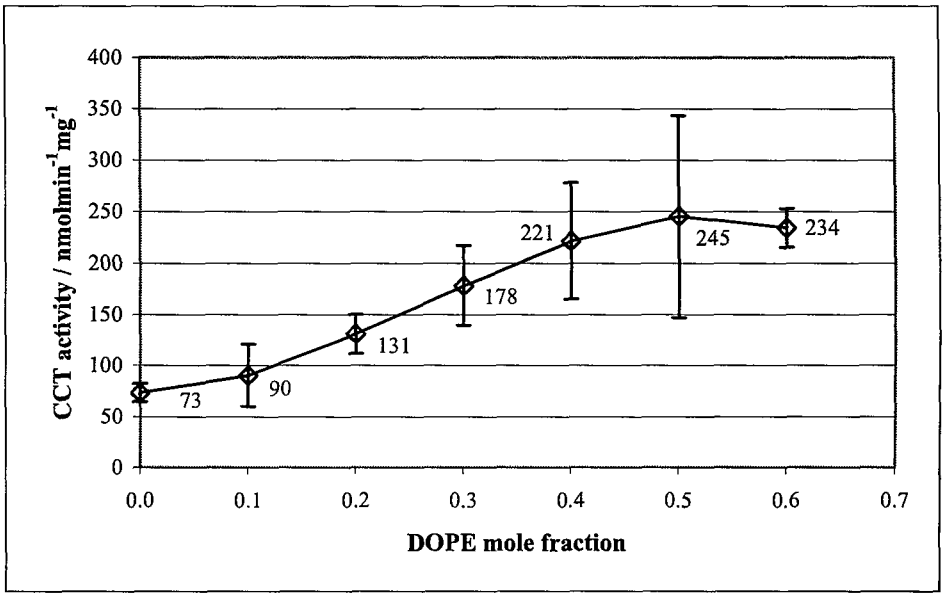

Figure 10.10 CCTα activity is plotted as a function of the mole fraction of DOPE in the DOPC/DOPE mixture. The error bars correspond to ± the standard deviation of three different samples. All data are reported in Table 10.5.

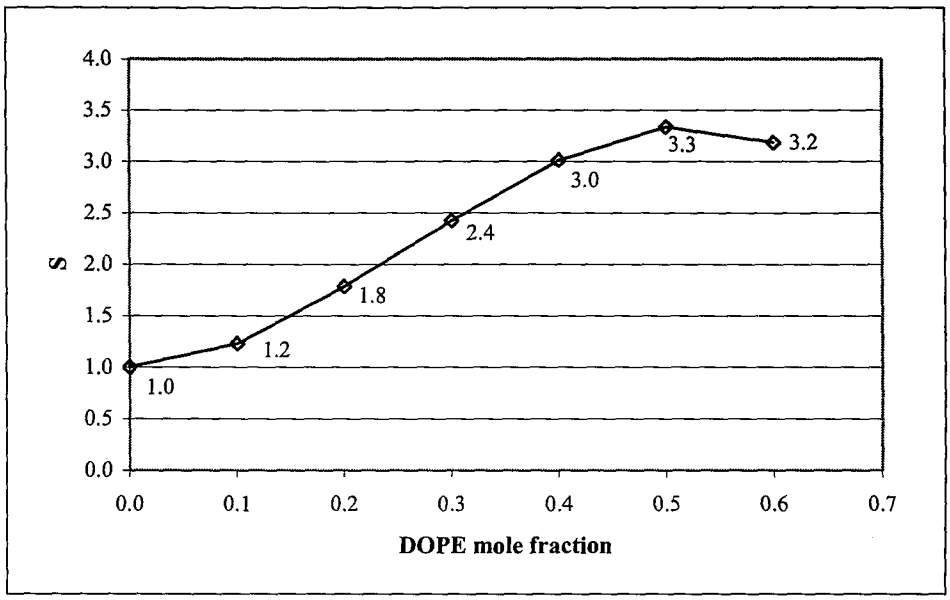

Figure 10.11 CCTα relative activity S for the DOPC/DOPE. Relative activity was calculated using Eq. 10.1. Relative activity data are reported in Table 10.5.

Table 10.6 This tabulation reports CCTα activity and relative activity, S, measured in the presence of DOPC/DOPE LUVs. Relative activity was calculated using Eq. 10.1. All the data reported in the table are plotted in Figure 10.12 and Figure 10.13.

DOPE mole fraction	CCTα activity ($nmol \cdot min^{-1} \cdot mg^{-1}$)	Std. Dev. ($nmol \cdot min^{-1} \cdot mg^{-1}$)	S
No LUVs	18	1	0.08
0.0	216	61	1.00
0.1	223	70	1.04
0.2	298	116	1.38
0.3	315	64	1.46
0.4	415	81	1.92
0.5	530	105	2.45
0.6	729	99	3.38

10.5.1.5 Comparison of CCTα activity in DOPC/DOPE LUVs

All the CCTα activity and relative activity curves for the DOPC/DOPE system are plotted in Figure 10.14 and Figure 10.15, respectively, and reported in Table 10.7. The whole set of DOPC/DOPE data indicates that the basal CCTα activity (i.e. the activity in absence of vesicles) is generally, but not always, more than ten fold lower than the activity measured in the presence of DOPC LUVs, confirming that the lipid causes a significant activation of the enzyme. Moreover, the basal activities shown in Figure 10.16 appear to be similar for all the four sets of experiments, in which CCTα aliquots from the 1st batch were used.

Different CCTα activity is shown in the presence of DOPC and DOPC/DOPE LUVs (Figure 10.17 shows the activity in the presence of DOPC/DOPE (4:6)), which were prepared in four different ways. The vesicles size analyses conducted on DOPC and DOPC/DOPE showed that only the DOPC sample from the 3rd set contained ~ 10% of particles smaller than 100 nm and that all the other vesicles contained at least 95% of vesicles bigger than 2000 nm. As discussed in 9.1, the decrease in the vesicle diameter should cause an increase in the stored bending energy due to an increased contribution from the geometric stress. Hence, it might have been expected that CCTα activity should have been higher for the DOPC sample containing a higher percentage of small vesicles, but it does not. Clearly, this is not the case. As the same CCTα aliquot was used for 2nd and the 3rd set of experiments, the difference in the enzyme activity should be dependent exclusively on the vesicles properties. The low CCTα activity found in correspondence with the sample having a higher population of small vesicles seems to indicate that the method used for the preparation of the vesicles could affect their properties in a way that cannot be revealed by scattering measurements. It is hypothesised that the freezing and the thawing process enlarges the vesicle and could increases the stress stored in the vesicle, possibly introducing defects in the bilayer structure [26]. It is also possible that the heating at 65°C (for 10 minutes during the final thawing) could have affected the vesicle structure causing the partial dissipation of either the

stored bending energy or the stress due to the structural defects. However, it has to be noted that the trends in the activity (increasing enzyme activity with DOPE content) are similar to the trends reported in the literature [1, 2].

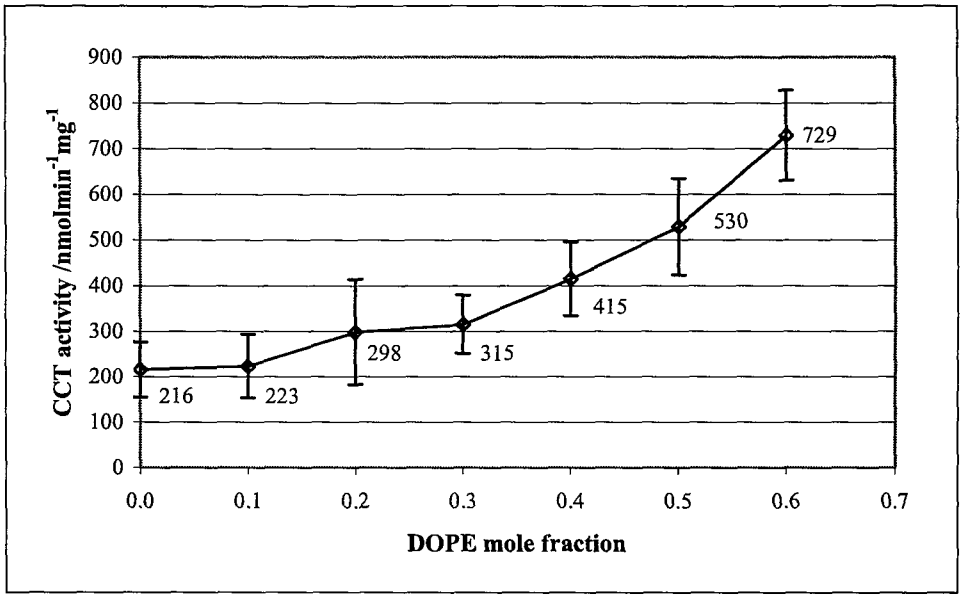

Figure 10.12 CCTα activity is plotted as a function of the mole fraction of DOPE in the DOPC/DOPE mixture. The error bars correspond to ± the standard deviation of three different samples. All data are reported in Table 10.6.

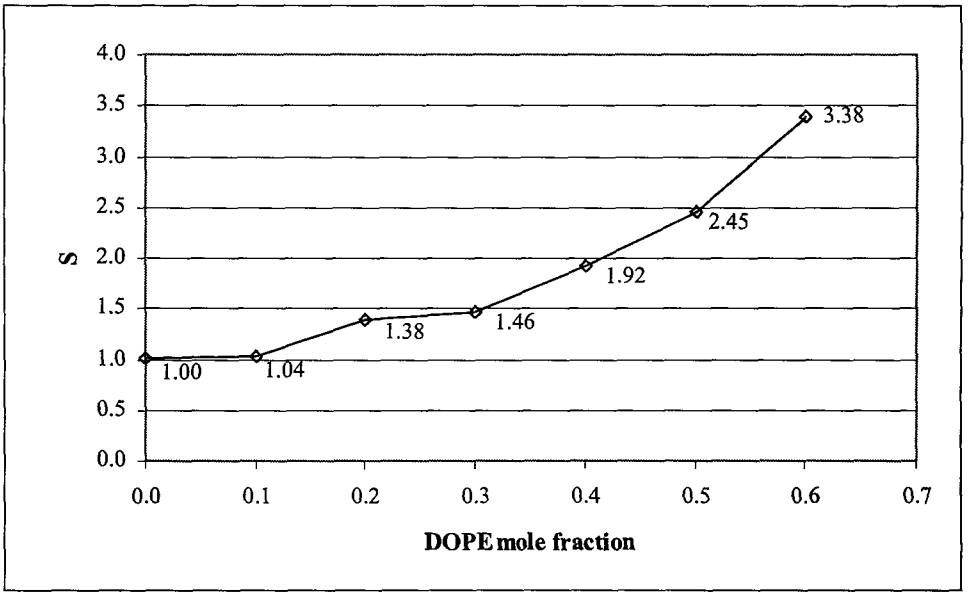

Figure 10.13 CCTα relative activity S for the DOPC/DOPE. Relative activity was calculated using Eq. 10.1. Relative activity data are reported in Table 10.6.

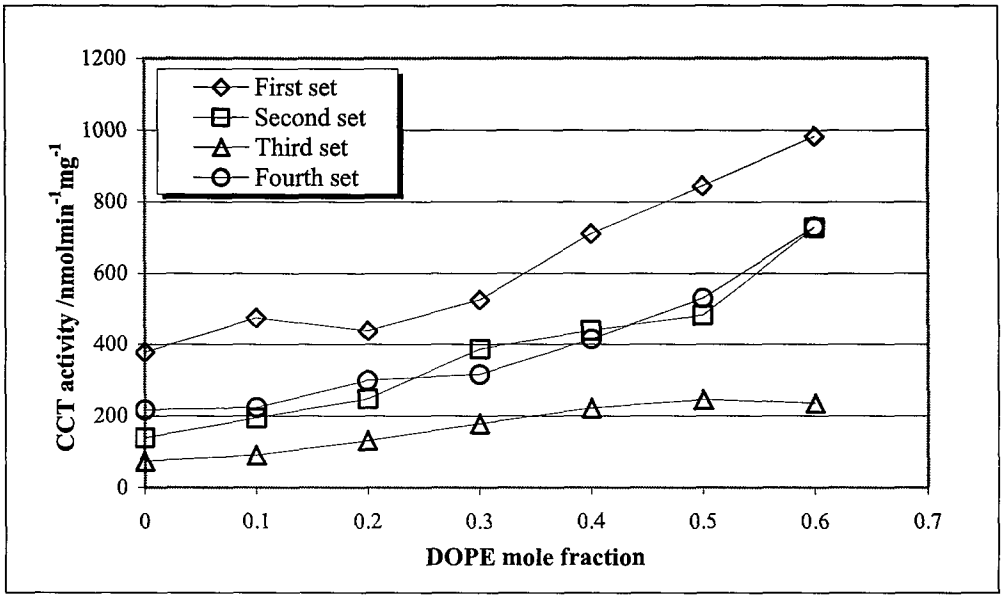

Figure 10.14 Comparison of the four curves obtained for the CCTα activity as a function of the mole fraction of DOPE in the DOPC/DOPE lipid mixtures. The four curves are plotted singularly in Figure 10.6, Figure 10.8, Figure 10.10 and Figure 10.12.

Table 10.7 The table summarises all the CCTα activities reported in the previous tables. All the curves are plotted in Figure 10.14

DOPE mole fraction	CCTα activity ($nmol \cdot min^{-1} \cdot mg^{-1}$)			
	First set	Second set	Third set	Fourth set
No LUVs	29	15	15	18
0	377	138	73	216
0.1	474	194	90	223
0.2	438	248	131	298
0.3	525	387	178	315
0.4	710	439	221	415
0.5	844	482	245	530
0.6	983	728	234	729

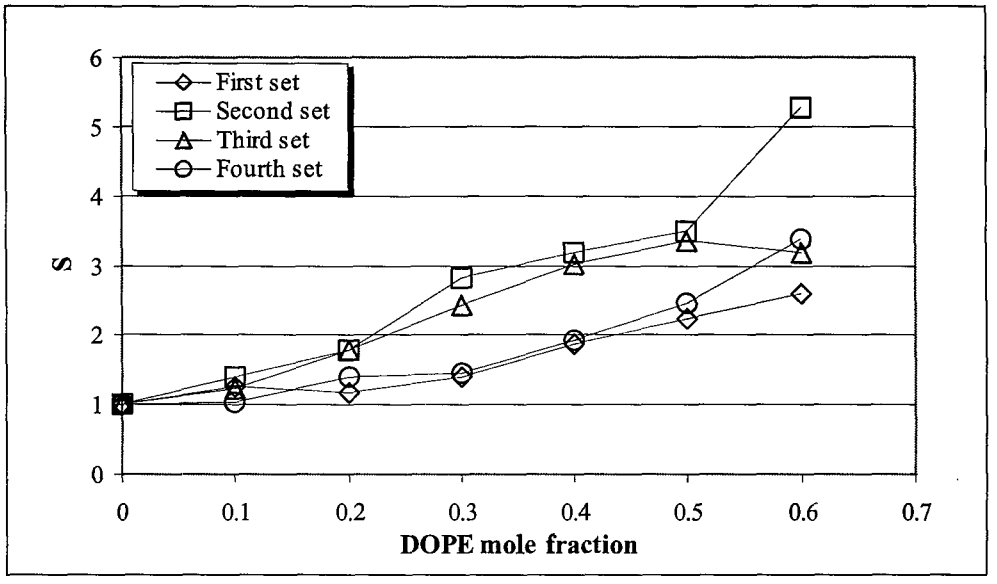

Figure 10.15 The four curves in the above plot correspond to the CCTα relative activity reported previously and shown in Figure 10.7, Figure 10.9, Figure 10.11 and Figure 10.13.

Table 10.8 The table reports all the CCTα activities reported in the previous tables and plotted together in Figure 10.15

DOPE mole fraction	CCTα relative activity			
	First set	Second set	Third set	Fourth set
No LUVs	0.08	0.11	0.21	0.08
0	1.00	1.00	1.00	1.00
0.1	1.26	1.41	1.23	1.04
0.2	1.16	1.80	1.78	1.38
0.3	1.39	2.81	2.42	1.46
0.4	1.88	3.19	3.01	1.92
0.5	2.24	3.50	3.33	2.45
0.6	2.61	5.29	3.18	3.38

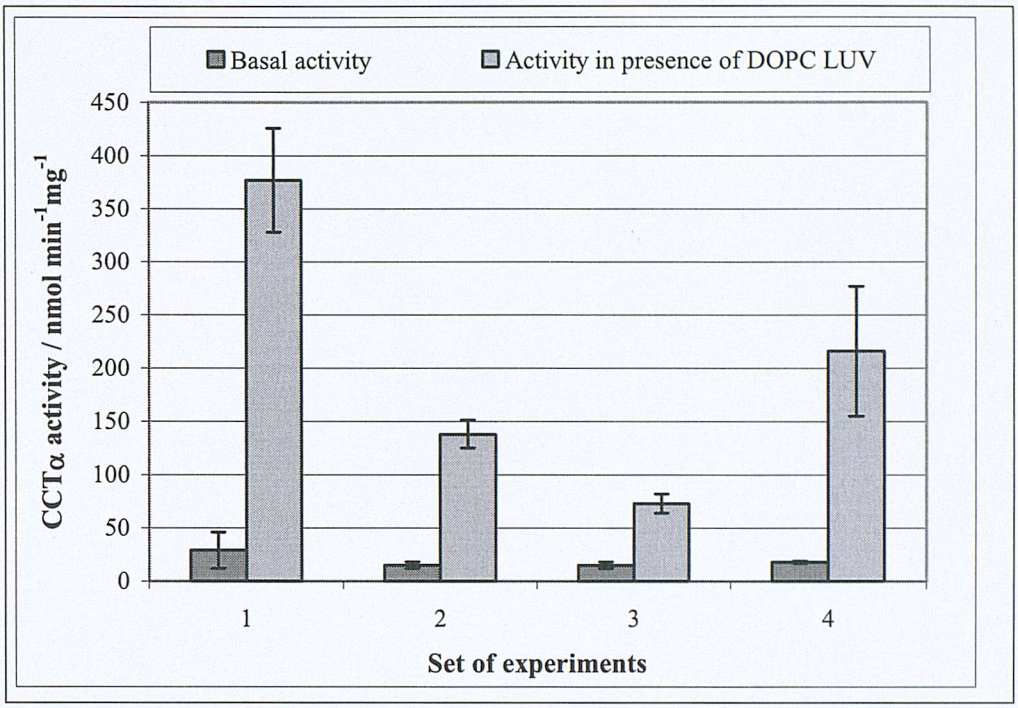

Figure 10.16 Comparison of the CCTα activity measured in Basal CCTα activity was measured in absence of vesicles. The same enzyme was used for the second and the third set of experiments. The error bars correspond to ± the standard deviation of three different samples.

While the trends in enzyme activity as function of DOPE concentration are consistent, it is clear that the absolute changes in activity are not reproducible. The reasons underlying this have not been determined. In part, irreproducibility in the magnitude of activation may be due to variations in the vesicles properties due to the presence of high energy defects which do not anneal prior to the assay. However, it is also possible that variations may be due to the protein. For example, the protein may dimerise when in solution. Furthermore, variation in basal activity indicates that there is significant variability in specific activity. In particular, it has been noted that the specific activity decreases significantly following each freeze-thaw cycle that the enzyme undergoes. The origin of this phenomenon is not known.

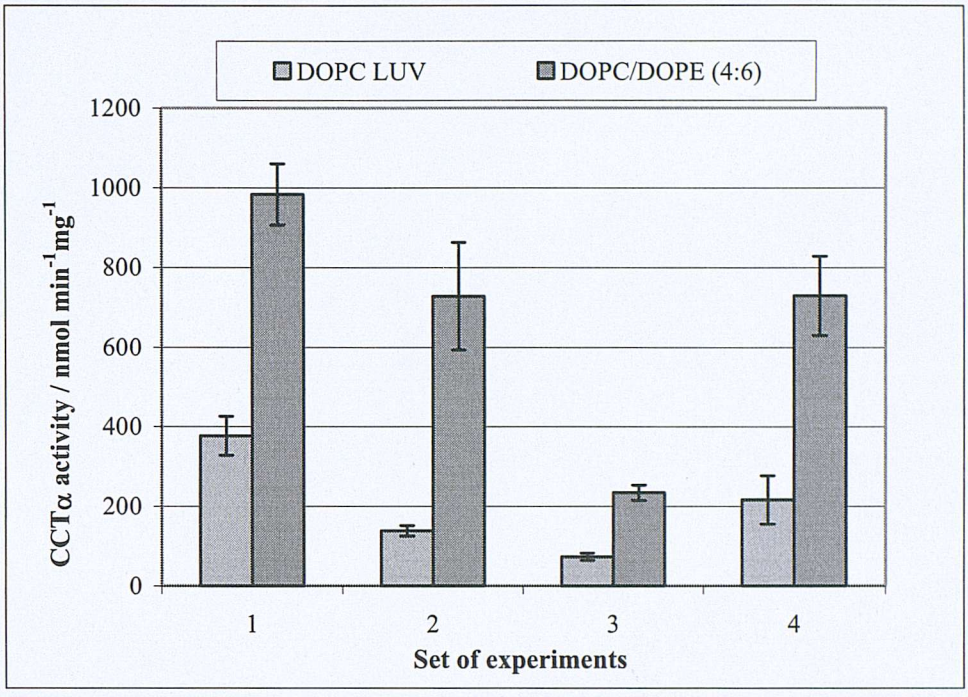

Figure 10.17 CCTα activity measured in presence of DOPC or DOPC/DOPE (4:6) LUVs. The enzyme used for the four sets of experiments came from three different aliquots of the first batch

Another possible source of variability could have been CCTα oxidation, followed by enzyme dimerisation and inactivation, as it has been reported in the literature [18]. The addition of DTT to the enzyme has been employed as a safeguard against enzyme denaturation. However, comparison of the four sets of experiments (1-3 without and 4 with DTT) suggests that DTT does not significantly affect the activity of the enzyme. The implication is therefore that oxidation may not be the cause of the observed variability. However, in view of the variability in specific activity, the trends are remarkably consistent, and hence in the following experiments the analysis of the data focuses on identifying trends rather than absolute changes in activity.

10.5.2 DOPC/DOPA LUVs

Two sets of experiments were done employing DOPC/DOPA mixtures. The differences between the two sets are highlighted in Table 10.9. As the previous sets

of experiments have shown that DTT might have no effect, the enzyme and vesicle preparation are the only differences that will taken into account during the discussion of the results.

Table 10.9 Difference between the two sets of experiment employing the DOPC/DOPA lipid mixtures.

Set of experiment	CCTα batch	DTT (mM)	Vesicle treatment
First	First	0.0	Thawing in the 11th step of Table 10.1 at 65 °C
Second	Second	4	As in Table 10.1

10.5.2.1 First set of experiments

DOPC/DOPA LUVs used to assay the CCTα activity were prepared according to the method reported in 10.4.3 and modified by thawing at 65 °C at the 11th step (10.5.1.3). The enzyme (first batch) activity was measured as described in 10.4.4 and 10.4.5 and no DTT was present in the reaction mixture. The results of the assays are reported in Table 10.10 and Table A-5, and plotted in Figure 10.18 and Figure 10.19. CCTα relative activity S (Table 10.10) was calculated using Eq. 10.1.

10.5.2.2 Second set of experiments

DOPC/DOPA LUVs used for the enzymatic assays were prepared according to the method reported in 10.4.3. The activity of CCTα (second batch) was measured as described in 10.4.4 and 10.4.5. The experimental results are reported in Table 10.11 and Table A-6, and plotted in Figure 10.20 and Figure 10.21. CCTα relative activity S (Table 10.11) was calculated using Eq. 10.1.

Table 10.10 This tabulation reports CCTα activity and relative activity, S, measured in the presence of DOPC/DOPA LUVs. Relative activity was calculated using Eq. 10.1. All the data reported in the table are plotted in Figure 10.18 and Figure 10.19.

DOPA mole fraction	CCTα activity ($nmol \cdot min^{-1} \cdot mg^{-1}$)	Std. Dev. ($nmol \cdot min^{-1} \cdot mg^{-1}$)	S
No LUVs	15	3	0.10
0.000	77	1	1.00
0.025	80	24	1.04
0.050	132	23	1.71
0.075	250	55	3.24
0.1	440	56	5.69
0.2	1677	47	21.71
0.3	1611	37	20.85

Table 10.11 This tabulation reports CCTα activity and relative activity, S, measured in the presence of DOPC/DOPA LUVs. Relative activity was calculated using Eq. 10.1. All the data reported in the table are plotted in Figure 10.20 and Figure 10.21.

DOPA mole fraction	CCTα activity ($nmol \cdot min^{-1} \cdot mg^{-1}$)	Std. Dev. ($nmol \cdot min^{-1} \cdot mg^{-1}$)	S
No LUVs	38	5	0.76
0.00	51	11	1.00
0.025	67	18	1.32
0.050	194	17	3.84
0.075	213	90	4.20
0.10	342	32	6.74
0.15	629	137	12.42
0.20	923	130	18.22
0.25	1038	77	20.49
0.30	1007	128	19.87

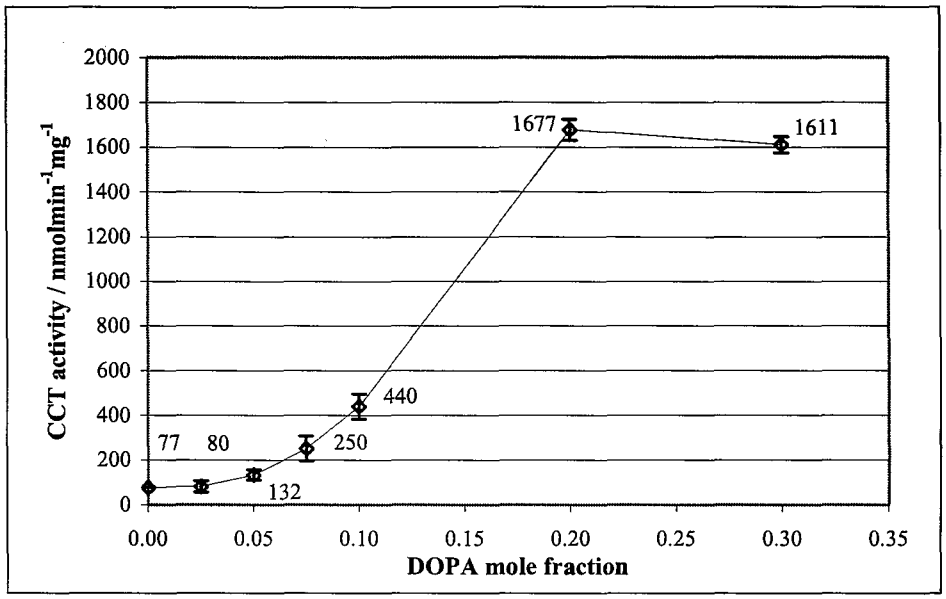

Figure 10.18 CCTα activity is plotted as a function of the mole fraction of DOPA in the DOPC/DOPA mixture. The error bars correspond to ± the standard deviation of three different samples. All data are reported in Table 10.10.

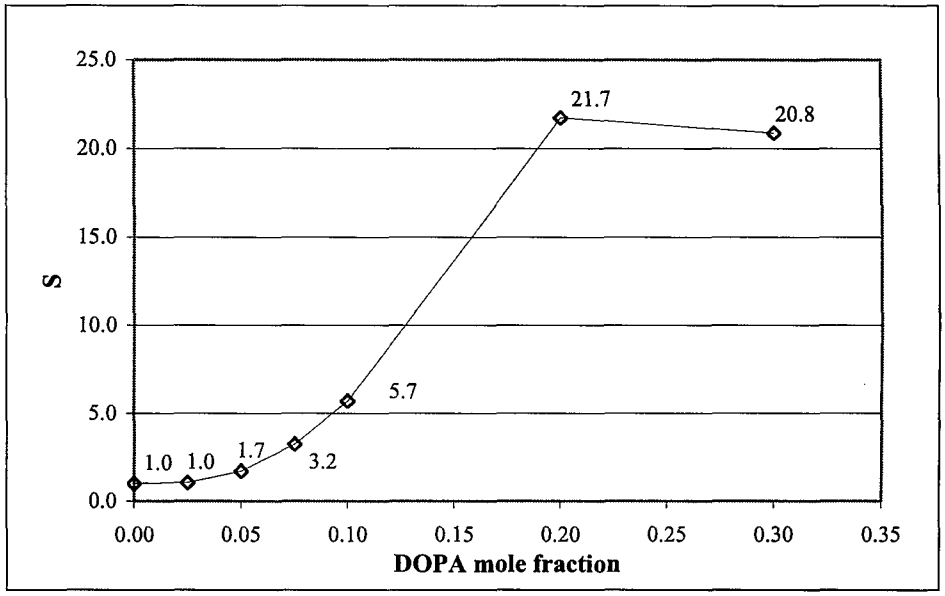

Figure 10.19 CCTα relative activity S for the DOPC/DOPA. Relative activity was calculated using Eq. 10.1. Relative activity data are reported in Table 10.10.

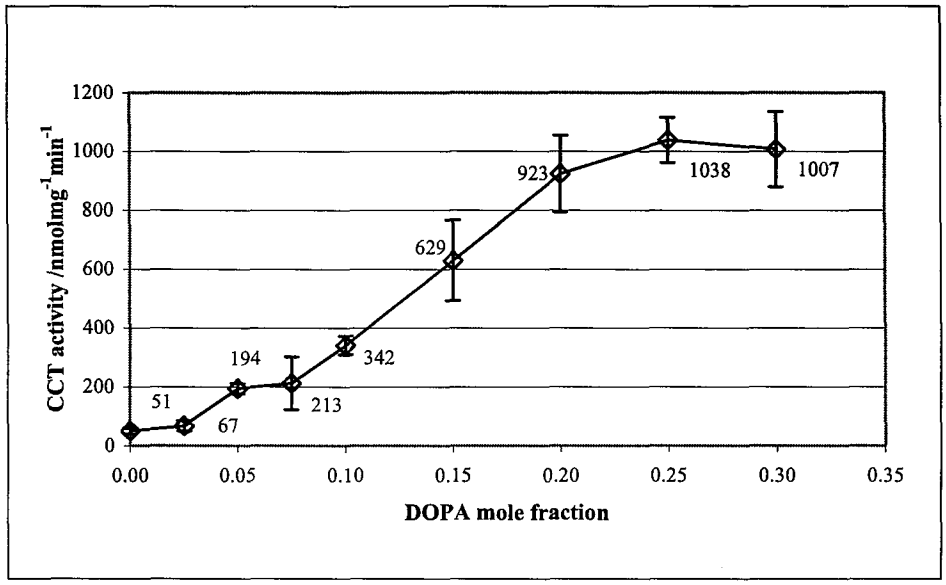

Figure 10.20 CCTα activity is plotted as a function of the mole fraction of DOPA in the DOPC/DOPA mixture. The error bars correspond to ± the standard deviation of three different samples. All data are reported in Table 10.11.

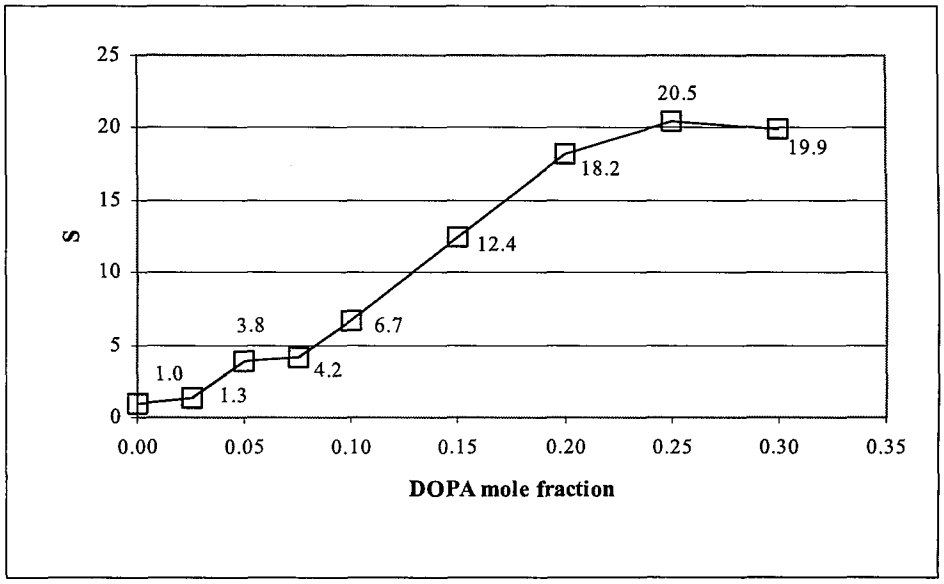

Figure 10.21 CCTα relative activity S for the DOPC/DOPA. Relative activity was calculated using Eq. 10.1 (10.4.4). Relative activity data are reported in Table 10.11.

10.5.2.3 DOPC/DOPA LUVs and CCTα activity

The assays in the presence of DOPC/DOPA LUVs show a dramatic increase in enzyme activity, as expected for charged lipids [3], and the trend of the relative activity seems to be consistent, although the two sets of experiments have differences in both the enzyme and the vesicle preparation. The enzyme preparation could be the cause of the difference in the enzyme specific activity. In contrast to the results obtained using the DOPC/DOPE mixtures, the basal activity of CCTα from the second batch of enzyme is higher than that from the first batch (Figure 10.22). This difference is difficult to explain, but may be due to either the presence of residual lipids in the enzyme or the presence of other unknown contaminant. However, in spite of the higher basal activity, the activity in the presence of DOPC LUVs is lower for the second CCTα batch. The enzyme activity measured for the two different batches of CCTα is plotted in Figure 10.23 and it appears that, except for the basal activity, the enzyme activity is consistently low for the entire set of assays in which the enzyme from the second batch was used. The difference is in the vesicles preparation seems to be similar to the one observed for the experiments with DOPC/DOPE: different enzyme specific activity but similar relative activity. Although a direct comparison between the specific activity of the two enzyme preparations in presence of DOPC/DOPA is not reasonable without a common reference point[n], the relative activity (Figure 10.24) is similar for both batches of enzyme, suggesting that the effect of DOPC/DOPA vesicles on the enzyme activity is qualitatively reproducible.

[n] The question of the common reference point will be addressed in the final discussion at the end of the chapter.

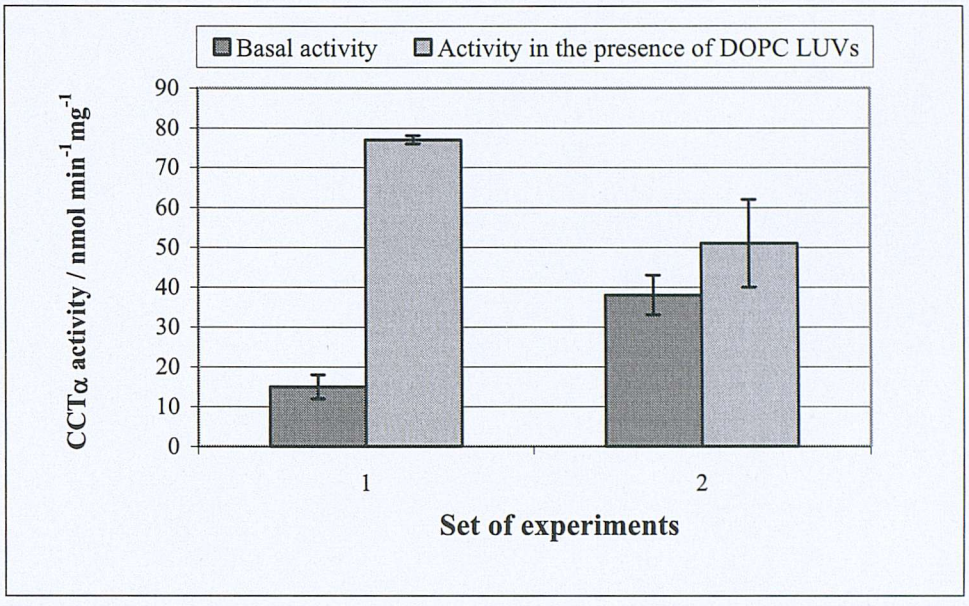

Figure 10.22 The basal activity and the activity in presence of DOPC/DOPA LUVs show differences that could be due essentially to the different batch of enzyme used for the experiments. The enzyme from the first batch was used for the first set of experiments, whilst the enzyme from the second batch was used for the second set of experiments.

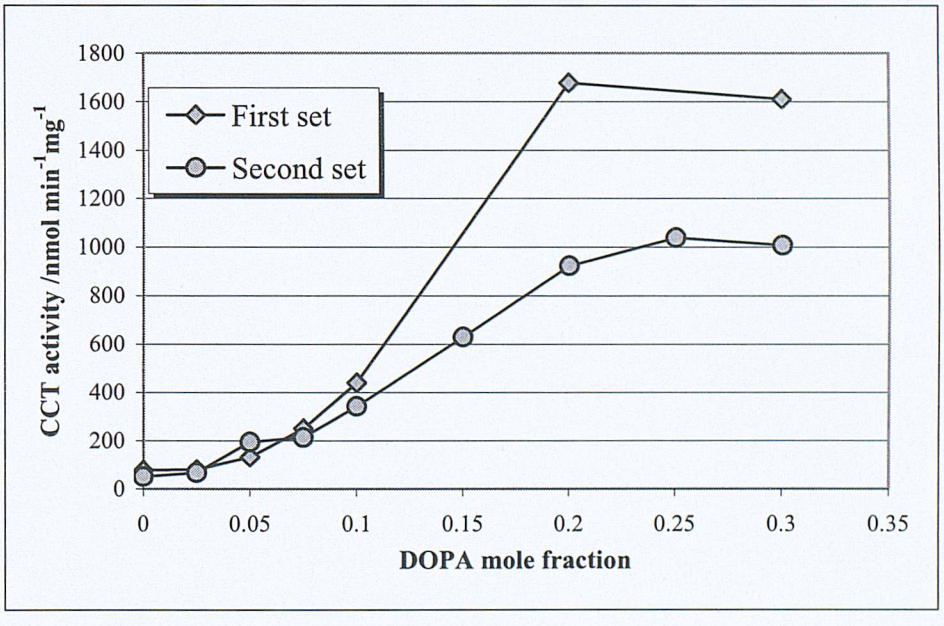

Figure 10.23 All the enzymatic relative activity curves obtained in the previous sets of experiments are plotted in the above graph.

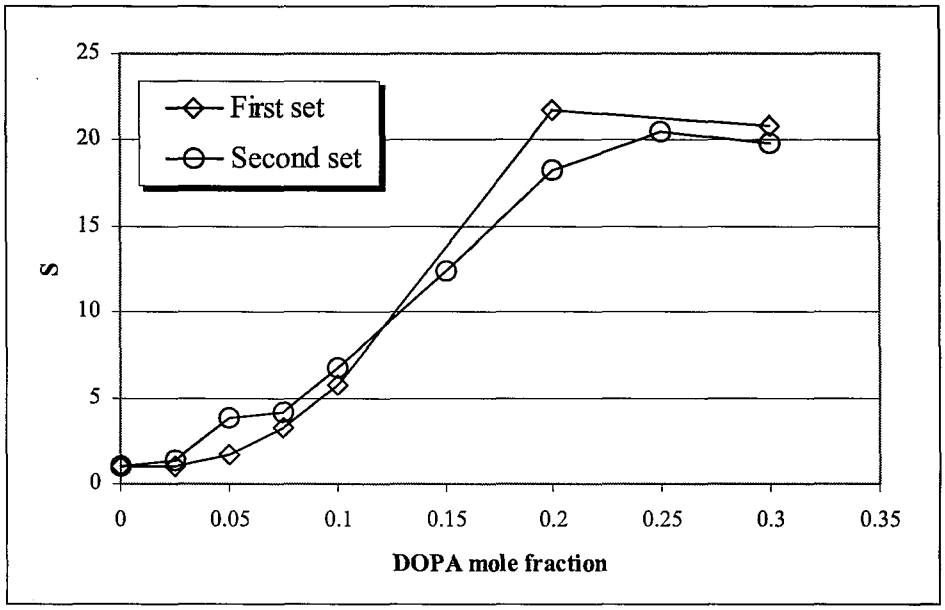

Figure 10.24 Comparison of the two curves for the CCTα relative activity in the presence of DOPC/DOPA LUVs, shown separately in Figure 10.18 and Figure 10.20.

10.5.3 DOPC/DPPA system

DOPC/DPPA LUVs were prepared according to the method reported in 10.4.3. The enzyme activity (first batch) was assayed as described in 10.4.4 and 10.4.5. The experimental results are reported in Table 10.12 and Table A-9, and plotted in Figure 10.25 and Figure 10.26. CCTα relative activity S (Table 10.12) was calculated using Eq. 10.1. The curves in Figure 10.25 and Figure 10.26 differ from all the others seen previously, showing a high activity in the presence of DOPC LUVs; moreover, the enzyme activity increases reaching a maximum in correspondence to a low mole percentage of DPPA (~ 7.5 mole percentage) and decreases for high mole fraction of DPPA. It has to be noted that in this set of experiments, and the one with the DOPC/DPPS mixtures, the enzyme activity was very high, even in the presence of pure DOPC. Although no enough data have been collected for the DOPC/DPPA system, it is reasonable to hypothesise that the DPPA phase transition from the gel to the liquid crystalline phase (~67 °C [28]) could cause a phase separation between DOPC and DPPA for the higher mole fraction of DPPA.

Table 10.12 This tabulation reports CCTα activity and relative activity, S, measured in the presence of DOPC/DPPA LUVs. Relative activity was calculated using Eq. 10.1. All the data reported in the table are plotted in Figure 10.25 and Figure 10.26.

DPPA mole fraction	CCTα activity ($nmol \cdot min^{-1} \cdot mg^{-1}$)	Std. Dev. ($nmol \cdot min^{-1} \cdot mg^{-1}$)	S
No LUVs	30	1	0.03
0.0	861	246	1.00
0.025	1797	358	2.09
0.050	2342	192	2.72
0.075	2626	294	3.05
0.100	2286	168	2.66
0.150	2097	107	2.44
0.200	1833	65	2.13
0.250	1564	109	1.82
0.300	989	78	1.15

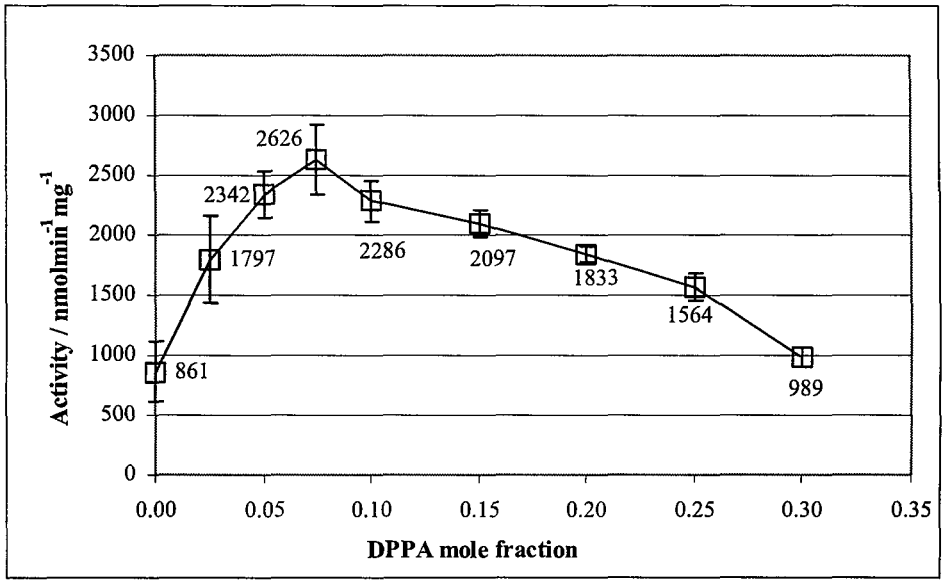

Figure 10.25 CCTα activity is plotted as a function of the mole fraction of DPPA in the DOPC/DPPA mixtures. The error bars correspond to ± the standard deviation of three different samples. All data are reported in Table 10.12.

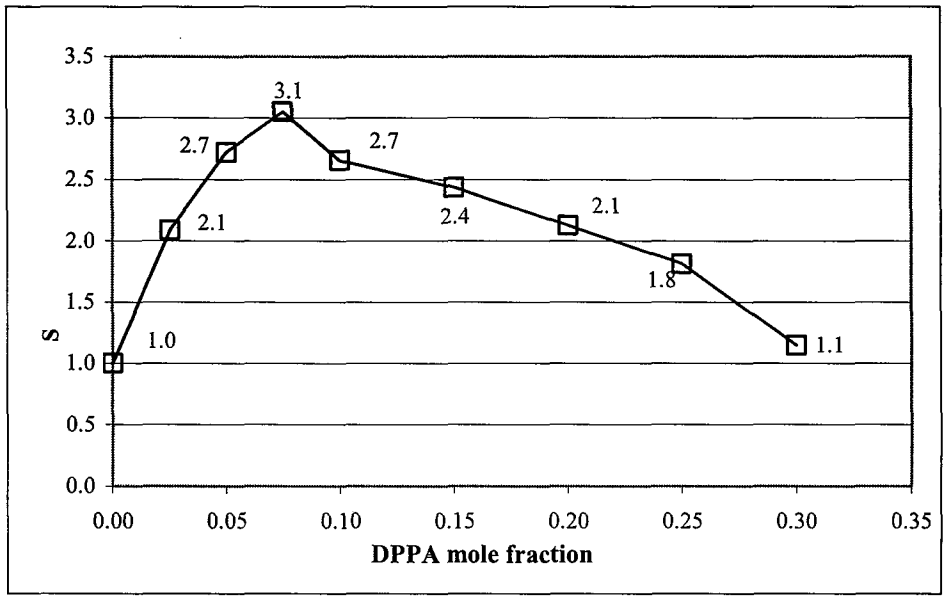

Figure 10.26 CCTα relative activity S for the DOPC/DPPA. Relative activity was calculated using Eq. 10.1. Relative activity data are reported in Table 10.12.

No phase diagram is available for the DOPC/DPPA mixtures and it is not possible to predict the effect of a phase separation onto the bending energy. However, the phase separation remains an hypothesis that could reasonably explain the increase and the subsequent decrease in the enzyme activity: the initial miscibility of DPPA into DOPC could count for the starting increase in the enzyme activity, while the following phase separation could count for the decreased enzyme activity (the phase separation could have reduced the mole fraction of DPPA in the DOPC).

10.5.4 DOPC/OPA LUVs

The following two sets of experiments differ only in the enzyme preparation, whilst the vesicles were prepared following the same protocol (10.4.3).

10.5.4.1 First set of experiments

DOPC/OPA LUVs were prepared as described in 10.4.3. The enzyme activity (first batch) was measured as described in 10.4.4 and 10.4.5. Because of the limited supply of enzyme from the first batch, a single sample for each lipid mixture was

used for these experiments. Moreover, the enzyme was subjected to a further step of freezing and thawing. The experimental results are reported in Table 10.13 and Table A-11, and plotted in Figure 10.27 and Figure 10.28. CCTα relative activity S (Table 10.13) was calculated using Eq. 10.1.

Table 10.13 This tabulation reports the CCTα activity and CCTα relative activity, S, measured in the presence of DOPC/OPA LUVs. Relative activity was calculated using Eq. 10.1. All the data reported in the table are plotted in Figure 10.27 and Figure 10.28.

OPA mole fraction	CCTα activity ($nmol \cdot min^{-1} \cdot mg^{-1}$)	S
No LUVs	4.9	0.15
0	31.9	1
0.025	91.7	2.87
0.05	172	5.40
0.075	254	7.97
0.1	318	9.96
0.2	360	11.26
0.3	242	7.58

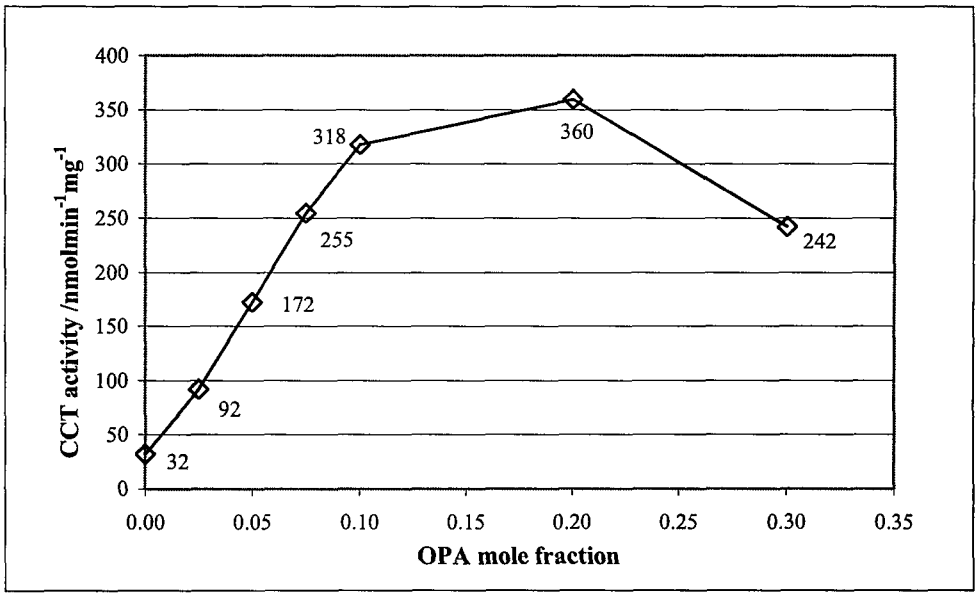

Figure 10.27 CCTα activity plotted as a function of the mole fraction of OPA in the DOPC/OPA mixture. All data are reported in Table 10.13.

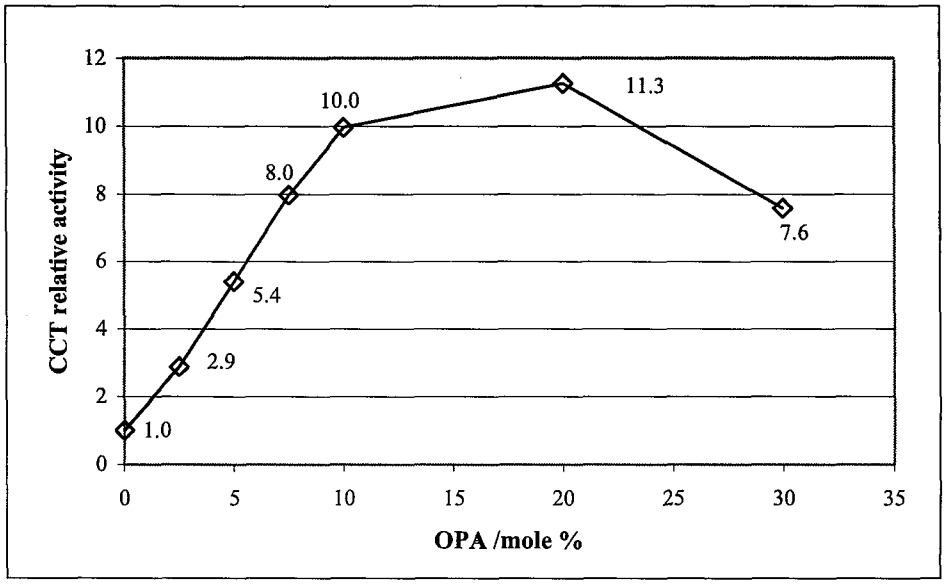

Figure 10.28 CCTα relative activity S for the DOPC/OPA. Relative activity was calculated using Eq. 10.1. Relative activity data are reported in Table 10.13.

10.5.4.2 Second set of experiments

DOPC/OPA LUVs were prepared according to the method reported in 10.4.3. The enzyme activity (second batch) was assayed as described in 10.4.4 and 10.4.5. The experimental results are reported in Table 10.14 and Table A-12, and plotted in Figure 10.29 and Figure 10.30. CCTα relative activity S (Table 10.14) was calculated using Eq. 10.1.

10.5.4.3 CCTα activity in DOPC/OPA LUVs

CCTα from two different batches was used for the two sets of experiments and this could account for the differences observed between the curves (Figure 10.31 and Figure 10.32). Moreover, an additional freeze-thaw step was applied to the first batch of enzyme and could account for its low basal activity and for the low activity in the presence of DOPC. However, the trend of the two curves resembles the trend seen for the case of DOPC/DPPA LUVs. As for the previous cases, miscibility/phase transition data for the DOPC/OPA mixtures are not available, making it difficult to rationalize the observed increase-decrease activity.

Table 10.14 This tabulation reports CCTα activity and relative activity, S, measured in the presence of DOPC/OPA LUVs. Relative activity was calculated using Eq. 10.1. All the data reported in the table are plotted in Figure 10.29 and Figure 10.30.

OPA mole fraction	CCTα activity ($nmol \cdot min^{-1} \cdot mg^{-1}$)	Std. Dev. ($nmol \cdot min^{-1} \cdot mg^{-1}$)	S
No LUVs	89	0.1	1.2
0.0	74	4	1.0
0.025	208	14	2.8
0.050	306	55	4.1
0.075	312	45	4.2
0.10	333	29	4.5
0.15	431	30	5.8
0.20	366	38	4.9
0.30	444	5	6.0
0.40	328	50	4.4

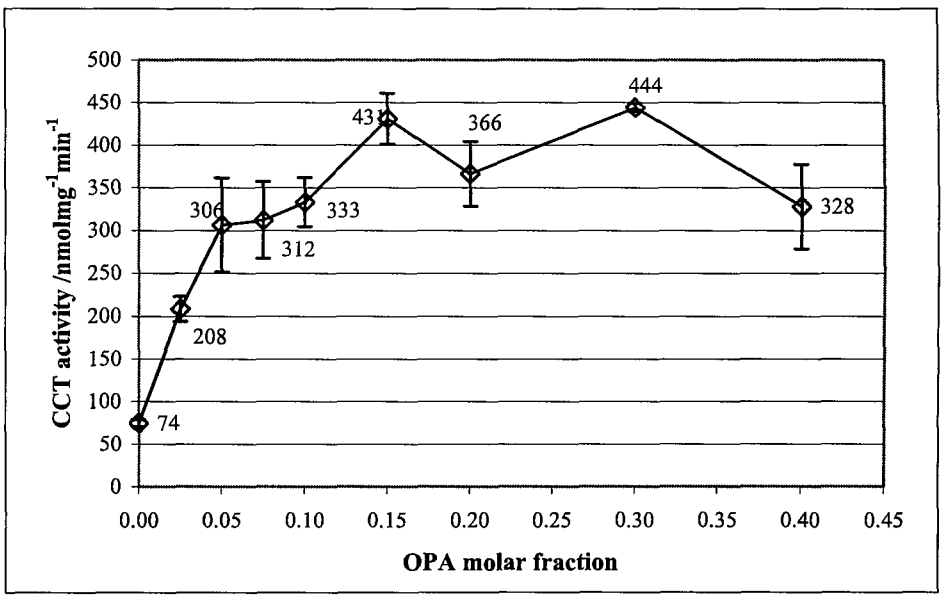

Figure 10.29 CCTα activity plotted as a function of the mole fraction of DOPS in the DOPC/OPA mixture. The error bars correspond to ± the standard deviation of three different samples. All data are reported in Table 10.14.

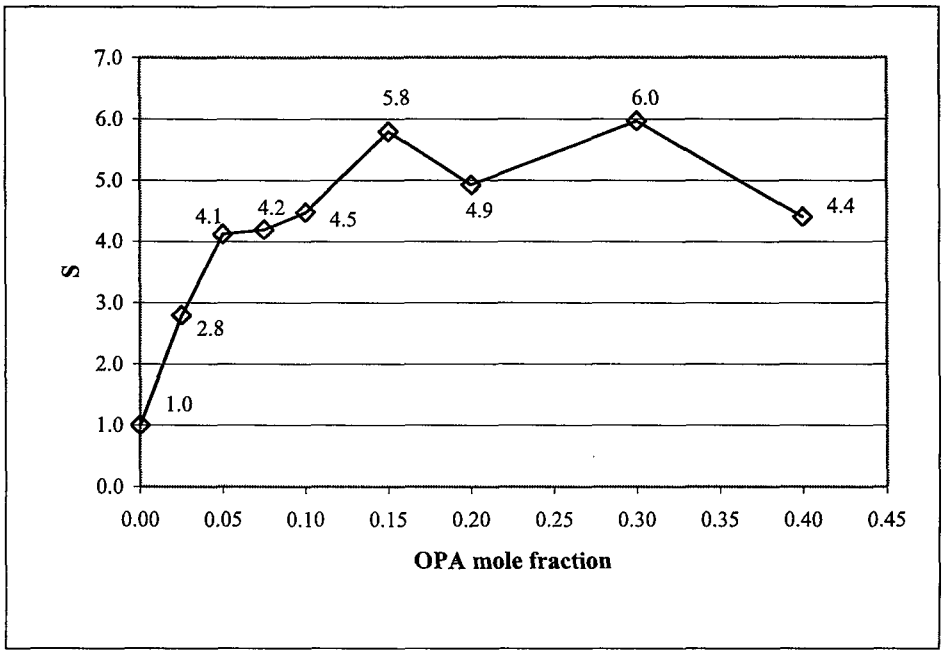

Figure 10.30 CCTα relative activity S for the DOPC/OPA. Relative activity was calculated using Eq. 10.1. Relative activity data are reported in Table 10.14.

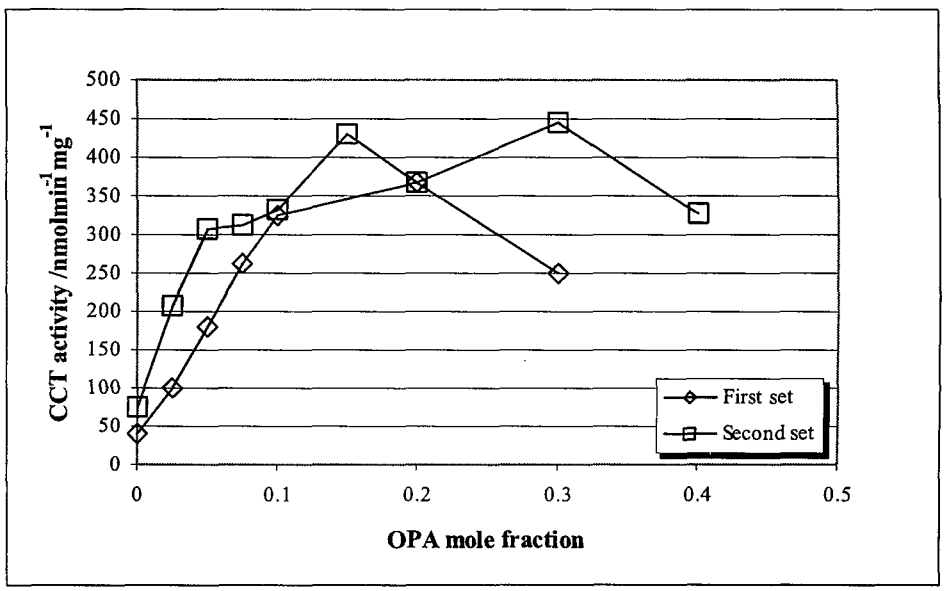

Figure 10.31 The two curves show a similar trend, even if the activity was found to be lower in the first set of experiments at low OPA mole fraction. The two curves are plotted singularly in Figure 10.27 and Figure 10.29.

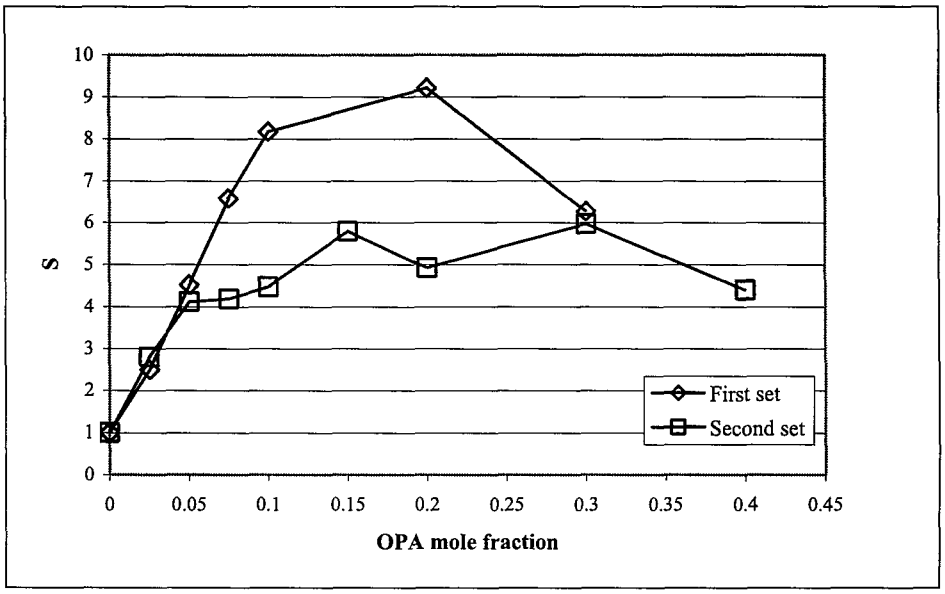

Figure 10.32 The relative activity of CCTα shows an initial increase that is similar in both the curves at low OPA mole percentage. The two curves are plotted singularly in Figure 10.28 and Figure 10.30.

10.5.5 DOPC/DOPS LUVs

The anionic phospholipid mixed with DOPC in the following two sets of experiments was DOPS. The differences between the two sets are highlighted in Table 10.15. As for the DOPC/DOPA experiments, the employing of enzyme from two different preparations constitutes the maybe most substantial difference. Again, the difference in the vesicle preparation is more difficult to assess, as no data is available about the properties variability of the lipid mixtures that have been used.

Table 10.15 Difference between the two sets of experiment employing the DOPC/DOPS lipid mixtures.

Set of experiment	CCTα batch	DTT (mM)	Vesicle treatment
First	First	0.0	Thawing in the 11th step of Table 10.1 at 65 °C
Second	Second	4	As in Table 10.1

10.5.5.1 First set of experiments

DOPC/DOPS LUVs were prepared as described in 10.4.3 and modified by thawing at 65 °C at the 11th step (10.5.1.3). The enzyme (first batch) activity was assayed as described in 10.4.4 and 10.4.5 (no DTT was added to the reaction mixture, 10.5.1.1). The results of the assays are reported in Table 10.16 and Table A-7, and plotted in Figure 10.33 and Figure 10.34. CCTα relative activity S (Table 10.16) was calculated using Eq. 10.1.

Table 10.16 This tabulation reports CCTα activity and relative activity, S, measured in the presence of DOPC/DOPS LUVs. Relative activity was calculated using Eq. 10.1. All the data reported in the table are plotted in Figure 10.33 and Figure 10.34.

DOPS mole fraction	CCTα activity ($nmol \cdot min^{-1} \cdot mg^{-1}$)	Std. Dev. ($nmol \cdot min^{-1} \cdot mg^{-1}$)	S
No LUVs	15	3	0.10
0.00	77	0	1.00
0.025	51	5	0.66
0.050	110	33	1.42
0.075	79	12	1.03
0.1	81	17	1.05
0.2	168	36	2.18
0.3	370	16	4.79

10.5.5.2 Second set of experiments

DOPC/DOPS LUVs were prepared as described in 10.4.3. The activity of the enzyme (second batch) was assayed as described in 10.4.4 and 10.4.5. The experimental results are reported in Table 10.17 and Table A-8, and plotted in Figure 10.35 and Figure 10.36. CCTα relative activity S (Table 10.17) was calculated using Eq. 10.1.

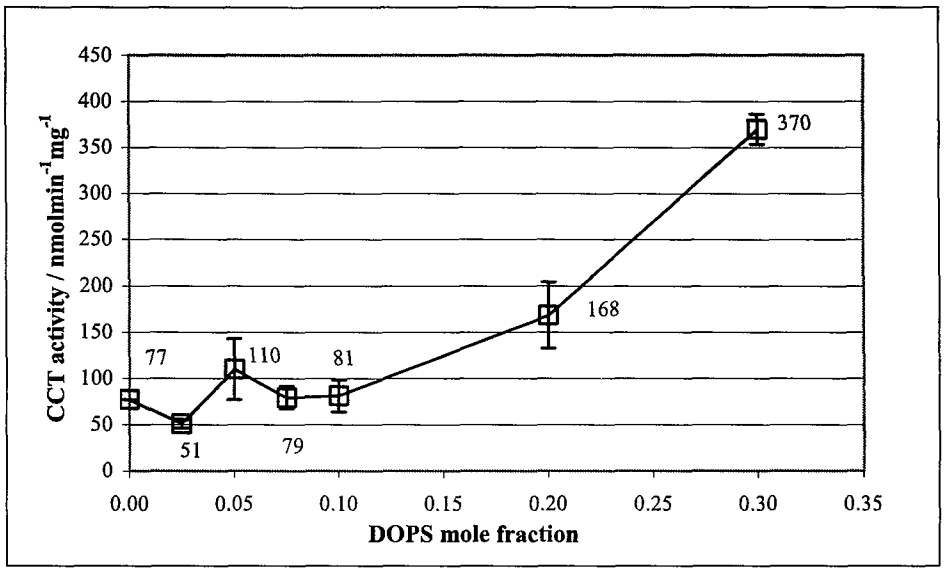

Figure 10.33 CCTα activity is plotted as a function of the mole fraction of DOPS in the DOPC/DOPS mixture. The error bars correspond to ± the standard deviation of three different samples. All data are reported in Table 10.16.

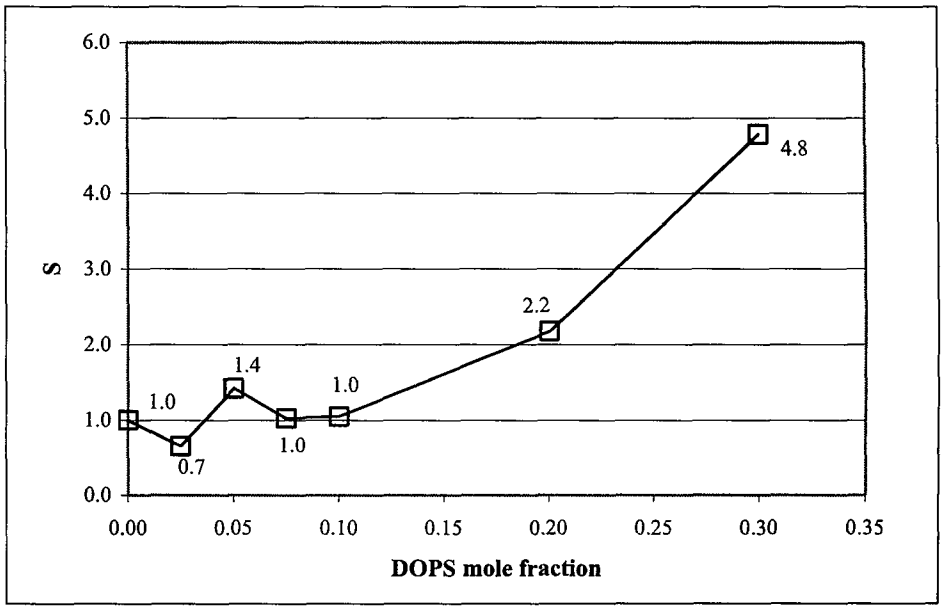

Figure 10.34 CCTα relative activity S for the DOPC/DOPS. Relative activity was calculated using Eq. 10.1. Relative activity data are reported in Table 10.16.

10.5.5.3 DOPC/DOPS LUVs and CCTα activity

Figure 10.38 shows the two curves obtained from the first and the second set of experiments with the DOPC/DOPS mixtures. In contrast to what is reported in the literature (maximal CCT activation with 20 % DOPS [3]), the results obtained herein show that the enzyme activity did not reach either a maximum or a plateau even with 30 % of DOPS. The curves for the relative activity from the first and the second set of experiments are shown in Figure 10.39. The activity measured with DOPC/DOPS vesicles is lower than the one measured with DOPC/DOPA vesicles, the lower DOPS head-group charge being a possible cause of the decreased activation (Figure 10.37). The head-group size of the two phospholipids could reasonably explain the difference in enzyme activation. Because of the differences between those lipids (zwitterions DOPC and DOPS, charged DOPA and DOPS, and size), it is not possible to determine quantitatively the effect of charge and stored bending energy.

Table 10.17 This tabulation reports CCTα activity and relative activity, S, measured in the presence of DOPC/DOPS LUVs. Relative activity was calculated using Eq. 10.1 (10.4.4). All the data reported in the table are plotted in Figure 10.35 and Figure 10.36.

DOPS mole fraction	CCTα activity ($nmol \cdot min^{-1} \cdot mg^{-1}$)	Std. Dev. ($nmol \cdot min^{-1} \cdot mg^{-1}$)	S
No LUVs	97	13	1.3
0.00	74	4	1.0
0.025	173	22	2.3
0.050	160	13	2.1
0.075	172	39	2.3
0.10	198	58	2.7
0.15	200	27	2.7
0.20	443	21	5.9
0.25	433	12	5.8
0.30	513	83	6.9

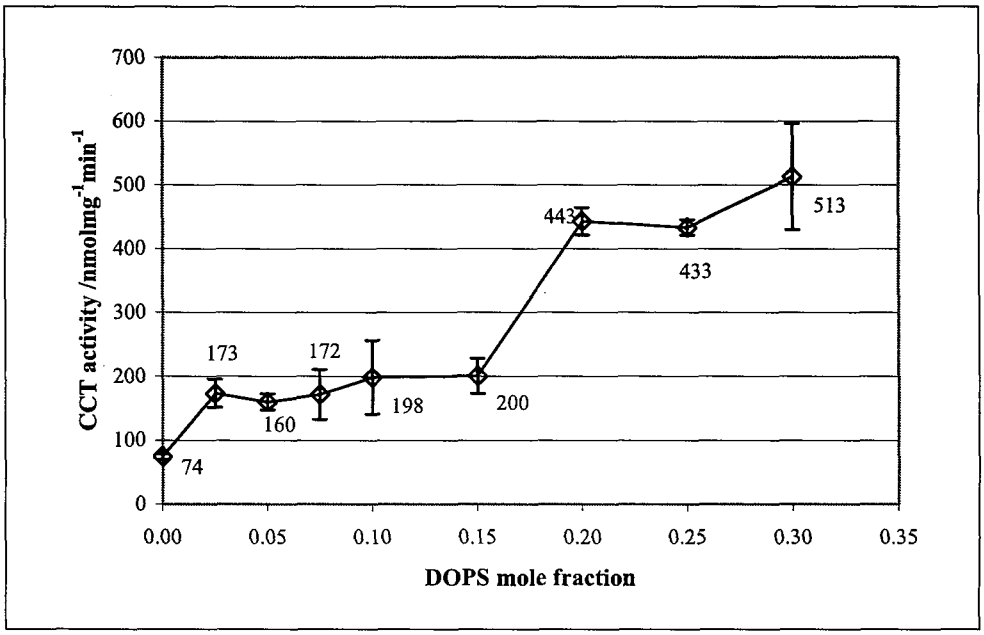

Figure 10.35 CCTα activity is plotted as a function of the mole fraction of DOPS in the DOPC/DOPS mixture. The error bars correspond to ± the standard deviation of three different samples. All data are reported in Table 10.17.

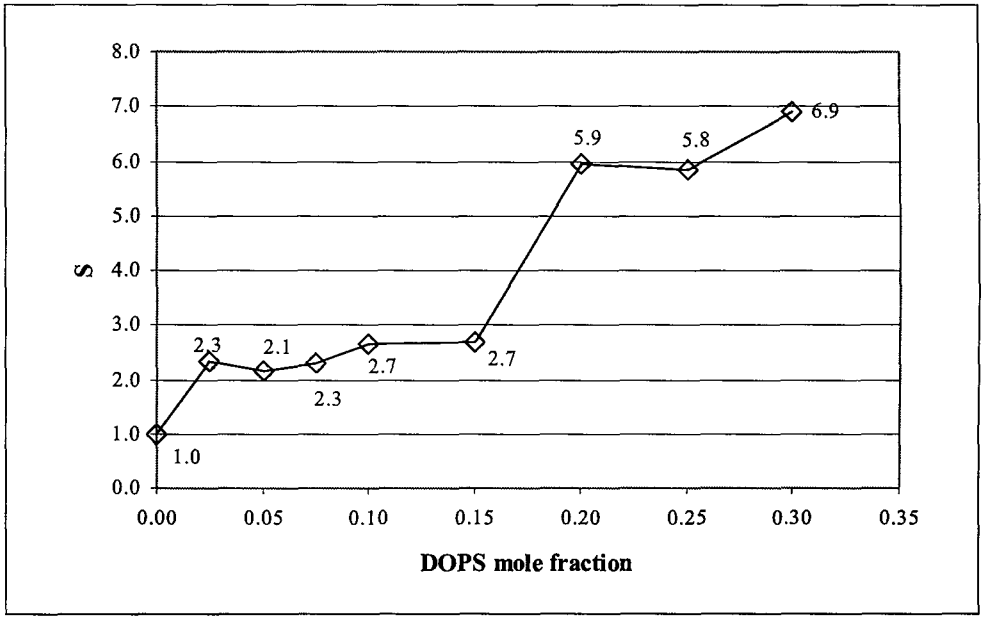

Figure 10.36 CCTα relative activity S for the DOPC/DOPA. Relative activity was calculated using Eq. 10.1. Relative activity data are reported in Table 10.17.

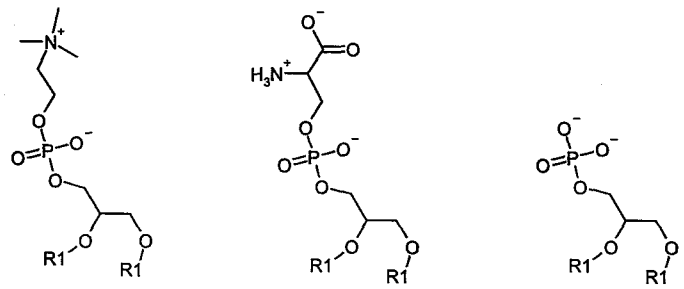

DOPC **DOPS** **DOPA**

Figure 10.37 The three phospholipids differ in the charge and in the size of the polar head-group, being the acyl chain R1 (oleyl) the same. DOPC has a neutral zwitterion head-group (net charge 0), DOPS has a negatively charged zwitterion head-group (nominal charge –1) and DOPA has a negatively charge head-group (nominal charge –2).

It is noted that CCTα from different batches shows different basal activity (Figure 10.40) as was the case for the DOPC/DOPA set of experiments. However, in this particular case, the basal activity of the enzyme from the second batch was higher than the activity measured in presence of DOPC vesicles, which is very similar to the activity measured for the enzyme from the first batch in presence of DOPC vesicles. As for the DOPC/DOPA results, the data available are not sufficient for an explanation of the observed different activities. However, although it is reasonable to hypothesise that, being the DOPS head-group bigger than the DOPA one, the DOPC/DOPS bilayer stores less bending energy than DOPC/DOPA and hence it is less effective to active the enzyme.

10.5.6 DOPC/DPPS LUVs

DOPC/DPPS LUVs were prepared following the method reported in 10.4.3. The enzyme activity (first batch) was assayed as described in 10.4.4 and 10.4.5. The experimental results are reported in Table 10.18 and Table A-10, and plotted in Figure 10.41 and Figure 10.42. CCTα relative activity S (Table 10.18) was calculated using Eq. 10.1.

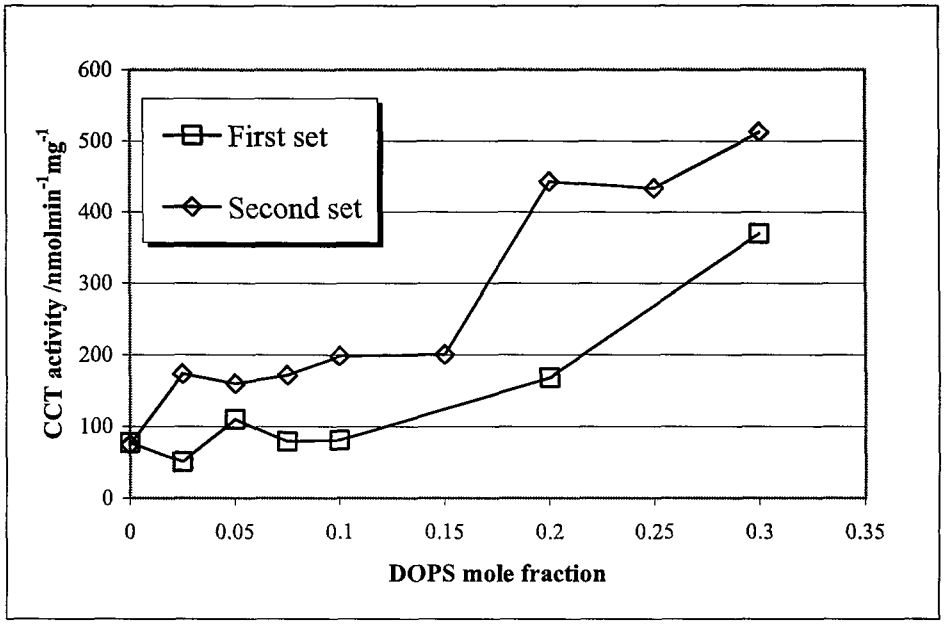

Figure 10.38 CCTα activity showed no plateau or maximal activation even at high mole fraction of DOPS in mixture with DOPC. Curves from the first and the second set.

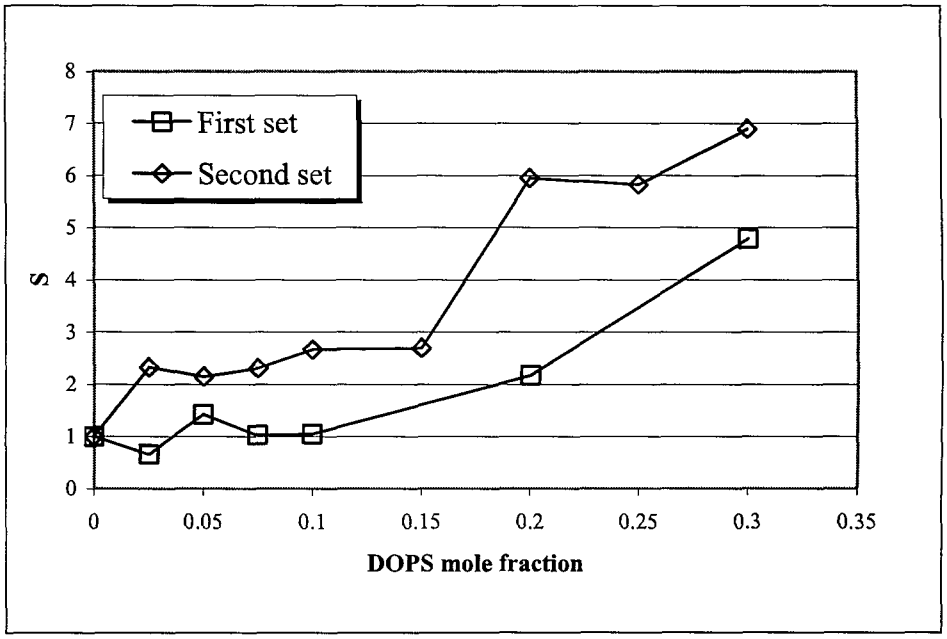

Figure 10.39 CCTα relative activity curves obtained from the first and the second set of experiments in the presence of DOPC/DOPS LUVs, and shown separately in Figure 10.34 and Figure 10.36.

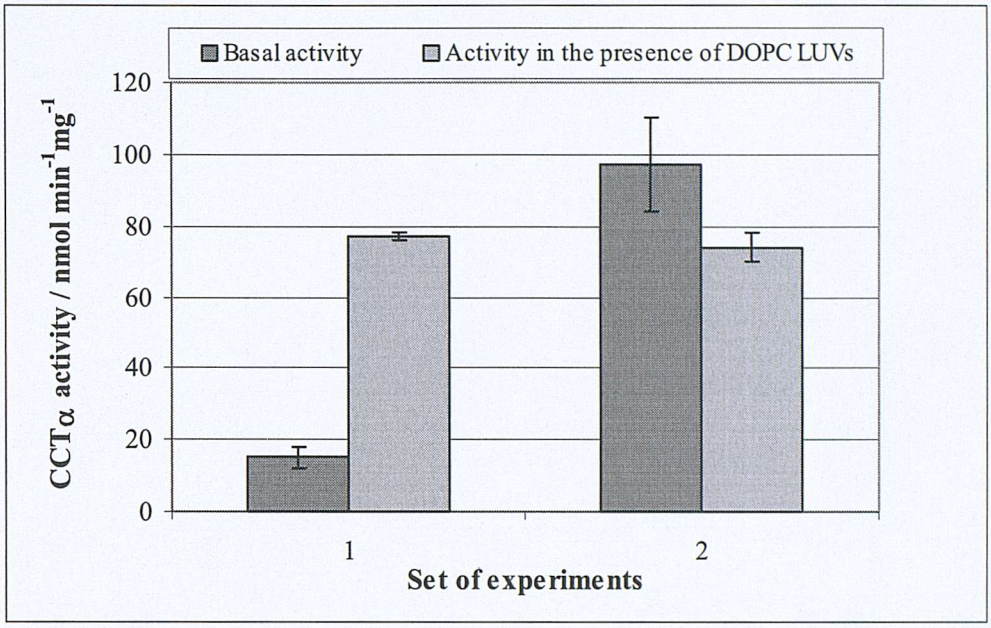

Figure 10.40 The basal activity and the activity in presence of DOPC/DOPA LUVs show differences that could be due essentially to the different batch of enzyme used for the experiments. The enzyme from the first batch was used for the first set of experiments, whilst the enzyme from the second batch was used for the second set of experiments. Differently from the previous cases, the basal activity measured during the second set of experiments is higher than the activity measured in presence of DOPC vesicles.

Table 10.18 This table reports CCTα activity and relative activity, S, measured in the presence of DOPC/DPPS LUVs. Relative activity was calculated using Eq. 10.1. All the data reported in the table are plotted in Figure 10.41 and Figure 10.42.

DPPS mole fraction	CCTα activity ($nmol \cdot min^{-1} \cdot mg^{-1}$)	Std. Dev. ($nmol \cdot min^{-1} \cdot mg^{-1}$)	S
No LUVs	30	1	0.03
0.00	861	246	1.00
0.025	1409	467	1.64
0.050	1218	219	1.41
0.075	1448	539	1.68
0.100	2374	506	2.76
0.150	3108	198	3.61
0.200	3301	96	3.83
0.250	3430	33	3.98
0.300	3457	288	4.02

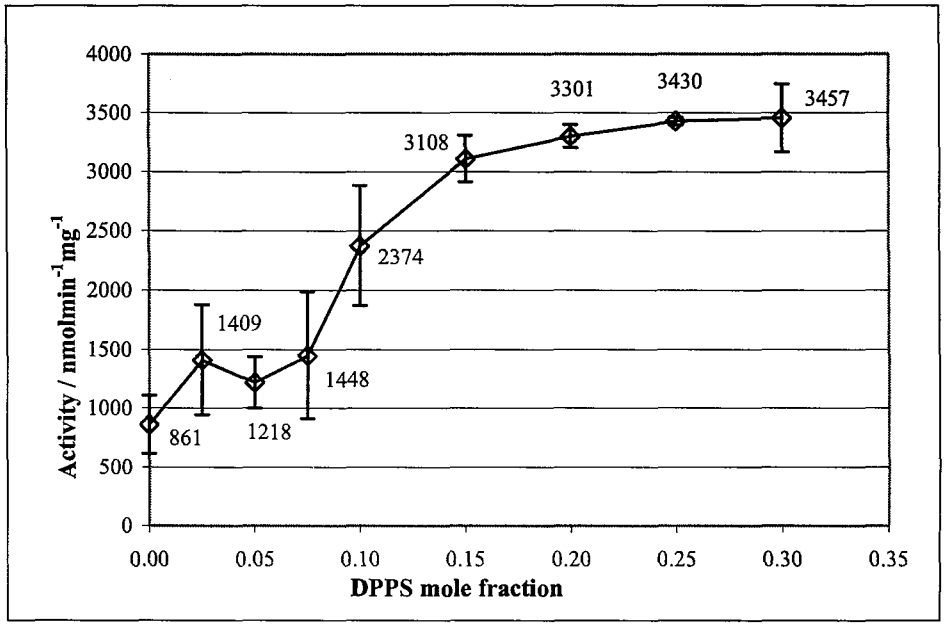

Figure 10.41 CCTα activity is plotted as a function of the mole fraction of DPPS in the DOPC/DPPS mixture. The error bars correspond to ± the standard deviation of three different samples. All data are reported in Table 10.18.

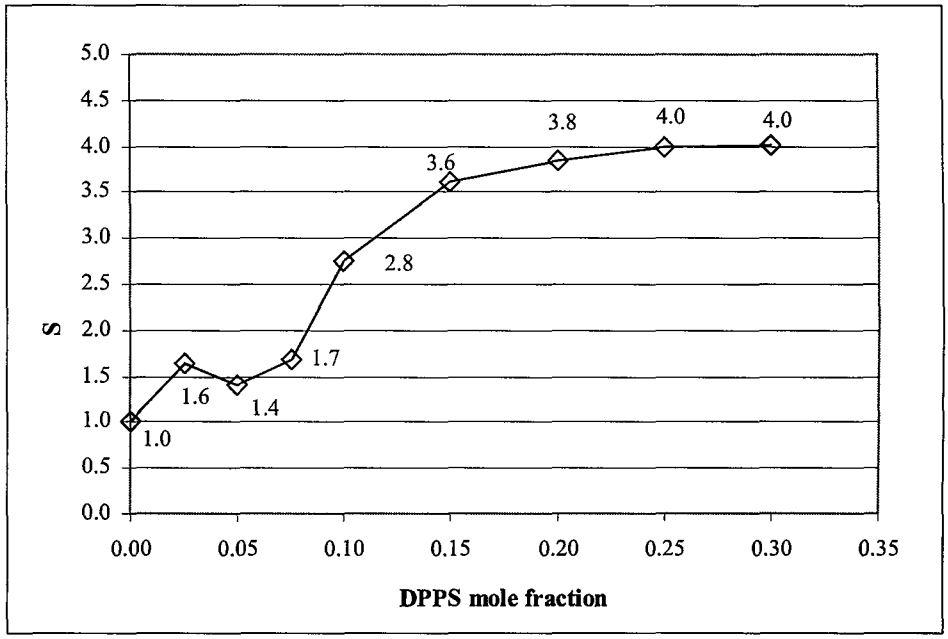

Figure 10.42 CCTα relative activity S for the DOPC/DPPS. Relative activity was calculated using Eq. 10.1. Relative activity data are reported in Table 10.18.

The enzyme aliquot used for this set of experiments is the same used for the DOPC/DPPA mixtures and shows the same high activity. Differently from what was seen with the DOPC/DOPA and DOPC/DOPS, the enzyme relative activity was very similar for both DOPC/DPPA (3.1) and DOPC/DPPS (4.0). Moreover, because DPPS phase transition occurs at 54° C [28], the DOPC/DPPS lipid mixtures could go through miscibility/phase transition phenomena. However, as previously mentioned, there are no sufficient data to interpret properly, and correctly, the effect of the DOPC/DPPS mixtures on the enzyme activation, in term of either charge or torque tension.

10.5.7 DOPC/OPS LUVs

As for the case of OPA, the following experiments were aimed to investigate the effect a PtdSer on the enzyme activation while the pressure in the hydrocarbon region was reduced. The following two sets of experiments differ only in the enzyme preparation: CCTα from the first batch for the fist set and from the second batch for the second set.

10.5.7.1 First set of experiments

DOPC/OPS LUVs were prepared following the method reported in 10.4.3. The enzyme activity (first batch) was assayed as described in 10.4.4 and 10.4.5 using the same enzyme aliquot used for the first DOPC/OPA experiment (10.5.4.1). Because of the limited supply of enzyme from the first batch, a single sample for each lipid mixture was used for the experiments reported here. The experimental results are reported in Table 10.19 and Table A-11, and plotted in Figure 10.43 and Figure 10.44. CCTα relative activity S (Table 10.19) was calculated using Eq. 10.1.

Table 10.19 This tabulation reports CCTα activity and relative activity, S, measured in the presence of DOPC/OPS LUVs. Relative activity was calculated using Eq. 10.1. All the data reported in the table are plotted in Figure 10.43 and Figure 10.44.

OPS mole fraction	CCTα activity ($nmol \cdot min^{-1} \cdot mg^{-1}$)	S
No LUVs	4.9	0.15
0.0	32	1.00
0.025	45	1.42
0.050	85	2.66
0.075	176	5.50
0.100	206	6.46
0.200	501	15.68
0.300	719	22.52

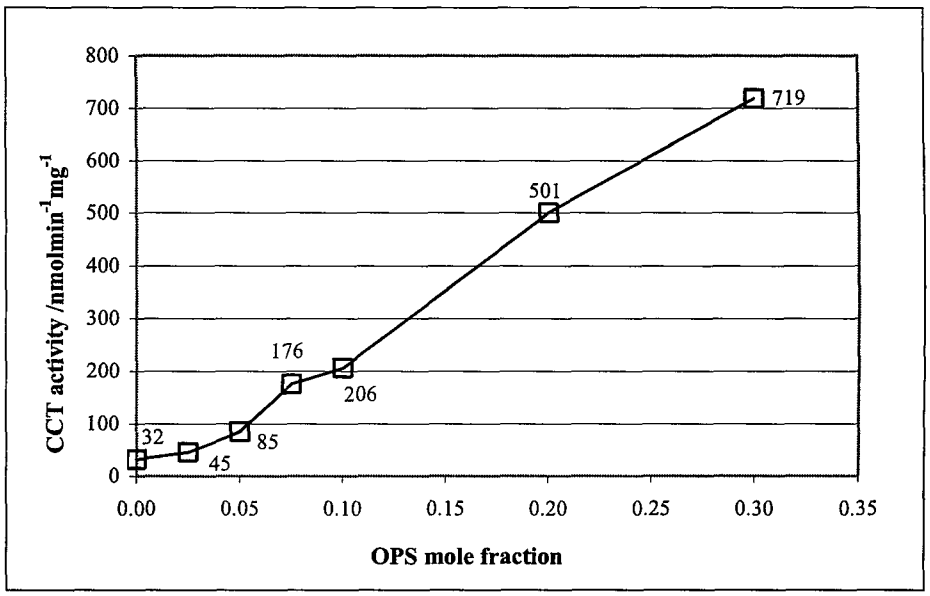

Figure 10.43 CCTα activity plotted as a function of the mole fraction of OPS in the DOPC/OPS mixture. All data are reported in Table 10.19.

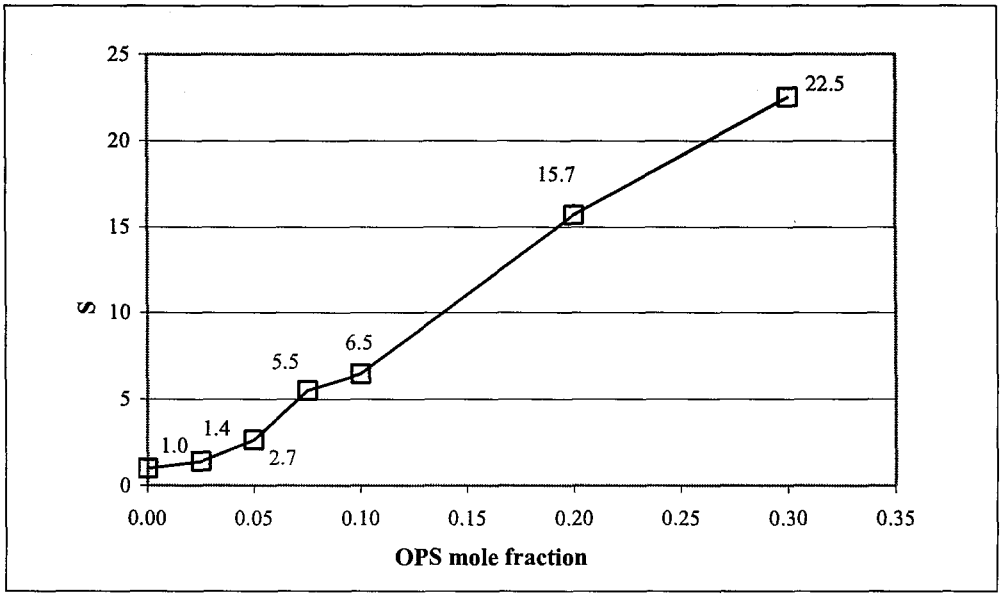

Figure 10.44 CCTα relative activity S for the DOPC/OPS. Relative activity was calculated using Eq. 10.1. Relative activity data are reported in Table 10.19.

10.5.7.2 Second set of experiments

DOPC/OPS LUVs were prepared according to the method reported in 10.4.3. The enzyme activity (second batch) was assayed as described in 10.4.4 and 10.4.5. The experimental results are reported in Table 10.20 and Table A-12, and plotted in Figure 10.45 and Figure 10.46. CCTα relative activity S (Table 10.20) was calculated using Eq. 10.1.

10.5.7.3 CCTα activity in DOPC/OPS LUVs

CCTα activity was strongly affected by the presence of OPS in mixture with DOPC. Differently from what was expected, the DOPC/OPS behaved more like DOPC/DOPA than like DOPC/DOPS. This behaviour was unexpected for two reasons: the lower charge and the smaller hydrophobic region (one oleyl group instead of two). However, it is reasonable to exclude the charge from the observed behaviour. In this case, we could speculate that immiscibility of the two phospholipids could be the reason. However, as no data are available, the immiscibility hypothesis has to be considered as a mere speculation.

Table 10.20 This tabulation reports CCTα activity and relative activity, S, measured in the presence of DOPC/OPS LUVs. Relative activity was calculated using Eq. 10.1. All the data reported in the table are plotted in Figure 10.45 and Figure 10.46.

OPS mole fraction	CCTα activity ($nmol \cdot min^{-1} \cdot mg^{-1}$)	Std. Dev. ($nmol \cdot min^{-1} \cdot mg^{-1}$)	S
No LUVs	97	13	1.3
0.00	74	4	1.0
0.025	152	7	2.0
0.050	169	25	2.3
0.075	184	23	2.5
0.10	148	25	2.0
0.15	333	74	4.5
0.20	407	29	5.5
0.30	598	50	8.0
0.40	891	23	12.0

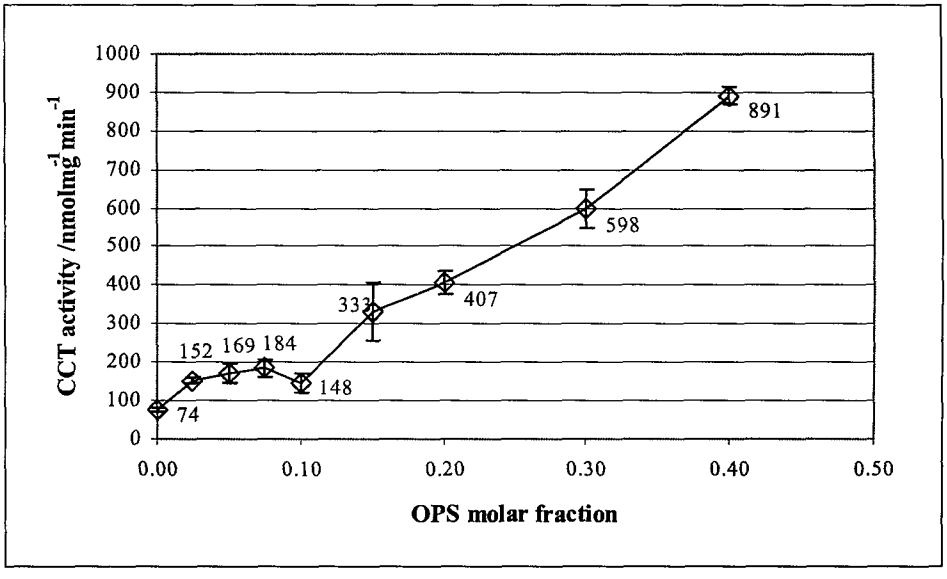

Figure 10.45 CCTα activity plotted as a function of the mole fraction of DOPS in the DOPC/OPS mixture. The error bars correspond to ± the standard deviation of three different samples. All data are reported in Table 10.20.

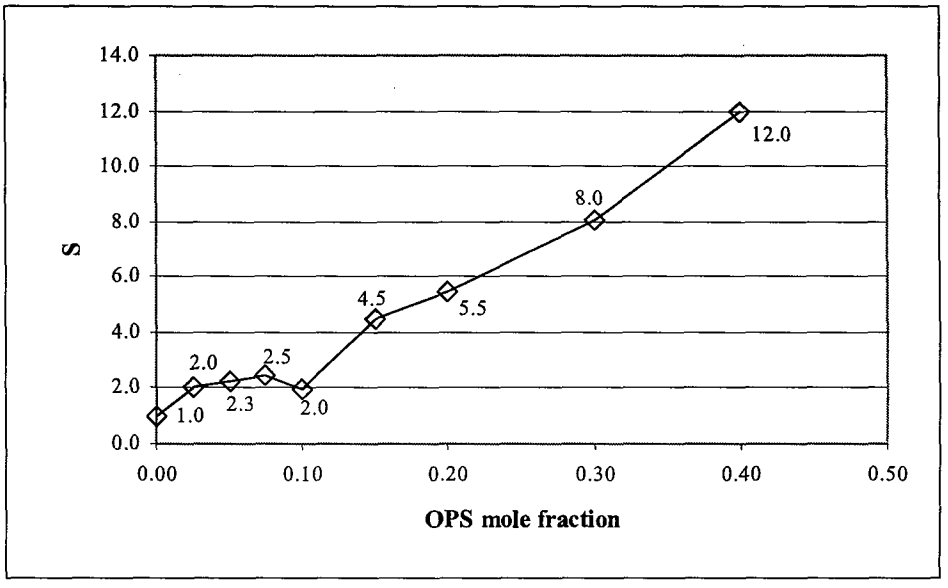

Figure 10.46 CCTα relative activity S for the DOPC/OPS. Relative activity was calculated using Eq. 10.1. Relative activity data are reported in Table 10.20.

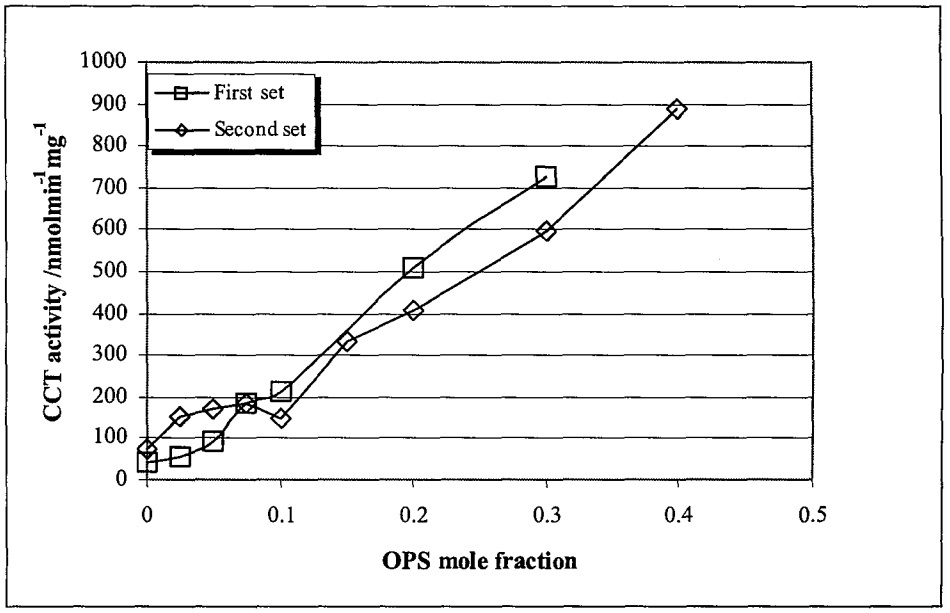

Figure 10.47 CCTα activity increases in a similar way in both the experiments with DOPC/OPS LUVs. The two curves are shown singularly in Figure 10.43 and Figure 10.45.

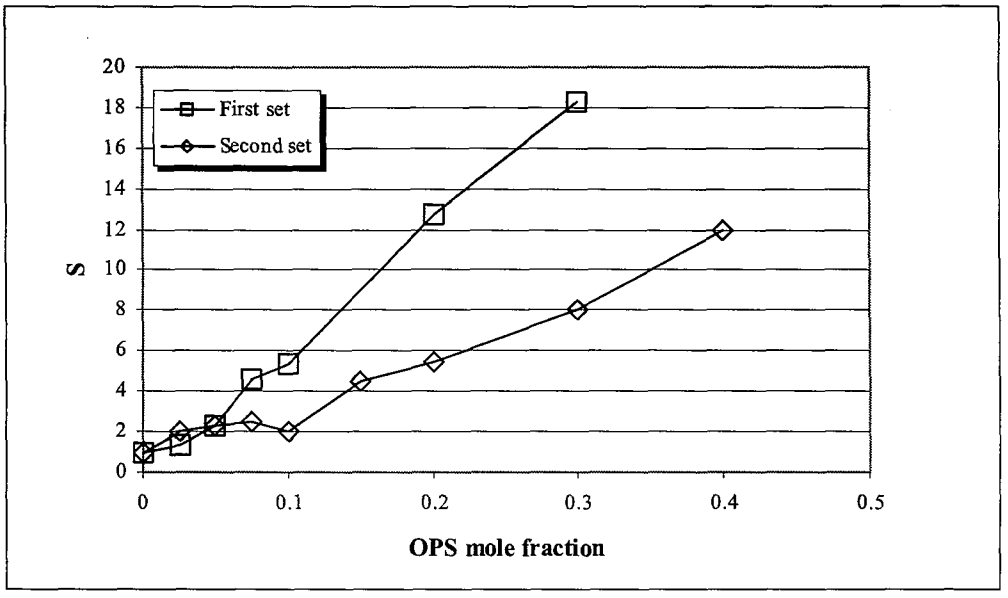

Figure 10.48 CCTα relative activity in the first set of experiments increases and shows a much higher activity than that obtained from the second set. The two curves are shown singularly in Figure 10.44 and Figure 10.46.

The results obtained with the DOPC/OPS mixtures are different from the others also for the specific and relative activity. In fact, while the enzyme specific activity is similar in both the experiments (Figure 10.47), whilst they differ in the relative activities (Figure 10.48).

10.5.8 DOPC/OA LUVs

DOPC/OA LUVs were prepared following the method reported in 10.4.3. The enzyme activity (second batch) was measured as described in 10.4.4 and 10.4.5. The experimental results are reported in Table 10.21 and Table A-14, and plotted in Figure 10.49 and Figure 10.50. CCTα relative activity S (Table 10.21) was calculated using Eq. 10.1. The mixture DOPC/OA proved to be very effective in activating the enzyme and giving the highest CCTα relative activity among those mixtures reported so far in this thesis. As expected from the results involving egg-PC/OA (1:1), the DOPC/OA mixtures are highly effective in activating the enzyme, especially the mixture DOPC/OA (1:1).

Table 10.21 This tabulation reports CCTα activity and relative activity, S, measured in the presence of DOPC/OA LUVs. Relative activity was calculated using Eq. 10.1. All the data reported in the table are plotted in Figure 10.49 and Figure 10.50.

OA mole fraction	CCTα activity ($nmol \cdot min^{-1} \cdot mg^{-1}$)	Std. Dev. ($nmol \cdot min^{-1} \cdot mg^{-1}$)	S
No LUVs	39	5	0.7
0.00	52	10	1.0
0.05	80	36	1.5
0.10	155	54	3.0
0.15	291	32	5.5
0.20	445	43	8.5
0.30	692	91	13.2
0.40	1009	134	19.2
0.50	1427	125	27.2
0.60	1283	98	24.5

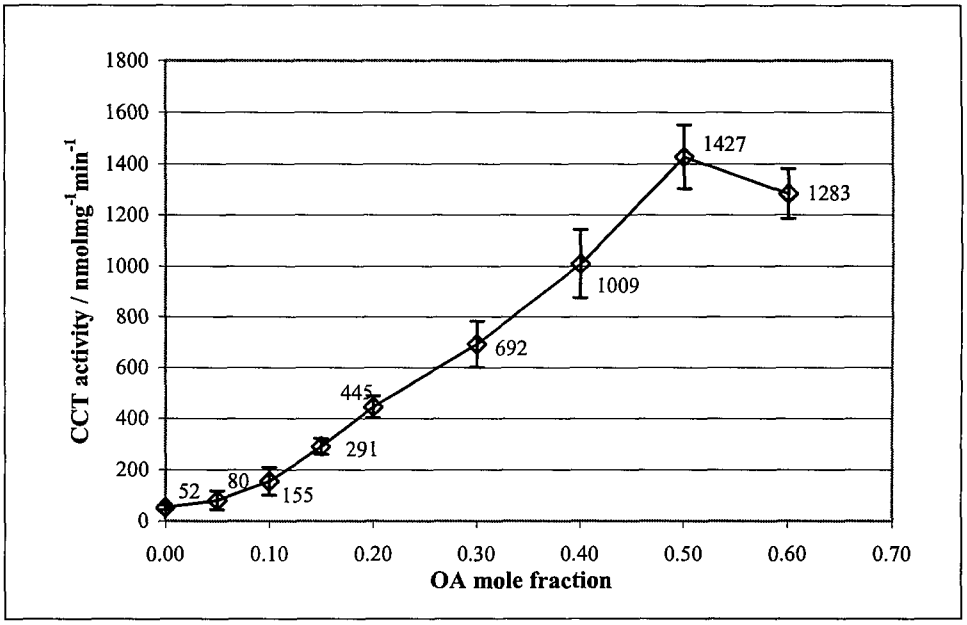

Figure 10.49 CCTα activity plotted as a function of the mole fraction of PA in the DOPC/OA mixture. The error bars correspond to ± the standard deviation of three different samples. All data are reported in Table 10.21.

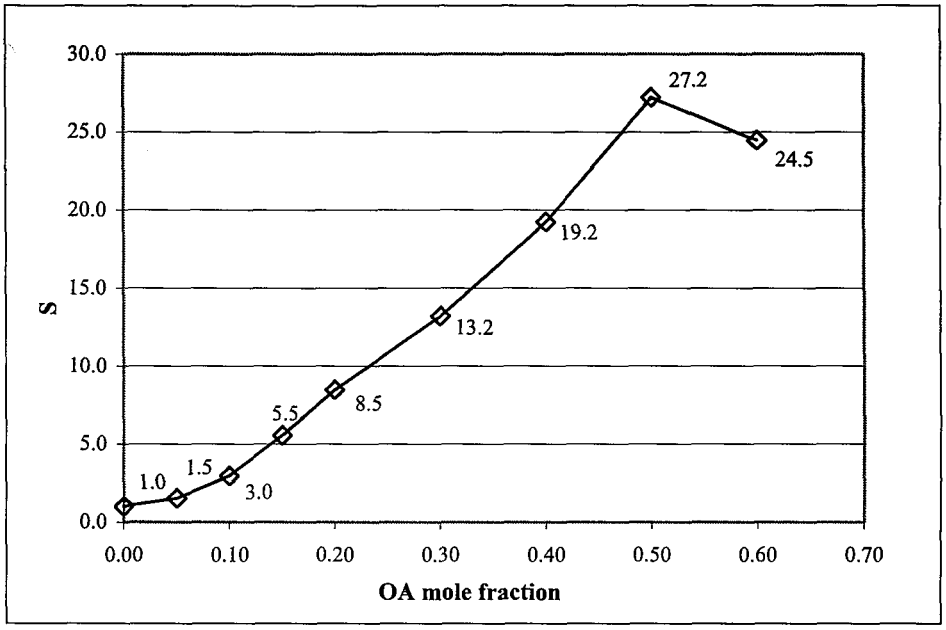

Figure 10.50 CCTα relative activity S for the DOPC/OA lipid mixtures. Relative activity was calculated using Eq. 10.1. Relative activity data are reported in Table 10.21.

10.6 Conclusions

A number of lipid mixtures and two enzyme preparations have been employed to obtain the results reported in this chapter. Several aspects of the results of this study have been analyzed: enzyme substrate concentrations, maximal and relative activity, lipid preparations and the correlation between lipid compositions and enzyme relative activities.

10.6.1 Enzyme activity and substrate concentrations

The mechanism of CCTα activation has been discussed in the introduction of the chapter. Some of the known key elements of CCTα activity and regulation are:

1. The enzymatic reaction behaves according to an ordered bi bi mechanism [22, 24].
2. The soluble form of CCTα is essentially inactive whilst the membrane bound is active.

3. Membrane biophysical properties can trigger the enzyme activation through the modulation of the enzyme partitioning onto the lipid.
4. The binding to the lipids activates the enzyme by increasing the affinity for CTP [12][o].

The velocity (V) of an enzymatic reaction proceeding through an ordered bi bi mechanism is given, for the case in which the binding of one substrate does not affect the binding of the second substrate, by Eq. 10.2 [29]

$$\text{Eq. 10.2 } V = \frac{V_{Max} \cdot [A][B]}{K^A K^B + K^B[A] + K^A[B] + [A][B]}$$

where $[B]$ and $[A]$ are the substrate concentrations, K^A and K^B the Michaelis constant for the substrates, and V_{Max} is the maximum velocity, which is proportional to the enzyme catalytic constant (k_{cat}) and the total enzyme concentration ($[E_T]$)

$$\text{Eq. 10.3 } V_{Max} = k_{cat}[E_T]$$

Eq. 10.2 can be rewritten in the form of Eq. 10.4

$$\text{Eq. 10.4 } V = V_{Max}\left(\frac{[A]}{K^A + [A]}\right)\left(\frac{[B]}{K^B + [B]}\right)$$

The calculation of V using Eq. 10.4 for different concentration of the substrates shows that only the 83% of V_{Max} is observed when $[A]$=10x K^A and $[B]$=10x K^B[p]. In case of CCTα, the percentage of enzyme that is saturated (which is the same as the percentage of V_{Max}) cannot be calculated because no kinetic study has been done to determine the K_ms. Moreover, complete saturation is only a theoretical condition because of the extremely high concentration of the substrates

[o] It has been reported that the presence of lipids decreases the Km for CTP from 24.7 mM in to 0.7 mM [12]

[p] 91% of V_{Max} is observed when $[A]$=20x K^A and $[B]$=20x K^B and only the 96% of V_{Max} is observed when $[A]$=50x K^A and $[B]$=50x K^B.

required. The value of V_{Max} is extrapolated from the enzyme kinetics for infinite concentration of the substrates. However, because the same substrate concentrations have been used in all the experiments reported herein, and because the k_{cat} is independent of the concentration of both enzyme and the substrates, Eq. 10.4 can be rewritten as

Eq. 10.5 $V = [E_T] \cdot V_{A,B}$

where $V_{A,B}$ is referred to the specific concentration of the substrates A and B. To establish conditions that most closely represent enzyme saturated with either or both substrates, one can only work at substrate concentrations ≥ those that yield the V_{Max}. Although the same enzyme concentration and the same range of substrate concentration has been used in all the assays, the velocity of the enzymatic reaction varied among the experiments, leading to the conclusion that a variable fraction of the total enzyme was active[q]. The following section will demonstrate that the enzyme relative activity, used to correlate the results obtained with different enzyme preparations, is independent of the fraction of active enzyme.

10.6.2 CCTα basal and maximal activity

Enzymes from different preparations have different histories: details of the purification procedures, handling, and storage. Although the actual causes of the decrease in the enzyme activity are still unknown[r], the storage, and especially the

[q] Someone could argue that the variability could be due to the k_{cat}, which is related to the affinity of the enzyme for the substrates and to the rate of conversion of the substrate to the products [8, 29-32]. However, because k_{cat} is empirically calculated from V_{Max} with the assumption that the entire enzyme is active (Eq. 10.3), the variability of k_{cat} and $[E_T]$ are dependent on one another and, hence, discussion of active enzyme is equivalent to discussion of k_{cat}.

[r] Enzyme oxidation might be one of the causes; however, the experiments with and without DTT have shown that, if this is the case, the process has occurred during the preparation and storage, and that the process is irreversible under the assay conditions that have been used.

freeze-thawing, are probably major factors[s]. Because the absolute enzyme specific activity was not constant, the relative activity (Eq. 10.1) has been employed to normalize the data for a qualitative analysis. The following demonstration, showing the independence of the relative activity from the absolute activity, is based on the assumption that the loss of activity is an irreversible process independent of and unaffected by the presence of lipids in the assay mixture. The demonstration will consider two possibilities: the inactive enzyme cannot partition onto the lipid membrane or it can partition onto the membrane but is not active.

If $[E_T]$ is the initial concentration of enzyme in the reaction mixture and $[L]$ the lipid concentration, we postulate that the enzyme will partition onto the lipid soon after they are mixed. Being $[E_L]$ and $[E_W]$ the enzyme concentrations on the lipids and in solution respectively, $[L]$ and $[W]$ the lipid and the water concentration, the partition constant K_P of the enzyme between the soluble and the lipid bound form is given by

$$\text{Eq. 10.6} \quad K_P = \frac{[E_L]/[L]}{[E_W]/[W]}$$

Because the lipid and the water concentration were constant in all the experiments that have been reported herein, the partition constant can be expressed in the form of Eq. 10.7

$$\text{Eq. 10.7} \quad K_L = K_P \frac{[L]}{[W]} = \frac{[E_L]}{[E_W]}$$

in which $[E_L]$ and $[E_W]$ are correlated to the initial concentration of enzyme by Eq. 10.8

$$\text{Eq. 10.8} \quad [E_T] = [E_L] + [E_W]$$

[s] During the course of this study it has been observed a 40% lost of activity occurred during one freeze-thaw step. Studies conducted on the lactate dehydrogenase have shown that 30 % of activity went lost after only one freeze-thaw step [33].

If V_L and V_W are the specific activities of the enzyme in presence and in absence of lipids respectively[t], then the enzyme activity (V) is given by

Eq. 10.9 $$V = [E_W] \cdot V_W + [E_L] \cdot V_L$$

If V^0 is the activity measured for the reference lipid system (DOPC in the present study), and $[E_L^0]$ and $[E_W^0]$ are the concentration of enzyme on the lipid and in water in the reference, the relative activity S is given by

Eq. 10.10 $$S = \frac{V}{V^0} = \frac{[E_W] \cdot V_W + [E_L] \cdot V_L}{[E_W^0] \cdot V_W + [E_L^0] \cdot V_L}$$

Because it is unknown how the decrease of activity affects the enzyme sensitivity to lipids, we hypothesise that the decrease of activity can affect both the partition and the specific activity. If φ is the molar fraction of enzyme that has retained the specific activity and χ is the molar fraction of active enzyme that has retained the sensitivity to the lipids, the concentration of active enzyme is given by

Eq. 10.11 $$[E_T]_{\chi,\varphi} = [E_L]_{\chi,\varphi} + [E_W]_{\chi,\varphi}$$

in which the subscript χ,φ refers to the active enzyme. The relative activity $S_{\chi,\varphi}$ is then given by

Eq. 10.12 $$S_{\chi,\varphi} = \frac{[E_W]_{\chi,\varphi} \cdot V_W + [E_L]_{\chi,\varphi} \cdot V_L}{[E_W^0]_{\chi,\varphi} \cdot V_W + [E_L^0]_{\chi,\varphi} \cdot V_L}$$

We will demonstrate that the relative activity is independent of the molar fraction of active enzyme, that is

Eq. 10.13 $$S_{\chi,\varphi} = S$$

Being χ the molar fraction of lipid sensitive enzyme, the concentration of the enzyme subjected to partition, $[E_T]_\chi$, is given by

Eq. 10.14 $$[E_T]_\chi = \chi \cdot [E_T]$$

[t] V_L and V_W correspond to $V_{A,B}$ of Eq. 10.5, and the subscript is referred to the enzyme form.

Eq. 10.8 is then rewritten in terms of concentration of the lipid sensitive enzyme bound to the lipid ($[E_L]_\chi$) and in solution ($[E_W]_\chi$)

Eq. 10.15 $[E_T]_\chi = [E_L]_\chi + [E_W]_\chi$

The substitution of Eq. 10.14 into Eq. 10.15 gives the correlation between the lipid sensitive enzyme concentrations and the total enzyme

Eq. 10.16 $\chi \cdot [E_T] = [E_L]_\chi + [E_W]_\chi$

Because $[E_L]_\chi$ and $[E_W]_\chi$ are the only enzyme concentrations taking part to the partition, Eq. 10.7 is rewritten as

Eq. 10.17 $K_L = \dfrac{[E_L]_\chi}{[E_W]_\chi}$

combining Eq. 10.7 with Eq. 10.17 gives Eq. 10.18

Eq. 10.18 $\dfrac{[E_L]}{[E_W]} = \dfrac{[E_L]_\chi}{[E_W]_\chi}$

that can be rewritten as

Eq. 10.19 $\dfrac{[E_W]_\chi}{[E_W]} = \dfrac{[E_L]_\chi}{[E_L]}$

Dividing both terms of Eq. 10.16 by $[E_L]$ it follows that

Eq. 10.20 $\chi \dfrac{[E_T]}{[E_L]} = \dfrac{[E_L]_\chi}{[E_L]} + \dfrac{[E_W]_\chi}{[E_L]}$

Because of Eq. 10.19, Eq. 10.20 can be rewritten in the form of Eq. 10.21

Eq. 10.21 $\chi \dfrac{[E_T]}{[E_L]} = \dfrac{[E_W]_\chi}{[E_W]} + \dfrac{[E_W]_\chi}{[E_L]}$

which can be recast to explicit $[E_W]_\chi$

Eq. 10.22 $\chi \dfrac{[E_T]}{[E_L]} = [E_W]_\chi \left(\dfrac{[E_L] + [E_W]}{[E_W][E_L]} \right)$

Finally, being $[E_T]=[E_L]+[E_W]$, it follows that

Eq. 10.23 $[E_W]_\chi = \chi \cdot [E_W]$

dividing Eq. 10.16 by $[E_W]$ and following the steps described for Eq. 10.20, it follows

Eq. 10.24 $[E_L]_\chi = \chi \cdot [E_L]$

Because φ has been defined as the molar fraction of activity lipid-sensitive enzyme, the concentration of active enzyme $[E_T]_{\chi,\varphi}$ is given by

Eq. 10.25 $[E_T]_{\chi,\varphi} = \varphi \cdot [E_T]_\chi = \varphi \cdot ([E_L]_\chi + [E_W]_\chi)$

The substitution of Eq. 10.23 and Eq. 10.24 into Eq. 10.25 gives

Eq. 10.26 $[E_T]_{\chi,\varphi} = \varphi \cdot (\chi \cdot [E_L] + \chi \cdot [E_W])$

From Eq. 10.26 and Eq. 10.11 it follows that

Eq. 10.27 $[E_L]_{\chi,\varphi} = \chi\varphi \cdot [E_L]$

Eq. 10.28 $[E_W]_{\chi,\varphi} = \chi\varphi \cdot [E_W]$

Because the active fraction of enzyme is independent of the lipids, the substitution of $[E_L]_{\chi,\varphi}$ and $[E_W]_{\chi,\varphi}$ of Eq. 10.12 with Eq. 10.27 and Eq. 10.28 gives the relative activity $S_{\chi,\varphi}$ expressed as in Eq. 10.29

Eq. 10.29 $$S_{\chi,\varphi} = \frac{\chi\varphi \cdot [E_W] \cdot V_W + \chi\varphi \cdot [E_L] \cdot V_L}{\chi\varphi \cdot [E_W^0] \cdot V_W + \chi\varphi \cdot [E_L^0] \cdot V_L}$$

Eq. 10.29 can then been rewritten to give

Eq. 10.30 $$S_{\chi,\varphi} = \frac{\chi\varphi \cdot ([E_W] \cdot V_W + [E_L] \cdot V_L)}{\chi\varphi \cdot ([E_W^0] \cdot V_W + [E_L^0] \cdot V_L)} = \frac{[E_W] \cdot V_W + [E_L] \cdot V_L}{[E_W^0] \cdot V_W + [E_L^0] \cdot V_L}$$

The right term of Eq. 10.30 is the relative activity given by Eq. 10.10 and then

$S_{\chi,\varphi} = S$

which confirms that the relative activity, calculated from data obtained using the same enzyme during the same session of experiments, is independent of the molar fraction of active enzyme and does not require either any estimate of the fraction of enzyme that is saturated nor the enzyme to be saturated.

10.6.3 Enzyme activity variability and LUVs

The Freeze-thaw (F-T) method was employed in this study to obtain lipid vesicles with properties satisfying two conditions: they had to be unilamellar and they had to be large. Although the vesicles obtained through this procedure satisfy the two key conditions of unilamellarity and size (9.5.29 and tables in the appendix), the F-T procedure has some limitations: it is not possible to predict the degree of unilamellarity and the amount of structural stress, and the vesicles have a non-homogeneous size.

The non-homogeneous size distribution affects the sizing result and, in an unpredictable way, the enzymatic assays. As discussed in 9.2.2.2, the analysis of the size distribution dependents on both the angle at which the scattered light is measured and the accumulation time: the larger the size distribution, the longer the accumulation time, the higher the number of angles at which the accumulation time has to be run [34]. Because it is not possible to have a precise knowledge of the size distribution of the vesicle sample, it is not possible to correlate variations in the enzyme activity to vesicles size[u]. Although Cornell showed that small unilamellar vesicles (SUVs, 29-42 nm) stimulate CCTα activity more than multilamellar vesicles (MLVs, size not reported) [35], a correlation between size and enzyme activity has

[u] The measurements have revealed that almost all the lipid mixtures sized were constituted by a high percentage of vesicles by far bigger than 100 nm (size of the most commonly used LUVs) and that only in few samples a low percentage of light was scattered by small vesicles. The vesicles were sized by measuring the light scattered at 90°, conditions under which the smaller particles scatter more light than the bigger ones. Hence, it is reasonable to say that the percentage of small vesicles is an overestimation of the real one.

never been reported[v]. Only few vesicle samples used for the assays were sized (essentially the ones used for the DOPC/DOPE). Although the sizing of the vesicles used for the assays could have been of some utility in the analysis of the data, this has not been done. The sizing tabulated in the appendix refers to lipid samples used to test the effect of the increasing anionic lipid on the apparent size distribution. Moreover, any correlation between enzyme activity and vesicle size distribution could have been done only if:

1. The viscosity and the refractive index of the buffer, used for the vesicles preparation and for the sizing, and the lipid refractive index the sizing of the vesicles used for the assays. In fact, those values are required for the calculation of vesicle size distribution by SDP weight analysis.

2. The elastic parameters and the surface density charge of the lipid mixtures used herein were known. In fact, those values are necessary to estimate the amount of stored elastic energy of the vesicle samples due to the size of the vesicles and to the effect of the surface charge on the elastic moduli.

However, despite of the above observations, the effect of vesicle size on the enzyme activation could be qualitatively accomplished using vesicles with fixed and narrow diameter distribution, such the ones obtained by extrusion[w].

Albeit the presence of small vesicles (subjected to a high geometric stress) could have been present and could have contributed to the observed variability of the enzymatic activity, we hypothesize that the stored bending energy and structural defects have significantly contributed to the enzymatic variability. The low degree of multilamellarity and the presence of structural defects in vesicles prepared by the F-T method have been previously discussed (9.6). Recent studies have also shown that multilamellar vesicles seem to be more susceptible to structural changes than the unilamellar ones when subjected to freeze-thaw steps [36]. Other possible

---

[v] However, because the available lipid surface area is smaller in MLVs than in SUVs, Cornell's data suggest that CCTα is more active in presence of small highly curved vesicles than in presence of the larger MLVs.

[w] Several kind of membranes are commercially available for the preparation of vesicles as small as 30 nm of diameter. Other sizes commercially available are 50 and 80 nm, from 0.1 to 5 μm.

contributions to the stored elastic energy and to structural defects could be: phase separation/segregation (liquid/liquid, liquid/solid, or solid/solid)[x], coexistence of different morphologies, and variability in the topology (for reviews see [37-40]). As previously mentioned, we do not have sufficient data to properly correlate enzyme activity and vesicles properties. We do not have any information for all the mixtures (except DOPC/DOPE) about spontaneous curvature, bending modulus, surface density charge, phase transition or lipid segregation. Despite the above limitations, we believe that the results presented are qualitative valid and contribute to the understanding of the enzyme regulation.

10.6.4 The basal activity and the reference lipid

Two issues need to address before proceeding with the discussion of the relative activity in relation to the lipid mixtures. The first issue is about the activity measured in absence of lipids and the second concern the use of DOPC as reference lipid system.

CCTα activity measured in the absence of vesicles was supposed to be negligible compared to the activating lipids DOPC. The basal activity measured for the enzyme from the second batch was 3-6 times higher than the activity of the enzyme from the first batch. As the basal activities appear to be comparable for enzyme aliquots of the same batch, it is reasonable to attribute to the enzyme preparation the origin of the differences in the activity. Contaminants and differences in the enzyme preparation or in the fold purification could be the cause of the variability in the basal activity; because no study was conducted on those particular sources of variability, the questions about the different basal activities remains unanswered. However, the relative activity has been demonstrated to be the proper variable for the comparison of results obtained with different enzyme preparation as long as the

[x] Cornell suggested that lipids in the liquid phase are more effective than lipids in the gel phase in the activation of CCTα [35].

specific activity (the basal activity and the activity measured in the presence of lipids) is used to normalize the data under the same optimal assay conditions.

Because the relative activity appears to be a convenient variable, for this kind of study at least, the choice of a proper lipid reference system is the primary issue. The question is then: is the DOPC lipid system a good reference? The answer is yes and no.

The answer is yes because DOPC has been used as a major constituent of all the lipid mixtures that have been studied. Moreover, because the enzyme does not show either a high or the maximal activity, it is possible distinguish between small changes in the enzyme activity, especially at the low concentration of the second component used in lipid mixtures[y].

Despite of the above considerations, DOPC is not a good reference because its stored elastic energy can be affected by geometric stress or structural defects. DOPC has shown the lowest activation among he lipid mixtures that have been studied. Although the net effect of membrane charge and bending energy on the enzyme partition is still undefined, it is reasonable to hypothesize that DOPC is more susceptible than some of the other lipids investigated herein to variations of membrane biophysical properties. Impurities could for example affect localised portion of the membrane by changing the surface charge or by creating local alteration in the membrane morphology.

One possible solution to the problem inherent in the use of a low activator lipid, such as DOPC, could be the use of a high activator lipid. The experiments reported herein have shown that DOPC/DOPA could be that reference for at least two reasons:

1. CCT has shown high (S~20) relative activity in a range of DOPA molar fraction between 0.2 and 0.3.

[y] The homeostatic control of the PtdCho has been shown by Jackowski in relation to the cell cycle [41]. In particular, Jackowski has shown that a change in the rate of synthesis and hydrolysis of PtdCho is one of the parameters affecting net synthesis of PtdCho.

2. Because of the plateau in the relative activity, it is reasonable to conclude that, at least in the centre of the plateau, minimum significance will be due to those biophysical modifications affecting DOPC.

However, because DOPC/DOPA has a so strong effect on CCTα, it could be more difficult to differentiate between lipids featuring low enzyme activation. Despite the possible flattening of results at low activity, DOPC/DOPA remains a suitable and possibly a reliable reference.

10.6.5 Torque tension and surface charge

Despite these issues, the trends in the changes of CCT activity as a function of lipid composition are broadly reproducible and do provide qualitative insights into the differential activation of the enzyme by membrane lipid composition. CCTα is sensitive to both vesicle torque tension and charge, but the distinction between charge and torque tension effect is difficult to estimate because values for the bending modulus, κ_M, spontaneous curvature, c_0, surface density charge and phase diagrams are not known for the lipid mixtures used herein.

The torque tension in membranes constituted by neutral lipids (such as DMPC, DOPC and DOPE in Figure 10.2) and the release of the bending energy, as the driving force for the enzyme partitioning, have been found to be sufficient conditions for activating the enzyme. Data reported in the literature have shown that short chain fatty acids ($<C_{14}$) mixed with egg-PC have no effect on CCT [35], suggesting that the vesicle charge is not a sufficient condition for the enzyme activation. However, Arnold and Cornell have shown that surface charge and torque tension can synergistically activate the enzyme [3]. They observed that CCT activity measured in the presence of egg-PC containing 2.5 mol% of 1-palmitoyl-2-oleoyl-phosphatidic acid increased from 20 to 430 nmol·min^{-1}·mg^{-1} when 2.5 mol% of diacylglycerol where added that lipid mixture; they also reported an increase of

activity from 90 to 380 nmol·min^{-1}·mg^{-1} when the same percentage of diacylglycerol was added to egg-PC containing 2.5 mol% of DOPS [3][z].

The present study was aimed to determine if the charge effect on the enzyme activation was due to electrostatic interaction or due to the effect on the bending energy. In fact, both the bending (k) and the Gaussian (k_G) elastic moduli are affected by the surface density charge (σ) according to Eq. 10.31 and Eq. 10.32

Eq. 10.31 $$\delta k^{el} = \sigma^2 \cdot f(\varepsilon_W, \varepsilon_{oil}, t, \lambda_D)$$

Eq. 10.32 $$\delta k_G^{el} = \sigma^2 \cdot g(\varepsilon_W, t, \lambda_D)$$

Where δk^{el} and δk_G^{el} are the electrostatic contribution to the respective moduli, ε_W and ε_{oil} are the dielectric constant of the water and the hydrophobic region of the bilayer respectively, t is the bilayer thickness and λ_D is the Debye-Huckel screening length [42]. However, as we have no sufficient data to determine neither the bending energy nor the contributions defined by Eq. 10.31 and Eq. 10.32, it is useless any attempt to obtain quantitative information from the results herein reported. However, the dissimilarity of the enzyme activity observed in the presence of phospholipids having the same head-group and differing for the acyl chains suggests that the charge is not the key element in the CCTα regulation.

10.7 References

[1] G. S. Attard, Templer, R.H., Smith, W.S., Hunt, A.N., and Jackowski, S., "Modulation of CTP: phosphocholine cytidylyltransferase by membrane curvature elastic stress," in *Proceedings of the National Academy of Sciences of the United States of America*, vol. 97, 2000, pp. 9032-9036.

[z] However, a direct comparison between those data and the ones reported in this chapter is not possible because they did not use any reference lipid system (they use egg-PC, which is not a CCT activator, as bulk lipid in all the mixtures they studied) and because they used egg-PC and 1-palmitoyl-2-oleoyl-phosphatidic acid instead of DOPC and DOPA. In fact, the data reported herein shown clearly that differences in the acyl group of a phospholipid can have a strong and unpredictable effect on the enzyme activity.

[2] S. M. A. Davies, Epand, R.M., Kraayenhof, R., and Cornell, R.B., "Regulation of CTP: phosphocholine cytidylyltransferase activity by the physical properties of lipid membranes: an important role for store curvature strain energy," in *Biochemistry*, vol. 40, 2001, pp. 10522-10531.

[3] R. S. Arnold, and Cornell, R.B., "Lipid regulation of CTP: phosphocholine cytidylyltransferase: electrostatic, hydrophobic, and synergistic interactions of anionic phospholipids and diacylglycerol," in *Biochemistry*, vol. 35, 1996, pp. 9917-9924.

[4] R. B. Cornell, "Regulation of CTP: phosphocholine cytidylyltransferase by lipids. 1. Negative surface charge dependence for activation," in *Biochemistry*, vol. 30, 1991, pp. 5873-5880.

[5] R. S. Arnold, DePaoli-Roach, A.A., and Cornell, R.B., "Binding of CTP: phosphocholine cytidylyltransferase to lipid vesicles: diacylglycerol and enzyme dephosphorylation increase the affinity for negatively charged membranes," in *Biochemistry*, vol. 36, 1997, pp. 6149-6156.

[6] A. Lykidis, Jackson, P., and Jackowski, S., "Lipid activation of CTP: phosphocholine cytidylyltransferase α: characterization and identification of a second activation domain," in *Biochemistry*, vol. 40, 2001, pp. 494-503.

[7] B. Alberts, Bray, D., Lewis, J., Raff, M., Roberts, K., and Watson, J.D., *Molecular biology of the cell*, Third ed. New York: Garland Publishing, 1994.

[8] L. Stryer, *Biochimica*, Fourth Edition ed. Bologna: Zanichelli, 1996.

[9] E. P. kennedy, Borkenhagen, L.F., and Smith, S.W., "Possible metabolic functions of deoxycytidine diphosphate choline and deoxycytidine diphosphate ethanolamine," in *Journal of Biological Chemistry*, vol. 234, 1959, pp. 1998-2000.

[10] G. Spyrou, and Reichard, P., "Compartmentation of dCTP pools," in *Journal of Biological Chemistry*, vol. 262, 1987, pp. 16425-16432.

[11] P. S. Sohal, and Cornell, R.B., "Sphingosine inhibits the activity of rat liver CTP: phosphocholine cytidylyltransferase," in *Journal of Biological Chemistry*, vol. 265, 1990, pp. 11746-11750.

[12] W. Yang, Boggs, K.P., and Jackowski, S., "The association of lipid activators with the amphipathic helical domain of CTP: phosphocholine cytidylyltransferase accelerates catalysis by increasing the affinity of the enzyme for CTP," in *Journal of Biological Chemistry*, vol. 270, 1995, pp. 23951-23957.

[13] A. Lykidis, Barburina, I., and Jackowski, S., "Distribution of CTP: phosphocholine cytidylyltransferase (CCT) isoforms," in *Journal of Biological Chemistry*, vol. 274, 1999, pp. 26992-27001.

[14] F. Mages, Rey, C., Fonlupt, P., and Pacheco, H., "Kinetic and biochemical properties of CTP: choline-phosphate cytidylyltransferase from the rat brain," in *European Journal of Biochemistry*, vol. 178, 1988, pp. 367-372.

[15] X. Wang, and Moore, T.S., "Partial purification and characterization of CTP: cholinephosphatase cytidylyltransferase from castor bean endosperm," in *Archives of Biochemistry and Biophysics*, vol. 274, 1989, pp. 338-347.

[16] P. A. Weinhold, Rounsifer, M.E., and Feldman, D.A., "The purification and characterization of CTP: phosphocholine cytidylyltransferase from rat liver," in *Journal of Biological Chemistry*, vol. 261, 1986, pp. 5104-5110.

[17] J. I. S. MacDonald, Kent, C, "Baculovirus-mediated expression of rat liver CTP: phosphocholine cytidylyltransferase," in *Protein Expression and Purification*, vol. 4, 1993, pp. 1-7.

[18] R. Cornell, "Chemical cross-linking reveals a dimeric structure for CTP: phosphocholine cytidylyltransferase," in *Journal of Biological Chemistry*, vol. 264, 1989, pp. 9077-9082.

[19] S. L. Pelech, Pritchard, P.H., and Vance, D.E., "cAMP analogues inhibit phosphatidylcholine biosynthesis in cultured rat hepatocytes," in *Journal of Biological Chemistry*, vol. 256, 1981, pp. 8283-8286.

[20] S. L. Pelech, and Vance, D.E., "Regulation of Rat liver cytosolic CTP: phosphocholine cytidylyltransferase by phosphorylation and dephosphorylation," in *Journal of Biological Chemistry*, vol. 257, 1982, pp. 14198-14202.

[21] J. A. Friesen, Campbell, H. A., and Kent, C., "Enzymatic and cellular characterization of a catalytic fragment of CTP: phosphocholine cytidylyltransferase α," in *Journal of Biological Chemistry*, vol. 274, 1999, pp. 13384-13389.

[22] D. P. Veitch, and Cornell, R.B., "Substitution of Ser for Glycine-91 in the HXGH motif of CTP: phosphocholine cytidylyltransferase implicayes this motif in CTP binding," in *Biochemistry*, vol. 35, 1996, pp. 10743-10750.

[23] L. F. Borkenhagen, and Kennedy, E.P., "The enzymatic synthesis of cytidine diphosphate choline," in *Journal of Biological Chemistry*, vol. 227, 1957, pp. 951-962.

[24] B. A. Helmink, Braker, J.D., Kent, C, and Friesen, J.A., "Identification of Lysine 122 and Arginine 196 as important functional residues of rat CTP:phosphocholine cytidylyltransferase alpha," in *Biochemistry*, vol. 42, 2003, pp. 5043-5051.

[25] G. R. Bartlet, "Phosphorous assay in column chromatography," in *Journal of Biological Chemistry*, vol. 234, 1959, pp. 466-468.

[26] U. Pick, "Liposome with a large trapping capacity prepared by freezing and thawing of sonicated phospholipid mixtures," in *Archives of Biochemistry and Biophysics*, vol. 212, 1981, pp. 186-194.

[27] M. Kasahara, and Hinkle, P.C., "Reconstitution and purification of the α-glucose transporter from human erythrocytes," in *Journal of Biological Chemistry*, vol. 252, 1977, pp. 7384-7390.

[28] J. R. Silvius, *Thermotropic phase transitions of pure lipids in model membranes and their modifications by membrane proteins*. New York: John Wiley & Sons, Inc., 1982.

[29] R. A. Copeland, *Enzymes: a practical introduction to structure, mechanism, and data analysis*. New York, NY: Wiley & Sons, 2000.

[30] R. Chang, *Physical Chemistry for the chemical and biological sciences*, 3rd ed. Sausalito, CA 94965: University Science Books, 2000.

[31] A. Fersht, *Structure and mechanism in protein science*: W.H. Freeman & Com., 2002.

[32] K. Wilson, and Walker, J., *Principles and techniques of practical biochemistry*, Fifth ed. Cambridge: Cambridge University Press, 2000.

[33] T. J. Anchordoquy, Izutsu, K.-I., Randolph, T.W., and Carpenter, J.F., "Maintenance of Quaternary Structure in the Frozen State Stabilizes Lactate Dehydrogenase during Freeze-Drying," in *Archives of Biochemistry and Biophysics*, vol. 390, 2001, pp. 35-41.

[34] C. Coulter, *Coulter® N4 Plus Submicron Particle Sizer, Reference Manual*. Miami, FL 33196, 1995.

[35] R. B. Cornell, "Regulation of CTP: phosphocholine cytidylyltransferase by lipids. 2 Surface curvature, acyl chain length, and lipid-phase dependence for activation," in *Biochemistry*, vol. 30, 1991, pp. 5881-5888.

[36] T. Kaasgaard, Mouritse, O.G., and Jorgensen, K., "Freeze/thaw effects on lipid-bilayer vesicles investigated by differential scanning calorimetry," in *Biochimica et Biophysica Acta*, vol. 1615, 2003, pp. 77-83.

[37] R. M. Epand, "Lipid polymorphism and protein-lipid interactions," in *Biochimica et Biophysica Acta*, vol. 1376, 1998, pp. 353-368.

[38] J. M. Seddon, "Structure of the inverted hexagonal (H_{II}) phase, and non-lamellar phase transitions of lipids," in *Biochimica et Biophysica Acta*, vol. 1031, 1990, pp. 1-69.

[39] J. M. Seddon, and Templer, R.H., "Polymorphism of lipid-water systems," in *Structure an dynamics of membranes*, vol. 1A, *Handbook of biological physics*, R. Lipowsky, and Sackmann, E., Ed. Amsterdam, The Netherlands: ELSEVIER SCIENCE B.V., 1995, pp. 97-160.

[40] E. Sackmann, "Physical basis of self-organisation and function of membranes: physics of vesicles," in *Structure and dynamics of membranes*, vol. 1A, *Handbook of biological physics*, R. Lipowsky, and Sackmann, E., Ed. Amsterdam, The Netherlands: ELSEVIER SCIENCE B.V., 1995, pp. 213-304.

[41] S. Jackowski, "Coordination of membrane phospholipid synthesis with the cell cycle," in *Journal of Biological Chemistry*, vol. 269, 1994, pp. 3858-3867.

[42] D. Andelman, "Electrostatic properties of membranes: the Poisson-Boltzmann theory," in *Structure and dynamics of membranes*, vol. 1B, *Handbook of biological physics*, R. Lipowsky, and Sackmann, E., Ed. Amsterdam, The Netherland: ELSEVIER SCIENCE B.V., 1995, pp. 603-642.

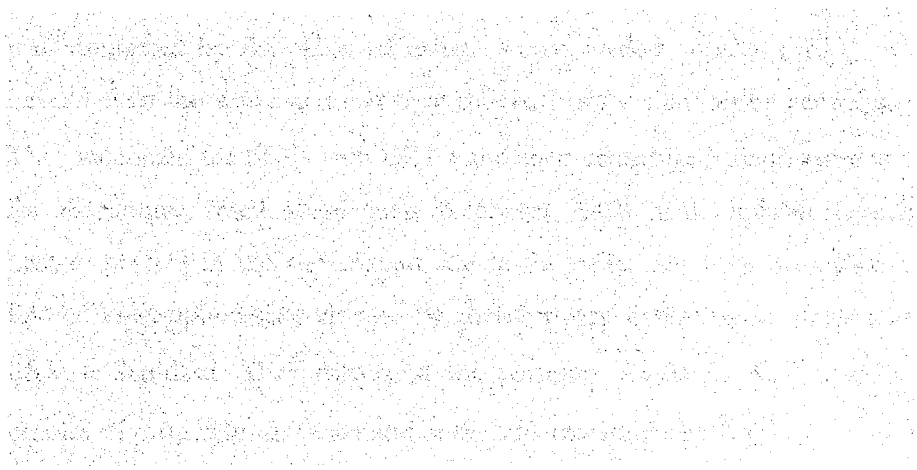

11 CCTα partitioning and activation

11.1 CCTα partition

According to the hypothesis proposed by Attard, the way in which the partition coefficient of CCTα (i.e. the ratio of the amount of enzyme in solution to the amount bound to the membrane) varies as a function of vesicle lipid composition should reflect the stored elastic energy of the membrane. Although a number of methods have been reported for the determination of partition coefficients in vesicle systems, these tend to have questionable error.

Cornell and Vance were the first that attempted a determination of the affinity of CCT for vesicles having different lipid composition [1]. The approach they used was based on the separation of lipid bound enzyme from the unbound using either sucrose density gradient or gel-filtration chromatography. The affinity of the enzyme for the vesicles was estimated assaying the percentage of total initial activity recovered with the lipid fractions (by either density gradient or chromatography). Although they were not able to determine any partition constant, they noticed that the membrane binding does not result necessary in the enzyme activation.

The determination of the partition constant of CCTα onto different lipid mixtures was attempted by Arnold *et al.* using sucrose loaded vesicles (SLVs), which are heavier than the water and can be removed from a solution by centrifugation [2]. They incubated the SLVs with CCTα and then centrifuged the mixture at 10000xg for 30 minutes, which aloud them to recover ~90% of the lipid in the pellet. The protein present in the supernatant and in the pellet was then quantified by SDS-PAGE electrophoresis followed by densitometry of Comassie-stained gel using BSA as standard. They calculated the partition constant (K_x) introducing the nmoles of protein in the pellet and in the supernatant in the Eq. 11.1

$$\text{Eq. 11.1 } K_x = \left(\frac{CCT_P}{CCT_S}\right)\left(\frac{W}{L}\right)$$

where CCT_P and CCT_S are the nmol of CCTα in the pellet and in the supernatant respectively, and W and L are the nmol of water and accessible lipid (half of the total concentration) respectively. Although the above method is based on protein quantification, there are several possible sources of error inherent with this method. The sucrose loading and the strong centrifuge force could have unpredictable effect on the vesicle properties and then on the enzyme partitioning. The quantification of the enzyme in the pellet and in the supernatant could be another source of error (they used radioactive lipids to estimate the amount of lipid recovered in the supernatant).

This Chapter describes a new approach, based on an analysis of enzyme activity data, to estimating partition coefficients for CCT. Although this method should be free of some of the limitations of the two methods previously reported, one possible limitation could be related to the absolute enzyme activity. However, the effect of the absolute enzyme activity on the method proposed herein and the results obtained using this method will be discussed in relation to the above two methods at the end of the chapter.

11.2 Partition constant and enzyme activity

The method is based on four assumptions:

1. In presence of vesicles, CCTα partitions between vesicles and water according to the simple equilibrium

$$\text{CCT}\alpha\text{(water)} \rightleftarrows \text{CCT}\alpha\text{(vesicles)}$$

2. The enzyme is present only as soluble CCTα (E_W) and vesicle-bound CCTα (E_L), so that at the equilibrium, the total concentration of the enzyme $[E_T]$ is given by

Eq. 11.2 $$[E_T]=[E_L]+[E_W]$$

where $[E_W]$ and $[E_L]$ are the concentration of CCTα in water and onto the lipid vesicles, respectively.

3. The equilibrium between the two CCTα forms is described by the equilibrium constant K_P [3, 4]

Eq. 11.3 $$K_P = \frac{[E_L]/([E_L]+[L])}{[E_W]/([E_W]+[W])}$$

where $[W]$ and $[L]$ are the concentrations of water and lipid respectively.

4. As discussed in the previous chapter (10.6.2), the rate of the enzymatic reaction v (represented by V in 10.6.2 and Eq. 10.9) is constituted by two terms: one for the vesicle-bound form and one for the unbound form:

Eq. 11.4 $$v = [E_W]\cdot V_W + [E_L]\cdot V_L$$

Where V_L and V_W are the specific activities of the enzyme measured when the whole enzyme is vesicle-bound or unbound. V_L and V_W are given by

Eq. 11.5 $$V_W = \left(\frac{v}{[E_W]}\right)_{[E_W]\to[E_T]}$$

Eq. 11.6 $$V_L = \left(\frac{v}{[E_L]}\right)_{[E_L]\to[E_T]}$$

If $[E_L]\ll[L]$ and $[E_W]\ll[W]$, Eq. 11.3 can be re-written in the simplified form

Eq. 11.7 $$K_P = \frac{[E_L]\cdot[W]}{[E_W]\cdot[L]}$$

Since the water concentration can be considered constant, the equilibrium constant K_P can be converted into partition constant K, defined as

Eq. 11.8 $$K = \frac{K_P}{[W]}$$

The combination of Eq. 11.9 with Eq. 11.7 yields

Eq. 11.9 $$K = \frac{[E_L]}{[E_W]\cdot[L]}$$

Eq. 11.9, solved for $[E_W]$, is then combined with Eq. 11.2, resulting in Eq. 11.10

Eq. 11.10 $$[E_T] = [E_L] + \frac{[E_L]}{K\cdot[L]} = [E_L]\cdot\left(1 + \frac{1}{K\cdot[L]}\right)$$

Recasting Eq. 11.10, the concentration of the enzyme adsorbed onto the vesicles is then given by Eq. 11.11

Eq. 11.11 $$[E_L] = [E_T]\cdot\left(1 + \frac{1}{K\cdot[L]}\right)^{-1}$$

Eq. 11.4 is then combined with Eq. 11.2, solved for $[E_W]$, to give

Eq. 11.12 $$v = [E_T]\cdot V_W + [E_L]\cdot(V_L - V_W)$$

The substitution of Eq. 11.11 into Eq. 11.12 gives

Eq. 11.13 $$v = [E_T]\cdot V_W + [E_T]\cdot\left(1 + \frac{1}{K\cdot[L]}\right)^{-1}\cdot(V_L - V_W)$$

which can be recast giving

Eq. 11.14 $$v - v_0 = [E_T]\cdot\left(1 + \frac{1}{K\cdot[L]}\right)^{-1}\cdot(V_L - V_W)$$

where $v_0 = [E_T]\cdot V_W$ is the enzymatic reaction rate measured in absence of vesicles. As V_W and V_L are considered to be independent from both the enzyme and vesicle concentrations, the specific activation of the enzyme ΔV, is given by

Eq. 11.15 $$\Delta V = (V_L - V_W)$$

Eq. 11.14 is then re-written as

$$\text{Eq. 11.16} \quad \Delta v = [E_T] \cdot \left(1 + \frac{1}{K \cdot [L]}\right)^{-1} \cdot \Delta V$$

where $\Delta v = v - v_0$. Recasting the reciprocal of Eq. 11.16 yields

$$\text{Eq. 11.17} \quad \frac{[E_T]}{\Delta v} = \left(\frac{1}{\Delta V}\right) + \left(\frac{1}{K \cdot \Delta V}\right) \cdot \left(\frac{1}{[L]}\right)$$

The double-reciprocal plot of $[E_T]/\Delta v$ versus $1/[L]$ is then a straight line (Figure 11.1) having the general form

$$\text{Eq. 11.18} \quad y = ax + b$$

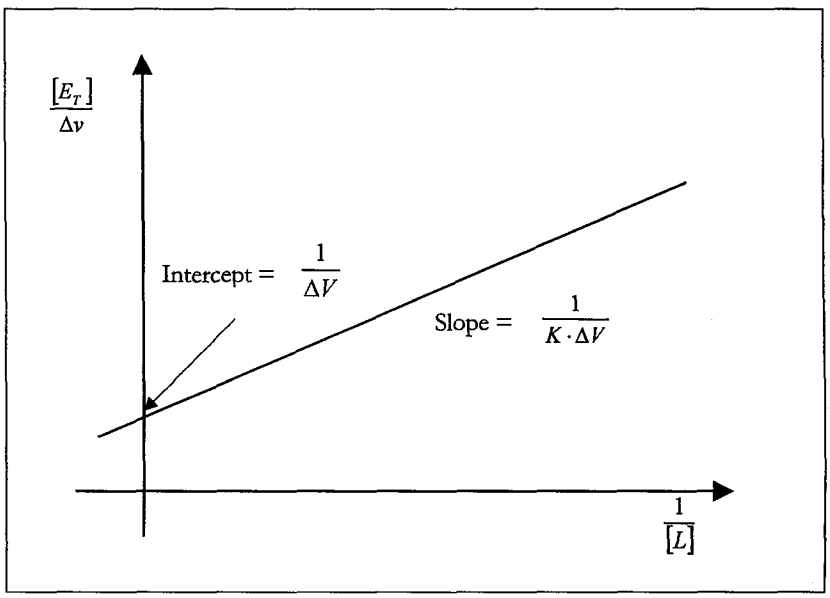

Figure 11.1 Double-reciprocal plot of Eq. 11.17.

where $y = [E_T]/\Delta v$, $x = 1/[L]$, the intercept is

$$\text{Eq. 11.19} \quad b = \frac{1}{\Delta V}$$

and the slope is

Eq. 11.20 $$a = \frac{1}{K \cdot \Delta V}$$

The specific activity of the enzyme in solution (V_W) can be obtained from the reaction rate in absence of vesicles (v_0) with an enzyme concentration $[E_T]$:

Eq. 11.21 $$V_W = \frac{v_0}{[E_T]}$$

The specific activity for the enzyme on the vesicles (V_L) is then obtained by combining Eq. 11.15 and Eq. 11.19

Eq. 11.22 $$V_L = \frac{1}{b} + V_W$$

Finally, the partition constant is then obtained dividing the intercept (Eq. 11.19) by the slope (Eq. 11.20)2

Eq. 11.23 $$K = \frac{b}{a}$$

The partition constant can be converted into the equilibrium constant using the relationship given in Eq. 11.8. The free energy (ΔG_P) for the partitioning can be calculated from K_P

Eq. 11.24 $$\Delta G_P = -RT \ln K_P$$

where $R = 8.314$ J·K·mol^{-1} and T is the absolute temperature.

The method of calculating partition coefficients for CCT by using Eq. 11.19 and Eq. 11.20, has been applied to a number of binary mixtures in an attempt to identify trends that correlate with the predictions of the qualitative model for CCT activity proposed by Attard.

11.3 Materials and methods

11.3.1 Materials (see 11.2.1)

11.3.2 CCTα assay and vesicle preparation

LUVs were prepared as described in 11.2.2 and constituted four different lipid mixtures: DOPC/DOPA (7:3), DOPC/DOPS (7:3), DOPC/OA (1:1) and DOPC/DOG (84:16). CCTα from the second batch was used for the experiments reported in this chapter. Conditions used for the CCTα assays were reported in 11.2.3 except for the vesicle concentrations, which are specified in the results section. In all the partition experiments, CCTα concentration was constant (10 μg/ml= ~$2.4 \cdot 10^{-7}$ M) and the lipid/enzyme mole ratio ranged between 42 (for 10 μM lipid samples) and 4200 (for 1.0 mM lipid samples). Enzymatic activity was determined by the TLC method (11.2.4).

11.3.3 Equilibrium and partition constants, specific enzymatic activity and standard deviation

Assay data, all in triplicate, were used to calculate the average and the standard deviation for the enzymatic activity as a function of the lipid concentration. These values were then used to obtain three data sets: ($[E]/\Delta v$, $1/[L]$), ($[E]/(\Delta v + SD)$, $1/[L]$) and ($[E]/(\Delta v - SD)$, $1/[L]$), where SD is the standard deviation relative to Δv. v and v_0 correspond to the mole of CDP-choline synthesised in one minute with or without vesicles respectively.

Linear regression analysis applied to the data set $([E]/(\Delta v), 1/[L])$ resulted in the regression estimates a and b of Eq. 11.18 that were used to calculate $\tilde{V}_L$, $\tilde{K}_P$, $\tilde{K}$ and $\Delta\tilde{G}$ (Eq. 11.19-Eq. 11.24). The same procedure applied to the data set $([E]/(\Delta v + SD), 1/[L])$ allowed the calculation of $V_L(+SD)$, $K_P(+SD)$, $K(+SD)$ and $\Delta G(+SD)$ (Eq. 11.19-Eq. 11.24). Finally, linear regression analysis of the data set $([E]/(\Delta v - SD), 1/[L])$ resulted in the regression estimates used to calculate $V_L(-SD)$, $K_P(-SD)$, $K(-SD)$ and $\Delta G(-SD)$ (Eq. 11.19-Eq. 11.24).

V_L, K_P, K, ΔG and the relative $S.D.$ were calculated using Eq. 11.25-Eq. 11.28:

Eq. 11.25 $$V_L = \widetilde{V}_L \pm \frac{|V_L(+SD) - V_L(-SD)|}{2}$$

Eq. 11.26 $$K_P = \widetilde{K}_P \pm \frac{|K_P(+SD) - K_P(-SD)|}{2}$$

Eq. 11.27 $$K = \widetilde{K} \pm \frac{|K(+SD) - K(-SD)|}{2}$$

Eq. 11.28 $$\Delta G = \Delta\widetilde{G} \pm \frac{|\Delta G(+SD) - \Delta G(-SD)|}{2}$$

11.4 Results

11.4.1 CCTα partitioning

Conditions used for the assays are reported in 11.3.2 and the data were treated as discussed in 11.1. The coefficients of Eq. 11.18 were obtained by regression analysis. Enzyme specific activity and partitioning, measured at different lipid concentrations, are reported and plotted in the following tabulations and figures: DOPC/DOG (84:16) (Table 11.1, Table 11.2, Table A-15, Figure 11.2 and Figure 11.3), DOPC/DOPA (7:3) (Table 11.3, Table 11.4, Table A-16, Figure 11.4 and Figure 11.5), DOPC/DOPS (7:3) (Table 11.5, Table 11.6, Table A-17, Figure 11.6 and Figure 11.7), and DOPC/OA (1:1) (Table 11.7, Table 11.8, Table A-18, Figure 11.8 and Figure 11.9).

The specific activities, the partition constants, the equilibrium partition constants and the partition free energies relative to the four lipid mixtures, calculated as described in 11.3.3, are reported and plotted in Table 11.9, Table 11.10 and Figure 11.10.

Table 11.1 CCTα partitioning into DOPC/DOG (84:16) LUVs. The least squares method was used for the linear regression.

[L]	Activity ($nmol \cdot min^{-1}mg^{-1}$)	Std. Dev. ($nmol \cdot min^{-1}mg^{-1}$)	1/[L]	$[E_T]/\Delta v$	Regression estimates
1.00	350	63	1.00E+03	3.71E+03	
0.50	272	11	2.00E+03	5.22E+03	
0.25	272	38	4.00E+03	5.20E+03	a = 0.282
0.10	230	17	1.00E+04	6.66E+03	b = 4863
0.05	151	22	2.00E+04	1.41E+04	R^2 = 0.971
0.025	139	40	4.00E+04	1.69E+04	
0.010	111	13	1.00E+05	3.22E+04	
0.0	80	4	-	-	

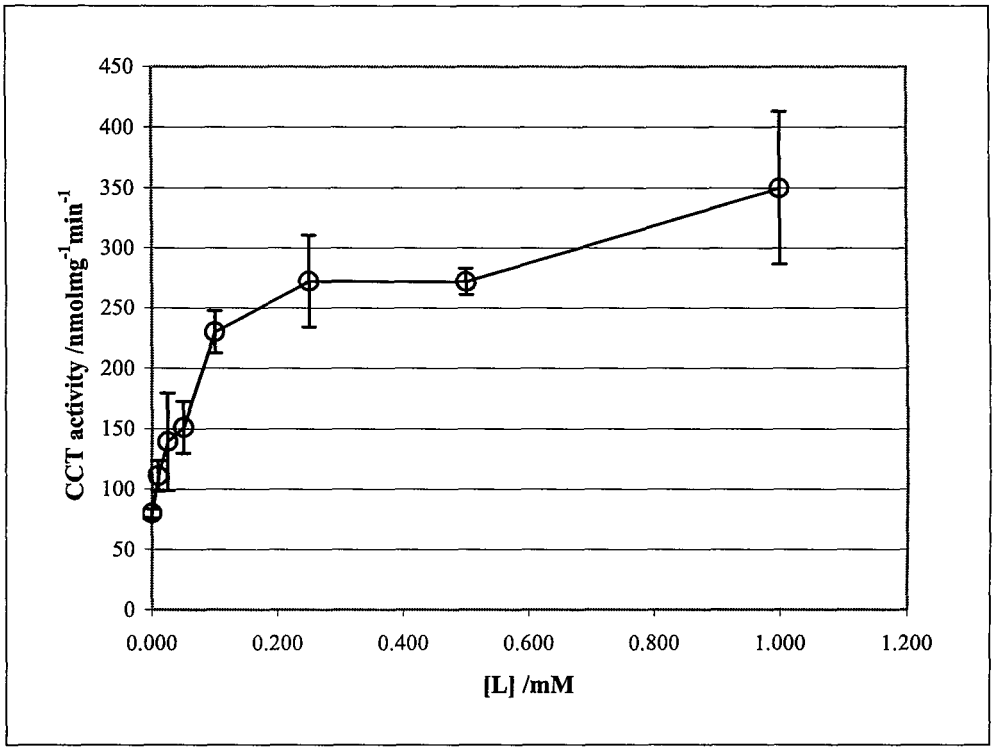

Figure 11.2 CCTα, activity measured for different concentrations of DOPC/DOG (84:16). [CCTα] = 10 μg/ml= ~$2.4 \cdot 10^{-7}$ M. The error bars represent ± the standard deviation.

Table 11.2 Data for the evaluation of the standard deviation for the results of CCTα partitioning into DOPC/DOG (84:16) LUVs. Lipid concentration ([L]) is expressed in mM. The least squares method was used for the linear regression.

[L]	1/[L]	$[E_T]/\Delta\nu$+SD	$[E_T]/\Delta\nu$-SD	Regression estimates
1.00	1.00E+03	3.00E+03	4.84E+03	**+SD data set**
0.50	2.00E+03	4.92E+03	5.55E+03	a = 0.185
0.25	4.00E+03	4.33E+03	6.50E+03	b = 4141
0.10	1.00E+04	5.95E+03	7.56E+03	R^2 = 0.952
0.05	2.00E+04	1.08E+04	2.04E+04	**-SD data set**
0.025	4.00E+04	1.00E+04	5.28E+04	a = 0.566
0.010	1.00E+05	2.26E+04	5.57E+04	b = 7574
0.0	-	-	-	R^2 = 0.791

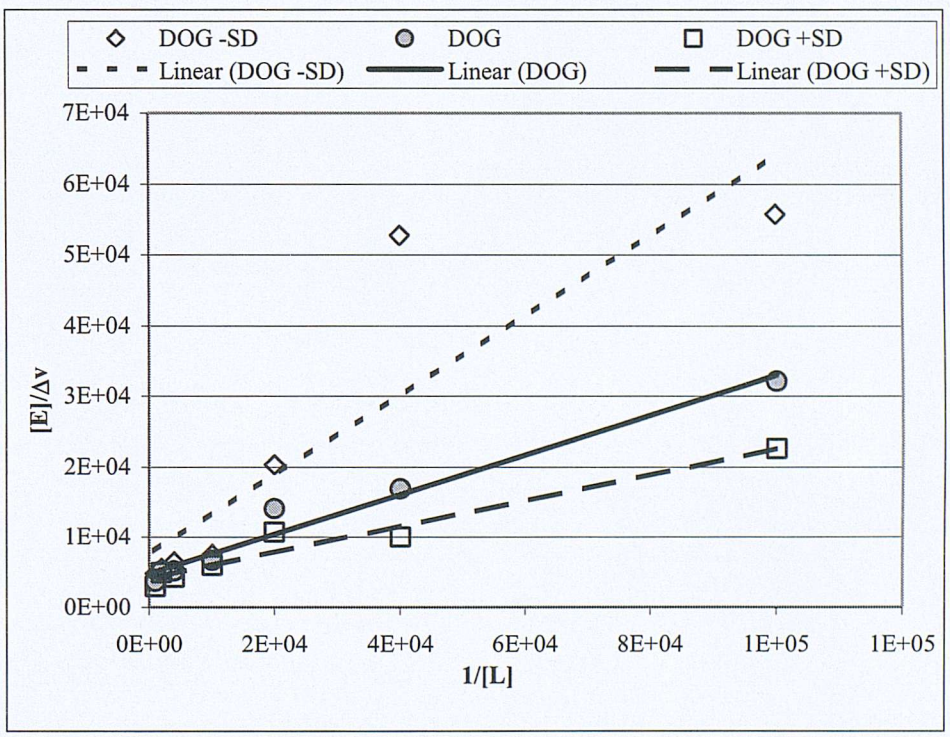

Figure 11.3 Double-reciprocal plots of CCTα partitioning into DOPC/DOG (84:16) LUVs and of the curve for the calculation of the standard deviation. [CCTα] = 10 μg/ml= ~$2.4 \cdot 10^{-7}$ M. Data are reported in Table 11.1 and Table 11.2.

Table 11.3 CCTα partitioning into DOPC/DOPA (7:3) LUVs. The least squares method was used for the linear regression.

[L]	Activity (nmol·min^{-1}mg^{-1})	Std. Dev. (nmol·min^{-1}mg^{-1})	1/[L]	$[E_T]/\Delta v$	Regression estimates
1.000	1206	52	1.00E+03	9.02E+02	
0.500	1060	123	2.00E+03	1.04E+03	
0.250	928	40	4.00E+03	1.20E+03	a = 0.103
0.100	716	77	1.00E+04	1.62E+03	b = 773
0.050	437	54	2.00E+04	2.94E+03	R^2 = 0.996
0.025	301	28	4.00E+04	4.90E+03	
0.00	97	13	-	-	

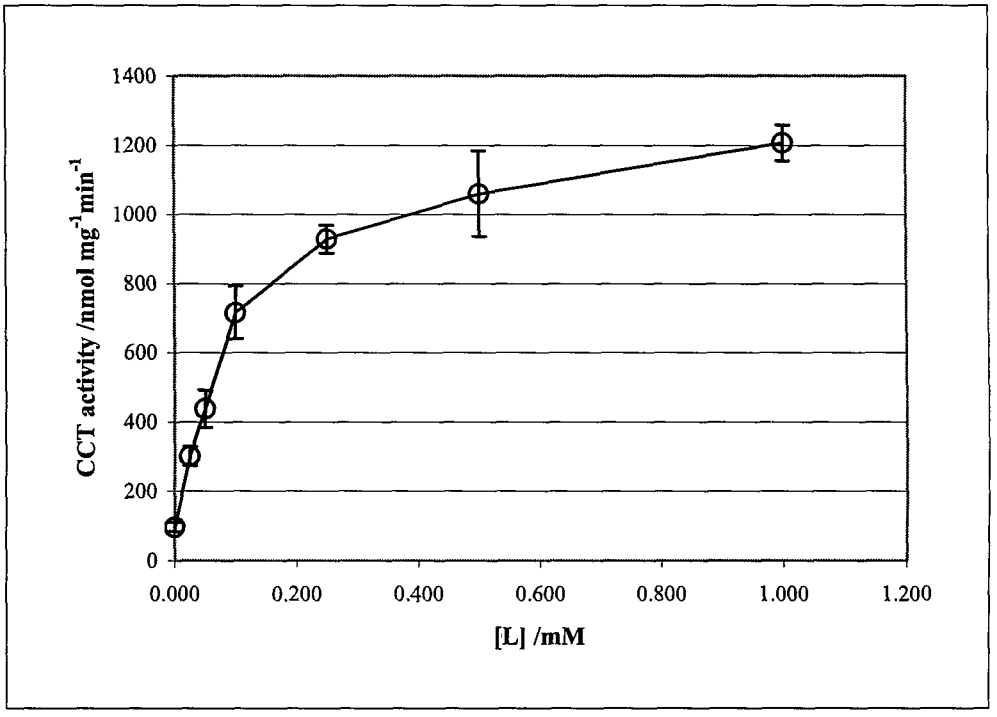

Figure 11.4 CCTα activity measured for different concentrations of DOPC/DOPA (7:3). [CCTα] = 10 μg/ml= ~2.4·10^{-7} M. The error bars represent ± the standard deviation.

Table 11.4 Data for the evaluation of the standard deviation for the results of CCTα partitioning into DOPC/DOPA (7:3) LUVs. Lipid concentration ([L]) is expressed in mM. The least squares method was used for the linear regression.

[L]	1/[L]	$[E_T]/\Delta\nu$+SD	$[E_T]/\Delta\nu$-SD	Regression estimates
1.000	1.00E+03	8.60E+02	9.47E+02	**+SD data set**
0.500	2.00E+03	9.20E+02	1.19E+03	a = 0.0878 b = 730 R^2 = 0.996
0.250	4.00E+03	1.14E+03	1.27E+03	
0.100	1.00E+04	1.43E+03	1.85E+03	**-SD data set**
0.050	2.00E+04	2.53E+03	3.51E+03	a = 0.124 b = 821 R^2 = 0.994
0.025	4.00E+04	4.26E+03	5.77E+03	
0.0	-	-	-	

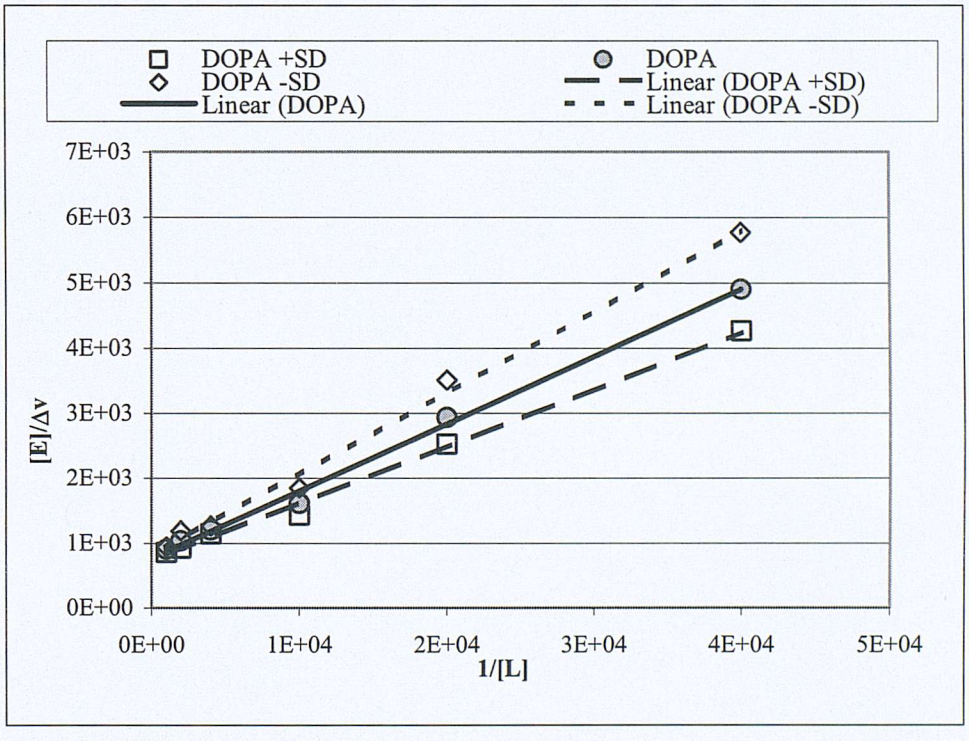

Figure 11.5 Double-reciprocal plot of the CCTα partitioning into DOPC/DOPA (7:3) LUVs and of the curve for the calculation of the standard deviation. [CCTα] = 10 μg/ml= ~$2.4 \cdot 10^{-7}$ M. Data are reported in Table 11.3 and Table 11.4.

Table 11.5 CCTα partitioning into DOPC/DOPS (7:3) LUVs. The least squares method was used for the linear regression.

[L] (mM)	Activity (nmol·min^{-1}mg^{-1})	Std. Dev. (nmol·min^{-1}mg^{-1})	1/[L]	$[E_T]/\Delta v$	Regression estimates
1.000	450	102	1.00E+03	2.70E+03	
0.500	394	87	2.00E+03	3.18E+03	
0.250	305	61	4.00E+03	4.44E+03	a = 0.400
0.100	206	30	1.00E+04	7.96E+03	b = 2900
0.050	166	22	2.00E+04	1.16E+04	R^2 = 0.986
0.025	134	13	4.00E+04	1.84E+04	
0.0	80	4	-	-	

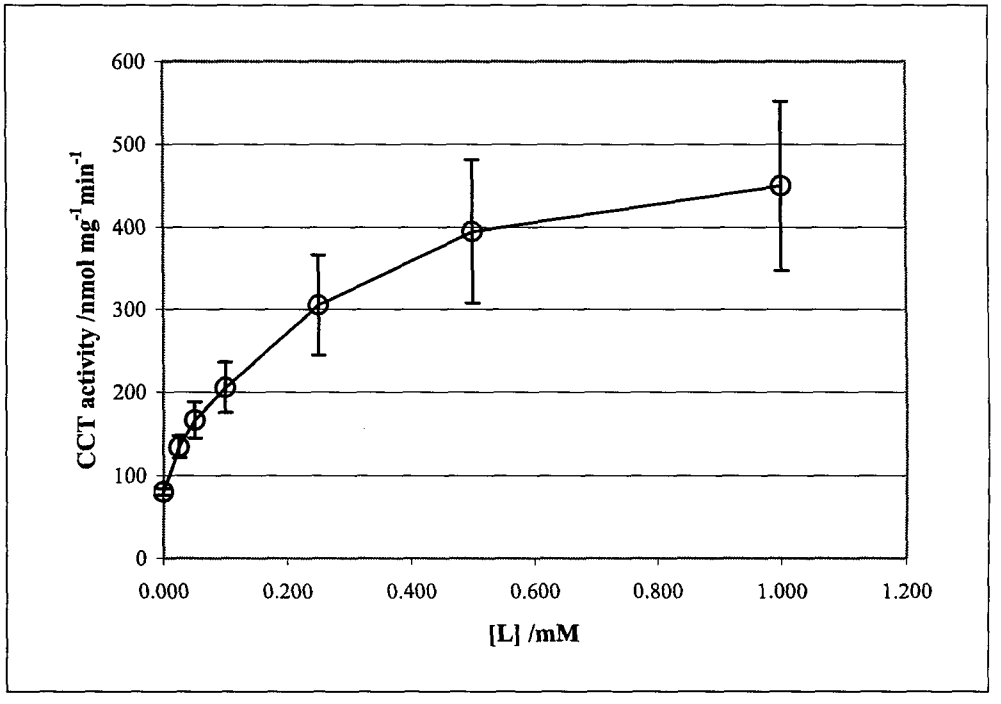

Figure 11.6 CCTα activity measured for different concentrations of DOPC/DOPS (7:3). [CCTα] = 10 μg/ml= ~2.4·10^{-7} M. The error bars represent ± the standard deviation.

Table 11.6 Data for the evaluation of the standard deviation for the results of CCTα partitioning into DOPC/DOPS (7:3) LUVs. Lipid concentration ([L]) is expressed in mM. The least squares method was used for the linear regression.

[L]	1/[L]	$[E_T]/\Delta\nu$+SD	$[E_T]/\Delta\nu$-SD	Regression estimates
1.000	1.00E+03	2.12E+03	3.74E+03	**+SD data set**
0.500	2.00E+03	2.49E+03	4.40E+03	a = 0.321
0.250	4.00E+03	3.50E+03	6.09E+03	b = 2280
0.100	1.00E+04	6.40E+03	1.05E+04	R^2 = 0.986
0.050	2.00E+04	9.22E+03	1.56E+04	**-SD data set**
0.025	4.00E+04	1.47E+04	2.45E+04	a = 0.532
0.0	-	-	-	b = 3985
				R^2 = 0.988

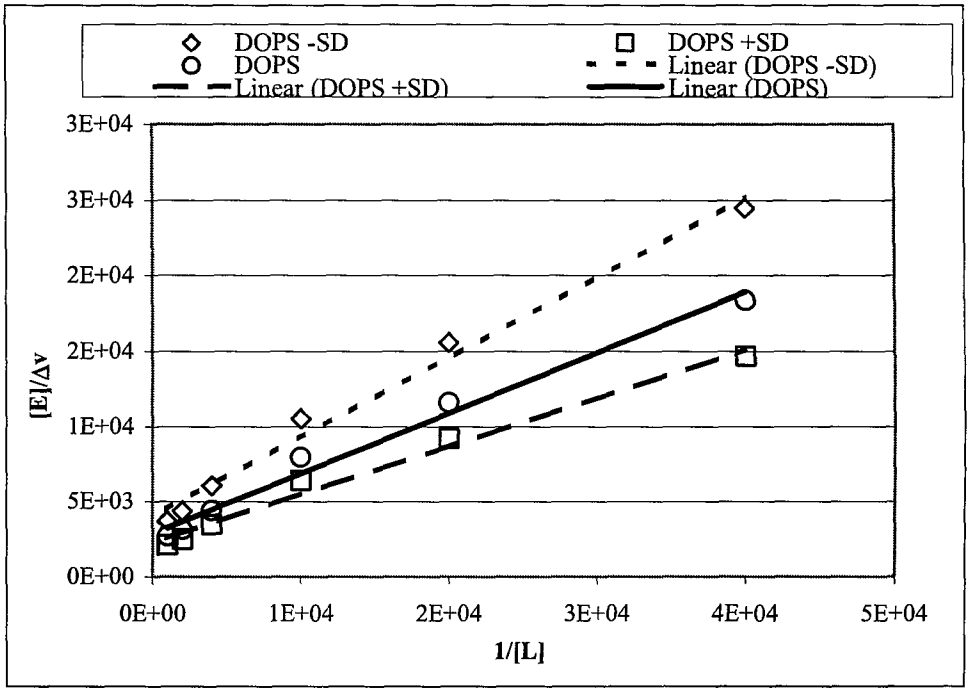

Figure 11.7 Double-reciprocal plots of CCTα partitioning into DOPC/DOPS (7:3) LUVs and of the curve for the calculation of the standard deviation. [CCTα] = 10 μg/ml= ~$2.4 \cdot 10^{-7}$ M. Data are reported in Table 11.5 and Table 11.6.

Table 11.7 CCTα partitioning into DOPC/OA (7:3) LUVs. Lipid concentration ([L]) is expressed in mM; activity and standard deviation are expressed in nmol·min^{-1}mg^{-1}. The least squares method was used for the linear regression.

[L]	Activity (nmol·min^{-1}mg^{-1})	Std. Dev. (nmol·min^{-1}mg^{-1})	1/[L]	$[E_T]/\Delta v$	Regression estimates
1.000	1295	102	1.00E+03	8.34E+02	
0.250	1277	100	4.00E+03	8.47E+02	
0.100	1155	74	1.00E+04	9.45E+02	a = 0.0146
0.050	1076	153	2.00E+04	1.02E+03	b = 791
0.025	809	176	4.00E+04	1.41E+03	R^2 = 0.975
0.0	97	13	-	-	

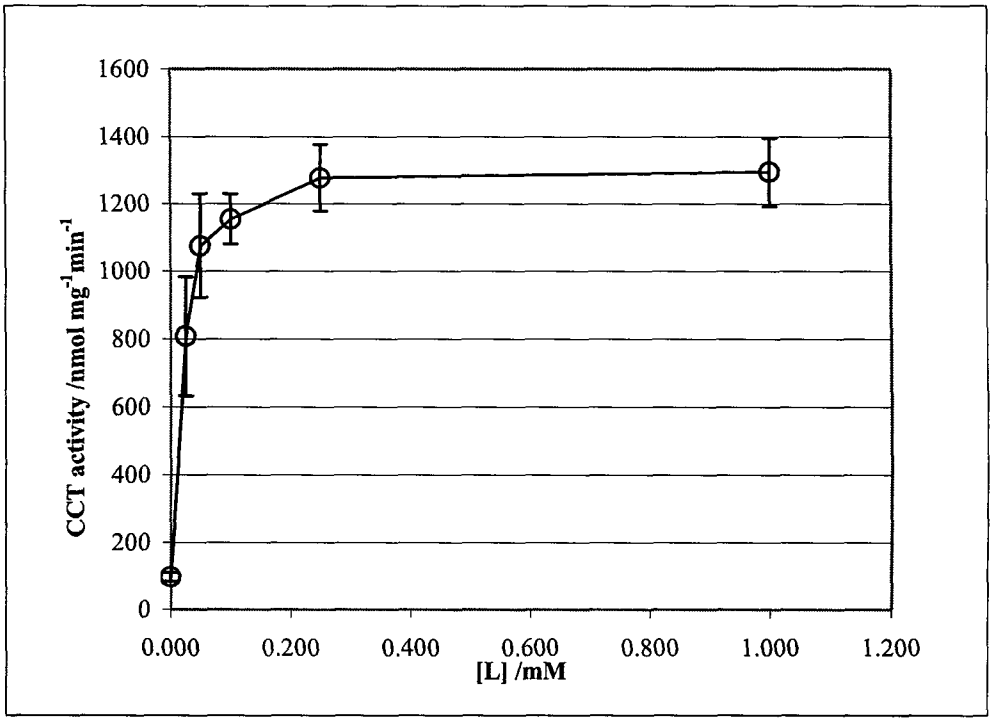

Figure 11.8 CCTα activity measured for different concentrations of DOPC/OA (1:1). [CCTα] = 10 μg/ml= ~2.4·10^{-7} M. The error bars represent ± the standard deviation.

Table 11.8 Data for the evaluation of the standard deviation for the results of CCTα partitioning into DOPC/OA (1:1) LUVs. Lipid concentration ([L]) is expressed in mM. The least squares method was used for the linear regression.

[L]	1/[L]	$[E_T]/\Delta v$+SD	$[E_T]/\Delta v$-SD	Regression estimates
1.000	1.00E+03	7.69E+02	9.13E+02	**+SD data points**
0.250	4.00E+03	7.81E+02	9.26E+02	a = 8.86E-03 b = 755 R^2 = 0.948
0.100	1.00E+04	8.82E+02	1.02E+03	
0.050	2.00E+04	8.83E+02	1.21E+03	**-SD data points**
0.025	4.00E+04	1.13E+03	1.87E+03	a = 0.025 b = 813 R^2 = 0.967
0.0	-	-	-	

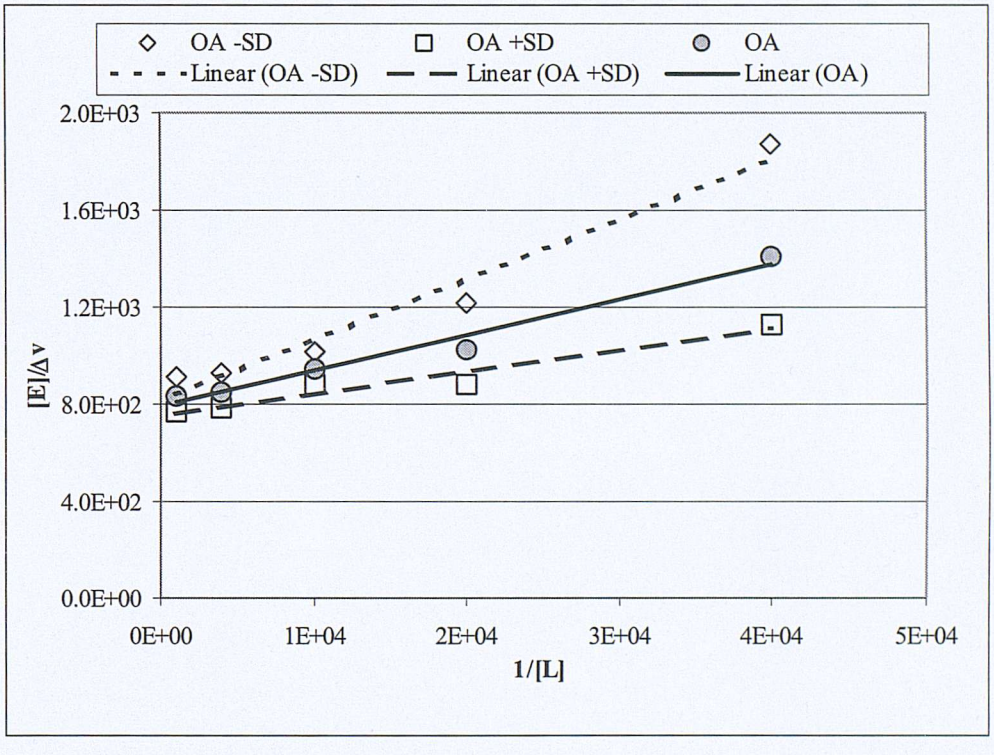

Figure 11.9 Double-reciprocal plots of CCTα partitioning into DOPC/OA (1:1) LUVs and of the curve for the calculation of the standard deviation. [CCTα] = 10 μg/ml= ~$2.4 \cdot 10^{-7}$ M. Data are reported in Table 11.7 and Table 11.8.

Table 11.9 All the constants were calculated using the equations reported in 11.1 and 11.3.3. The specific enzymatic activation and the partition constant for the four lipid mixtures are plotted in Figure 11.10.

Lipid mixture	V_M ($mol \cdot min^{-1} g^{-1}$)	K ($mol^{-1}l$)	K_P	ΔG_P ($J \cdot mol^{-1}$)
DOPC/DOG (84:16)	2.86E-04	1.73E+04	9.6E+05	-3.55E+04
DOPC/DOPA (1:1)	1.39E-03	7.49E+03	4.16E+05	-3.33E+04
DOPC/DOPS (1:1)	4.25E-04	7.24E+03	4.02E+05	-3.33E+04
DOPC/OA (1:1)	1.36E-03	5.4E+04	3.0E+06	-3.84E+04

Table 11.10 Standard deviation for the constants reported in Table 11.9.

Lipid mixture	S.D.(V_M) ($mol \cdot min^{-1} g^{-1}$)	S.D.(K) ($mol^{-1}l$)	S.D.(K_P)	S.D.(ΔG_P) ($J \cdot mol^{-1}$)
DOPC/DOG (84:16)	3.9E-05	3.2E+03	1.8E+05	4.7E+02
DOPC/DOPA (1:1)	5.4E-05	6.1E+02	3.4E+04	2.1E+02
DOPC/DOPS (1:1)	6.6E-05	1.4E+02	7.8E+03	4.9E+01
DOPC/OA (1:1)	3.47E-05	1.9E+04	1.0E+06	8.8E+02

11.5 Conclusions

11.5.1 CCTα partition/activation

As for the previous chapter, the enzyme activity has shown variability within the same preparation. However, the previous chapter showed that the relative activity is independent of the fraction of enzyme that is active. The same is only partially true for the partitioning experiments reported in this chapter. In fact, as shown in the previous chapter (10.6.2, Eq. 10.26) the fraction of active enzyme ($[E_T]_{\chi,\varphi}$) can be represented by Eq. 11.29

Eq. 11.29 $[E_T]_{\chi,\varphi} = \chi\varphi[E_T]$

where χ and φ refer to the mole fraction of enzyme that has retained its activity (see previous chapter for a discussion of χ and φ). Because V_W and V_L are independent of χ and φ (10.6.2), $[E_T]_{\chi,\varphi}$ can be substituted into Eq. 11.17, which gives

$$\text{Eq. 11.30} \quad \frac{[E_T]_{\chi,\varphi}}{\Delta\nu} = \left(\frac{1}{\Delta V}\right) + \left(\frac{1}{K \cdot \Delta V}\right) \cdot \left(\frac{1}{[L]}\right)$$

Eq. 11.30 can be recast and expressed in terms of χ and φ

$$\text{Eq. 11.31} \quad \frac{[E_T]}{\Delta\nu} = \left(\frac{1}{\chi\varphi \cdot \Delta V}\right) + \left(\frac{1}{K \cdot \chi\varphi \cdot \Delta V}\right) \cdot \left(\frac{1}{[L]}\right)$$

From Eq. 11.31 it follows that, while the partition constant is independent of the enzyme activity (Eq. 11.23), the enzyme activity in solution and on the lipid depends on the fraction of active enzyme. In particular, the measured enzyme activities are only apparent V'_W and V'_L that are linked to the real value (measured when all the enzyme molecules are active) by Eq. 11.32 and Eq. 11.33

$$\text{Eq. 11.32} \quad V'_W = \chi\varphi \cdot V_W$$

$$\text{Eq. 11.33} \quad V'_L = \chi\varphi \cdot V_L$$

From Eq. 11.32 and Eq. 11.33 follows that it is possible to estimate the real enzyme activity from the partition experiments only if the active fraction of enzyme is known. A reference lipid system together with a calculation of the relative activity would help to correlate the activity of enzymes from different preparations[a]. However, this approach was not used in this study.

11.5.2 CCTα partitioning

As discussed in the previous chapters, the release of the membrane bending energy is the driving force behind the enzyme activation through partitioning onto the

[a] The relative activity would help to determine if the different activities of two different experiments with different lipid mixtures are due to the nature of the lipids or to the effect of the enzyme variability.

membrane surface. Hence, the differences in the activity could be due to differences in the partition: the higher the partition, the higher is the activity. A model was developed herein for the determination of the partition coefficient and the specific enzymatic activity, which is supposed to be constant and independent of vesicle concentration. Partition constants and specific activities for CCTα have been measured in presence of four different lipid mixtures and are plotted in Figure 11.10, which shows that CCTα partitioning and activation could be independently regulated by the biophysical properties of the vesicle. As demonstrated in the previous section, while the absolute activity cannot be estimated, the partition constant should be independent of the enzyme activity and should be consistent with other values reported in the literature. Arnold *et al.* have estimated values for the partition constant of CCTα using different lipid mixtures [2]. Although they used egg-PC as the major lipid in the mixtures (DOPC has been used herein), some of those results can still be used for a comparison.

Table 11.11 Partition constant for CCTα calculated using the method described herein (K_P) and calculated by Arnold *et al.* ($1/2 \cdot K_X$) [2]. The partition constant determined by Arnold has been divided by two because they the used [L]/2 instead of [L] for the determination of K_X and K_P respectively (Eq. 11.1 and Eq. 11.7).

Determination by activity measurement		Determination by centrifugation	
Lipid mixture	K_P (x10^{-5})	Lipid mixture	$1/2 \cdot K_X$ (x10^{-5})
DOPC/DOPA (7:3)	4.16 ±0.3	Egg-PC/POPA (75:25)	5.5 ± 0.7
DOPC/DOPS (7:3)	4.0 ± 0.1	Egg-PC/DOPS (6:4)	1.1 ± 0.2

The comparison of the partition constants, reported in Table 11.11, shows that there is a good agreement between the results obtained using the two different methods. However, Arnold *et al.* used egg-PC and 1-palmitoyl-2-oleyl-phosphatidic acid, which differ in acyl chain composition from DOPC, different temperature (20 °C), different buffer composition and a different method of protein preparation and

these factors may contribute to the observed differences. However, the constants estimated using the two methods have the same order of magnitude, leading to the conclusion that the method reported herein could be adopted for the determination of the partition constant. Despite the general agreement between the partition constants, further experiments need to be done to verify that the partition constant is independent of the enzyme absolute activity and that the measured activity is the only parameter affected by the decreased enzyme activity. Although it is not possible so far to give a detailed description of the mechanism involved in the modulation of the enzyme activity, the analysis of Figure 11.10 leads to some observations:

1. The partition constant for the DOPC/DOG mixture is higher than the correspondent constant estimated for DOPC/DOPA and DOPC/DOPS. Due to its small head-group, DOG is expected to be a strong type II lipid; hence, the high bending energy stored in the vesicles could be responsible for the high partition constant.

2. The DOPC/DOPA mixture, which is the most effective for the enzyme activation, shows a very low partition constant. In this case, it is possible that the high specific activity is due to the synergism between the electrostatic and the hydrophobic interactions with the membrane interface. As the head-group of DOPA is bigger than that of DOG, it is expected that the membrane has a lower stored bending energy and consequently that the enzyme partition constant is low.

3. The ratio between the specific activation constants (V_L) for DOPC/DOPA and DOPC/DOPS could be related to the ratio between the charges C of those lipids (C ≈ -2 for DOPA and ≈ -1 for DOPS),

$$\frac{V_L(DOPC/DOPA)}{V_L(DOPC/DOPS)} \approx 3.3 \quad \text{and} \quad \frac{C(DOPA)}{C(DOPS)} \approx 2$$

4. The mixture DOPC/OA is the most effective on both partitioning and activation. The partitioning, in particular, is an order of magnitude higher than for all the other mixtures. Oleic acid mixed with phosphatidylcholine

behaves as strong type II lipids; hence, as for DOPC/DOPA, high bending energy and surface charge could act synergistically and increase the partition constant and the specific activity.

Although the results reported in this chapter support the model described herein, further experiments are needed to confirm or disprove the above results.

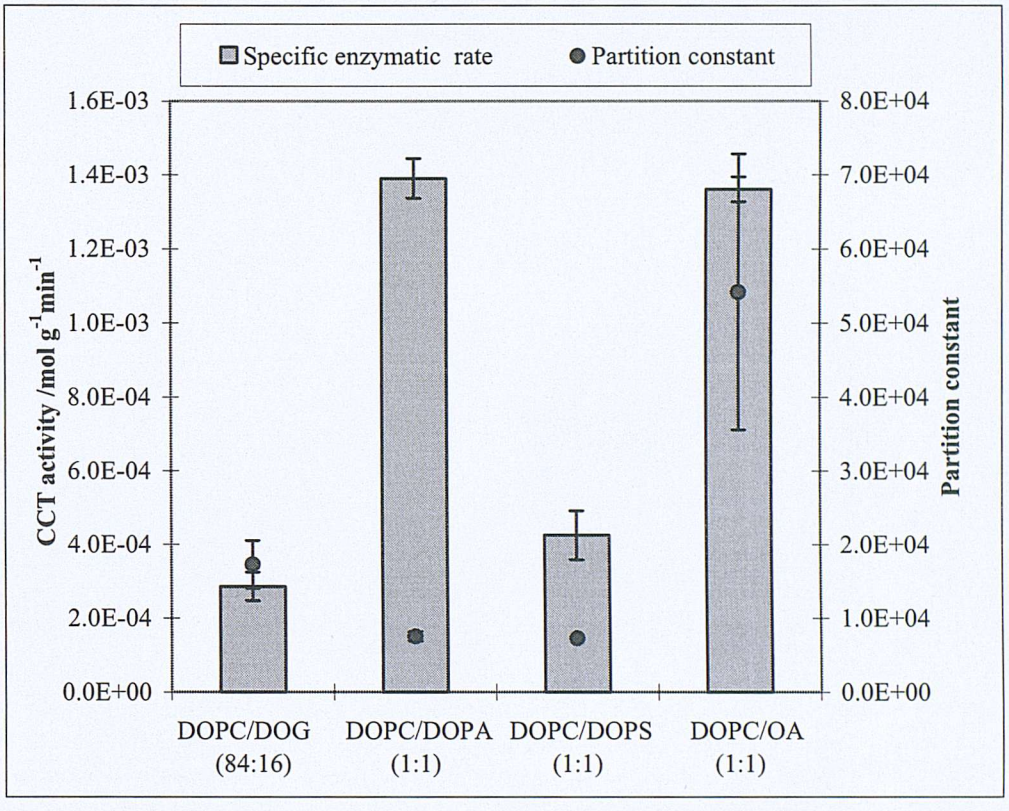

Figure 11.10 Plot of the specific enzymatic activities and the partition constants reported in Table 11.9. The error bars correspond to ± the standard deviations reported in Table 11.10.

11.5.3 Hypothesis of enzyme activity modulation

Although the mechanism of CCTα activation is still unknown, a hypothetical mechanism has been reported in the literature to differentiate charge and hydrophobic effect on the enzyme activation [5, 6]. In the proposed mechanism, the enzyme inhibition is caused by the formation of an intramolecular complex

between the C-terminal domain and the M-domain, which should triggers the enzyme activation through the interaction of the hydrophobic strip with the membrane. According their model, the partition of the enzyme onto the membrane surface begins with an electrostatic interaction through a positively charged segment of the enzyme (5 lysine residues in the short segment 248-254) and the negative charge of the membrane. Hence, while the electrostatic interaction (dependent on the lipid charge) aloud the enzyme to sit inactive on the membrane surface, the hydrophobic interaction (dependent on the torque tension and the stored elastic energy of the membrane) through the M-domain results in the enzyme activation [5, 6]. However, that hypothesis is not consistent with the results reported by Lykidis *et al.* [7]. Lykidis *et al.* have shown that CCTα mutants lacking the M-domain or the C-terminal domain are active, although they are sensitive to different properties of the membrane. In particular, they have shown that mutants lacking the M-domain (CCTα[Δ257-309]) are active and sensitive to the lipid charge, whilst mutant lacking the C-terminal domain (CCTα[Δ312-367]) are active and sensitive to the stored elastic energy [7]. Because CCTα[Δ257-309] was shown to be active, it is reasonable to exclude that the enzyme activation is triggered by the hydrophobic interaction mediated by the M-domain.

Although further experiments are required to study the effect of charge and torque tension on the enzyme activation, a hypothetical mechanism of enzyme regulation is presented based on the preliminary results reported herein. The mechanism is based on the hypothesis that the lipid membrane is a required component for the folding of the enzyme into the active form. We hypothesize that the hydrophobic interaction (mediated by the M-domain) is the key factor leading the enzyme on the membrane, whilst the electrostatic interaction (mediated by 5 lysine residues in the short segment 248-254) is the key factor triggering the enzyme activation Figure 11.11. However, as the DOPC/DOPE and DOPC/DOG mixtures are able to activate the enzyme, it follows that the stored elastic energy can partially activate the enzyme (maybe because the hydrophobic strip and the 5-lysine segment are connected in the amino acid sequence of the enzyme) Only further experiments will

prove/disprove the results and the method reported herein, and will help to have a better understanding of the role played by the membrane biophysical properties on the enzyme activity modulation.

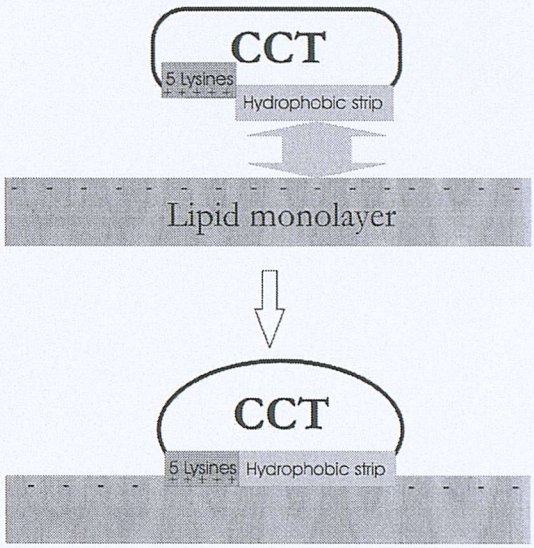

Figure 11.11 The hydrophobic interaction (light grey arrow), sensitive to the torque tension and the stored elastic energy, could the enzyme partition onto the vesicle surface. When the enzyme reaches the membrane surface, the membrane binding through the hydrophobic strip could aloud electrostatic interaction between the negatively charged lipids and the enzyme positively charged segment (5 lysine residues in the short segment 248-254, 3.1) to trigger the folding of CCTα into the active form.

11.6 References

[1] R. Cornell, and Vance, D.E., "Binding of CTP: phosphocholine cytidylyltransferase to large unilamellar vesicles," in *Biochimica et Biophysica Acta*, vol. 919, 1987, pp. 37-48.

[2] R. S. Arnold, DePaoli-Roach, A.A., and Cornell, R.B., "Binding of CTP: phosphocholine cytidylyltransferase to lipid vesicles: diacylglycerol and enzyme dephosphorylation increase the affinity for negatively charged membranes," in *Biochemistry*, vol. 36, 1997, pp. 6149-6156.

[3] S. H. White, Wimley, W.C., Ladokhin, A.S., and Hristova, K., "Protein folding in membrane: determining energetics of peptide-bilayer interactions," in *Methods in Enzymology*, vol. 295, 1998, pp. 62-87.

[4] H. S. Chan, and Dill, K.A., "Solvation: how to obtain microscopic energies from partitioning and solvation experiments," in *Annual Review of Biophysical and Biomolecular Structure*, vol. 26, 1997, pp. 425-259.

[5] R. Cornell, and Northwood, I. C., "Regulation of CTP: phosphocholine cytidylyltransferase by amphitropism and relocalization," in *TIBS*, vol. 25, 2000, pp. 441-447.

[6] J. A. Friesen, Campbell, H. A., and Kent, C., "Enzymatic and cellular characterization of a catalytic fragment of CTP: phosphocholine cytidylyltransferase α," in *Journal of Biological Chemistry*, vol. 274, 1999, pp. 13384-13389.

[7] A. Lykidis, Jackson, P., and Jackowski, S., "Lipid activation of CTP: phosphocholine cytidylyltransferase α: characterization and identification of a second activation domain," in *Biochemistry*, vol. 40, 2001, pp. 494-503.

12 Conclusions

Integral and peripheral membrane proteins operate in conjunction with membranes and are sensitive to their molecular composition or affected by their biophysical properties. Membrane proteins interact with the lipid bilayer in different ways: hydrophobic and/or electrostatic interaction, molecular recognition of specific lipids present in the membrane. Spectrin dimers[a] bind lipids containing the negatively charged phosphatidylserine by electrostatic interaction [1]. Some cytoskeletal proteins such as spectrin, dynamin or myosin X bind specifically phosphorylated phosphatidylinositol ($PtdIns(3,4)P_2$, $PtdIns(4,5)P_2$, $PtdIns(3,4,5)P_3$)[b] trhough a plecktrin-homology domain that recognise not only the charge but also the shape of those phospholipids [2]. The annexins are a family of proteins that bind negatively charged phospholipids and some specific proteins (annexin-binding proteins) in a Ca^{2+}-dependent manner [3-5]; moreover, some member of the annexin family (Annexin V and XII) can also for ion channels as function of the pH [6]. Apolipoprotein A-I, the major constituent of high density lipoprotein (HDL) is present as soluble and membrane bound form: the presence of lipid trigger a conformational change in the C-terminal region of the protein (from random coil to α-helix) and increase the enzyme affinity for the membrane [7]. The protein kinase C (PKC) family is activated by diacylglycerol and by phosphatidylserine and appears to be sensitive to the presence of DAG-enriched and DAG-poor domains [8]. Phospholipase A_2 and C hydrolysis of PtdCho is strongly enhanced by the presence of structural defects in the lipid bilayer [9-11]. The folding of Bacteriorhodopsin

---

[a] Spectrin dimmers are involved in the determination of the deformability and dynamic properties of erythrocyte membrane and cell shape.

[b] $PtdIns(3,4)P_2$: phosphatidylinositol-3,4-biphosphate; $PtdIns(4,5)P_2$: phosphatidylinositol-4,5-biphosphate; $PtdIns(3,4,5)P_3$: phosphatidylinositol-3,4,5-triphosphate.

seems to be sensitive to the membrane torque tension [12]: decrease of protein folding in correspondence of increase in the torque tension.

Because membrane enzymes are affected by imbalance in the membrane biophysical properties, it is necessary for the cell to monitor and to maintain the membrane properties in a functional physiological range. The membrane fluidity is dependent on the amount of cholesterol (in eukaryotes), saturated and unsaturated lipids and homeostatic control is exerted on their synthesis. CCTα could be involved in the control the elastic membrane properties: the torque tension. Despite the low reproducibility of the enzyme specific activity, the results reported in his thesis, in accordance with the data reported in the literature [13-15], support the key role played by the elastic membrane properties in the CCTα activity modulation. Moreover, the equations developed herein, which describe the enzyme activity modulation in terms of partitioning and activation, could be a useful tool to be used to achieve a better understanding of the modulation of CCTα activity by membrane biophysical properties.

12.1 References

[1]R. Maksymiw, Sui, S.-F., Gaub, H., and Sackmann, E., "Electrostatic coupling of spectrin dimers to phosphatidylserine containing lipid lamellae," in *Biochemistry*, vol. 26, 1987, pp. 2983-2990.

[2]V. Niggli, "Structural properties of lipid-binding sites in cytoskeletal proteins," in *Trends in Biochemical Sciences*, vol. 26, 2001, pp. 604-611.

[3]V. Gerke, and Moss, S.E., "Annexins: from structure to function," in *Physiological Reviews*, vol. 82, 2002, pp. 331-371.

[4]E. Babiychuk, and Draeger, A., "Annexins in cell membrane dynamics: Ca^{2+}-regulated association of lipid microdomains," in *Journal of Cell Biology*, vol. 150, 2000, pp. 1113-1123.

[5]H. Sohma, Creutz, C.E., Saitoh, M., Sano, H., Kuroki, Y., Voelker, D.R., and Akino, T., "Characterization of the Ca^{2+}-dependent binding of annexin IV to surfactant protein A," in *Biochemical Journal*, vol. 341, 1999, pp. 203-209.

[6]J. M. Isas, Cartailler, J.-P., Sokolov, Y., Patel, D.R., Langen, R., Luecke, H., Hall, J.E., and Haigler, H.T., "Annexins V and XII insert into bylayers at mildly pH and form ion channels," in *Biochemistry*, vol. 39, 2000, pp. 3015-3022.

[7]M. N. Oda, Forte, T.M., Ryan, R.O., and Voss, J.C., "The C-terminal domain of apolipoprotein A-I contains a lipid-sensitive conformational trigger," in *Nature Structural Biology*, vol. 10, 2003, pp. 455-460.

[8]A. K. Hinderliter, Dibble, A.R.G., Biltonen, R.L., and Sando, J.J., "Activation of protein kinase C by coexisting diacylglycerol-enriched and diacylglycerol-poor lipid domains," in *Biochemistry*, vol. 36, 1997, pp. 6141-6148.

[9]J. A. F. o. d. Kamp, Kauerz, M.T.H., and Deenen, L.L.M. van, "Action of pancreatic phospholipase A_2 on phosphatidylylcholine bilayers in different physical states," in *Biochimica et Biophysica Acta*, vol. 406, 1975, pp. 169-177.

[10]J. Rashba-Step, Tatoyan, A, Duncan, R., Ann, D., Pushpa-Rehka, T.R., and Sevanian, A., "Phospholipid peroxidation induces cytosolic phospholipase A_2

activity: membrane effects versus enzyme phosphorylation," in *Archives of Biochemistry and Biophysics*, vol. 343, 1997, pp. 44-54.

[11]Q. He, and Li, J., "Dynamic and morphological investigation of phospholipid monolayer hydrolysis by phospholipase C," in *Biochemical and Biophysical Research Communications*, vol. 300, 2003, pp. 541-545.

[12]A. R. Curran, Templer, R.H., and Booth, P.J., "Modulation of folding and assembly of the membrain protein Bacteriorhodopsin by intermolecular forces within the lipid bilayer," in *Biochemistry*, vol. 38, 1999, pp. 9328-9336.

[13]R. B. Cornell, "Regulation of CTP: phosphocholine cytidylyltransferase by lipids. 2 Surface curvature, acyl chain length, and lipid-phase dependence for activation," in *Biochemistry*, vol. 30, 1991, pp. 5881-5888.

[14]R. B. Cornell, "Regulation of CTP: phosphocholine cytidylyltransferase by lipids. 1. Negative surface charge dependence for activation," in *Biochemistry*, vol. 30, 1991, pp. 5873-5880.

[15]G. S. Attard, Templer, R.H., Smith, W.S., Hunt, A.N., and Jackowski, S., "Modulation of CTP: phosphocholine cytidylyltransferase by membrane curvature elastic stress," in *Proceedings of the National Academy of Sciences of the United States of America*, vol. 97, 2000, pp. 9032-9036.

13 Appendices

Sample radioactivity is reported as 10^3 count per minute (cpm).

Table A-1 (DOPC/DOPE LUVs: first set of experiments)

DOPE mole fraction	I sample		II sample		III sample	
	PhoCho	CDP-Cho	PhoCho	CDP-Cho	PhoCho	CDP-Cho
No CCTα	325.8	0.55	319.03	0.26	348.81	0.14
No vesicles	269.38	1.44	329.57	0.59	354.3	0.61
0	316.29	8.67	324.42	7.45	344.34	10.21
0.1	320.21	12.3	313.69	9.19	343.64	11.32
0.2	315.62	8.41	358.94	10.42	342.29	12.75
0.3	318.85	11.51	335.9	12.03	330.03	13.06
0.4	318.53	16.46	326.51	15.48	335.79	17.63
0.5	318.99	20.18	333.97	19.33	331.81	19.99
0.6	319.1	22.04	322.15	21.42	327.59	25.35

Table A-2 (DOPC/DOPE LUVs: second set of experiments)

DOPE mole fraction	I sample		II sample		III sample	
	PhoCho	CDP-Cho	PhoCho	CDP-Cho	PhoCho	CDP-Cho
No CCTα	322.6	0.18	339.04	0.19	309.06	0.4
No vesicles	350.98	0.59	346.91	0.5	295.92	0.65
0	341.99	3.33	346.92	3.1	326.16	3.72
0.1	334.19	5.05	342.32	4.04	356.79	5.17
0.2	345.91	6.69	338.19	6.29	328.13	4.82
0.3	335.23	9.5	329.64	9.76	336.99	7.99
0.4	337.36	11.72	329.96	5.86	331.86	13.43
0.5	317.63	11.61	332.05	12.53	332.01	9.17
0.6	317.46	15.86	317	13.54	318.31	20.01

Table A-3 (DOPC/DOPE LUVs: third set of experiments)

DOPE mole fraction	I sample		II sample		III sample	
	PhoCho	CDP-Cho	PhoCho	CDP-Cho	PhoCho	CDP-Cho
No CCTα	322.6	0.18	339.04	0.19	309.06	0.4
No vesicles	350.98	0.59	346.91	0.5	295.92	0.65
0	346.49	2.04	340.72	1.75	356.01	1.67
0.1	343.74	1.97	347.23	1.64	346.64	3.01
0.2	342.94	2.63	349.11	3.35	345.92	3.51
0.3	348.17	5.35	341.75	3.78	336.95	3.57
0.4	337.48	5.84	341.08	6.06	347.43	3.77
0.5	331.96	5.87	337.34	3.33	331.24	7.73
0.6	342.4	5.95	332.76	5.43	333.47	4.94

Table A-4 (DOPC/DOPE LUVs: fourth set of experiments)

DOPE mole fraction	I sample		II sample		III sample	
	PhoCho	CDP-Cho	PhoCho	CDP-Cho	PhoCho	CDP-Cho
No CCTα	344.34	2.56	302.86	2.26	324.79	2.45
No vesicles	340.63	2.95	330.89	2.9	335.73	2.93
0	324.51	7.74	315.89	8.07	322.4	5.65
0.1	332.09	7.51	313.35	8.73	327.81	5.92
0.2	339.45	7.66	300.15	11.27	325.83	7.9
0.3	311.33	7.65	319.87	10.75	319.67	9.49
0.4	324.31	12.88	291.42	11.59	332.85	9.89
0.5	284.94	15.03	319.83	11.98	324.25	14.21
0.6	317.69	16.88	309.03	17.79	304.55	20.58

Table A-5 (DOPC/DOPA LUVs: first set of experiments)

DOPA mole fraction	I sample		II sample		III sample	
	PhoCho	CDP-Cho	PhoCho	CDP-Cho	PhoCho	CDP-Cho
No CCTα	322.6	0.18	339.04	0.19	309.06	0.4
No vesicles	350.98	0.59	346.91	0.5	295.92	0.65
0	341.99	3.33	346.92	3.1	326.16	3.72
0.025	337.7	1.54	350.27	2.65	340.71	1.7
0.05	337.07	3.39	343.73	2.54	344.67	3.5
0.075	332.42	7.17	346.14	4.9	347.11	5.62
0.1	328.52	10.83	337.72	11.03	346.4	8.98
0.2	305.83	39.36	306	39.27	318.37	38.72
0.3	311.35	37.72	314.25	38.78	321.22	37.67

Table A-6 (DOPC/DOPA LUVs: second set of experiments)

DOPA mole fraction	I sample		II sample		III sample	
	PhoCho	CDP-Cho	PhoCho	CDP-Cho	PhoCho	CDP-Cho
No CCTα	346.85	0.61	356.37	0.87	362.21	0.83
No LUVs	358.33	1.61	357.67	1.83	362.63	1.71
0.00	347.78	2.22	358.49	1.79	363.93	2.07
0.03	354.39	2.00	361.03	2.34	365.17	2.93
0.05	-	-	351.92	5.71	345.17	5.03
0.08	-	-	358.57	4.40	349.88	7.37
0.10	346.28	8.51	282.54	7.96	357.40	8.61
0.15	338.73	14.31	340.74	19.65	347.50	13.50
0.20	330.49	20.78	324.58	25.84	337.60	20.90
0.25	327.11	26.48	327.59	26.13	338.80	23.75
0.30	314.93	25.59	356.08	22.53	341.36	27.00

Table A-7 (DOPC/DOPS LUVs: first set of experiments)

DOPS mole fraction	I sample		II sample		III sample	
	PhoCho	CDP-Cho	PhoCho	CDP-Cho	PhoCho	CDP-Cho
No CCTα	322.6	0.18	339.04	0.19	309.06	0.4
No vesicles	350.98	0.59	346.91	0.5	295.92	0.65
0	341.99	3.33	346.92	3.1	326.16	3.72
0.025	349.13	1.32	349.98	1.18	345.73	1.38
0.05	343.44	2.07	351.35	2.41	326.15	3.34
0.075	348.23	2.27	353.89	1.74	335.27	1.83
0.1	346.89	1.57	344.77	2.03	329.91	2.26
0.2	345.77	4.52	343.57	3.04	331.2	4.32
0.3	342.76	8.36	338.95	8.71	328.45	8.77

Table A-8 (DOPC/DOPS LUVs: second set of experiments)

DOPS mole fraction	I sample		II sample		III sample	
	PhoCho	CDP-Cho	PhoCho	CDP-Cho	PhoCho	CDP-Cho
No CCTα	372.29	0.45	374.31	0.48	340.31	0.42
No LUVs	374.50	3.30	370.21	2.68	372.07	2.69
0.00	372.76	2.36	357.53	2.31	374.77	2.22
0.025	379.51	4.54	361.31	5.32	370.73	4.51
0.05	369.46	4.63	354.89	4.45	353.33	3.90
0.075	368.27	4.37	365.37	3.94	364.69	5.79
0.10	373.86	5.43	360.97	3.89	355.34	6.66
0.15	363.17	5.36	358.60	6.00	374.89	4.86
0.20	360.73	11.84	354.78	10.64	354.38	11.47
0.25	353.21	11.29	347.10	10.76	360.88	10.92
0.30	360.93	15.29	358.53	10.93	346.87	12.98

Table A-9 (DOPC/DPPA LUVs)

DPPA mole fraction	I sample		II sample		III sample	
	PhoCho	CDP-Cho	PhoCho	CDP-Cho	PhoCho	CDP-Cho
No CCTα	374.26	1.40	370.83	1.37	365.72	1.40
No LUVs	375.43	2.16	374.54	2.16	410.07	2.35
0.00	354.29	16.19	335.97	27.69	349.44	23.72
0.025	335.66	36.14	320.40	53.81	320.00	47.66
0.05	325.93	55.94	304.04	58.31	313.51	65.18
0.075	312.83	59.71	306.27	65.78	302.61	75.35
0.10	325.29	55.14	317.45	58.71	315.50	63.46
0.15	312.87	55.72	327.99	54.38	322.95	51.35
0.20	327.13	45.57	336.23	47.93	324.80	48.86
0.25	333.35	41.82	337.36	42.91	337.21	37.34
0.30	344.03	27.64	349.07	26.42	341.56	23.43

Table A-10 (DOPC/DPPS LUVs)

DPPS mole fraction	I sample		II sample		III sample	
	PhoCho	CDP-Cho	PhoCho	CDP-Cho	PhoCho	CDP-Cho
No CCTα	374.26	1.4	370.83	1.37	365.72	1.4
No LUVs	375.43	2.16	374.54	2.16	410.07	2.35
0	354.29	16.19	335.97	27.69	349.44	23.72
0.025	325.033	49.3	346.56	34.57	345.53	26.29
0.05	333.07	33.52	351.16	25.68	332.93	35.05
0.075	321.67	47.24	333.84	42.55	355.27	22.58
0.1	305.4	52.16	298.75	75.03	324.34	52.57
0.15	289.3	78.58	252.37	72.25	298.41	73.05
0.2	292.65	80.89	286.18	83.6	287.58	85.34
0.25	286.91	87.84	286.06	85.44	287.35	87.18
0.3	292.71	79.47	275.31	92.42	283.56	88.48

Table A-11 (DOPC/OPA and DOPC/OPS LUVs: first set of experiments)

Anionic lipid mole fraction	DOPC/OPA LUVs		DOPC/OPS LUVs	
	PhoCho	CDP-Cho	PhoCho	CDP-Cho
No CCTα	298.85	0.18	298.85	0.18
No LUVs	309.58	0.27	309.58	0.27
0.00	303.87	0.81	303.87	0.81
0.025	294.48	1.97	302.07	1.08
0.05	276.8	3.37	305.08	1.90
0.075	298.07	5.31	300.87	3.73
0.10	297.49	6.61	301.61	4.37
0.20	295.82	7.43	296.34	10.40
0.30	302.61	5.13	295.67	15.06

Table A-12 (DOPC/OPA LUVs: second set of experiments)

OPA mole fraction	I sample		II sample		III sample	
	PhoCho	CDP-Cho	PhoCho	CDP-Cho	PhoCho	CDP-Cho
No CCTα	372.29	0.45	374.31	0.48	340.31	0.42
No LUVs	374.50	3.30	370.21	2.68	372.07	2.69
0.00	372.76	2.36	357.53	2.31	374.77	2.22
0.025	368.92	6.04	368.33	5.64	361.53	5.20
0.05	365.57	7.29	356.66	9.49	363.32	7.24
0.075	357.37	8.70	362.07	6.86	356.59	8.68
0.10	360.37	8.47	349.11	9.16	365.67	8.16
0.15	360.15	11.87	362.08	11.22	364.02	10.46
0.20	361.51	10.63	361.11	8.85	359.47	9.03
0.30	357.36	11.33	356.33	11.25	362.87	11.69
0.40	351.66	9.25	373.86	7.38	360.19	8.97

Table A-13 (DOPC/OPS LUVs: second set of experiments)

OPS mole fraction	I sample		II sample		III sample	
	PhoCho	CDP-Cho	PhoCho	CDP-Cho	PhoCho	CDP-Cho
No CCTα	372.29	0.45	374.31	0.48	340.31	0.42
No LUVs	374.50	3.30	370.21	2.68	372.07	2.69
0.00	372.76	2.36	357.53	2.31	374.77	2.22
0.025	384.26	4.44	379.56	4.52	355.20	3.89
0.05	350.65	5.14	377.04	4.43	383.13	4.46
0.075	361.89	5.02	373.78	4.52	366.63	5.57
0.10	377.78	3.58	356.91	4.05	346.32	4.45
0.15	361.33	8.46	353.45	10.40	372.85	7.13
0.20	370.92	9.97	360.44	10.84	360.20	11.03
0.30	366.25	15.95	374.48	14.59	344.84	15.92
0.40	341.59	21.40	350.66	23.11	365.57	23.82

Table A-14 (DOPC/OA LUVs: second set of experiments)

OA mole fraction	I sample		II sample		III sample	
	PhoCho	CDP-Cho	PhoCho	CDP-Cho	PhoCho	CDP-Cho
No CCTα	372.29	0.45	374.31	0.48	340.31	0.42
No LUVs	374.50	3.30	370.21	2.68	372.07	2.69
0.00	347.78	2.22	358.49	1.79	363.93	2.07
0.05	346.10	2.75	365.51	1.81	358.51	3.53
0.10	340.94	5.55	356.66	4.58	361.58	3.20
0.15	338.23	6.89	356.17	7.54	355.94	8.73
0.20	333.13	9.78	351.17	12.18	353.71	12.23
0.30	343.13	17.42	342.85	19.70	347.03	15.30
0.40	321.01	26.97	338.60	21.54	334.65	25.53
0.50	314.06	36.66	325.93	35.87	326.83	31.60
0.60	319.77	30.44	325.00	28.86	321.36	33.57

Table A-15 (CCTα partitioning into DOPC/DOG (84:16) LUVs)

[Lipid] (mM)	I sample		II sample		III sample	
	PhoCho	CDP-Cho	PhoCho	CDP-Cho	PhoCho	CDP-Cho
No CCTα	325.40	0.46	370.78	0.52	278.27	0.51
1.000	354.97	9.46	344.19	7.10	356.56	10.43
0.500	358.63	7.30	354.15	6.80	359.43	7.41
0.100	356.62	6.37	360.92	5.70	335.32	6.00
0.025	361.99	3.47	357.10	5.04	370.69	3.40
0.000	350.28	2.49	355.83	2.40	-	-

Table A-16 (CCTα partitioning into DOPC/DOPA (7:3) LUVs)

[Lipid] (mM)	I sample		II sample		III sample	
	PhoCho	CDP-Cho	PhoCho	CDP-Cho	PhoCho	CDP-Cho
No CCTα	372.29	0.45	374.31	0.48	340.31	0.42
1.000	335.95	30.29	343.60	28.98	331.00	30.52
0.500	312.95	26.27	326.75	26.78	350.93	23.38
0.250	351.48	22.72	348.11	24.61	346.59	23.17
0.100	355.87	17.22	343.67	19.96	362.39	17.43
0.050	352.60	12.26	367.48	10.01	363.59	11.66
0.025	370.63	7.62	371.00	8.90	396.61	8.24
0.000	374.50	3.30	370.21	2.68	372.07	2.69

Table A-17 (CCTα partitioning into DOPC/DOPS (7:3) LUVs)

[Lipid] (mM)	I sample		II sample		III sample	
	PhoCho	CDP-Cho	PhoCho	CDP-Cho	PhoCho	CDP-Cho
No CCTα	325.40	0.46	370.78	0.52	278.27	0.51
1.000	341.85	12.07	340.06	8.29	346.67	13.21
0.500	345.27	10.43	340.87	7.47	351.80	11.91
0.250	344.89	8.21	345.32	6.09	357.32	9.19
0.100	355.65	5.83	346.10	4.54	359.81	6.11
0.050	359.54	4.32	354.29	4.20	364.96	5.30
0.000	350.28	2.49	355.83	2.40	-	-

Table A-18 (CCTα partitioning into DOPC/OAS (1:1) LUVs)

[Lipid] (mM)	I sample		II sample		III sample	
	PhoCho	CDP-Cho	PhoCho	CDP-Cho	PhoCho	CDP-Cho
No CCTα	372.29	0.45	374.31	0.48	340.31	0.42
1.000	336.19	34.17	341.29	29.60	330.44	32.97
0.500	343.62	29.82	354.03	33.06	346.45	28.59
0.100	347.45	28.80	349.55	28.08	336.97	30.83
0.050	352.11	24.45	334.73	30.88	356.09	26.58
0.025	348.02	20.68	353.03	25.11	372.14	16.70
0.000	374.50	3.30	370.21	2.68	372.07	2.69

Table A- 19 Vesicles were diluted in buffer and sized measuring the light scattered at 90°. Vesicle diameter was estimated by SDP intensity analysis. Analysis conditions were: 300 seconds accumulation and automatic sampling time, 3-200 nm diameter range and 24 bins.

DOPC/DOPE mole ratio	Vesicle size (nm)	Standard deviation (nm)	Percentage of scattered light
9/1	≥2000	137	86
	237	31	12
	84	14	2
8/2	≥2000	137	85
	166	21	15
7/3	≥2000	137	82
	162	14	18
6/4	≥2000	137	86
	157	12	14
5/5	≥2000	137	88
	152	15	12
4/6	≥2000	137	96
	67	13	4

Table A- 20 Vesicles were diluted in buffer and sized measuring the light scattered at 90°. Vesicle diameter was estimated by SDP intensity analysis. Analysis conditions were: 300 seconds accumulation and automatic sampling time, 3-200 nm diameter range and 24 bins.

DOPC/DOPA mole ratio	Vesicle size (nm)	Standard deviation (nm)	Percentage of scattered light
97.5/2.5	≥2000	137	97
	105	19	3
95/5	≥2000	137	98
	210	32	1
	52	10	1
92.5/7.5	≥2000	137	99
	52	9	1
90/10	≥2000	137	100
85/15	≥2000	137	100
80/20	≥2000	137	100
75/25	≥2000	137	96
	95	14	4
70/30	≥2000	137	95
	111	16	5

Table A- 21 Vesicles were diluted in buffer and sized measuring the light scattered at 90°. Vesicle diameter was estimated by SDP intensity analysis. Analysis conditions were: 300 seconds accumulation and automatic sampling time, 3-200 nm diameter range and 24 bins.

DOPC/DOPS mole ratio	Vesicle size (nm)	Standard deviation (nm)	Percentage of scattered light
97.5/2.5	≥2000	137	99
	80	6	1
95/5	≥2000	137	99
	179	23	1
92.5/7.5	≥2000	137	100
90/10	≥2000	137	99
	45	6	1
8/2	≥2000	137	98
	72	17	2
75/25	1941	158	85
	351	75	10
	120	34	5
7/3	≥2000	137	100

Table A- 22 Vesicles were diluted in buffer and sized measuring the light scattered at 90°. Vesicle diameter was estimated by SDP intensity analysis. Analysis conditions were: 300 seconds accumulation and automatic sampling time, 3-200 nm diameter range and 24 bins.

DOPC/DPPA mole ratio	Vesicle size (nm)	Standard deviation (nm)	Percentage of scattered light
97.5/2.5	1863	214	77
	236	110	23
95/5	≥2000	137	86
	165	30	14
92.5/7.5	1924	175	80
	331	66	12
	133	33	8
9/1	1865	212	87
	192	46	11
	82	13	2
85/15	≥2000	137	89
	204	37	11
80/20	≥2000	137	93
	139	35	7
75/25	1264	220	98
	75	8	2
70/30	≥2000	137	97
	68	20	3

Table A- 23 Vesicles were diluted in buffer and sized measuring the light scattered at 90°. Vesicle diameter was estimated by SDP intensity analysis. Analysis conditions were: 300 seconds accumulation and automatic sampling time, 3-200 nm diameter range and 24 bins.

DOPC/DPPS mole ratio	Vesicle size (nm)	Standard deviation (nm)	Percentage of scattered light
97.5/2.5	≥2000	137	97
	242	22	3
95/5	≥2000	137	100
92.5/7.5	≥2000	137	99
	80	5	1
90/10	≥2000	137	98
	195	15	2
85/15	≥2000	137	97
	200	30	2
	52	10	1
80/20	≥2000	137	98
	173	29	2
75/25	≥2000	137	98
	76	17	2
70/30	≥2000	137	99
	61	14	1

Table A- 24 Vesicles were diluted in buffer and sized measuring the light scattered at 90°. Vesicle diameter was estimated by SDP intensity analysis. Analysis conditions were: 300 seconds accumulation and automatic sampling time, 3-200 nm diameter range and 24 bins.

DOPC/OPA mole ratio	Vesicle size (nm)	Standard deviation (nm)	Percentage of scattered light
97.5/2.5	1865	213	22
	268	85	78
95/5	1233	511	57
	253	129	43
92.5/7.5	≥2000	137	83
	147	28	17
90/10	283	36	100
80/20	≥2000	137	92
	110	28	8
70/30	≥2000	137	92
	72	19	8
60/40	≥2000	137	95
	41	13	5

Table A- 25 Vesicles were diluted in buffer and sized measuring the light scattered at 90°. Vesicle diameter was estimated by SDP intensity analysis. Analysis conditions were: 300 seconds accumulation and automatic sampling time, 3-200 nm diameter range and 24 bins.

DOPC/OPS mole ratio	Vesicle size (nm)	Standard deviation (nm)	Percentage of scattered light
97.5/2.5	≥2000	137	78
	145	21	22
95/5	≥2000	137	84
	170	29	16
92.5/7.5	≥2000	137	91
	101	21	9
90/10	≥2000	137	82
	121	30	8
85/15	≥2000	137	88
	177	36	12
70/30	≥2000	137	100
60/40	≥2000	137	100

Table A- 26 Vesicles were diluted in buffer and sized measuring the light scattered at 90°. Vesicle diameter was estimated by SDP intensity analysis. Analysis conditions were: 300 seconds accumulation and automatic sampling time, 3-200 nm diameter range and 24 bins.

DOPC/OA mole ratio	Vesicle size (nm)	Standard deviation (nm)	Percentage of scattered light
90/10	≥2000	137	87
	170	30	13
80/20	≥2000	137	84
	250	17	16
70/30	≥2000	137	89
	188	41	11
60/40	1770	259	66
	255	61	34
50/50	1944	154	80
	205	39	20
40/60	≥2000	137	94
	144	33	6

14 GLOSSARY[a]

Amphipathic Of protein molecules with one surface containing hydrophilic and the other hydrophobic amino acid residues.

Apoptosis Pathway that results in cell death in multi-cellular organism. It occurs as a defined series of events, regulated by a conserved machinery. Apoptosis is essential in development for the removal of unwanted cells. In apoptosis, the chromatin in the cell nucleus condensed and becomes fragmented. The cells detach from neighbours, shrink and then fragment into apoptotic bodies. Neighbouring cells recognise apoptotic bodies and remove them by phagocytosis.

Axon The long process which grows out from the cell bodies of some neurones towards a specific target with which it connects and carriers impulses away from the cell body.

Brain Enlargement of the central nervous system of most bilaterally symmetrical animals with an antero-posterior axis. Three dilations of the neural tube give rise to forebrain, midbrain and hindbrain. The **forebrain** comprises the diencephalons anteriorly and the telencephalon posteriorly. Primitively, this is olfactory but in higher vertebrates the telencephalon roof is expanded to form the paired cerebral hemispheres and dominates the rest of the brain in its sensory and motor function. The telencephalon retains its association with smell, forming a pair of olfactory lobes. The **midbrain** is primitively an optic centre, the pair of optic nerves entering after decussation (crossing of the nerve tracts from one side of the brain to the other) at the optic chiasma. Although terminations of these fibres enter the visual cortex of the cerebrum in higher vertebrates, the midbrain still retains integrative functions and is the origin of some cranial nerves. The **hindbrain** generally has its anterior roof enlarged to form a pair of cerebellar hemispheres associated with

---

[a] M. Thain, and Hickman, M., *The penguin dictionary of biology*, Tenth edition ed. London: Penguin Books Ltd, 2000.

proprioceptive coordination of muscle activity in posture and locomotion. Its floor is thickened to form the pons anteriorly and the medulla oblongata posteriorly. The central canal of the spinal cord expands to form the brain ventricles, and the whole is surrounded by meninges.

Endocytosis Collective term for phagocytosis and pinocytosis. An essential process in much eukaryotic cell locomotion.

Eukaryotes Organism in whose cell or cells chromosomal genetic material is (or was) contained within one or more nuclei and so separated from the cytoplasm by two nuclear membranes. Some eukaryote cells (e.g. mammalian erythrocytes) lose their nuclei during development.

Exocytosis Process whereby a vesicle (e.g. secretory vesicle), often budded from the endoplasmic reticulum or golgi apparatus, fuses with the plasma membrane of the cell, with release of vesicle contents to exterior. Common process in secretion. When restricted to anterior region of cell it is an important stage in much eukaryotic cell locomotion.

Forebrain see **Brain**

Haemostasis Several homeostatic mechanisms maintaining blood in a fluid state, and within blood vessel.

Hindbrain see **Brain**

Homeostasis Term given to those processes, commonly involving negative feed-back, by which both positive and negative control are exerted over the values of a variable or set of variables, and without which control the system would fail to function

Hyperplasia Increase in amount of tissue resulting from cell division (each remaining the same size). The opposite is hypoplasia.

Hypoplasia see **Hyperplasia**

Midbrain see **Brain**

Myelin sheath Many layers of membrane of Schwann cell or of oligodendrocyte wrapped in a tight spiral round a nerve axon forming a sheath preventing leakage of current across the surrounded axon membrane.

Phagocytosis One form of endocytosis in which large particles/cell debris are taken up into large endocytic vesicles (phagosomes).

Pinocytosis The bulk-phase component of endocytosis, involving ingestion of surrounding extracellular fluid by part of the eukaryotic plasma membrane by invagination to form an endocytic vesicle.

Prokaryotes They are typically unicellular or filamentous. Their DNA is not housed within a nuclear envelope and no prokaryotic cell is descendent from such nucleated cells. Mitochondria and chloroplasts are absent, but they possess structures that functions similarly (mesosome, chromatophore).

Systemic Generally distributed throughout an organism.

Vasoactive Having an effect upon rate of blood flow or tissue fluid production; e.g. affecting dilation or permeability of blood vessels.

Promoters About 100 base pairs long, it lies a short distant upstream of the coding part of the gene of which it forms a part and it is the region to which an RNA polymerase molecule binds to initiate transcription. Promoters of genes which transcribe large amounts of product are similar to one another (share similar consensus sequence) and have a TATA box about 30 base pairs upstream from where the transcription begins.

TATA box Short nucleotide consensus sequence in eukaryote promoter sequences bound by RNA polymerase II and III. It is an AT-rich region, commonly including the interrupted sequence TATAT...AAT...A.

Consensus sequence Conserved nucleotide sequences found in all examples of a regulatory region in DNA, such as promoter regions.

"...ed ho posto il mio cuore a ricercare ed investigare con saggezza tutto ciò che viene fatto sotto il sole: é questa una occupazione molesta, che Dio ha dato ai figli dell'uomo perchè in essa si affatichino."

(*Sacra Bibbia*, Ec 1,13)

("...and I devoted my heart to pursue and investigate wisely everything which is done under the sun: this is an annoying occupation, which God gave to the sons of the man so that they could get tired.")

(*Holy Bible*, Ec 1,13)